In vitro and in vivo models to investigate tissue remodelling in Graves' ophthalmopathy

Glynn R.C. Baker

PhD

Cardiff University

2006

ProQuest LLC
789 East Eisenhower Parkway
P.O. Box 1346
Ann Arbor, MI 48106-1346

Summary

In chapter one the aim was to establish and extend the characterization of murine models of thyroiditis and Graves' ophthalmopathy (GO), induced by transfer of TSH receptor (TSHR) primed T cells. In the first experiment, genetic immunization or TSHR fusion protein induced TSHR antibodies in all nine mice. Some of the antibodies functioned as thyroid-stimulating antibodies and/or TSH binding inhibiting Igs with 2/7 mice having elevated T4. Splenocyte transfer induced no immune response in naive BALB/cbyJico recipients. Subsequently genetic immunization or fusion protein-treated mice were maintained in either local or Brussels conditions (water, chow, and bedding). TSHR antibodies were induced in 9/9 Brussels (with decreased T4 in 1/9) but 5/9 local mice. No thyroiditis or orbital changes were induced, but misleading fixation artefacts in extraocular muscles were noted. Thyroids from many TSHR-treated and control mice contained ectopic thymus. Ectopic thymus can masquerade as thyroiditis, and care is required to avoid muscle artefacts.

In chapter 2 the biological effects of TSHR activation in vitro, in adipose tissue - the site of orbital TSHR expression was examined. Activating mutant TSHR (TSHR*) or wild type (WT), were introduced into human orbital preadipocytes using retroviral vectors. Their proliferation, basal cAMP accumulation, spontaneous and PPARγ induced adipogenesis were assessed and compared with non-modified cells. Expression of TSHR* significantly inhibited the proliferation of preadipocytes and produced an increase in unstimulated cAMP. PPARγ induced adipogenesis in non-modified cells produced morphological changes, but not in TSHR* expressing cells. TSHR activation renders preadipocytes refractory to PPARγ induced adipogenesis. The failure to develop lipid-containing vacuoles suggested the terminal stages of differentiation have been inhibited.

In chapter 3 tears from patients with Graves' disease (GD), GO and smokers were examined for TSHR activation and protein changes. Reflex tears were collected from 37 normal non-smokers (NNS), 33 normal smokers (NS), 51 GD and 85 GO patients. Specific thyrotropin receptor stimulating activity (TSHRSA) was measured and also serum thyroid stimulating antibodies (TSAB). Pooled NNS, NS and GO tears were separated by SDS-PAGE and silver stained. Proteins expressed in the NS and GO pools but not NNS, were excised and analysed by MALDI-TOF mass spectrometry. Specific TSHRA was detected in 25% NS, 32% GD and 41% GO. A thyroid blocking antibody did not inhibit TSHRA. Clinical activity score correlated with serum TSAB but not tear TSHRSA. SDS-PAGE analysis revealed a higher vol/vol protein concentration in GO tears and additional proteins of 30 to 41 kD, in GO and NS compared with NNS. These were identified as zinc-alpha-2-glycoprotein (ZAG) and lactoferrin (LF). ZAG (also known as lipid mobilising factor) and LF do not have TSHRSA. Therefore, similar changes in tear composition are present in GO and NS compared with NNS. We postulate that TSHRSA is a protease enzyme. ZAG and LF expression is increased and their molecular weights are modified, suggesting degradation and/or changes in glycosylation, which may affect their bioactivities.

In chapter 4, transgenic adiponectin elevation in FVB mice produced profound changes in interscapular and orbital fat depots. No previous models have demonstrated orbital fat proliferation and these changes could be followed by orbital MRI. TSHR expression increases with adipogenesis but does not in this case lead to autoimmunity directed towards the TSHR. A wide range of circulating adiponectin levels are present GO patients and no clinical correlations were evident.

Publications

Baker GRC, Morton M, Rajapaska RS, Bullock M, Gullu S, Mazzi B, Ludgate M. "Altered Tear Composition in Smokers and Patients with Graves' Ophthalmopathy". Arch Ophthalmol 2006. In press.

Lei Zhang, Glynn Baker, D. Janus, C. Paddon, D. Fuhrer, M. Ludgate. Biological Effects of Thyrotropin Receptor Activation on Human Orbital Preadipocytes. IOVS 2006. In press.

Baker G, Mazzioti G, Von Rhuland C, Ludgate M (2005). "Reevaluating thyrotropin receptor-induced mouse models of graves' disease and ophthalmopathy". Endocrinology 146(2):835-44.

Ludgate M and G Baker (2004). "Inducing Graves' ophthalmopathy" J Endocrinol Invest 27(3):211-15.

Combs T, Pajvani U, Berg A, Lin Y, Jelicks L, Laplante M, Nawrocki A, Rajala M, Parlow A, Cheeseboro L, Ding Y, Russell R, Lindemann D, Hartley A, Baker G, Obici S, Deshaies Y, Ludgate M, Rossetti L, Scherer P (2004). "A Transgenic Mouse with a Deletion in the Collagenous Domain of Adiponectin Displays Elevated Circulating Adiponectin and Improved Insulin Sensitivity". Endocrinology 145:367-383

Starkey K, Janezic A, Jones G, Jordan N, Baker G, Ludgate M (2003). "Adipose thyrotrophin receptor expression is elevated in Graves' and thyroid eye diseases ex vivo and indicates adipogenesis in progress in vivo." J Mol Endocrinol 30(3): 369-80.

Starkey K, Heufelder A, Baker G, Joba W, Evans M, Davies S, Ludgate M (2003). "Peroxisome proliferator-activated receptor-gamma in thyroid eye disease: contraindication for thiazolidinedione use?" J Clin Endocrinol Metab 88(1):55-9.

Ludgate M. and G. Baker (2002)."Unlocking the immunological mechanisms of orbital inflammation in thyroid eye disease" Clin Exp Immunol 127(2):193-8.

Ludgate M. and G. Baker (2001). Animal models of Graves' ophthalmopathy. Thyroid Eye Disease. R. Bahn. Boston/Dordecht/London, Kluwer Academic Publishers: 67-81.

Acknowledgements

This work was carried out under the clear supervision and inspiration of Dr Marian Ludgate.

Mrs Carol Lane facilitated research by allowing access to her thyroid eye disease clinic and biopsy material from surgery as well as continuing my ophthalmic training in parallel to research work.

I am grateful for the co-operation of all the patients providing samples for study.

Funding by the Welsh Office for Research and Development provided a salary for two years of full-time study and some consumables were covered by the Cardiff and Vale NHS Trust Research and Development small grant award.

Dr Terry Combs and Dr Phillip Sherer allowed us access to study the transgenic adiponectin mice and measure serum adiponectin from Graves' ophthalmopathy patients.

Chris von Rhuland in the department for medical microscopy assisted with embedding the plastic specimens and performed the electron microscopy.

Dr Bill Stewart performed the initial MRI scans and established a protocol for me to follow.

Dr Nicola Jordan provided instruction for TSAB assays.

Dr Mark Lewis provided instruction on western blotting and his general lab experience was invaluable.

Dr Gherado Mazziotti helped perform intracellular cytokine analysis by flow cytometry.

Dr Sevim Gullu, Dr Barbara Mazzi and Dr Sam Rajapaska performed the initial tear TSHR stimulating assays and protein gels.

Dr Mike Morton performed the MALDI-TOF analysis.

Mr Martin Bullock performed purification of ZAG.

Dr Catherine Winder performed SYPRO ruby staining of tear proteins.

Specific acknowledgement of those performing procedures that contributed to this work are mentioned again at the appropriate area in the text, otherwise all other experiments were performed by myself.

Abbreviations

ACTH	adrenocorticotropin
ACHE	acetylcholinesterase
ADD1	adipocyte differentiation and determination factor-1
APC	antigen presenting cell
aP2	adipocyte lipid binding protein
BAT	brown adipose tissue
cAMP	cylic adenosine monophosphate
CAS	clinical activity score
cDNA	complementary DNA
C/EBP	CCAAT/ enhancer binding protein
CHO	Chinese hamster ovary
CRE	cAMP response element
CREB /ATF1	cAMP responsive element binding protein/activated transcription factor 1
CS	calf serum
DAB	diaminobenzidine tetrahydrochloride
DMEM	Dulbecco's modified Eagle medium
DNA	deoxyribonucleic acid
ECD	extracellular domain of TSHR
ELAM	endothelial leucocyte adhesion molecule
ELISA	enzyme linked immunoabsorbent assay
EOM	extra-ocular muscle
ERK	extracellular signal related kinase
FACS	fluorescence activated cell sorting
FCS	fetal calf serum
GAG	glycosaminoglycan
GD	Graves' disease
GO	Graves' ophthalmopathy
GPI	glycophosphatidylinositol
HBSS	Hanks balanced salt solution
HLA	human leucocyte antigen
HRE	hormone resonse element
HSP	heat-shock protein
IBMX	isobutylmethylxanthine
ICAM	intracellular adhesion molecules
ICC	immunocytochemistry
IFN	interferon
IL	interleukin
IP_3	inositol triphosphate
KW	Kruskall Wallis
LATS	long acting thyroid stimulator
LFA	lymphocyte function-associated antigen
LIF	leukaemia inhibitory factor
LPL	lipoprotein lipase
MALDI-TOF	matrix assisted laser desorption ionisation-time of flight
MCP	monocyte chemotractic protein
MHC	major histocompatibility antigen

mRNA messenger RNA
MRI magnetic resonance imaging

NF-κB nuclear factor κB
NIS sodium iodide symporter
NSB non-specific binding

ORO oil red-O

PBS phosphate buffered saline
PEG polyethyleneglycol
PGT PBS-gelatine-tween
PM pretibial myxoedema
PPAR perioxisome proliferator activated receptor

RANTES Regulated on Activation, Normal T Expressed and Secreted
RIA radio immunoassay
RNA ribonucleic acid
RXR retinoid x receptor

SREBP sterol regulatory element binding protein

TBAB thyrotropin receptor blocking antibody
TBII thyrotropin receptor inhibiting immunoglobulin
TE tris edta (maxiprep buffer)
TG thyroglobulin
TGF transforming growth factor
Thy
TNF tumour necrosis factor
TPO thyroidperoxidase
TRH thyrotropin releasing hormone
TSAB thyrotropin receptor stimulating antibody
TSH thyrotropin
TSHR thyrotropin receptor
TTF thyroid transcription factor
TZD thiazolidinedione
T3 tri-iodothyronine
T4 tetra-iodothyronine

UCP uncoupling protein
UHW university hospital of Wales

VCAM vascular cell adhesion molecules

WAT white adipose tissue

CONTENTS

3 INCREASING TSHR ACTIVATION IN DIFFERENTIATED ORBITAL PREADIPOCYTES HAS VARIABLE EFFECTS ON LIPID ACCUMULATION 101

Figures

Tables

1 Introduction

1.1 Graves' ophthalmopathy

1.1.1 Introduction to Graves' ophthalmopathy

Graves' disease is a common autoimmune condition in which thyroid stimulating antibodies (TSAB) mimic the action of thyrotropin (TSH) [1]. Since both the growth and function of the thyroid are controlled by TSH, TSAB lead to hyperthyroidism and diffuse goitre [2]. The target of the autoimmune response in Graves' disease is the thyrotropin receptor (TSHR) [3]. The majority of patients with Graves' disease have some degree of ocular involvment that is self limiting, but 3 to 5% of patients develop Graves' ophthalmopathy, an autoimmune condition that requires intervention [4]. Graves' ophthalmopathy is also known as thyroid eye disease and thyroid associated ophthalmopathy, but as they share a common clinical and histological spectrum the use of the term Graves' ophthalmopathy is used throughout this work.

The main clinical features of Graves' ophthalmopathy present with varying degrees of severity are; proptosis, conjunctival injection, chemosis, diplopia and, in extreme cases, loss of sight due to compression of the optic nerve or in years gone by, corneal ulceration and globe perforation. These signs and symptoms can be explained by the increase in volume of the orbital contents by three mechanisms; oedema, production of hydrophilic glycosaminoglycans (GAG) and hypertrophy of the adipose tissue by adipogenesis [5]. The mechanism by which orbital fat proliferates in Graves' ophthalmopathy is not well characterised. Performing biopsies on actively inflamed tissue can exacerbate the situation and is therefore unethical. Models offer surrogate opportunities to investigate such a condition. There are four experimental chapters in this thesis; each comprises an introduction, methods, results and discussion section. As a background to this some general introductions are given on Graves' ophthalmopathy, thyroid biology, thyroid autoimmunity and lipid metabolism. We have used in vivo and in vitro models to examine:

1. TSHR induced thyroiditis and ophthalmopathy.
2. Effects of TSHR activation during adipogenesis.
3. TSHR stimulation by tears and protein changes therein.
4. Orbital adipogenesis induced by transgenic adiponectin expression and its possible relationship to Graves' ophthalmopathy.

1.1.2 Historical aspects of Graves' ophthalmopathy

This thesis has at its core a clinical spectrum of thyroid and eye disease reported by a respected physician in Bath, Caleb Parry in a posthumous publication [6]. The first patient in his series of 8 with thyrotoxicosis also had proptosis and was seen in 1786. Graves went on to describe patients more in terms of their thyrotoxicosis while Basedow focussed on the ophthalmopathy [7; 8]. For many years the presence of a diffuse toxic goitre and raised basal metabolic rate, had proptosis as an accepted feature but anomalies in this contented description soon emerged. Duke-Elder's 1952 'Text-book of Ophthalmology' gives a historical perspective to the considered wisdom half a century ago [9]. The anomalies included; persistence of proptosis after normalising metabolic rate and goitre, worsening proptosis after apparent spontaneous remission or thyroidectomy, proptosis that developed when basal metabolic rate was low and in the presence of myxoedema and most confounding, proptosis that developed preceding hyperthyroidism. The main cause of proptosis, that of Graves' disease, was soon labelled as "thyrotoxic exophthalmos" and the hypothyroid causes called "thyrotropic" or "exophthalmic ophthalmoplegia". Some authors thought that the manifestations of eye disease were completely removed from the thyroid and were dependent on pituitary activity. So as to not lose track of those who originally described various features of the ophthalmopathy Table 1-1 records some rarely used medical eponyms.

Table 1-1 Historical medical eponyms relating to Graves' ophthalmopathy

Sign	Description
Enroth's	Puffy, oedematous, upper and lower lid swelling
Jellinek's	Abnormal upper lid pigmentation
Dalrymple's	The frightened appearance of upper lid retraction
Kocher's	Increased upper lid retraction on holding fixation
Von Graefe's	Lid lag on downgaze
Boston's	Jerky irregular upper lid descent in down gaze
Joffroy's	Absence of forehead creases on upgaze
Rosenbach's	Trembling eyelids on gentle closure
Stellwag's	Infrequent and incomplete blinking reflex
Gifford's	Difficulty inverting the upper lids
Moebius'	Convergence weakness
Suker's	Inability to maintain extreme lateral gaze
Ballet's	Partial or complete immobility of one or all the ocular muscles

Early observations were that thyrotoxic exophthalmos occurred in early adult life and had a male to female ratio of 1:9 and most cases had a relatively benign course resolving without much disfigurement [9]. In contrast cases of exophthalmic ophthalmoplegia were a disorder of middle age and roughly equal sex incidence. The severity of exophthalmic ophthalmoplegia was such that it was not uncommon to exenterate an eye on the suspicion of tumour only to find nothing and then have the condition develop in the remaining eye. An ocular muscle traction test was advocated to assist in such diagnostic dilemmas; ophthalmoplegia due to neurological causes would still allow free movement of the anaesthetised globe when pulled on with forceps, in exophthalmic ophthalmoplegia no such movement would be possible due to fibrosis. The number of patients dying with complications of the disease was greater and there was ready access to whole orbit pathological specimens. Histological descriptions of thyrotoxic exophthalmos commented on the near normal appearance of most cases apart from fat proliferation within the orbit, ocular muscles and other skeletal muscles. More severe cases had lymphocytic infiltrates in connective tissue, fat and muscle, oedema and nerve fibre degeneration. In exophthalmic ophthalmoplegia all the orbital tissues were involved with oedema, patchy lymphocytic infiltrates and fibrosis of muscles and lacrimal gland. Severely affected muscles would take on a cartilaginous appearance. The changes were largely due to degeneration rather than inflammation, the oedema accentuated by strangulation of the circulation in the closed orbital space [9]. The changes seen are not dissimilar to those described in an unrelated set of experiments examining Volkman's ischaemic paralysis, whereby venous return from the forearm is impeded and arterial supply initially continues. Lymphocytic infiltration, oedema and progressive fibrosis develop followed by contracture [10].

Attempts to explain the proptosis revolved around four main theories. The first, "muscular activity", specifically the contraction of smooth muscle within the orbit was severely hamstrung by the minimal presence of such a tissue within the orbit, the only real candidate for this would be Muller's muscle beneath the levator which could account for lid retraction but none of the other signs. The second, "vascular congestion", smooth muscle fibres crossing the inferior orbital fissure obstruct orbital venous drainage when stimulated sypmpathetically, but again no such structure exists. The third, "muscular weakness", proposed that weakness and elongation of the recti had a permissive effect on proptosis. Lastly, "increased orbital tissue bulk", clear histological demonstration of fat, oedema and hydrophillic hyaluronic acid was thought by most to be the cause of proptosis.

Therefore, explaining the cause of proptosis in mechanical terms had some consensus 50 years ago but how this accumulated or was related to thyroid or pituitary function was unclear and without adequate explanation. In terms of treatment, iodine or thyroidectomy for thyrotoxicosis, crude thyroid extract for hypothyroidism, relying on basal metabolic rate to titrate dosage, tarsorrhaphy for corneal exposure, orbital decompressions were crude and used as a last resort and once burnt out the proptosis could be reduced by shortening the recti.

Before continuing on with more current work one individual case report by Stallard is noteworthy [11]. He reports a hypothesis of Russell Brain who suggested that exophthalmic ophthalmoplegia with thyrotoxicosis is due to an excessive production of an X-factor, believed to by thyrotropic hormone of the pituitary and hyperthyroidism was a subordinate part of the process. A 31 year old man with mild signs of thyrotoxicosis, bilateral proptosis worse on the left, had a slightly reduced basal metabolic rate and was treated with thyrotropic hormone injection on three consecutive days. Over the next month his left sided proptosis dramatically worsened to the point where corneal exposure and ulceration ultimately lead to perforation and enucleation. While the TSH preparation may be crude and the worsening of the ophthalmopathy put down as coincidence it is suggestive that a TSH like factor is involved in the mechanism of proptosis. Early evidence of the role of TSH in animal models is reviewed in chapter 2.

1.1.3 Autoantigens in Graves' ophthalmopathy

Oedema and glycosaminoglycans induce expansion of the extra-ocular muscles (EOM) which are greatly enlarged and have been the focus of investigations to identify the autoantigen in Graves' ophthalmopathy and the link with the thyroid gland. A variety of methods, including screening EOM expression libraries [12] and western blotting [13], have identified a number of potential antigens e.g. flavoprotein subunit of mitochondrial succinate dehydrogenase [14] and extracellular matrix proteins [15]. A 64kD protein 'D1' or tropomodulin, which is expressed in thyroid and EOM but not skeletal muscle, was isolated from a thyroid expression library [16]. Other investigators have studied the orbital connective tissue and adipose compartments and identified a 23 kD protein present in orbital fibroblasts as a potential Graves' ophthalmopathy autoantigen [17]. Ocular muscle biopsies from normal and Graves' ophthalmopathy patients show fibroblasts expressing

HLA class II antigens, no expression was present on muscle cells which all had a normal morphology, this lead the authors to question the likelihood of clinically significant reaction to muscle antigen [18]. In fact fibroblasts are a prime suspect for the target of the autoimmune response, not only in Graves' ophthalmopathy but also in another extra-thyroidal manifestation, pretibial myxoedema (PM). In this context, it has been reported that immunoglobulins from Graves' disease patients stimulate the production of ICAM-1 from Graves' disease fibroblasts but not normal fibroblasts [19]. This highlights the presence of fibroblast antibodies in the circulation of patients and also a difference in the response to these antibodies between normal and Graves' disease fibroblasts. Finally the similarity between thyroglobulin (TG), an autoantigen in Hashimoto's thyroiditis, and acetylcholinesterase (ACHE) led to the proposal that a TG/ACHE shared epitope could provide the link between the thyroid and the orbit [20]. Graves' ophthalmopathy sera were shown to bind to the neuromuscular junction [21] in vitro but, as in all of the preceding examples, even though a proportion of Graves' ophthalmopathy patients' sera were found to contain antibodies, their presence did not correlate with disease activity. In contrast, disease severity, as measured by the clinical activity score (CAS) [22], correlates with TSAB [23]. The role of the target antigen, TSHR is introduced in chapter 3

1.1.4 Graves' ophthalmopathy; a TH2 disorder?

Graves' disease and ophthalmopathy have an underlying autoimmune pathogenesis [24]. Adequate immunoregulation depends on a range of mechanisms that maintain discrimination between self and non self. These include elimination of auto reactive T cells in the thymus, peripheral tolerance and anergy (the requirement of a second signal in the immune synapse). The T cell has a central control role in these processes, with $CD4^+$ cells having "helper" and $CD8^+$ "cytotoxic" phenotypes. $CD4^+$ (and $CD8^+$) cells are further classified into TH1 (TC1) or TH2 (TC2) on the basis of the cytokines they secrete; IL-2 and IFN-γ from TH1 and IL-4,5,6,9,10,13 from TH2. TH1 are associated with cell mediated responses and TH2 with humoral immunity. Organ specific autoimmune diseases are considered to result from an imbalance between TH1 and TH2. This is elegantly demonstrated in a human model of Graves' disease and ophthalmopathy happened on by chance. In patients with multiple sclerosis (MS) treated in vivo with a monoclonal antibody to CD52, greater than 95% of their circulating T lymphocytes were eliminated and there was considerable amelioration of their disease. Five to twenty-one months after

this treatment, T cell numbers had returned to 35% and B cells to 180% of pre-treatment values but 14/47 patients had developed Graves' disease with TSAB, with 5 also having Graves' ophthalmopathy symptoms [25] (and personal communication). The deviation from TH1 to TH2, although beneficial for MS, was permissive for Graves' disease and stresses the importance of balance in maintaining appropriate immune responsiveness.

Additional support for the Th2 skew of Graves' ophthalmopathy comes from the positive correlation of levels of soluble CD30 with TBII activity and it is suggested that it could be used as a marker as to when to complete anti-thyroid drug therapy [26]. Part of the TNF/nerve growth factor superfamily, sCD30 is preferentially expressed and secreted from TH2 cells. Cross-linking has expansion and effector functions particularly on B cells while blocking promotes TH1 phenotype cells developing [27]. In contrast, studies of T cell clones derived from Graves' ophthalmopathy patients indicate a predominance of TH1 type autoreactivity in early stages of the disease and TH2 as the condition develops [28; 29]. The culture conditions could influence the clonal phenotype and ex vivo analysis of cytokines in orbital tissues by RT-PCR has found a TH2 spectrum [30].

One feature of TH2 reactivity, the participation of mast cells, has been shown to induce prostaglandin synthesis and GAG production in human orbital fibroblasts, at least in vitro [31]. Mast cells have been reported in Graves' ophthalmopathy biopsies [30] but their precise role warrants further investigation. Furthermore increases in circulating IgE, which could activate mast cells [32] and stem cell factor, a mast cell growth factor [33], have been reported in Graves' disease. It has been demonstrated by flow cytometry that IgE antibodies bind directly to the TSHR in a small number of patients with Graves' ophthalmopathy [34]. Interestingly IgE production by B cells requires T-cells, however mast cells are capable of this via their expression of CD154 (CD40 ligand) that activates CD40 on B cells and is dependent on Il-4 [35]. Il-4 production by mast cells has also been demonstrated to augment fibroblast proliferation via cell-cell adhesion [36].

As will be discussed further in chapter 4, smoking is a major risk factor for Graves' ophthalmopathy and when cells from the mast cell lineage were exposed to cigarette smoke in vitro, the release of several cytokines including IL-4, 5, 10 and 13 and TNFα was induced. IL-4 and 13 induce class switching to IgE whilst TNFα is a major Graves' ophthalmopathy cytokine implicated in several aspects of pathogenesis [37]. Smoking and other possible environmental factors appear to have a greater contribution to Graves'

ophthalmopathy than genetic susceptibility and would seem unrelated to TSHR, CTLA-4, HLA and TNF-β genes [38].

1.1.5 Cellular mechanisms producing Graves' ophthalmopathy

The activity of cytokines marshals the recruitment of inflammatory cells to the orbit and their subsequent responses. A wide range of techniques has been used in the examination of the limited number of surgical specimens that are available for research investigation. The cellular protagonists are lymphocytes, macrophages, mast cells and fibroblasts/preadipocytes. From an initial standpoint that IFNγ, TNFα and IL-1 are the primary effectors [37], have evolved the following mechanisms.

Facilitating entry to the orbit of lymphocytes and monocytes requires activation of adhesion molecules. In situ demonstration of ICAM-1, ELAM-1, VCAM-1 and LFA-3 on blood vessels and vascular endothelium from TED orbits has been linked with in vitro fibroblast production of ICAM-1 and LFA-1 stimulated by IFNγ, TNFα and IL-1 [39]. The expression of ICAM-1, ELAM-1, VCAM-1 and leucocyte integrins CD11a-c is greater in early disease in perimysial connective tissue and vascular endothelium in Graves' ophthalmopathy [40].

Chemoattractants implicated include IL-6, 8 and 16, RANTES and monocyte chemotactic protein (MCP)-1. IL-16 is important in T-cell trafficking as a ligand for CD4+ cells that is believed to follow RANTES production in orbital and thyroid fibroblasts [41]. This activity is induced by IL-1β simulating a pathological state. The IL-16 promolecule is cleaved by caspase 3 and is basally expressed by lymphocytes and stored preformed in mast cells. The production of these chemoattractants has recently been shown to be due to a specific interaction between IgG from Graves' disease patients and Graves' disease fibroblasts insulin-like growth factor 1 receptor (IGF-1R) [42]. This is a new concept and adds IGF-1R to the list of possible autoantigens mentioned previously. Similarly IL-6, 8 and MCP-1 chemokine production is induced by proinflammatory cytokines from orbital fibroblasts [43; 44]. The CD40/CD154 costimulatory pathway has been demonstrated to have a potential role in IL-6, 8 expression. T-cells and mast cells express CD154 that activates the TNFα related CD40 receptor on orbital fibroblasts and is upregulated by IFNγ [43]. CD154 triggers

nuclear mobilization of NF-κB that in turn has binding sites within the promoter regions of IL-6, 8.

Once in the orbit, specific antigen presentation to T-cells is suggested to occur via major histocompatibility complex (MHC) class II HLA-DR antigen [45]. IFNγ can induce orbital fibroblasts expression of HLA-DR [43; 46]. Antigen intracellular processing and presentation may also be facilitated by expression of heat shock proteins (HSP) present in Graves' ophthalmopathy orbital and pretibial fibroblasts [45; 47].

Fibroblastic activation follows one of two divergent routes, denoting a heterogeneous population. One engages in prostanoid synthesis and GAG production [48; 49] the other, the preadipocyte undergoes an inflammatory mediated program of adipogenesis [50]. Both production of hyaluronan and prostaglandin E2 (PGE_2), via prostaglandin endoperoxidase H synthase-2 (PGHS2), in the former can be stimulated by CD40/154 activation [51]. PGE_2 is a determinant for B cell maturation, mast cell activation and the phenotypic bias of TH0 lymphocytes to become TH2. Orbital fibroblasts from Graves' ophthalmopathy have recently been demonstrated to proliferate in the presence of autologous T cells [52]. Proliferation required cell contact, MHC II and CD40/154 signaling. The interruption of CD40 activation may represent a specific site for therapeutic intervention [53].

Just as orbital fibroblasts appear heterogeneous in their adipogenic potential so too is their expression of Thy-1 (CD90) [54]. Two major sub-populations of lung fibroblast can be defined, one expresses Thy-1 and accumulates lipid, and the non-expressing population does not express lipid but does express MHC II when stimulated [55]. Thy-1 expression is associated with a distinct pattern of cellular events regarding cytokine, collagen and fibronectin production [55; 56; 57]. Approximately 65% of orbital fibroblasts express Thy-1 [54]. Curiously opposite to lung fibroblasts, it has subsequently been shown that orbital and myometrial fibroblasts expressing Thy-1 have TGF-β driven myofibroblastic potential whereas fibroblasts not expressing Thy-1 had a PPAR-γ driven lipoblastic potential [58]. The ligands for Thy-1 are not well characterized but endothelial cells expressing Thy-1 have been shown to interact specifically with the leukocyte integrin Mac-1 (CD11b/CD18) and be important in leukocyte extravasation [59]. This perhaps further suggests orbital fibroblasts fall into two subsets, those interacting with leukocytes express Thy-1 and those

participating in adipogenesis do not (or simply lose expression as initial commitment to differentiation occurs).

The process described in sections 1.3-5 are summarised in Figure 1.1 and have in part been published in this format in a review article by us previously [60]. Additional recent information is reported in a recent review of the pathogenesis of Graves' ophthalmopathy [61].

Figure 1.1 Summary of the steps involved in the initiation of Graves' ophthalmopathy

(1) T cells recognize TSHR on orbital fibroblasts. (2) Activated mast cells aid fibroblast activation, stimulate a TH2 response and (3) stimulate TSAB production. (4) Fibroblast activation results in the production of proinflammatory mediators and adhesion molecules with the preadipocyte fraction undergoing differentiation and increasing TSHR expression that heightens TSH/TSAB sensitivity. The resultant inflammation and adipogenesis produce the clinical manifestations of TED.

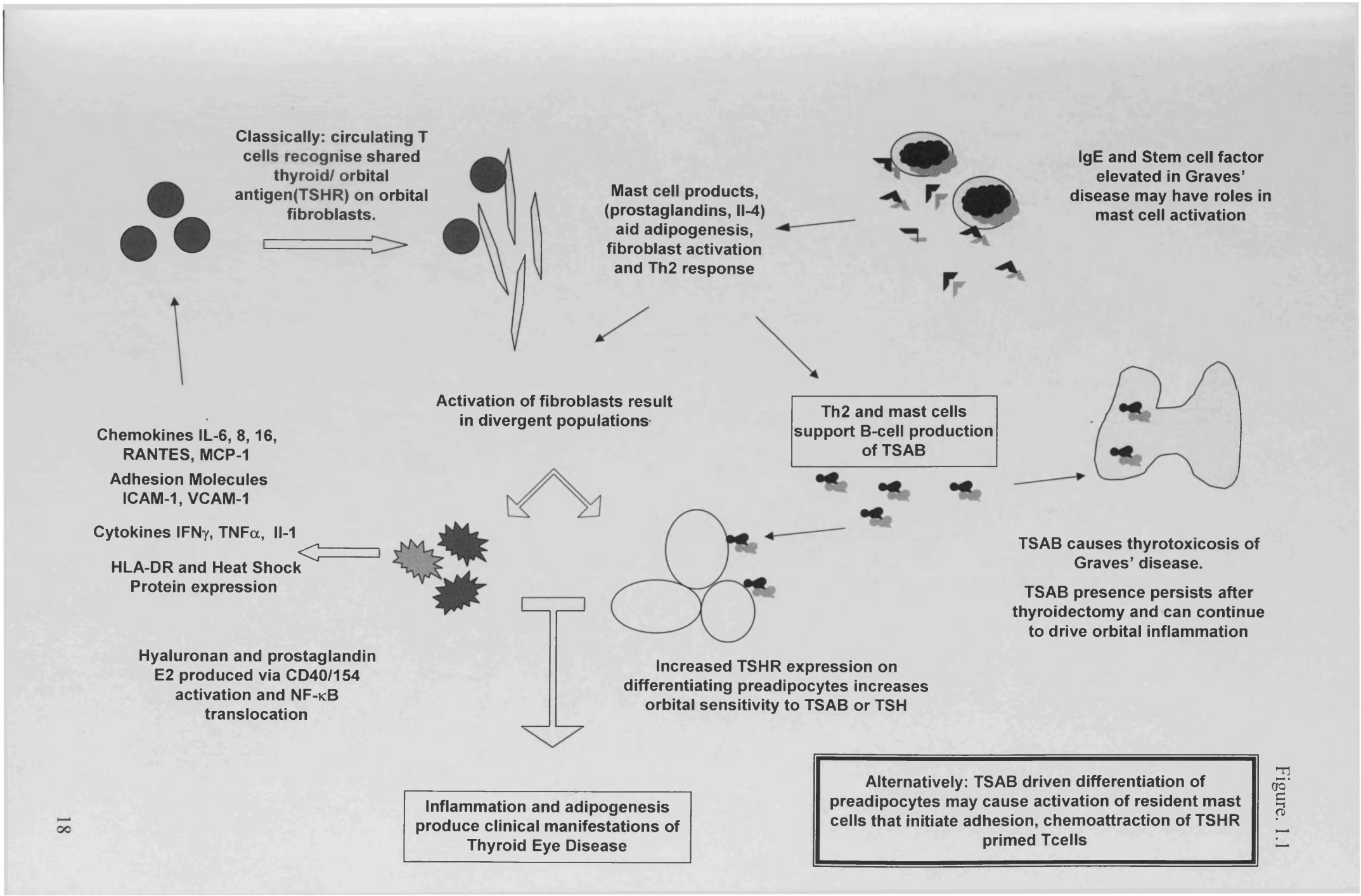
Classically: circulating T cells recognise shared thyroid/ orbital antigen(TSHR) on orbital fibroblasts.
Mast cell products, (prostaglandins, Il-4) aid adipogenesis, fibroblast activation and Th2 response
IgE and Stem cell factor elevated in Graves' disease may have roles in mast cell activation
Activation of fibroblasts result in divergent populations
Th2 and mast cells support B-cell production of TSAB
Chemokines IL-6, 8, 16, RANTES, MCP-1
Adhesion Molecules ICAM-1, VCAM-1
Cytokines IFNγ, TNFα, Il-1
HLA-DR and Heat Shock Protein expression
TSAB causes thyrotoxicosis of Graves' disease.
TSAB presence persists after thyroidectomy and can continue to drive orbital inflammation
Hyaluronan and prostaglandin E2 produced via CD40/154 activation and NF-κB translocation
Increased TSHR expression on differentiating preadipocytes increases orbital sensitivity to TSAB or TSH
Inflammation and adipogenesis produce clinical manifestations of Thyroid Eye Disease
Alternatively: TSAB driven differentiation of preadipocytes may cause activation of resident mast cells that initiate adhesion, chemoattraction of TSHR primed Tcells

Figure. 1.1

1.2 The thyroid axis and disease

1.2.1 Thyroid structure and function

This section is a basic review of thyroid structure and function [62]. The thyroid gland is a highly vascular, bilobed structure anterior to the trachea and its basic unit of structure is the follicle that produces thyroid hormones. Follicles are roughly spheres of polarised cells encasing a protein rich colloid. Development starts around day 24 from an outgrowth of pharyngeal endoderm, this descends into the neck and assumes its final position around week 7. Closely associated are the parathyroid glands and thymus, their development is discussed in chapter 2.

Follicular cells produce thyroglobulin and actively transport iodide using the sodium iodide symporter (NIS), an ATPase dependent transporter that allows concentration of iodide to 30-50 times that of plasma. Adjacent follicles are often at different levels of activity, those less active have a more cuboidal epithelium, those more active have columnar appearances and hence the normal follicular heterogeneity. Iodide in the follicular cell is oxidised to iodine by hydrogen peroxide catalysed by thyroid peroxidase (TPO) and then actively transported into the lumen. At the apical colloid interface, iodination of tyrosyl residues of thyroglobulin produces monoiodotyrosine (MIT) and diiodotyrosine (DIT). The coupling of DIT produces tetra-iodothyronine (thyroxine, T_4) or coupling DIT with MIT to produce tri-iodothyronine (T_3), both are catalysed by TPO. The follicle stores the thyroid hormones in this state, until the thyroglobulin is taken back up into the follicular cell by active pinocytosis under stimulation by TSH. Lysosomal fusion hydrolyses the thyroglobulin molecules to release T_3 and T_4. On average 100μg of hormone is secreted daily, 10% of which is the more active T_3, 80% of the T_4 then undergoes peripheral conversion mainly in liver and kidneys by deiodinase type 1, to T_3 or inactive reverse T_3. The hormones are transported bound to thyroxine binding globulin, thyroxine binding prealbumen or albumen.

Cellular signaling of thyroid hormone is via nuclear receptors that remain bound to DNA apart from in the presence of hormone. On ligand binding the receptors either dimerise or couple with other nuclear receptors such as retinoid X receptor. "Zinc finger" binding of hormone response elements (HRE) on the nuclear receptors ultimately controls gene

transcription. Thyroid hormone also has non transcriptional effects on glucose, calcium and sodium transport by unknown mechanisms [62].

Thyroid hormone raises cellular metabolic rates by transcription of respiratory chain enzymes, sodium and potassium ATPase and increasing mitochondria in most tissues. Up to 40% of a cells energy requirement can be in maintaining its electrochemical gradient so increasing its sodium and potassium ATPase can alone increase expenditure greatly. From this we understand patients with excess hormone (thyrotoxic) have a high metabolic rate, weight loss, fatigue, palpitations, atrial fibrillation and heat intolerance. Patients deficient in hormone (hypothyroid) conversely have a low metabolic rate, weight gain, lethargy and cold intolerance [63].

Normal secretion of thyroid hormone is under control by the hypothalamic-pituitary axis [62]. Hypothalamic secretion of thyrotropin releasing hormone (TRH) to pituitary thyrotrophs is via the hypothalamo-hypophyseal capillaries and stimulates secretion of TSH. Thyroid hormone negatively feeds back on pituitary thyrotrophs not on TRH secretion. When thyroxine is low the thyrotrophs increase TRH receptor expression and vice versa. Inhibition can also occur at the pituitary by hormonal (dopamine/somatostatin) or cytokine (IL-1β & 6/ TNF-α) effects. Cold exposure increases TRH secretion raising metabolic rate.

TSH is a glycoprotein composed of a generic α unit (identical to that of lutenising hormone and follicle stimulating hormone) and a specific β unit and its circulation half life is 30 minutes (reviewed [64]). Secretion follows a diurnal pattern with a midnight peak and is pulsatile.

The TSH receptor (TSHR) is an archetypal G-protein linked structure with 3 external and internal loops, 7 transmembrane helices, an external amino terminus and an internalized carboxyl terminus (reviewed [65]). Ligand binding activates the αβγ G protein trimer by GTP displacing bound GDP on the Gα subunit. This unit (Gα) dissociates and activates adenylate cyclase to produce cAMP ($G_s\alpha$ pathway) until GTP is hydrolysed back to GDP. cAMP activates protein kinase A (PKA) which in turn phosphorylates cAMP response element binding protein (CREB). CREB translocates to the nucleus and stimulates transcription by binding cAMP responsive elements (CRE). This results in follicle cells

increasing iodine and colloid uptake and producing hydrogen peroxide and TPO to elevate circulating thyroxine. Another pathway is also stimulated, $G_q\alpha$ stimulates phospholipase C to hydrolyse phosphoinositides to inositol triphosphate (IP_3) and diacylglycerol. IP_3 elevates intracellular calcium and diacylglycerol activates protein kinase C [62; 66].

1.2.2 Thyroid Autoimmunity

1.2.2.1 Central and peripheral tolerance

Graves' disease is the commonest cause of thyrotoxicosis and is a well characterized autoimmune condition (reviewed [1; 3; 24; 67]). It evolves from abnormal immune surveillance that allows T and B lymphocytes to circulate that recognize autoantigens in the thyroid, most importantly, the TSHR. This represents a loss of tolerance of self antigens and a brief background to tolerance is described here (reviewed [68]). T and B cells have a common lymphoid progenitor; T cells are matured in the thymus while B cells remain in the bone marrow before relocating to the spleen.

Thymic T cell maturation is stepwise, early thymocytes have dual expression of CD4 and 8, those unable to recognize major histocompatibility antigens (MHC) are deleted. The remaining cells expressing CD4 recognize class II MHC and those expressing CD8, class I. Further selection deletes cells recognizing auto antigens associated with MHC and therefore most auto-reactive T cells are removed due to central tolerance by clonal deletion. Clonal anergy can induce peripheral tolerance whereby T cells exposed to prolonged antigen are forced into apoptosis by Fas ligand binding, known as activation induced cell death. B cell maturation is initially in the bone marrow, auto-reactive surface IgM can be rearranged. Once rearranged, if auto-reactivity resolves, further maturation follows in the spleen otherwise apoptosis removes auto-reactive B cells [69].

1.2.2.2 Lymphocytes in autoimmunity

As mentioned previously, circulating T cells can be divided into cytotoxic (CD8) and helper (CD4) roles and are further divided into TH1 and TH2 cells that have different cytokine profiles. These distinct cytokine profiles are less rigid in humans but the diseases

they produce are contrasting; TH1, the inflammatory autoimmune diseases and TH2, allergy and antibody mediated diseases.

Activation of T and B cells is via surface receptors (T/BCR) that recognize antigens with appropriate co-stimulation (reviewed [24]). Antigen presenting cells (APC) digest antigen and present peptide fragments and human leucocyte antigen (HLA) that binds to TCRs. CD4 TCR interaction is restricted to HLA class II molecules (usually presenting exogenous proteins), while CD8 are restricted to class I (endogenous proteins). Additional co-stimulation between APC and T cells occur via B7-CD28 and CD40-CD40L, without this second signal anergy can be induced and no further stimulation develops. BCRs are membrane bound immunoglobulins identical to those they secrete. Bound antigen requires co-stimulation with either cytokines or via direct antigen, class 2 and T cell binding to activate antibody production.

Matured $CD4^+$ thymocytes contain a high frequency of cells capable of becoming regulatory T cells once in the periphery, that if present in sufficient numbers, can prevent disease [70]. A radiation and thymectomy-induced thyroiditis model provides clear evidence for regulatory T cells by demonstrating disease prevention when animals were reconstituted with peripheral $CD4^+$ cells from syngeneic donors [71]. Cells with such a phenotype, CD45RC-, are described as "memory" cells and imply the initial recognition of antigen in the periphery is an important event. In utero radio-iodide ablation of rat thyroids lead to depletion of peripheral regulatory T cells capable of preventing thyroiditis, despite the capacity of the thymus maintain their production [72]. A process of antigen-specific immuno-suppression in autoimmune thyroid disease is suggested by such experiments [73].

1.2.2.3 Mechanisms of loss of tolerance and susceptibility in Graves' disease

The highly ordered process of immunity breaks down in Graves' disease and tolerance is lost leading to production of antibodies that stimulate the TSHR relentlessly, producing thyrotoxicosis and goitre. Viral infections have been suggested to cause unmasking of proteins not seen by the adult immune system and have been sequestered away from immune surveillance, similar to the lens protein induced uveitis seen after traumatic rupture of a lens [74]. No similar model has been proposed for the thyroid. Coincident similarity between infectious agents and host proteins, "molecular mimicry" has been

postulated between Yersinia enterocolitica and the TSHR [75], but direct evidence that such infection leads to Graves' disease is not present. "Bystander activation" is a hypothesis suggesting a viral infection within the thyroid results in production of IFN-γ or other cytokines that induces MHC II expression on thyrocytes. The thyrocytes act as APCs to circulating or resident CD4 cells, however no evidence of concordant co-stimulatory signals and HLA expression are present (reviewed [1; 24; 76]).

The lack of genetic susceptibility in Graves' ophthalmopathy contrasts with Graves' disease in which familial links are evident, numerous genes have been identified; HLA-DR3, HLA-DR ß1, CTLA4, protein tyrosine phosphatase non-receptor type 22 and thyroglobulin (reviewed in [77]). Concordance rates between monozygotic twins is 25-30% and drops to 2-7% in dizygotic twins [78]. The fact that it is at best 30% in monozygotes and not much higher suggests other factors are important. As discussed in relation to Graves' ophthalmopathy smoking is an important risk factor in Graves' disease along with stress, pregnancy and radiation exposure [76; 79].

Models of Graves' disease and ophthalmopathy are discussed in chapter 2.

1.2.2.4 The TSHR and its antibodies

The TSHR as discussed briefly before has some homology with LH and FSH receptors but differs in having two subunits. This was deduced before cloning the gene and confirmed subsequently [80; 81; 82]. The α subunit is the ectodomain and the β unit is smaller, comprising the membrane spanning and carboxyl terminus. The 9 leucine rich repeats of the ectodomain binds TSH, while the transmembrane loops interact with the G proteins. Cysteine bonding in the ectodomain is important for ligand binding .[83] The creation of the two subunits requires cleavage of a 50 amino acid segment in the ectodomain possibly by a matrix metalloprotease, then disulphide bonds link the subunits and breaking these bonds leads to shedding of the α subunit (reviewed in [65]). TSHR exists in multimeric forms until bound by TSH [84]. On ligand binding, the ectodomian changes confirmation from a tethered inverse agonist (closed) to a full agonist (open) of the transmembrane domain that allows disinhibition of the natural constitutive activity of the receptor (reviewed in [85]).

Germline mutations in the TSHR can lead to inactivation and activation of the receptor. Some inactivating mutations cause partial resistance to TSH (normal thyroid hormone levels, normal sized thyroid with raised TSH) [86]. Complete resistance is seen in congenital hypothyroidism but can be due to defects in genes other than the TSHR [87]. Congenital hyperthyroidism due to activating mutations is rare and similar somatic mutations can cause benign and malignant nodular thyroid disease [67]. A large number of mutations have been identified (www.uni-leipzig.de/innere/tshr) most are present within exon 10 and code for amino acids in the transmembrane domain [88]. Retroviral transduction of a panel of activating mutations into human thyrocytes, a rat thyrocyte cell line and COS-7 cells showed the mutations result in varying levels of adenylate cyclase and phosphoinositide-3 kinase activation with roughly similar responses in the thyrocytes but differing in the COS-7, suggesting the cellular context influences the mutations activities [89]. It was also shown that the highest levels of cAMP did not necessarily induce the greatest proliferation. This may be due to differing mechanisms of phosphodiesterases and cAMP regulatory elements.

The autoimmune process in Graves' disease produces antibodies to the TSHR that can take several forms and are generically called thyrotropin receptor antibodies (TRAb). Stimulating antibodies were originally identified as IgG and called long acting thyroid stimulator (LATS) [90], they are currently referred to as thyrotropin receptor stimulating antibodies or immunoglobulin (TSAB/TSI). TSAB can be detected in up to 95% of untreated Graves' disease patients [91]. Immunoglobulin from Graves' disease patients can also compete for binding with both TSH and TSAB, blocking signal transduction, these antibodies have been called thyrotropin receptor binding inhibiting immunoglobulins (TBII) [2]. TSHR antibodies can also bind the receptor without blocking or stimulating it [34]. These thyrotropin receptor blocking antibodies (TBAB) occur in some cases of idiopathic myxoedema and are seen less commonly in Hashimoto's thyroiditis. The hypothyroidism of Hashimoto's is mainly due to a destructive process. It has a higher incidence in areas with adequate dietary iodine [92].

The TSHR has proved difficult to purify and therefore investigators have used a number of non thyroidal cells to express recombinant TSHR; prokaryotic bacteria, eukaryotic insect cells and mammalian cells [65]. Expression in Chinese hamster ovary (CHO) cells demonstrated a fully functional TSHR [93]. The use of recombinant TSHR was largely to

generate elusive antibodies mimicking TSAB, this was ultimately achieved using animal models similar to the plasmid DNA driven model investigated in chapter 2 [94].

Work 30 years ago showed the existence of adipocyte TSH receptor antibodies detected by immunoprecipitation of radiolabelled TSH, guinea pig fat tissue and Graves' patients sera [95]. The immunoprecipitation values did not correlate with antimicrosomal, antithyroglobulin, TBII and TSAB acitivities were weak. It was concluded they were antibodies that recognized different determinants to TBII and TSAB, research has not followed to study epitopes that may be involved. However the presence of a functional TSHR in adipose tissue has been the subject of recent attention and TSHR expression is upregulated during adipogenesis as described in chapter 3.

1.3 Adipocyte Biology and Differentiation

In the past 25 years the view of fat as a simple storage depot of triacylglycerol during times of plenty has undergone major revision. Obesity is increasing in prevalence, associated with NIDDM, Hypertension, Atherosclerosis, gallbladder disease, all with associated morbidity and mortality. Through the production of adipocytokines (adipsin, leptin, plasminogen activator inhibitor-1, TNF-α) the central role fat has to play in metabolism and diseases such as obesity and diabetes has become apparent [96]. Adipose tissue expansion is composed of both increased volume and increased cell number (hypertrophy and hyperplasia). Adipocytes can be differentiated from preadipocytes, adipocyte decrease occurs mainly by apoptosis (to a lesser extent dedifferentiation) both of which occur throughout life, although preadipocyte differentiation capacity may decrease with age [97]. Control of this system is a mixture of endocrine, paracrine and autocrine feedback [98]. Understanding the development and biology of fat pads is relevant to this thesis as the mechanism of orbital fat proliferation in Graves' ophthalmopathy is not well characterised.

1.3.1 White fat biochemistry

Fatty acids are important structurally in membranes, as hormones, second messengers and as a fuel source in white adipose tissue [99]. Fatty acids are esterified in the liver to glycerol

phosphate to form triacylglycerol (triglyceride) and then transported to adipose tissue as very low density lipoproteins. An extracellular lipoprotein lipase (stimulated by insulin) hydrolyses the triacylglycerol before uptake. The adipocyte then activates the fatty acids and transfers the resulting CoA derivatives to glycerol 3-phosphate. Glucagon and adrenaline stimulate reversible phosphorylation of hormone sensitive lipase (HSL) via cAMP activation of a protein kinase. HSL breaks down triacylglycerol while in contrast insulin inhibits lipolysis. The released fatty acids are then broken down to acetyl CoA and are transported to the inner mitochondrial membrane and degraded in the matrix to produce ATP. Insulin stimulates acetyl CoA carbxylase to promote fatty acid synthesis.

1.3.2 Adipocytokines

Adipose tissue as an organ is a relatively new concept, the proteins secreted have been called adipocytokines or adipokines. Leptin acting via its receptor (Ob-R) in the hypothalamus controls energy intake and expenditure [100]. The leptin deficient mouse is obese, diabetic, infertile and hyperphagic [101]. Human genetic mutations in the leptin gene result in a very similar phenotype [102]. However, in normal and obese individuals body fat correlates positively with leptin, suggesting obesity is associated with leptin insensitivity [100]. TNF-α is present in human adipose tissue and increased in obesity, it correlates inversely with lipoprotein lipase and is thought to cause insulin resistance [103]. When adipose TNF-α production is reversed in models of obesity and diabetes it leads to improved insulin sensitivity [104]. TNF-α while being secreted from fat pads might not enter the circulation and may have local autocrine or paracrine actions [105]. IL-6 plasma levels correlate positively with obesity and insulin resistance [106] and weight loss reduces IL-6 in plasma [107]. IL-6 is secreted into plasma (unlike TNF-α) and therefore could increase insulin resistance systemically [105]. Resistin is expressed during differentiation and secreted from 3T3-L1 cells, it appears to inhibit adipogenesis and may function as a negative regulator [108], however its role is not fully characterised and it may simply be a bystander product [109]. Other adipokines include angiotensin, acylation stimulation protein, plasminogen activator type-1 and TGF-β. Adiponectin is discussed in chapter 5.

1.3.3 Adipocyte differentiation and transcriptional control

Adipose tissue forms in loose connective tissue that is abundant subcutaneously and tends to cluster, suggesting autocrine or paracrine factors are acting. Human preadipocytes are harvested from stromal vascular sites and the close physical association of preadipocytes and endothelial cells is extended by them sharing surface markers, suggesting a possible common lineage [110]. It is likely they represent stem cells that have recently diverged, cells with pluripotent capacity to differentiate into cartilage, muscle and fat have been identified for many years [111]. The immortalisation of murine preadipocytes (3T3-L1 and 3T3-F442A) [112] committed to adipocyte differentiation expanded infinitely the experimental possibilities due to a defined differentiation cocktail of insulin, glucocorticoids and cAMP, which produces adipocytes over 4-6 days. T4 has been shown to aid fetal adipocyte development by inducing IGF-1 and IGF binding proteins [113].

The pathway of preadipocyte differentiation is well described commencing with growth arrest, usually at confluence, when the differentiation cocktail is added. Up to two more rounds of cell division occur (clonal expansion) and finishes with expression of the key adipogenic transcription factors; peroxisome proliferator-activated receptor γ (PPARγ) and CCAAT/enhancer binding protein α (C/EBPα), after which permanent growth arrest is followed by the full mature phenotype. Blockage of DNA binding by the E2F/DP transcription factor correlates with PPARγ expression [114], E2F binding can also be decreased by the retinoblastoma gene [115]. Early morphological changes are loss of the slender fibroblastic appearance with rounding. Early changes in mRNA expression are; increased lipoprotein lipase, transient elevation of C/EBPβ and C/EBPδ, before PPARγ and C/EBPα. Terminal differentiation is characterised by increased gene expression of aP2, Glut 4, malic enzyme, glycerophosphate dehydrogenase, fatty acid synthase and acetyl CoA carboxylase, amongst others [96]. With these proteins comes the lipid laden morphology of mature adipocytes.

Currently the key transcription factors are PPARγ, C/EBP's and adipocyte determination and differentiation factor-1/ sterol regulatory element binding protein-1c (ADD1/SREBP1c). PPARγ2 is the predominant isoform in adipose tissue [116] and like all nuclear hormone receptors are ligand activated. One clinically important set of ligands are the thiazolidinediones (TZD) that bind with moderately high affinity and are proadipogenic and reverse hyperglycaemia [117]. In terms of naturally occurring ligands the list is continually growing and include: 15 deoxy-$\Delta^{12,14}$ prostaglandin J_2 ($15dPGJ_2$)

polyunsaturated fatty acids, but these have low affinity, binding well below that of TZD's [118; 119]. PPARγ activation is so profoundly adipogenic that vector driven expression can lead to myoblasts trans-differentiating to adipocytes [120].

The role of C/EBPs (basic leucine zipper transcription factors) were demonstrated by ectopic expression in 3T3-L1 cells, C/EBPβ alone can induce differentiation while C/EBPδ still requires a differentiation cocktail [121]. C/EBPα expression can similarly induce differentiation and antisense C/EBPα mRNA can reciprocally block adipogenesis [122; 123]. ADD1/SREBP1c is a basic helix-loop-helix transcription factor and binds E-box sequences (CANNTG) and sterol regulatory elements on DNA[124; 125]. It is expressed early in adipogenesis and when over-expressed assists adipogenesis but cannot drive it independently of differentiation cocktails [126]. ADD1/SREBP1c is thought to produce an endogenous ligand of PPARγ [127]. The transcription factors involved with white and brown adipose tissue development seem identical and in keeping with this, short term TZD treatment of CD-1 rats lead to interscapular fat pad proliferation. This is a brown fat depot and no other pads were examined [128].

Numerous other transcription factors are implicated in adipogenesis and some are noteworthy in relation to this thesis. Nuclear factor of activated T cells (NFAT) is a transcription factor that promotes aP2 expression. Cyclosporine, used by some in the treatment Graves' ophthalmopathy [129], inhibits nuclear translocation of NFAT proteins to reduce adipogenesis but has no effect on differentiated cells [130]. Cyclic AMP response element binding protein (CREB) activation alone can induce adipogenesis and conversely blocking CREB can induce adipocyte apoptosis, this is discussed further in chapter 3 [131; 132]. Steroid receptor coactivators (SRC-1) have an important role in CREB induced transcription during in vitro adipogenesis [133; 134]. PPARγ co-activator (PGC) is found solely in brown fat, while lacking the histone acetyltransferase required to manipulate chromatin, it probably interacts with CREB that does [135]. Given that brown and white fat share essentially the transcription processes in differentiation it is striking they have such opposite functions. PGC must in part be responsible for the mitochondrial biogenesis and uncoupling protein (UCP)-1 expression that defines the thermogenic energy consuming brown fat.

Adipocyte differentiation and expression of TSHR is further discussed in chapter 3 and 5.

2 The thyroid, orbit and ectopic thymus in TSHR immunized BALB\c; A Graves' masquerade

2.1 Introduction

2.1.1 An early history of modelled Graves' ophthalmopathy

For an accurate model of Graves' disease one would want to demonstrate as many of the following as possible; thyrotoxicosis, thyroiditis, goitre, extrathyroidal involvement, an immune background of thyrotropin receptor stimulating antibodies (TSAB), generalised weight loss and tachycardia. The exploration of such models was underway in the early part of the last century (reviewed in [136]). They attempted to raise circulating thyrotropin (TSH) with pituitary extracts or methyl cyanide, to induce proptosis in ducks and rabbits [137; 138]. The proptosis could be reversed by cervical ganglion sympathectomy, suggesting the action was via the lid retractor, Mullers muscle. While lid lag is present in Graves', a more convincing feature is an increase in the volume of orbital contents that was demonstrated in guinea pigs following treatment with pituitary extracts in 1936 [139]. Weight loss, thyroid hypertrophy and mild proptosis were present but the addition of thyroidectomy to the protocol resulted in severe proptosis. The orbital volume increased by 40%, mainly in the fat and lacrimal gland, in which lymphocytes, oedema and mucopolysaccharides were present. Additional work showed degeneration and oedema that was specific to extraocular muscles [140]. A non-invasive attempt to measure proptosis in guinea pigs described a "camera lucida" that involved using a bright light to startle a dark adapted subject, while transfixed and motionless the proptosis could be measured [141]. The apparatus was not widely used probably due to the high sympathetic drive the startle induced. With hindsight these models were potentially liberating a range of thyroidal antigens during the thyroidectomy, followed by over stimulating extrathyroidal thyrotropin receptors with increasing TSH in animals spiraling into hypothyroidism.

More recent models have not all had an obvious antigen and have been driven by TSH alone. A factor in pituitary extracts given to goldfish produces proptosis, exophthalmic producing factor (EPS), this was initially thought to be TSH that had both thyrotropic and exophthalmic properties [142]. EPS was further defined as being a tryptic fragment of the nearly intact β subunit and the amino terminus of the α subunit of TSH [143]. Both this

fragment and TSH caused a doubling in glycosaminoglycan content of the Harderian gland in guinea pigs with induced proptosis [144]. EPS effects were dissociated from TSH in another guinea pig model where proptosis induced by thyroidectomy and augmented by radio-iodine or PTU was then treated with thyroxine replacement to remove any variation due to hypothyroidism [145]. This reduced TSH levels but EPS and proptosis were unaltered suggesting the two were separate effects. Further evidence was that treatment with TRH could raise circulating TSH but did not induce proptosis or raise EPS. In these models antigen liberation is required in addition to EPS/TSH activity to induce proptosis.

None of these models have survived in use into this century unlike protocols that induce thyroiditis using thyroglobulin (Tg) or Tg sensitized clones [146; 147; 148; 149]. Similarly the EPS bioassay has fallen from use and was reported to have low specificity that varies seasonally with normal serum able to induce proptosis in the atlantic minow (*fundus heteroclitus*) [150].

2.1.2 Thyrotropin Receptor in modelled Graves' disease

Until TSHR was formally cloned, the low level expression on thyroid membranes and extracts prevented its use as an antigen to attempt induction of thyroiditis as had been done for Tg. TSHR peptides have been reported to induce TSAB, TBAB, TBII, raised thyroxine, but without thyroiditis in mice, rabbits and chickens [151; 152; 153; 154]. Five different H-2 mouse strains were immunized with human TSHR that had been detergent extracted and affinity purified from a human thyroid cell line [155]. MHC class II expressing, H-2^s and H-2^q mice developed antibodies to the receptor, had transient rises in T3 and a mild lymphocytic thyroid infiltrate.

To examine the response to a more complete range of TSHR epitopes, the extracellular domain (ECD) was expressed as a bacterial fusion protein with maltose binding protein (MBP) and initially showed TBII and TBAB activity with lowering of serum thyroxine in H-2^d BALB/c mice [156]. An "atypical lymphoblastoid infiltration with follicular destruction" was present in some mice and further work confirmed the model phenotype as comprising; TBII, TBAB, lowered thyroxine, lymphocytic infiltration in 50% males and 100% females [157; 158]. Using the same protocol in C57 (H-2^b) or CBA (H-2^k) does not induce thyroiditis but TSHR antibodies are generated [159]. In the same experiment, NOD

(H-2^{g}) that develop a spontaneous thyroiditis in approximately 5%, had an increased incidence of destructive thyroiditis, with immunoreactivity for IFNγ and few B-cells in contrast with the BALB/c in which IL-4 and IL-10 and significant numbers of B-cells were present. From this profile it was assumed BALB/c have a Th2 based thyroiditis while NOD have a Th1 process. Interestingly the closely related NOD (H-2^{h4}) develop a spontaneous thyroiditis that increases with raised dietary iodine [160].

The human ECD produced by baculovirus was found to raise thyroxine levels in BALB/c while murine ECD expressed in insect cells behaved similarly to ECD/MBP vaccination, but significantly, none have induced thyroiditis [161; 162]. In common with these methods attempting to produce correctly folded and glycosylated TSHR, eukaryotic expression vectors encoding the TSHR have been used. Plasmids are efficiently taken up into myocytes in 50μl volumes due to hydrostatic pressure within the anterior tibial muscle sheath [163]. Myocytes then transfer the antigen to antigen presenting cells [164]. The pcDNA3 vector was cloned with the cDNA of human TSHR (pcDNA3-TSHR) downstream from its CMV promoter and used to immunize BALB/c [165]. In general they responded similarly to those receiving ECD/MBP, but when applied to NMRI mice; 30% had TBAB and reduced thyroxine while 13% had TSAB, raised T3 and T4, suppressed TSH and thyroid and orbital changes (described in 2.1.3) [166]. Confirmation of these models have not been forthcoming in particular the reproducibility of the thyroiditis [167; 168; 169; 170].

Elsewhere success in developing a model with TSAB, hyperthyroidism and thyroid hypertrophy utilizing fibroblasts coexpressing compatible MHC II and human TSHR has been achieved in AKR/N (H-2^{k}) mice [171]. These findings have been confirmed by others and at no time has a thyroidal lymphocytic infiltrate been detected [169; 172]. However when the technique was applied to Chinese hamsters some did develop the additional feature of focal lymphocytic infiltration [173]. The efficiency of TSHR inducing hyperthyroid TSAB models has significantly increased with the use of high transgene expressing adenovirus alone or infecting dendritic cells and lymphoblastoid B-cells known to coexpress MHC II and B-7 [170; 174; 175]. Infrequently the latter induces a focal thyroiditis and necrosis in older mice.

2.1.3 Thyrotropin Receptor in modelled Graves' ophthalmopathy

Relatively few models of orbitopathy or other extrathyroidal involvement have been developed. In contrast, evidence of human orbital expression of TSHR has gathered implicating it as a prime contender for the role of shared thyroid and orbital antigen [176; 177; 178; 179; 180; 181]. The transfer of TSHR primed T-cells to BALB/c results in changes to 68% of the mice orbits described as; "accumulation of adipose tissue, oedema caused by periodic acid Schiff positive material, dissociation of muscle fibers, the presence of TSHR immunoreactivity and infiltration by lymphocytes and mast cells" would seem to mimic Graves' ophthalmopathy [182]. Similar changes were present in NMRI mice immunized with pcDNA3-TSHR [166]. Oedema, muscle separation and mast cell infiltration were also reported in the orbits of BALB/c and CD-1 mice immunized using cDNA for TSHR and G2s with or without cDNA for IL-4 or IL-12 [183]. The reproducible models, where mice have TSAB and hyperplastic thyroids, have normal ocular muscles [170; 175]. Gross macroscopic changes such as proptosis or muscle hypertrophy have not been reported in any of the models and confirmation of the ophthalmopathy models has not been forthcoming from other laboratories. In fact the only ophthalmopathy model to develop oedema, proptosis, ocular restriction, lymphocytic infiltration and GAG accumulation was generated in cats by ligating orbital veins, the changes are noteworthy but in need of association to an autoimmune trigger [184]. Cats have an orbital venous system much closer in structure to humans than rats and mice.

2.1.4 Aims: Confirmation and further examination of pcDNA-TSHR and ECD/MBP induced Graves' ophthalmopathy model

The only TSHR induced model of Graves' disease reported to have a high incidence of thyroiditis with ophthalmopathy is that described by the Belgian group using TSHR primed splenocytes transferred to naïve recipients. Initially our investigation aimed to confirm this model, examine if the model follows a Rundle's-like curve and if frequency of disease differs between male and female BALBc from local and imported colonies. Inability to raise thyroiditis or ophthalmopathy by vaccination with TSHR either in protein or DNA plasmid form redirected us to investigate possible effects on the induced immune response resulting from regional dietary variations. We have been unable to replicate the existing model but demonstrate some interesting findings and propose areas of improvement in modelling Graves' ophthalmopathy.

2.2 Materials and Methods

2.2.1 Production of the extracellular domain of thyrotropin receptor in E. coli

To produce sufficient TSHR protein for use in immunization and ELISA, expression and purification from a bacterial system was used. Frozen glycerol stocks of E. coli (TOPP 1 strain, protein fusion and purification system, New England Biolabs) having previously been transformed with the vector pMAL-cR1-ECD containing the 1.2kb EcoR1-XbaI cDNA fragment of the human TSHR ECD (amino acids 20-414) were prepared for overnight culture [156]. Ten millilitres of Luria broth (LB appendix (app) A), containing ampicillin (100μg/ml), was inoculated with transformed cells and incubated overnight in an orbital incubator (S150, Stuart Scientific) at 37 C and 220rpm. The following morning the overnight culture (now cloudy in contrast with media not inoculated) was added to 1 litre of LB rich broth (app. A), containing ampicillin (100μg/ml). This culture was returned to the orbital incubator at 30 C until the optical density (600nm) reached 0.3. Fusion protein production was then induced with 50μM isopropylthiogalactoside (IPTG) and the culture continued for 3-4 hours. IPTG inhibits the repressor activity of the lacI gene on the tac promoter that initiates translation of the fusion protein. Cells were then harvested by centrifugation (Mistral 3000, MSE) at 4000g for 10 minutes and the supernatants discarded and the pellet resuspended in 10mls of lysis buffer (app. A). Protease inhibitors were then added, aprotinin (10μg/ml) and phenylmethylsulfonyl fluoride (PMSF) (1μg/ml). The pellets were stored on ice overnight at -20 C then subjected to four freeze thaw cycles followed by 3 pulses of sonication for 1 minute each. The lysed bacteria were then centrifuged (Rotina, Hettich) at 9000g for 20 minutes and the supernatants decanted and saved on ice.

2.2.2 Purification of ECD/MBP protein

Purification relies on the affinity of the maltose element of the fusion protein for amylose. Fifteen millilitres of pre-swelled amylose (New England Biolabs) was inserted into a 50ml sterile syringe with glass wool in the tip and equilibrated with column buffer (app. A). Following washing with 2 volumes of column buffer the column was transferred to a cold room. The crude protein lysate was diluted 1:2-5 with column buffer and applied to the

column, the flow through was reapplied to the column to maximize yield. Unbound protein was then washed off by running 7-8 volumes of column buffer through it. Elution buffer (column buffer with maltose and β-mercaptoethanol (both 10mM)) was applied to the column and 16 x 1.5ml aliquots were collected and stored at -20 C.

2.2.3 Protein estimation by trichloroacetic acid precipitation

A bovine serum albumin (BSA) standard was made by dissolving 10 mg of BSA in 10ml of elution buffer in a 37 C water bath. In a clear, 96-well plate, triplicates of 0, 5, 10, 25 and 50μl of the BSA standard were placed, to which 50, 45, 40, 25 and 0μl of elution buffer were added respectively to give a total well volume of 50μl in each. Duplicates of the eluted protein aliquots (sample (25μl) plus elution buffer (25μl)) were similarly added to the plate. 50μl of 60% trichloroacetic acid was then added to each well and precipitation developed over 30 minutes at room temperature. A fluffy white precipitate developed. The optical density was read on a plate reader at 570nm and sample protein concentration calculated after a standard curve was constructed from the BSA standards.

2.2.4 Detection of ECD/MBP protein by SDS PAGE

An SDS gel was run to examine the induced ECD/MBP production. A gel apparatus (Mini protean, Bio-Rad) was prepared with a 12% resolving and a 4% stacking gel. 25-30μg samples of protein and 10μg of protein markers (broad range 175-6 kDa, New England Biolabs) were denatured at 95 C for 5 minutes in Laemlli buffer and then loaded onto the gel. Electrophoresis was carried out in running buffer for 45 minutes at 200V (PS500X power pack, Hoeffer Scientific), followed by Coomassie staining for 30 minutes gently on an orbital mixer (Denley). Coomassie destaining solution was used to clear the gel after 3-4 changes every 20-30 minutes, gel drying solution was used for 30-40 minutes before dehydrating the gel onto blotting paper under a heated flat bed vacuum apparatus. (Gels and solutions see app. A).

2.2.5 Confirmation of ECD/MBP protein by Western blot

Western blotting was performed on affinity purified ECD/MBP to confirm the presence of TSHR. A 12% SDS gel was run in parallel as above without staining with Coomassie blue. The gel was transferred to blocking buffer for 15 minutes while an equal sized piece of PVDF membrane (Hybond-P, Amersham) was soaked in methanol briefly and then placed in blocking buffer for 10 minutes. The blotting apparatus (Mini protean, 3 cell, Bio-Rad) was loaded, according to instructions (app. A), with the gel and PVDF membrane, transfer was carried out for 1 hour at 350mA. The pink pyronin y tracking dye, confirmed protein transfer to the membrane. The membrane was equilibrated briefly in TBS-T buffer (app.A) before placing in blocking buffer for 1 hour with shaking. The membrane was then rinsed twice for 2 minutes in TBS-T and incubated with the primary antibody, p60 (1:500), for 1 hour with shaking. p60 is a polyclonal rabbit antibody previously raised against extracellular TSHR residues 350-369 (AHYYVFFEEQENEIIGFGQE) coded for by exon 10 of the human TSHR gene [156]. Washes of 1 x 15 minutes and 2 x 5 minutes were performed before the secondary antibody incubation with anti-rabbit polyclonal HRP IgG, diluted 1:5000, for one hour (Amersham Bioscience). Washes were repeated followed by detection using ECLplus reagent (Amersham Bioscience) that utilizes HRP breakdown of luminol to generate a sustained chemifluoresence at 440nm that was detected on Hyperfilm (Amersham).

2.2.6 Maxiprep purification of pcDNA3-TSHR

For each mouse the full course of DNA immunizations required 400μg of pcDNA3-TSHR. Therefore to obtain milligram quantities of plasmid a maxiprep plasmid purification kit (Qiagen) was used. It is based on alkaline lysis of bacteria and subsequent binding of DNA to resin on a column under low pH/salt conditions. A medium salt wash removed proteins and RNA, followed by a high salt elution of the plasmid DNA which is finally desalted and precipitated in isopropanol.

From glycerol stocks of E. coli transformed with pcDNA3-TSHR, an overnight culture was prepared in 250mls LB (app. A) containing ampicillin (100μg/ml) and incubated in an orbital incubator at 37 C, two or four flasks were prepared. The next morning the cell pellets were centrifuged at 2500g for 15 minutes at 4 C, supernatant removed and the

pellet vortexed in 10mls of resuspension buffer (all buffers app. A). After adding 10 mls of lysis buffer the mixture was inverted 6 times and left to stand for 5 minutes before adding 10mls of chilled neutralization buffer and inverting the mixture a further 6 times. The lysate was transferred to a filter cartridge and incubated for 10 minutes after which time a thick white protein and genomic DNA precipitate formed at the top of the cartridge. Meanwhile the anion exchange resin containing column was washed with 10mls of equilibration buffer and once drained completely, was filled with filtered lysate from the cartridge. The resin column was then washed twice with 30mls of wash buffer and eluted with 15mls of elution buffer. The DNA was precipitated by adding 10.5mls of isopropanol in a polypropylene tube, mixed and centrifuged (Rotina, Hettich) at 15000g for 30 minutes at 4 C. The supernatant was carefully removed and the pellet desalted with 5mls of 70% ethanol before further centrifugation at 15000g for 10 minutes and removal of the supernatant. The DNA pellet was air dried for 5 minutes and redissolved in 200µl of buffer TE (Tris/EDTA, app.A).

2.2.7 Measurement of pcDNA3-TSHR by spectrophotometry

An estimate of the quality and quantity of pcDNA3-TSHR was made by determining the absorbance ratios at 260 and 280nm in a spectrophotometer (Genequant pro, Biochrom ltd). For optical density readings to be reproducible, A_{260} values needed to be between 0.1-1.0, this required dilution of the resuspended DNA from 1:10-50 in buffer TE. The A_{260}/A_{280} ratios ranged between 1.7 and 2.0 indicating good quality DNA.

2.2.8 Restriction digest and agarose gel electrophoresis of pcDNA3-TSHR

To confirm the presence of the TSHR insert within the pcDNA3-TSHR purified by maxiprep a restriction digest was performed. Enzyme restriction using the single cloning sites BamH1 (cuts GGATCC) and Xho1 (cuts CTCGAG) linearized the plasmid and excised the 2.3kb TSHR insert.

The restriction was carried out on 0.5-1µg of DNA, using 5 units of Xho1 and BamH1 in buffer K (Amersham Bioscience) made up to a 20µl volume with distilled water and incubated for 1 hour at 37 C on a hot plate (QBT2, Grant Instruments). A 2% agarose gel

was prepared by heating 0.8g of agarose in 40mls of TAE buffer (app. A) in a microwave (950W, Proline) until melted. This was allowed to cool before adding 0.5μg/ml ethidium bromide and then poured onto a 9cm gel tray (Bio-Rad), well combs inserted and allowed to set. Then, 2μl of restriction products were added to 1μl of 10 x gel loading buffer (Promega) and mixed with 7μl water. These were loaded into the wells of the gel submerged under TAE in a horizontal electrophoresis cell (Mini sub cell GT, Bio-Rad). In addition, a 1kb ladder (Promega) and unrestricted plasmid DNA were loaded alongside and run at 80 volts for 1hour. Once completed, the electrophoretically separated DNA stained with ethidium bromide was visualized under ultraviolet light and recorded digitally (Alpha imager, Alpha Innotech).

2.2.9 Home office licensing and GM approval

In accordance with the Animals (Scientific Procedures) Act 1986, project and personal license approval was required before commencing procedures on live mice. The project license (30/2304) states all procedures are carried under general anaesthesia and termination by approved schedule 1 methods. The immunizations, blood sampling and splenocyte transfer are classified as mild in grading the overall severity of the experiments. The personal license was obtained after completing the accredited course within the Biomedical Services Department, UWCM, for rodents, modules 1 to 4 inclusive.

2.2.10 ECD/MBP and pcDNA3-TSHR vaccination

There was a high incidence of induced thyroiditis reported in naïve recipients of splenocytes primed against TSHR by the two step in vivo and in vitro protocol [185]. The splenocytes were stored and used as required.

In vivo priming was carried out on 6 week old female BALB/c by Jico (Iffa Credo, France). They were immunized according to two schedules under halothane anaesthesia. Anaesthesia was tolerated well overall but four out of the 94 mice were unable to be resuscitated following anaesthetic (female GI 1B, male BECD 0, female FNP 2R and male FECD 2B). Immunizations were carried out on day 0 (with pre-immune blood sampling) and at three, six and nine weeks. One group of six mice received 100μg of pcDNA3-TSHR

in 25% sucrose shared equally between both anterior tibialis muscles [165]. Another group of four mice had an initial 100μg of ECD/MBP intra-peritoneally (ip), in a 200μl volume of 0.9% saline with adjuvant, 0.1% aluminium oxide, 0.4% magnesium hydroxide (Maalox, Rhone-Poulenc Rorer) and 50μl of acellular bordetella pertussis vaccine (Wyeth) [156]. Thereafter immunizations used 50μg of ECD/MBP with adjuvant. Daily checks were made on mice after immunization to check vaccination sites, mobility, activity and tail bleeds. Generally DNA vaccination provoked little or no interruption to daily living with a full recovery by the following day. This contrasted with ECD/MBP which reduced activity and produced coat "staring" which settled 2-4 days after immunization. Mice were killed in a carbon dioxide chamber after 14 weeks, their serum stored and spleens, thyroids and orbital contents removed. Dissection of thyroids and orbits was initially performed using an operating microscope but once familiarized with the anatomy was performed without, apart from the dissection of ocular muscles from the globe.

Mice immunized with pcDNA3-TSHR were referred to as GI and those immunized with ECD/MBP as ECD. Individual mice were identified by rings of indelible marker around their tails that were redrawn every two weeks.

[NOTE: Pre-immune sampling of blood from young mice yielded 10-30μl volumes which once clotted and spun results in very small serum volumes 5-10μl. Pooling serum from the groups was the only way sufficient volumes were available for all the assays but is not ideal as it removes initial variations between individuals.]

2.2.11 Splenocyte storage and gradient separation

Spleens removed from immunized and control animals were transferred to RPMI (app. A), immediately mechanically disrupted using a blunt forceps and artery clips to empty the splenic capsule. The splenocytes were washed by centrifuging (Centaur 2, MSE) at 400g for 5 minutes, washed in RPMI, repeat centrifuged and resuspended in 1ml of freezing mix (fetal calf serum (FCS) with 10% dimethylsulfoxide (DMSO)). Splenocytes were stored in a 1.5ml cryovial, slow cooled to -80 C overnight before transferring to liquid nitrogen. Forty-eight hours prior to transfer, the frozen aliquots were rapidly thawed in a 37 C water bath, washed in 20mls of RPMI for 20 minutes to remove the DMSO and centrifuged at 400g for 5 minutes. Splenocytes were resuspended in 3mls of RPMI and layered onto an

equal volume of histopaque (1077, Sigma) gradient equilibrated to room temperature in a 15ml falcon tube and centrifuged (Mistral 3000, MSE) 400g for 30 minutes at room temperature. The upper aqueous layer was removed before aspirating the opaque interface containing the splenocytes which was transferred to a new tube containing 10mls of RPMI and centrifuged at 250g for 10 minutes. The supernatant was discarded and this wash step was repeated to remove histopaque.

2.2.12 Transfer and in vitro priming of TSHR primed T-cells

By transferring the splenocytes we aimed to determine the incidence of disease induced in male versus female mice either imported from the same colony as used in the previously described model or the local colony. In the absence of thyroiditis, spleen cells were arbitrarily selected from the animals with the highest TSAB activity to use in the transfer.

Following washing to remove histopaque, splenocytes were resuspended and cultured in RPMI 1640 supplemented with 10% FCS, β-mercaptoethanol and 20μg/ml ECD/MBP for 48 hours at 37 C (5% CO2, Sanyo incubator). Naïve 9-week-old mice were immunized via the tail veins, each with 5 x 10^5 splenocytes in 100μl phosphate buffered saline (PBS, app. A). In total, 36 BALB/c by J (Iffa Credo, France) were immunized, 7 male and female mice each received ECD/MBP or pcDNA3-TSHR primed cells and 4 male and female mice with non-primed cells. 28 BALB/c mice from the local colony were similarly immunized, 5 male and female with TSHR protein or DNA primed cells and 4 male and female mice with non-primed cells (Table 2-1). The non primed splenocytes were from 2 male and female, 9 week BALB/c by J, whose sera and thyroids were included in the control group. Mice were killed at 10 weeks, excluding 6 male and female BALB/c by J's that were re-immunized at 15 weeks with 5 x 10^6 ECD/MBP or pcDNA3-TSHR primed cells. These mice were killed 12 weeks later.

Mice from the local colony were given the prefix "B" and those from the French colony "F". This was suffixed by "ECD" for those receiving ECD/MBP primed cells and "GI" for those with pcDNA3-TSHR primed cells.

Table 2-1 Summary of T-cell transfer

Method of T-cell preparation	French BALB/c x J		Local BALB/c	
	Female	Male	Female	Male
pcDNA3-TSHR primed	7	7	5	5
ECD/MBP primed	7	7	5	5
Non primed	4	4	4	4

2.2.13 Environmental modification of Graves' ophthalmopathy model

The environment in which experimental models are housed can alter the induced disease. We attempted, as closely as possible, to reproduce the housing of the colony that developed disease in Belgium.

A second group of twenty imported BALB/c by J female mice were divided into two groups of ten. On arrival they were all fed standard feed and were established on this for 3 weeks. The two groups where then immunized (as above in 2.2.10) half with pcDNA3-TSHR and half with ECD/MBP with a modified adjuvant replacing acellular bordetella pertussis vaccine (now unavailable in monovalent form) with 0.2μg Pertussis toxin (Sigma). At immunization the two groups were subdivided; half continued standard local water, feed (Rat and Mouse (RM) No1 Maintenance, SDS) and bedding, the other had modifications of imported water, bedding and feed (RN-01-20K12, Carfil Nutrients) as used by IRIBHN, Brussels [182] (summarised in Table 2-2). After a total of four immunizations the mice were sacrificed at 14 weeks.

As before, mice were labeled as either "GI" or "ECD" depending on the vaccination method. With environment modifications the prefix "B" was used to denote Belgian environment modification and "L" for local conditions.

Table 2-2 Summary of second immunization

	French female BALB/c x J	
Immunization	pcDNA3-TSHR	ECD/MBP
Local conditions	5	5
Environment modified	5	5

2.2.14 ELISA evaluation of circulating anti-ECD/MBP IgG

To study the kinetics of the IgG response to the vaccination in the first immunized group and to test transfer of anti-TSHR activity in the single T-cell transfer group, an ELISA was performed. While ECD/MBP can be cleaved by factor Xa, this gives very small protein yields of pure ECD. The conjugated ECD/MBP in this ELISA did not give a solely TSHR specific target for mice immunized by the ECD/MBP or receiving T-cells primed by this route.

Clear 96-well plates were coated overnight at 4 C with 100µl/well of ECD/MBP (10µg/ml) in coating buffer and washed three times with wash buffer the following morning. Primary incubation was with test sera diluted 1:100 in diluent (100µl volume) and a positive control with anti-P59 [156] (1:1000), in duplicate for two hours at room temperature followed by three washes. Secondary incubation used 100µl of the conjugate, containing anti-mouse IgG horse radish peroxidase (HRP) for the test sera and anti-rabbit IgG HRP for the control, was for 30 minutes at room temperature followed by three washes. Detection used 100µl of substrate and the optical density change was measured in a plate reader at 410nm with positive controls giving readings of greater than two. (Substrate, conjugate and coating, wash and diluent buffers see app. A).

2.2.15 Flow cytometry evaluation of anti-TSHR IgG

To avoid the dual recognition of antigen with the ECD/MBP based ELISA all sera were additionally examined by flow cytometry. Anti-TSHR IgG in sera would bind to Chinese hamster ovary cells (CHO-K1) expressing the TSHR kindly provided by Dr Phil Watson [34]. The full length extracellular domain was anchored by a glycophosphatidylinositol (GPI) link and was highly expressed. Bound cells could then be detected by anti-mouse IgG conjugated to fluorescein isothiocyante (FITC). When the cell suspension was hydrodynamically focused by the cytometer, laser excitation at 488nm of FITC produced a fluorescence output around 530nm that was measured in photomultiplier tubes. The cell population could then be described in relation to its fluorescent characteristics; the greater the number of fluorescent cells, the more anti-TSHR binding.

Eighty to ninety percent confluent CHO-K1-GPI cells were detached with 5mM EGTA/EDTA in PBS, washed three times with 0.1% bovine serum albumen (BSA) in PBS

and then resuspended in PBS/BSA 0.1% at 2 x 10^6 cells/ml. Two microlitres of mouse serum was added to 100µl aliquots (2 x 10^5 cells) of the cell suspension and incubated for 1hr at room temperature. Cells were then washed in the same buffer three times before incubating with FITC conjugated $F(ab^1)_2$ fragment of goat anti-mouse immunoglobulins (DAKO, diluted 1:16) for 30 minutes at 4 C in the dark. Following three final washes, cells were counterstained with propidium iodide to allow gating out of damaged cells. FITC fluorescence from 5000 cells incubated with test sera was measured by a FACScan flow cytometer (Becton Dickinson) and compared to pre-immune sera.

Statistically analyzing fluorescence data from photomultiplier tubes has inherent flaws due to the non linear output. In representing data there were also compromises, reporting fluorescence geometric means did not allow experiments to be compared if different machines or instrument settings were used, as was the case. In an attempt to normalize between experiments, the shifts on histograms were examined using Kolmogorov Smirnov (KS) statistics (Cellquest Pro software, Becton Dickinson). Cumulative FITC fluorescence curves were automatically plotted with test sera vs pre-immune and a 'D' value is calculated indicating a level of spread. The range of D values of non-primed recipients was initially used to calculate the 97.5th centile, values lying above this were considered positive for anti-TSHR IgG. However, some non-primed recipients developed high D values and when considered alongside the histogram plots it became apparent that a descriptive scale can be applied whereby D values below 0.3 are negative (-), borderline (0.3-0.4(+/-)) and positive (>0.4 (+)).

2.2.16 Measurement of TSHR binding inhibiting immunoglobulins

TSH-binding inhibiting immunoglobulin (TBII) activity was measured by examining the binding of TSH to GPI cells expressing TSHR. Anti-TSHR antibodies in test sera competed with radio-labeled TSH binding of TSHR and any reduced radioactivity of solubilised cells was measured to give an index TSH binding inhibition (modified from [186]). TSHR expressing JPO9 cells were previously used [157] but in preliminary experiments GPI cells were found to have higher binding and sensitivity.

GPI cells were maintained in Hams F12 complete medium (app. A) until 70-90% confluent. On day 1 they were trypsinised, plated in 96-well plates at 2 x 10^4 cells/well and

cultured overnight. Following aspiration of the medium, working buffer (HBSS salt free, app. A) was used to rinse the cells twice. Working buffer was added to I^{125} labeled bovine TSH tracer (kindly provided by BRAHMS Diagnostica, Berlin, Germany) in equal volumes and 100µl aliquots added to 3 µl of serum (triplicates). Tracer was handled in a designated radioactive containment area. In addition to test and pre-immune sera, aliquots were made for total counts and non specific binding (NSB), by adding 100mU of bovine TSH). Following a three-hour incubation at room temperature the cells were washed twice in ice-cold buffer, lysed with 100µl 1N NaOH (30mins, 4°C), transferred to counting tubes and radioactivity measured in a gamma counter (Cobra II auto gamma, Pachard). Results were expressed as a percentage of the counts per minute (cpm) bound by the test sera relative to the pre-immune value of 100% tracer binding after subtracting the NSB cpm. The TBII indices were then plotted against 97th and 3rd centiles constructed from individual non-primed (transfer group) or pre-immune (immunized groups 1 and 2) sera.

$$\text{TBII} = \frac{\text{test sera (CPM)}}{\text{Pre-immune sera (CPM)}} \times 100$$

2.2.17 Measurements of TSHR stimulating activity

TSHR stimulating activity (TSAB) can be demonstrated on non-thyroid cells such as Chinese hamster ovary (CHO) cells expressing recombinant human TSHR by measuring increases in cAMP following receptor binding [187]. TSAB was assayed using LULU* cells expressing both hTSHR and cAMP- luciferase constructs [188] using a three day protocol. Sera containing either TSAB or TSH would stimulate cAMP accumulation via TSHR which in turn increased plasmid luciferase expression. When the cells were lysed, the luciferase acted on luciferase substrate to generate light output that was recorded in a luminometer.

On day one pre-confluent LULU* cells maintained in Hams F12 complete were trypsinised and plated in white opaque 96-well plates (Costar) at 2 x 10^4 cells/well. On day two, cells were switched to charcoal stripped Hams F12 (app. A), cultured overnight and finally on day three, cells were washed with working buffer (Hams F12 serum free medium, app. A). In triplicate, 5µl of test serum was added to 50µl of working buffer and incubated for 4 hrs at 37 C. A positive control of bovine TSH at 0.1, 1 and 10mU in 50µl working buffer was used. Following washing twice in 200µl of normal saline, the plates

were air-dried and either stored at -20 C or analyzed immediately. Lysis buffer x 5 (Promega) was thawed from -20 C, diluted 1:5 with distilled water and 50µl was added to each test well to lyse the cells while shaking (Microshaker, Camlab) for 20 minutes. Meanwhile, 1 bottle of luciferase assay buffer and luciferase assay reagent (Promega) were mixed to form the luciferase assay substrate. This was kept in the dark while equilibrated to room temperature and when ready to use was primed into the injector of the luminometer (Tropix Microplate luminometer, Applied Biosystems). The management of dispensing substrate and reading light output from test wells was under the control of proprietary software (Tropix Winglow, Applied Biosystems). The output of relative light units (RLU) from test sera was compared to pre-immune sera to give a stimulation index (SI). Test sera were considered positive when greater than the 97th centile of the non primed recipients this was calculated as SI>1.8.

$$\text{TSAB SI} = \frac{\text{Test sera RLU}}{\text{Pre-immune sera RLU}}$$

2.2.18 Measurement of serum thyroxine

Total serum free T4 was measured using a competitive radioimmunoassay (RIA). This commercial assay (Amerlex) relies on the competition between T4 in the test sera and labeled (I^{125}) T4 for sheep anti-T4 antibody bound to magnetizable particles. T4 binding to thyroxine binding globulin is prevented by the reaction buffer. Magnetic separation of the particles removes unbound tracer and the amount of remaining tracer is inversely proportional to the T4 in the sample which is compared to a standard curve.

The assay was carried out in areas designated for the use, monitoring and disposal of radioactive materials. Duplicate 10µl volumes of standards, NSB and sera were placed in tubes. 100µl of antibody suspension was added, the samples vortexed, covered and incubated at room temperature for 45 minutes. Magnetic separation was carried out for 15 minutes, then, while still attached to the separator, the tubes were inverted and blotted leaving a dry rim of particles at the bottom of the tube. The samples were counted in an automated counter (Cobra II auto gamma, Pachard) in which standard curves were generated by a logit-log plot giving results in nmol/l. A correction factor was applied (T4 nmol/l x 0.0777) to report T4 in µg/dl.

2.2.19 Splenocyte stimulation using TSHR or PMA/ionomycin

Splenocytes were used in the adoptive transfer of modeled Graves' ophthalmopathy. We examined the splenocytes primed with pcDNA3-TSHR and ECD/MBP to assess if environmental modification altered the cytokine production and compared them to splenocytes from two pcDNA3-TSHR mice immunized in Brussels (generously provided by Dr Sabine Costagliola, IRIHBN) and non-immunized splenocytes.

Splenocytes were thawed, washed twice in 10mls RPMI 1640, centrifuged (400G, 5 minutes), fluid aspirated, the pellet resuspended in 5mls RF10 medium (app. A) and cells allowed to recover overnight in an incubator (37 C, 5% CO_2). Splenocytes were counted the following day using trypan blue exclusion to determine viable cell proportions (greater than 85%), centrifuged (400G, 5 minutes), and resuspended at 2 x 10^6 cells/ml in RF10.

PMA/ionomycin stimulation

Activation of splenocytes was carried out using a polyclonal stimulus with phorbol 12-myristate, 13-acetate (PMA) and ionomycin (both Sigma). These agents induce cytokine production through protein kinase C and calcium ion influx [189]. Monensin (Sigma) was added to block cytokine secretion for intracellular cytokine staining (ICCS). Even after monensin, ICCS can be relatively insensitive and therefore we examined in parallel the accumulation of cytokines within the supernatant while the splenocytes were undergoing stimulation. High levels of monensin may also inhibit cytokine production as well as secretion and it was omitted from assays for supernatant cytokine measurement.

Four aliquots of 0.5ml splenocyte suspension (1 x 10^6 cells) were taken for each mouse. Two aliquots were used for ICCS and two used for supernatant estimation of cytokine production in parallel experiments. For ICCS, the control sample was incubated for 4 hours at 37 C with monensin (7μM) and then prepared for flow cytometry (2.2.20). The ICCS stimulated sample was incubated with PMA (25ng/ml), ionomycin (1μg/ml) and monensin (7μM), both for 4 hours. For supernatant cytokine measurements the cells were incubated as for ICCS but without monensin, centrifuged (400g, 5minutes), supernatants aspirated and stored at -80 C until assayed for cytokines (2.2.21).

TSHR stimulation

To compare the cytokine production induced by the polyclonal stimulus to a specific stimulus we used two sources of TSHR. Firstly, ECD/MBP was chosen because it was used in both in vitro and in vivo priming steps in the adoptive transfer model. Secondly, given that T-cells recognize short peptide fragments of antigens we also used synthetic peptides of the TSHR (listed app. A, kindly provided by Dr P Watson).

96-well microplates were loaded with 250µl of splenocyte suspension (5 x 10^5 cells) in RF10. Triplicates for stimulation with ECD/MBP and TSHR peptides and control un-stimulated conditions were plated. ECD/MBP was used at 10µg/ml and TSHR peptides (previously dissolved in DMSO) were used at 5µg/ml. After incubation at 37 C for 6 days, supernatants were pooled from the triplicate wells, centrifuged (400g, 5 minutes), supernatants aspirated and stored at -80 C until assayed for cytokines (2.2.21).

2.2.20 Splenocyte cytokine staining for flow cytometry, analysis of CD4, CD8, IL-4 and IFN-γ following PMA/ionomycin stimulation

Following polyclonal stimulation (2.2.19) surface staining of CD4 and CD8 was followed by permeabilisation for ICCS to asses their capacity to be stimulated to produce TH1 (interferon (IFN)-γ) and TH2 (IL-4) cytokines. Characterising the splenocytes used a four colour flow cytometer counting 10^5 events (FACSCaliber, Becton Dickinson).

Following the four hour incubation (2.2.19)10^6 splenocytes were washed in PBS/BSA 0.5%, centrifuged (400G, 5 minutes) and resuspended in 1 ml PBS/BSA. Surface antigen detection used peridinin chlorophyll-*a* protein (PerCP)-conjugated rat anti-mouse CD4 (L3T4) and allophycocyanin (APC)-conjugated rat anti-mouse CD8a (Ly-2) monoclonal antibodies (Pharmingen). Both antibodies (10µl) were added to each splenocyte suspension, incubated at room temperature in the dark for 30 minutes, washed in 3 ml PBS/BSA and centrifuged. Cells were then fixed and permeabilised using a kit (CPK-200, Cell permeabilisation kit, ImmunologicalsDirect.com). Two drops of solution A (formaldehyde based fixative) was added to the splenocytes, mixed, incubated in the dark for 15 minutes, PBS/BSA washed and centrifuged. Cells in the pellet were then permeabilised with 2 drops of solution B. Simultaneously, 10µl of anti-cytokine

monoclonal antibodies (Pharmingen) were added, r-phycoerythrin (PE)-conjugated rat anti-mouse IL-4 and FITC conjugated rat anti-mouse IFN-γ, and incubated at room temperature in the dark for 30 minutes. 400μl of 2% paraformaldehyde was finally added and after a minimum of 10 minutes either analyzed or kept overnight at 4 C.
Results were plotted on dot plots using WinMDI 2.8 * and regions containing CD4 and CD8 populations were selected. Once gated according to surface markers the percentage of cells expressing IL-4 and IFN-γ from control and stimulated splenocytes was measured using the same arbitrary quadrants for similar samples. The figure recorded was the percentage of cells expressing cytokines in the stimulated sample minus the un-stimulated, differences were examined for significance between groups.

A positive control for PMA/ionomycin stimulation was human peripheral blood mononuclear cells (PBMC) that were thawed and stimulated in parallel to the splenocytes. They were surface stained for anti-human CD4/8 and cytokine staining by anti-human IFN-γ FITC (both Pharmingen).

*(http://publish.uwcm.ac.uk/study/medicine/haematology/cytonetuk/documents/software.htm)

2.2.21 ELISA evaluation of IL-4 and IFN-γ in supernatants from TSHR and PMA/ionomycin stimulated splenocytes

Cytokines secreted from splenocytes stimulated by either polyclonal or specific stimuli were measured by commercial murine IFN-γ and IL-4 ELISA (Duoset, R&D systems). While not specifying the cells producing cytokines, the ELISAs are highly sensitive, capable of detecting pg/ml quantities in the supernatants.

The primary antibodies; rat anti-mouse, IFN-γ and IL-4 were diluted to 4μg/ml in PBS, 100μl/well was added to a 96-well plate (Costar), sealed and left overnight at room temperature. The following day plates were emptied by rapid inversion and washed three times in wash buffer. Blocking buffer was added, 300μl/well, incubated for 1 hour at room temperature and the wash step repeated. Samples were analysed in duplicate and standards in triplicate, 100μl/well, covered and incubated for 2 hours at room temperature. Standards

were prepared using a seven point, two-fold serial dilution in the appropriate reagent diluents, with the high standard for IFN-γ starting at 2000pg/ml and IL-4 at 1000pg/ml. The wash step was repeated and 100µl/well of the detection antibodies (biotinylated goat anti-mouse, IFN-γ (400ng/ml) and IL-4 (200ng/ml)) were added for a further 2 hour incubation followed by a repeat set of washes. The streptavidin-HRP provided in the kit was diluted 1:200, 100µl/well added, incubated for 20 minutes at room temperature away from direct light and the wash steps repeated. Substrate solution was added, 100µl/well, incubated for 20 minutes at room temperature away from direct light, before adding 50µl/well of stop solution. Optical densities were measured at 450nm with wavelength correction set at 570nm. (Reagent diluents, substrate, stop solution, wash and blocking buffers, app. A).

Standard curves were plotted and fitted with trendlines whose equations were used to calculate the concentration of cytokines in pg/ml of sample supernatants. The value recorded is the amount of cytokine present in the stimulated sample minus that of the unstimulated sample.

2.2.22 Thyroid and orbital histology

Thyroids and ocular muscles from the first immunized group were processed for light microscopy with haematoxylin and eosin (H&E) and periodic acid and Schiff's reagent (PAS) staining on paraffin sections. T-cell recipients and the second immunization group had the thyroids separated by dividing the trachea. The thyroids of T-cell recipients were processed for frozen and plastic sections and thyroids and ocular muscles from the second immunization group were all processed for plastic sections.

Paraffin sections

Specimens were fixed in 10% phosphate buffered formalin with 2% acetic acid for a minimum of 48hours. Processing was carried out in an Automated Duplex processor (app. A) and then embedded in paraffin wax using a Blockmaster II embedding machine. Sections were trimmed on a Bright microtome at 10µm, cut at 5µm and floated onto water before placing on a microscope slide and dried overnight in a 37 C oven.

Prior to staining, the sections were placed in a 60 C oven for 20 minutes, deparaffinised with two 5 minute changes of xylene, descending grades of alcohol (100% x 2, 90% and 70%, 2 minutes each), washed in tap water for 5 minutes and then a distilled water rinse. For H&E, sections were stained in Harris's haematoxylin for 5 minutes, washed in running water for 5 minutes, rinsed in distilled water, before 2 minutes staining in 1% eosin. For PAS, sections were treated with 1% periodic acid for 7 minutes, washed in distilled water (3 changes, 1 minute), transferred to Schiff's reagent for 10 minutes, rinsed in distilled water and then counterstained with haematoxylin for 5 minutes. Finally excess stain was washed off in tap water, dehydration was in ascending grades of alcohol (90% wash, 100% x 3 for 2 minutes each) and cleared in xylene (3 changes, 5 minutes). Sections were mounted in Ralmount on a charcoal filter extractor and left to set in an oven overnight at 45 C.

Plastic sections

Specimens were fixed overnight in 0.2% glutaraldehyde, 4% formaldehyde in Sorensons phosphate buffer, transferred to phosphate buffer and stored at 4 C the following day. The specimens were then dehydrated, post-fixed in uranyl acetate and embedded in LR white in the department of medical microscopic sciences (UWCM, app. A). Specimens were then cut from the plastic capsule using a hacksaw and re-orientated. Sections were trimmed with a hacksaw initially, then using a glass knife (knifemaker, LKB 7801) on an ultramicrotome (Ultracut, Reichert Jung), trimmed further and finally cut at 0.3-0.5μm. Series of sections at different levels were dried onto a microscope slide in a 40 C oven for 2 hours or on a hot plate for 10 minutes and stained with toluidine blue (3 minutes), rinsed in tap water, returned to the oven overnight, mounted in DPX and finally dried in an oven.

Frozen sections

Specimens were placed directly into OCT mount on a small piece of cork board and snap frozen in a cooling chamber containing hexane surrounded by solid CO_2 pellets in methylated alcohol. Once frozen through, the block was transferred to a cryo tube and stored in liquid nitrogen. For cutting sections the cork board was frozen to a cryostat chuck before cutting 6μm section that were allowed to dry overnight in a 40 C oven. Local non-primed mice had cryostat sections cut for staining with H&E and toluidine blue to practice

cryostat sectioning but in the absence of thyroiditis in the treated animals, further immunohistochemistry was not performed.

2.2.23 Statistical Analysis

Data was analysed using software, SPSS for Windows (version 11.0.1) or the DOS based INSTAT (version 2.0, GraphPad Software). Categorical data was examined using chi square with Fisher's exact test where required and continuous data using T tests, ANOVA or Kruskal Wallis where appropriate. Homogeneity of variance was assessed by Levene's (SPSS) or Bartlett's (INSTAT) statistics and post hoc testing mainly by Tukey honestly significantly different (HSD). Test values are reported with p values and test type.

2.3 Results

2.3.1 Confirmation of purified immunogens: ECD/MBP protein and pcDNA3-TSHR

The elution profile of protein concentration is shown in Figure 2.1 and represents the final products of a representative initial 1 litre culture. From this 1 litre approximately 62mg of ECD/MBP was affinity purified, this compares with New England Biolabs reported ranges of yields from 10-100mg/l of culture. The IPTG induction of the 89kDa ECD/MBP and its affinity purification is demonstrated in the coomassie stained gel of Figure 2.2. Western blotting confirmed the presence of TSHR like peptide in the affinity purified ECD/MBP of the appropriate size but also other smaller proteins that represent either breakdown or incompletely translated ECD/MBP as previously reported for this antibody [156] (Figure 2.3).

Following maxiprep purification, pcDNA3-TSHR concentrations ranged between 2.5-4μg/μl giving 500 to 800μg of DNA per maxiprep. This was enzyme restricted to demonstrate the 2.3kb TSHR insert on ethidium bromide stained agarose gels (Figure 2.4).

Figure 2.1 ECD/MBP fusion protein eluted from an amylose column

Fusion protein was eluted from an amylase column with maltose (10mM) and 1.5ml aliquots collected. Protein concentration was determined by trichloroacetic acid precipitation.

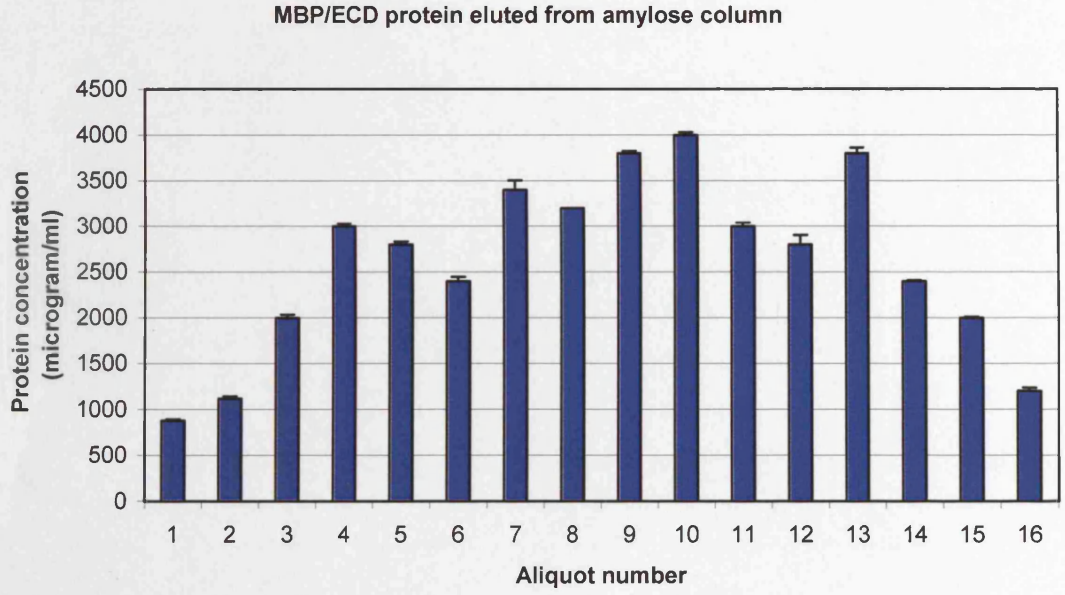

Figure 2.2 ECD/MBP IPTG induction and amylose column purification

Coomassie blue gel of crude bacterial lysate from TOPP1 E.coli transformed with the vector pMAL-cR1-ECD; pre-IPTG (lane 2) and post-IPTG induction (lane 3-6, samples taken at 30 minute intervals post-IPTG) of the 89kDa ECD/MBP. Affinity purified ECD/MBP (*) and the smaller 45kDa MBP protein (-): early elution fraction (lane 7), peak fraction (lane 8), late fraction (lane 9) and column flow through (lane 10). (Lane 1, protein markers).

Figure 2.3 Confirmation of TSHR production by Western blotting

Detection of the extracellular portion of TSHR used western blotting with polyclonal antibody p60: crude bacterial lysate (lane 1) and affinity purified ECD/MBP from early, peak and late column fractions (lanes 2, 3 and 4 respectively). Full length ECD/MBP is detected around 89kDa and a smaller protein is also detected that may represent either incomplete translation or breakdown of the full length protein.

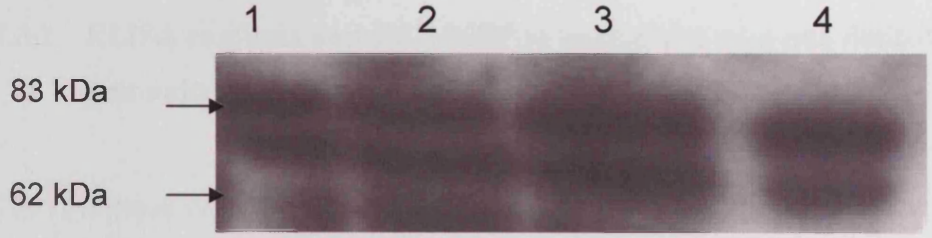

Figure 2.5 ECD/MBP ELISA, first immunized group

ELISA from the first immunized group (GI-genetically immunized, ECD-protein) showing immune response to TSHR-ECD/MBP. The ECD group has a rapid and robust response potentially recognizing both antigens. The GI group responds slower and less vigorously to the plasmid expressed single TSHR antigen.

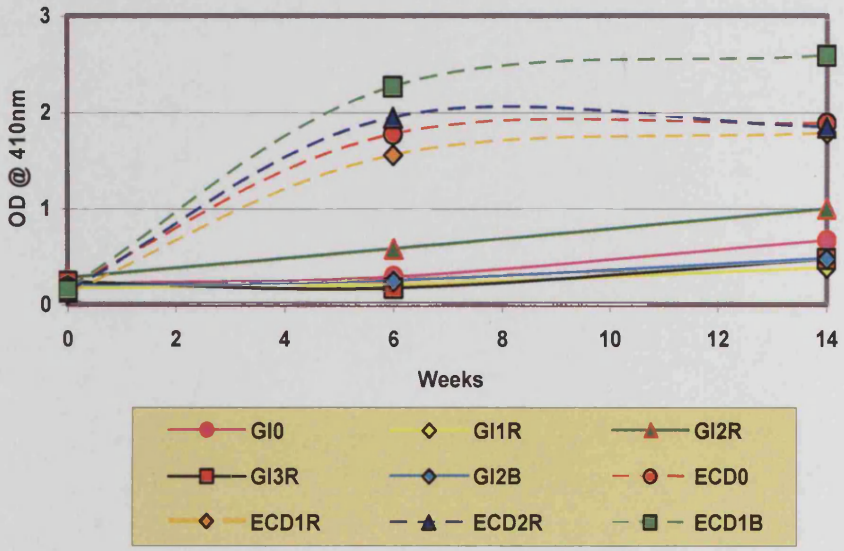

Much lower magnitudes of change in optical densities (OD) were seen in the single splenocyte transfer group. Local mice had ODs below or within the 3rd-97th centiles of their non-primed controls. Overall 0/19 local and 6/16 French mice had OD's greater than their controls (χ^2=8.588, p=0.003) suggesting an inability to transfer the anti-ECD/MBP immunity to local mice by splenocytes primed in the French mice (Figure 2.6).

Given there is a greater immune response with the protein immunization we also wanted to understand if immunological transfer was similarly influenced. The French recipients (male and female) of ECD/MBP primed splenocytes had, on average, greater optical densities than pcDNA3-TSHR primed cells, but did not achieve significance (0.4897 vs. 0.3737, p=0.065 (Welch's approximate t)). Alternatively, when considered as proportions, 1/8 were positive from the pcDNA3-TSHR primed cells and 5/8 from ECD/MBP primed cells, suggesting there may be transfer of combined reactivity to ECD/MBP with less from the pcDNA3-TSHR priming, however with the small sample size significance is not

achieved (χ^2=4.2, p=0.12, Fisher's exact). The difference between the local and French groups is due to immunity transferred in the main by ECD/MBP primed cells. Interestingly, average ODs for the local non-primed groups (females 0.61 and males 0.51) were higher than French non-primed groups (females 0.42 and males 0.36 (Table 2-3)). This is significant (F=6.9, p=0.007, ANOVA, (p=0.248 (Levene)) and is further defined as significant differences between local females versus; French males (p=0.006) and French females (p=0.043, Tukey-HSD). The non-primed recipients received 5 x 10^6 cells in contrast to 5 x 10^5 cells in the primed splenocyte group and this may be causing an increased polyclonal response.

Figure 2.6 ECD/MBP ELISA, single T-cell transfer group

Local mice receiving primed T-cells have statistically significant (* p<0.05) lower optical densities than their non-primed controls suggesting no transfer of immunity (shaded area represents non-primed range 3rd to 97th centiles). The French recipients of primed T-cells show some individual elevations in OD above their non primed controls but this does not achieve significance as a group and implies some limited transfer of immunity. French mice almost exclusively from TSHR-ECD/MBP primed T-cell transfer develop reactivity, while no local mice have any evidence of an immune response

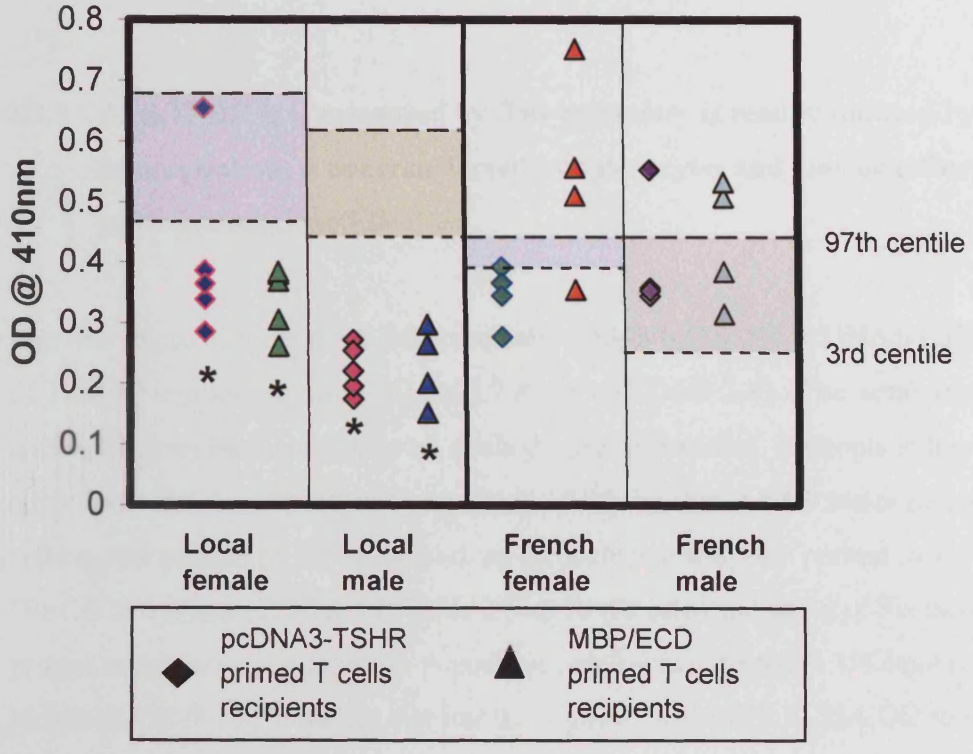

Figure 2.7 Anti-TSHR IgG flow histograms: Immunized group 1

Outlined histogram represents pre-immune sera and solid histogram sera at 14 weeks. All mice were positive for anti-TSHR IgG indicated by a right shift in the solid histogram. (GI-pcDNA3-TSHR and ECD-ECD/MBP immunized).

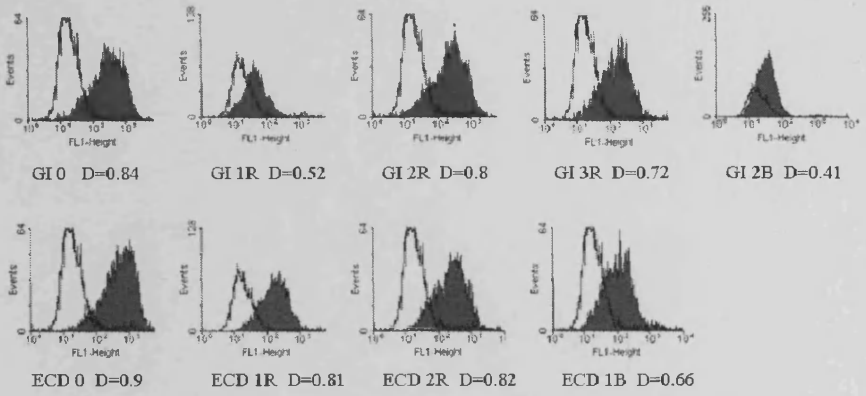

Figure 2.8 Anti-TSHR IgG flow histograms: Immunized group 2 with environment modifications

Histograms for GIL and GIB represent sera after 14 weeks whereas for MBL and MBB the sera was from 9 weeks. (pcDNA3-TSHR immunized/local environment (GIL), pcDNA3-TSHR immunized/Belgian environment (GIB), ECD/MBP immunized, local environment (MBL) and Belgian environment (MBB).

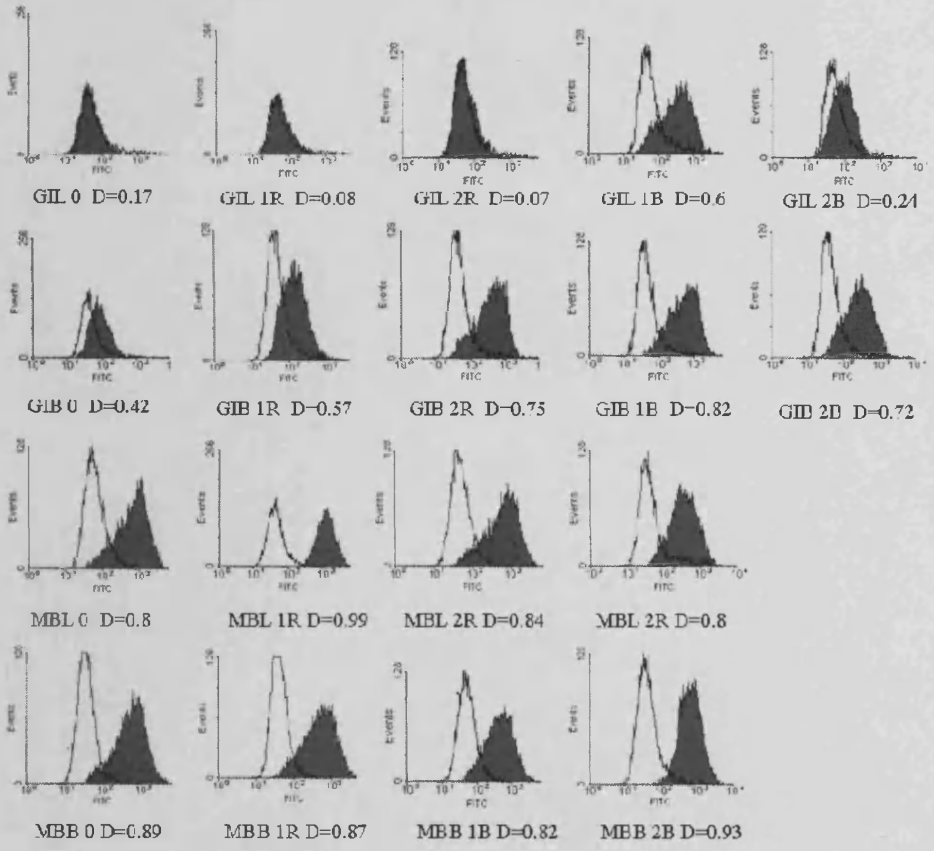

Figure 2.9 Anti-TSHR flow cytometer "D" values for groups 1 and 2 immunized mice

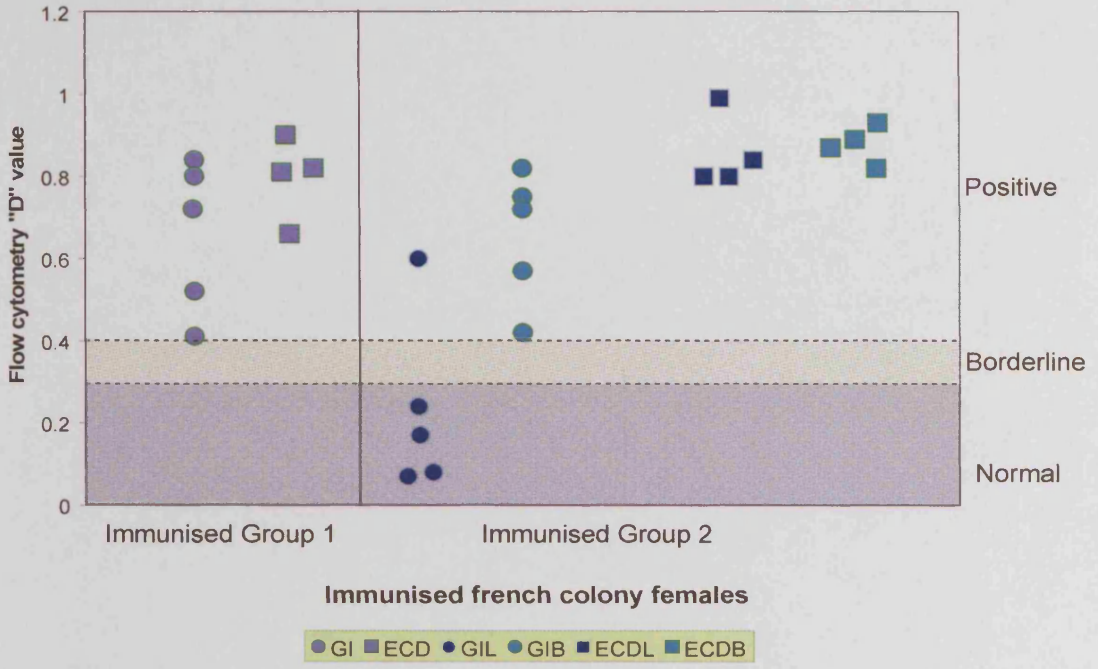

Figure 2.10 Anti-TSHR IgG flow histograms, splenocyte transfer to local colony females

All mice were negative for anti-TSHR. (B-local colony, GI-pcDNA3-TSHR primed splenocytes, ECD- ECD/MBP primed splenocytes, NP-non-primed splenocyte).

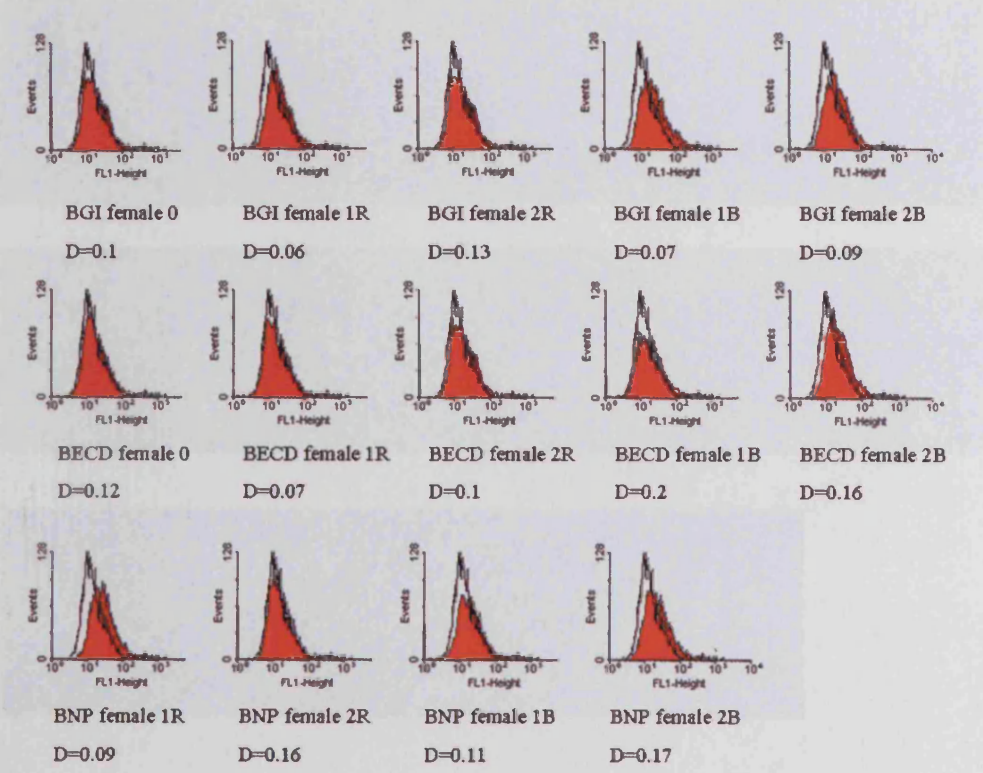

Figure 2.11 Anti-TSHR flow cytometer "D" values for splenocyte transfer groups

(B-local colony, F-French colony, GI-pcDNA3-TSHR primed splenocytes, ECD-ECD/MBP primed splenocytes). Circled is BECD 1R whose D value represents a left shift, not a positive right shift.

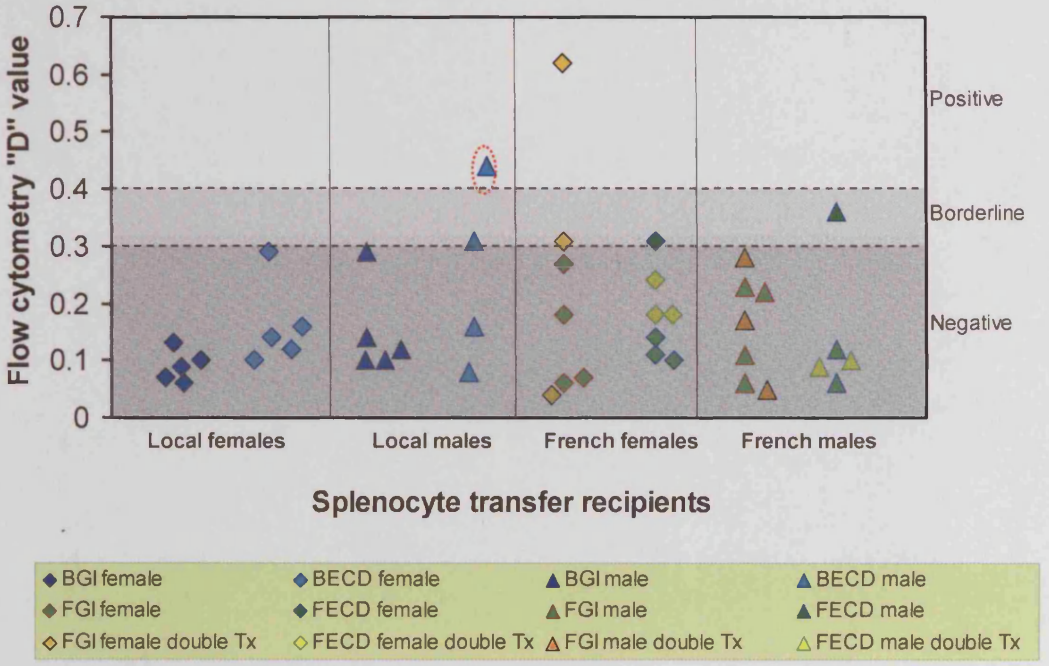

Amongst the French single splenocyte transfer group a similar overall picture of transfer failure is present (Figure 2.11 and Tables 2-11 and 2-12). Seven out of eight males and females were negative and 1/8 males (FECD 2R) and 1/8 females (FECD 1R) were inconclusive. Four out of four male and 2/3 female non primed recipients were negative, 1/3 female non-primed (FNP 1R) mouse was positive and this mouse did not have an elevated ECD/MBP ELISA OD. The second splenocyte transfer resulted in 4/6 female and 5/5 males that remained negative, 1/6 females inconclusive (FGI 3B) and 1/6 females positive (FGI 2B).

In total there were 12 groups divided by sex, colony, and type of splenocyte transferred. Analyzing mean D values demonstrates no significant difference between the groups ($F=0.926$, $p=0.524$, ANOVA, Levene $p=0.014$, therefore non-parametrically ($\chi^2=7.43$, $p=0.736$, Kruskal Wallis).

From the group of French male and female primed splenocyte recipients there was no correlation between elevated ECD/MBP ELISA ODs and anti-TSHR by flow cytometry ($rho=0.07$, $p=0.797$, Pearson).

In the second immunization group all mice from local and environment modified groups developed anti-TSHR when immunized with ECD/MBP (8/8, Figure 2.8). Whereas pcDNA3-TSHR immunization lead to the local group having significantly less mice with anti-TSHR (1/5) compared to the modified group (5/5) ($p=0.048$, Fisher's exact test). When the first and second groups mean D values were analyzed by ANOVA significant differences in variation are confirmed ($F=11.496$, $p<0.0001$) with post hoc testing confirming the pcDNA3-TSHR locally maintained group to have significantly lower anti-TSHR than all the other groups ($q=6.2\text{-}8.9$, $p<0.01\text{-}<0.001$, Tukey-Kramer multiple comparisons).

2.3.4 TBII activity is present in immunized group 1, is not reproducible in immunized group 2 irrespective of environmental modification and is not significantly transferred by splenocytes

TBII activity was detected in the first pcDNA3-TSHR immunized group in 3/5 and in 1/4 of the ECD/MBP mice (Figure 2.12). None of the 18 mice from the second immunized group had any TBII activity irrespective of environmental modification. The difference between the TBII activity when the groups are considered individually is just significant ($\chi^2=7.6$, $p=0.043$, Fisher exact) but analysis of small sample sets is inaccurate. Therefore, if considered as two different experiments; the first group have 4/9 positive for TBII and 0/18 for the second group, this becomes highly significant ($\chi^2=9.39$, $p=0.007$, Fisher exact). This demonstrates an inconstancy in TBII development between the two experiments.

Very little evidence of TBII activity was found in the transfer recipients, only 2/4 local male mice that received ECD/MBP primed splenocytes developed any significant activity (Figure 2.13). Considering all groups individually there was no significant difference in the proportions with significant TBII activity ($\chi^2=13.2$, $p=0.067$, Fisher exact) and as two groups, local (2/19) and French (0/26), there remained no significant difference ($\chi^2=2.86$, $p=0.173$, Fisher exact).

Figure 2.12 TBII activity in immunized groups 1 and 2

3/5 pcDNA3-TSHR and 1/4 ECD/MBP immunized mice from group 1 have TBII activity. No mice from group 2 have any TBII. (Values below the 3rd centile show significant TBII activity).

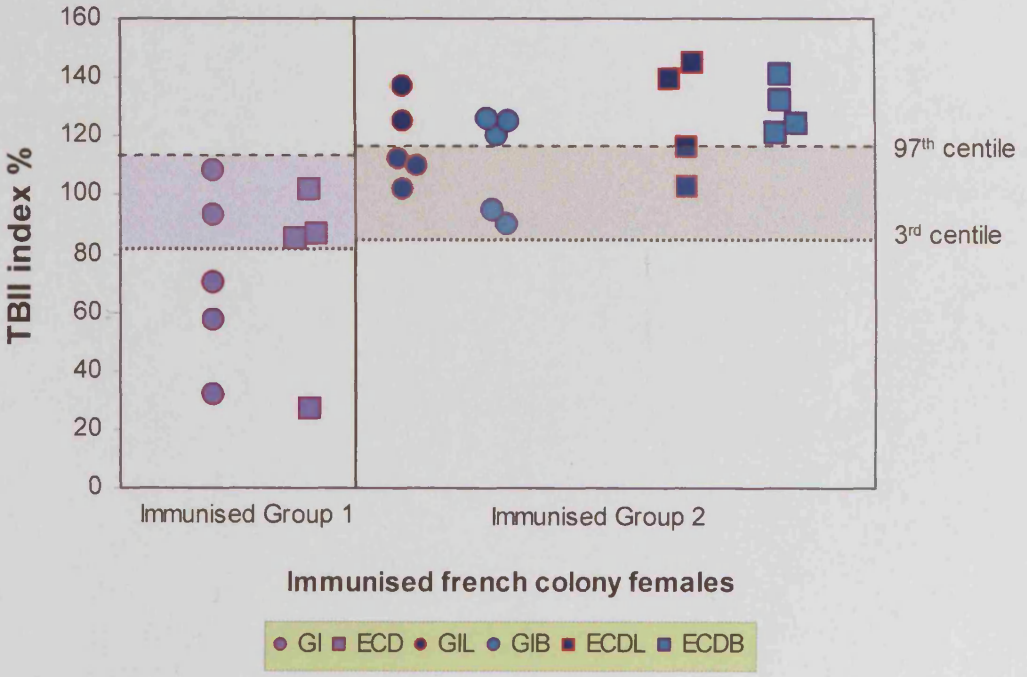

Figure 2.13 TBII activity in splenocyte transfer groups

Only 2/4 local colony male mice receiving ECD/MBP primed splenocytes demonstrated TBII activity.

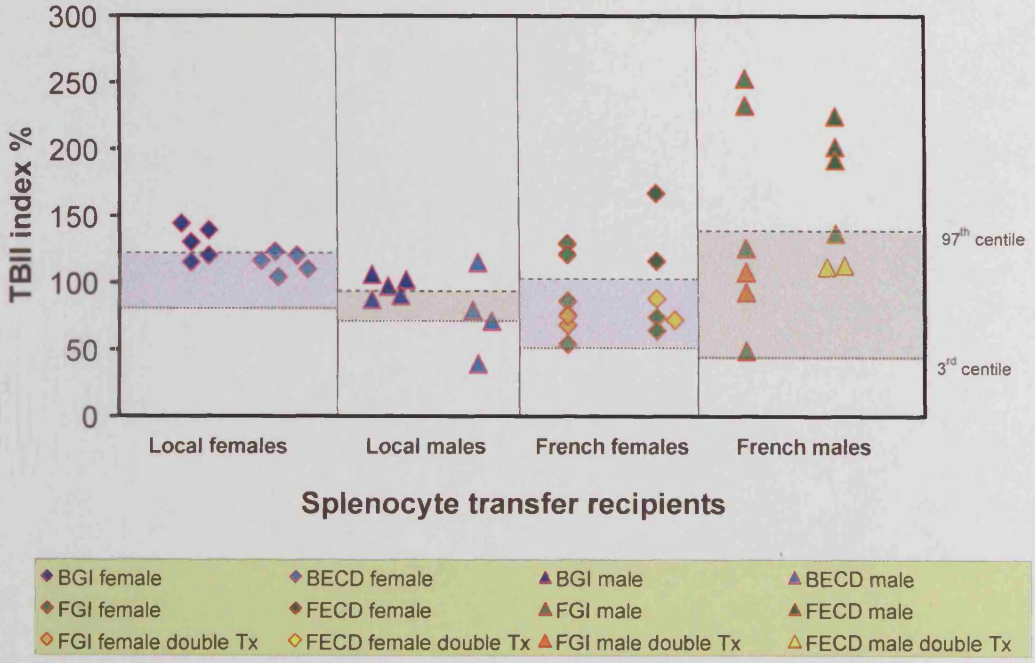

A considerable number of test samples in the splenocyte transfer experiments, rather than showing inhibition, demonstrate greater binding than the control pre-immune serum (Figure 2.13). The calculation of the TBII index using pooled pre-immune samples as the standard representing 100% TSH binding may be biased. When groups in the pool, like the female BNP, have some inherent capacity to bind TSHR, as evidenced by their ECD/MBP ELISA results, their sera might compete for TSH binding giving an artificially low cpm against which the TBII index is calculated. In an attempt to minimize this potential bias and reintroduce the range of individuals' activities, 97^{th}-3^{rd} centiles were constructed from non-primed sera in the transfer group and individual pre-immune sera in the second immunization group.

2.3.5 TSAB activity is exclusively found in group 1 immunized mice and were not transferred or reproduced

By luciferase assay, 3/5 pcDNA3-TSHR and 2/4 ECD/MBP immunized mice from group 1 had TSABs and 0/18 of those in group 2 (Figure 2.14 & Figure 2.15). The difference between the two groups is significant (χ^2=12.27, p=0.002, Fisher exact) and as for the TBII results there is inconstancy between experiments. No mice from the splenocyte transfer group had TSABs.

Figure 2.14 Relative light unit output from luciferase assay group 1 immunized mice (PI-pre-immune)

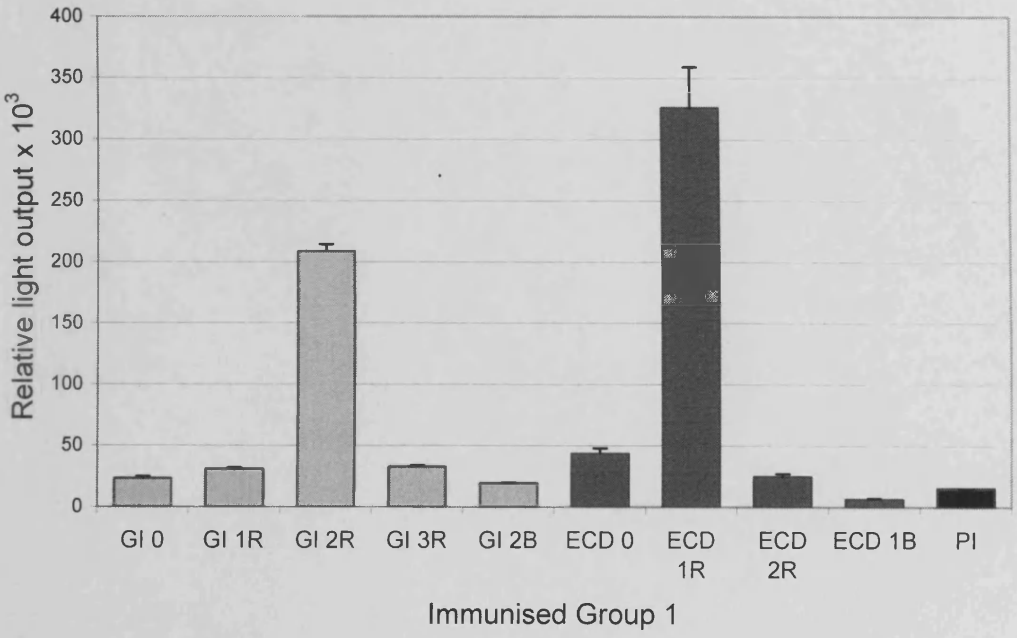

Figure 2.15 TSAB activity in immunized groups 1 and 2

In total, 5/9 group 1 and 0/18 group 2 mice had detectable TSABs.

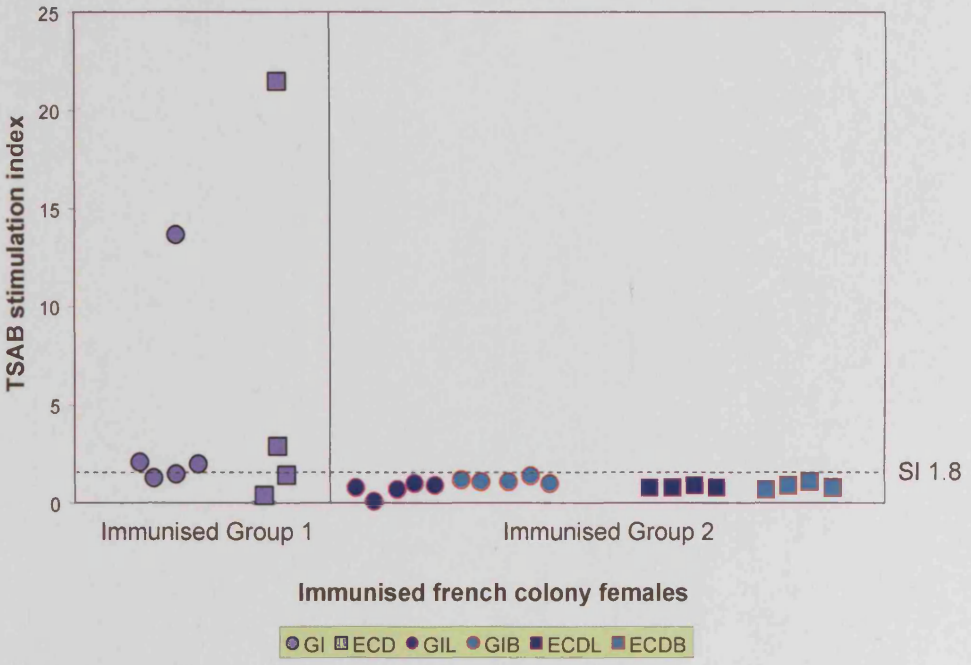

Some degree of caution should be mentioned about the methodology of this assay. The development of this in-house assay initially used serum free medium conditions to carry out the final incubation [188]. While our model was being investigated the TSAB luciferase assay was being optimized. When switched to a salt free/5% polyethylene glycol (PEG) buffer, the SI could be twice that of serum free conditions at four hours and a six hour incubation was optimum for TSAB binding in serum free media [190]. Therefore the results we report may lack sensitivity.

2.3.6 T4 values are higher in group 1 immunized mice than group 2

Total T4 values were largely within a wide normal range (Table 2-4) but differences existed between the two groups and within group 2 (Figure 2.16). Significantly higher average T4 was found in group 1 than group 2 immunized mice, 8.64 vs. 3.67μg/dl ($p<0.0001$, Mann Whitney U). While there are some differences present in the means of GIL (3.92), GIB (4.3), ECDL (3.86) and the lowest, ECDB (3.1), this does not achieve significance ($F=2.125$, $p=0.143$, ANOVA ($p=0.102$, Levene)).

The splenocyte transfer groups total T4 were largely within the normal range with variations present between the groups (χ^2=22.67, p=0.002, Kruskal Wallis) (Figure 2.17). One exception was the male BECD mice whose levels were low but differed significantly only from female BGI mice (p<0.01, Dunn's Multiple Comparison). The local colony BECD males were unusual in their T4 values were both low and homogenous (mean=2.5, sd=0.141) in contrast with the French FECD males heterogeneity (mean=7.7, sd=2.65). There is no significant correlation between TSAB, TBII, T4 or anti-TSHR in immunized group 1 and 2 or the splenocyte transfer group.

Table 2-4 Total T4 values from individual non-primed recipients, pre-immune and control mice

	Mean	Standard deviation	97th-3rd centiles
Female non-primed	5.77µg/dl n=7	2.75	10.22-3.34
Male non-primed	5.86µg/dl n=8	1.95	8.91-3.81
Pre-immune/control	4.27µg/dl n=9	2.40	8.91-2.57

Figure 2.16 Total thyroxine levels from immunized groups 1 and 2

Group 1 levels while within the normal range are higher than group 2 (p<0.0001, Mann Whitney U). The apparent difference between group ECDB and the other members of group 2 is not statistically significant.

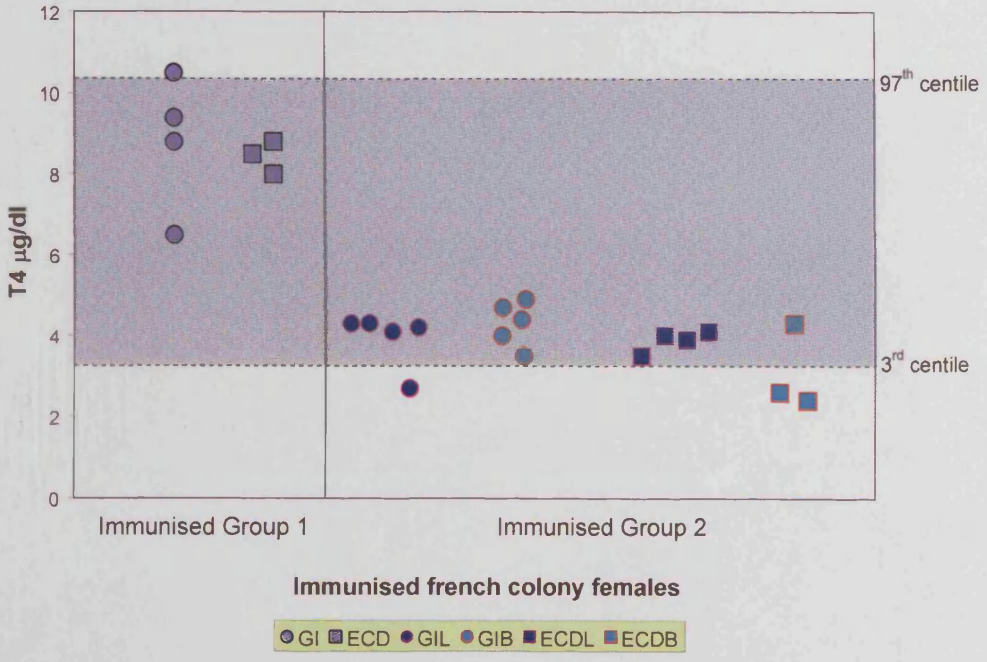

Figure 2.17 Total T4 values from splenocyte transfer group

Differences exist between groups (p=0.02, ANOVA). The means of FECD vs BECD male are significantly different (p=0.006, Tukey HSD) while there are no differences between the female groups.

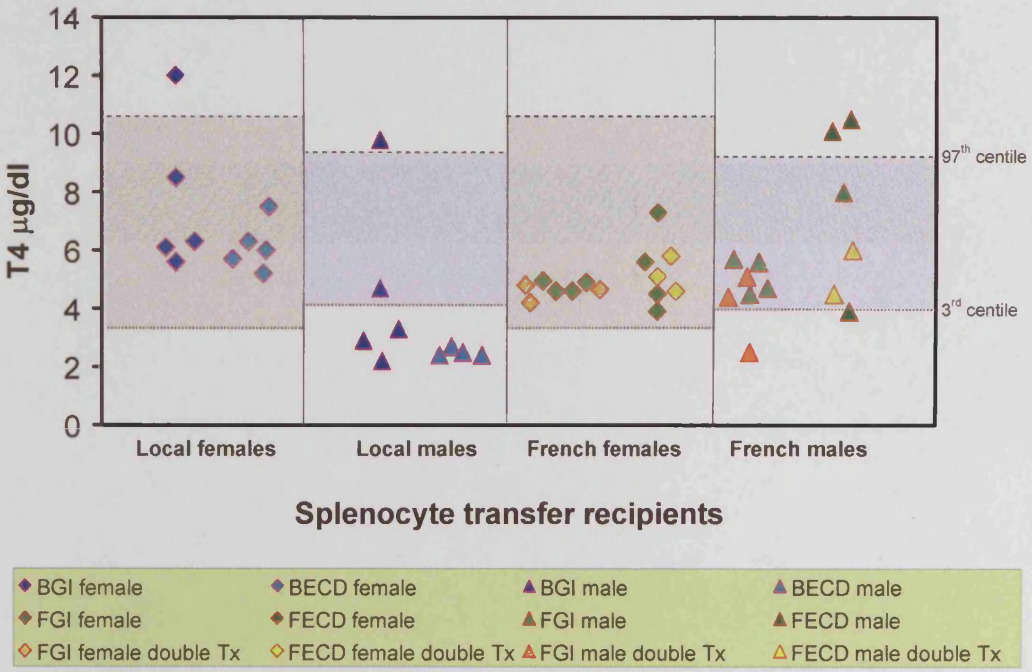

2.3.7 Splenocyte TH1 and TH2 cytokine expression determined by ICCS is similar in all groups, whereas CD4/CD8 ratio is altered by immunization

Increases in cytokine production from CD4 and CD8 splenocyte populations by PMA/ionomycin stimulation are shown in Table 2-5 and summarized in Figure 2.19. A representative output from the flow cytometer in the form of dot plots is shown in Figure 2.18. Graphically there is a suggestion the protein immunized environment modified (MBB) group have higher percentages of $CD4^+/IFN\text{-}\gamma^+$ and $IL\text{-}4^+$. However the average percentages of polyclonaly stimulated $CD4^+/IFN\text{-}\gamma^+$ splenocytes did not differ significantly between groups (χ^2=6.74, p=0.150, Kruskal Wallis). Differences in $CD4^+/IL\text{-}4^+$ percentages were present (χ^2=11.57, p=0.0419, Kruskal Wallis), but none of the groups differed significantly between experimental groups and controls on post hoc testing (Dunn Multiple Comparison).

Figure 2.18 Flow cytometry dot plots demonstrating CD4, CD8 surface staining and Il-4, IFN-γ intracellular cytokine staining of splenocytes

Plots (C-E) show that only low level increases in cytokine populations followed stimulation with PMA/ionomycin (Normal spleen 5).

A. Forward and side scatter plot for initial population gating.
B. $CD4^+/CD8^+$ plot for region selection of surface markers.
C. $CD4^+$/ IFN-γ^+. D. $CD4^+$/ Il 4^+. E. $CD8^+$/ INF-γ^+. F.$CD8^+$/ Il 4^+.

G. Positive control for PMA/ionomycin stimulation. Human peripheral blood mononuclear cells surface stained for anti-human CD3 PerCP and cytokine staining by anti-human IFN-γ FITC. Stimulation results in an 8% increase of the IFN-γ^+ population.

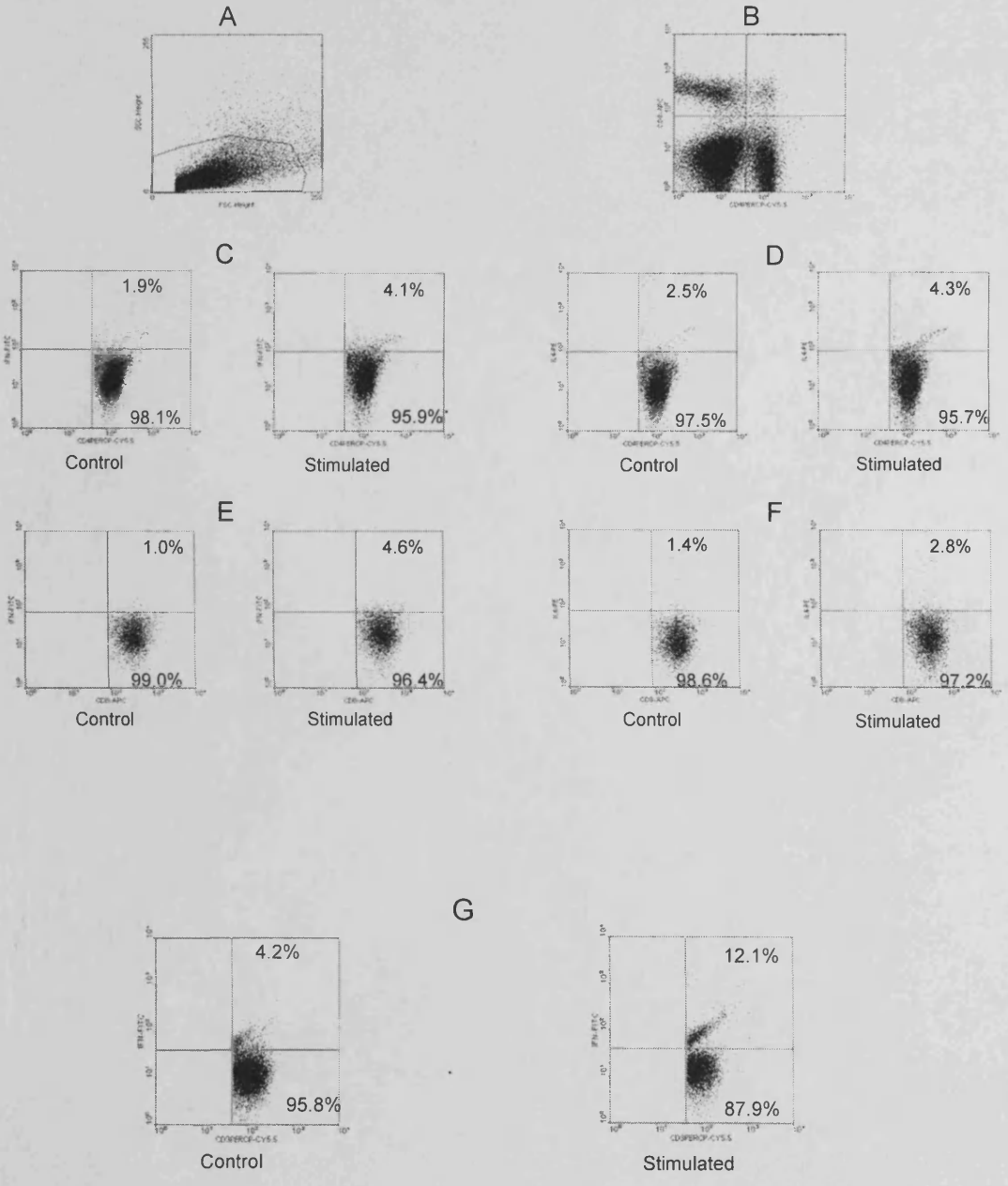

Figure 2.19 Percentages of $CD4^+$ and $CD8^+$ splenocytes stimulated to express IFN-γ and Il 4

Splenocytes from immunized group 2, Brussels (BRUS) and non-immunized (NORM) mice. Low levels of stimulation were detected in all groups and none were statistically different from the control normal splenocytes. The small Brussels group did not significantly differ from the locally immunized group 2 mice.

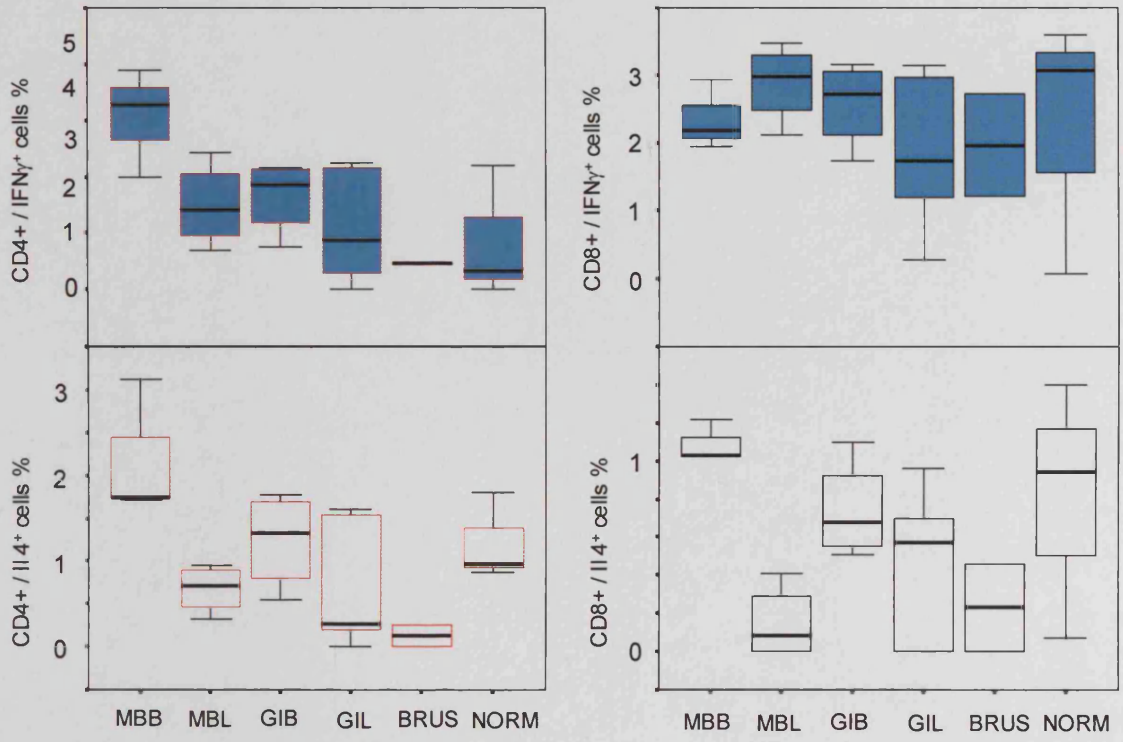

Figure 2.20 CD4/CD8 ratios from control and stimulated splenocytes

CD4/CD8 ratios are higher in protein immunized mice, lower with local and Brussels genetically immunized mice and lowest in non-immunized.

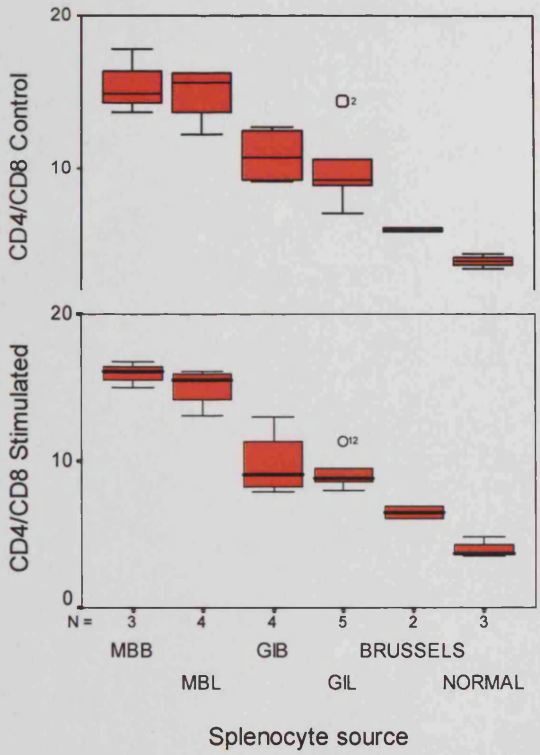

$CD8^+/IFN\text{-}\gamma^+$ percentages do not differ between the groups (χ^2=3.27, p=0.513, Kruskal Wallis). Neither are there differences between experimental and control groups of $CD8^+/IL\text{-}4^+$ (χ^2=10.96, p=0.0519, Kruskal Wallis).

While the MBB group appeared to have higher cytokine expression than a number of other groups it was never significantly greater than that of non-immunized mice. Overall the levels of cytokine stimulation were low in both CD4 and CD8 splenocyte populations. They did not differ between mice immunized in Brussels, local non-immunized and immunized mice, irrespective of the method of immunization or environmental modification. However, the protein immunized mice (MBB and MBL) had an accompanying elevation in the CD4/CD8 ratio with the highest ratio (mean=15.4) that differed significantly from the other groups (p<0.0001, Figure 2.20). The local genetically immunized mice (GIB and GIL) were the next highest (mean=9.46) and differed significantly from protein immunized and non-immunized (p<0.0001), but not from those genetically immunized in Brussels (p=0.061). The lowest ratio was found in the non-immunized group (mean=4.0) and this did not differ from the genetically immunized Brussels mice (mean=6.5, p=0.239(all Tukey HSD)). This relationship was not altered by stimulation of the splenocytes. [Note: Counting 10^5 cells the CD4+ events range from 2.8-4.0 x 10^4 and CD8+ from 0.2-0.4 x 10^4.]

Table 2-5 Percentage of $CD4^+$ and $CD8^+$ splenocytes stimulated to express IFN-γ and IL-4 from immunized group 2, Brussels and non-immunized mice

	$CD4^+$ Cytokine expression %		$CD8^+$ Cytokine expression %		$CD4^+$ /$CD8^+$ Ratio	
	IFN-γ	Il 4	IFN-γ	Il 4	Control	Stimulated
MBB 0	3.28	1.72	1.95	1.22	17.76	16.08
MBB 1R	2	1.74	2.19	1.02	13.60	16.74
MBB 2B	3.89	3.13	2.93	1.03	14.92	14.95
MBL 0	1.19	0.83	3.47	0	15.11	15.29
MBL 1R	2.43	0.6	3.13	0.41	16.28	16.06
MBL 2R	0.7	0.32	2.12	0	16.07	13.03
MBL 1B	1.66	0.95	2.84	0.17	12.24	15.67
GIB 0	0.75	0.54	1.74	0.6	12.14	13.01
GIB 1R	2.12	1.6	2.51	1.1	12.63	9.51
GIB 1B	2.16	1.77	2.95	0.75	9.35	8.61
GIB 2B	1.59	1.06	3.17	0.51	9.12	7.86
GIL 0	2.23	1.6	2.97	0.7	14.39	11.34
GIL 1R	2.16	1.54	3.14	0.96	10.55	9.46
GIL 2R	0.88	0.26	1.19	0	8.93	7.96
GIL 1B	0.27	0.2	1.73	0.57	9.30	8.83
GIL 2B	0	0	0.28	0	7.02	8.54
Brussels a	0.46	0.25	2.72	0.46	6.10	6.90
Brussels b	0.45	0	1.21	0	5.90	6.05
Normal 5	2.2	1.8	3.6	1.4	3.41	3.50
Normal 6	0.34	0.97	3.07	0.94	4.43	4.75
Normal 7	0	0.86	0.06	0.07	3.96	3.72

2.3.8 IFN-γ secreted is mostly below the limit of detection and can be stimulated in a small proportion of splenocytes by ECD/MBP. Low levels of IL-4 are detectable but none differ significantly from non-immunized mice

IFN-γ was below the limit of detection from all splenocytes stimulated by both peptides and PMA/ionomycin (Table 2-6, sample standard curves app. A). ECD/MBP stimulation resulted in low level IFN-γ production in 2/7 ECD/MBP immunized mice, 1/11 pcDNA3-TSHR mice and 0/3 normal mice. Neither in terms of proportions (χ^2=1.63, p=0.71, Fisher exact) or group means (F=2.02, p=0.163, ANOVA) was there a significant difference. The difference between detectable IFN-γ in the presence of ECD/MBP (3/21) with none stimulated by PMA/ionomycin (0/21) or TSHR peptide (0/21) achieved significance (χ^2=6.3, p=0.043).

Il-4 levels were low but generally within detectable ranges (Tables 2.6 & 2.7 and Figure 2.21)). TSHR peptides induced no significant difference in IL-4 between groups (F=1.805, p=0.172, ANOVA, (Levene p=0.203)). PMA/ionomycin was similar with no significant differences (F=0.519, p=0.758, ANOVA (Levene p=0.889)). ECD/MBP stimulation increased IL-4 secretion in four protein immunized mice above that of normal splenocytes but again no group differed significantly (p=0.064, ANOVA (Levene p=0.009, therefore, Kruskal Wallis, χ^2=6.63, p=0.085)).

Table 2-6 Levels of IFN-γ and IL-4 stimulated in splenocyte supernatants

	IFN-γ pg/ml			IL-4 pg/ml		
	Peptides	ECD/ MBP	PMA/ Ionomycin	Peptides	ECD/ MBP	PMA/ Ionomycin
MBB 0	0	0	0	1.9	0	0
MBB 1R	0	36.3	0	3.4	12.2	0
MBB 2B	0	0	0	0.3	2.8	14.1
MBL 0	0	0	0	0	12.5	3.6
MBL 1R	0	25.3	0	4.7	3.4	2.0
MBL 2R	0	0	0	1.6	22.2	15.8
MBL 1B	0	0	0	0	25.6	11.7
GIB 0	0	0	0	0	0	15.8
GIB 1R	0	0	0	2.2	2.2	0
GIB 1B	0	2.3	0	2.8	6.6	9.2
GIB 2B	0	0	0	0	1.6	14.2
GIL 0	0	0	0	6.8	7.3	0
GIL 1R	0	0	0	1.8	2.7	0.8
GIL 2R	0	0	0	5.9	0	0.8
GIL 1B	0	0	0	1.8	2.7	14.2
GIL 2B	0	0	0	3.6	2.7	7.5
Brussels a	0	0	0	0	1.4	6.7
Brussels b	0	0	0	0	0	0
Normal 5	0	0	0	1.8	3.2	13.3
Normal 6	0	0	0	1.4	8.2	10.8
Normal 7	0	0	0	4.1	0.5	1.7

Figure 2.21 IL-4 in splenocyte supernatants following stimulation with TSHR peptides, PMA/ionomycin and ECD/MBP

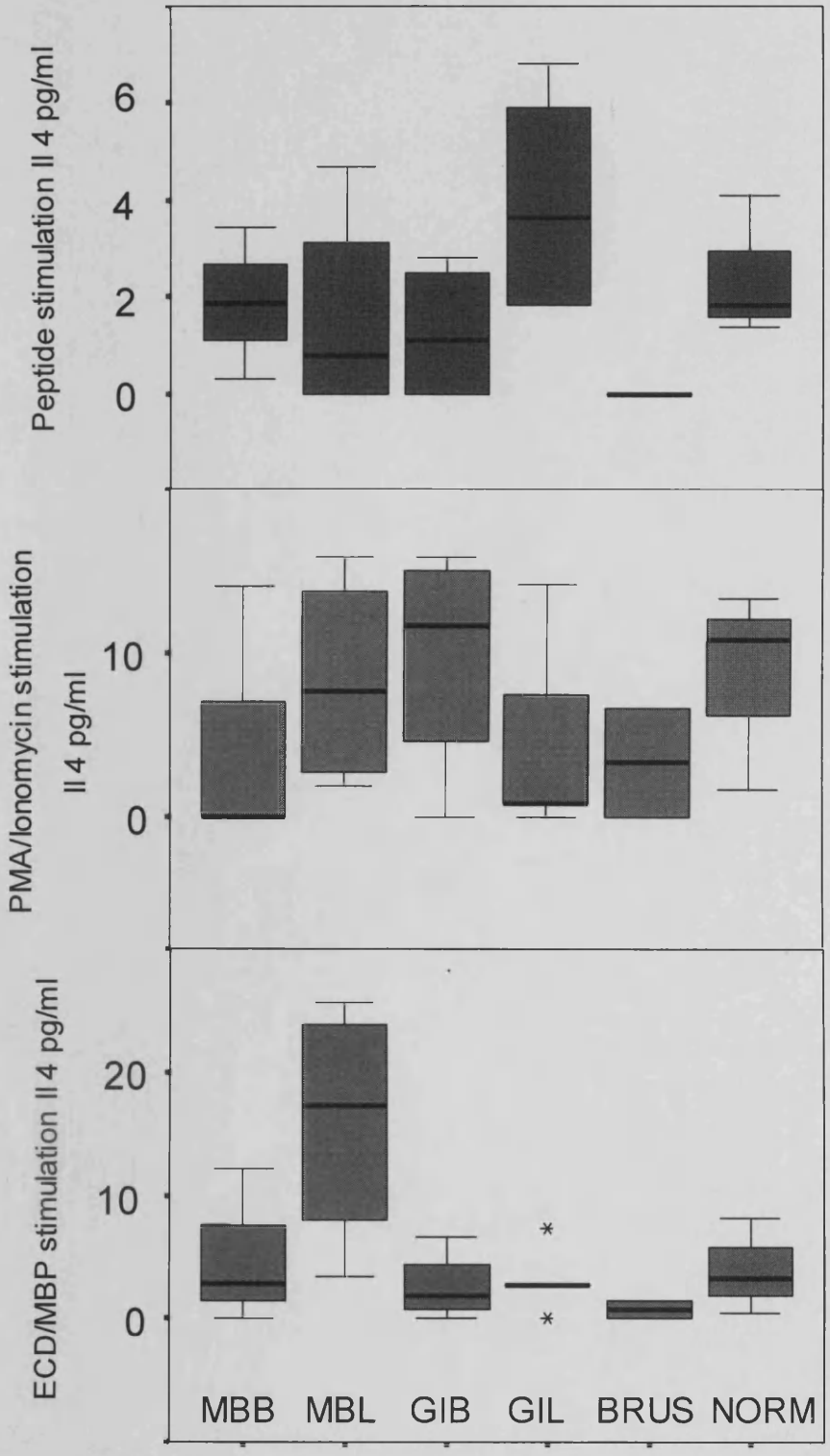

2.3.9 Thyroiditis is not induced or transferred. Thyroid follicles demonstrate normal ranges of appearances and intrathyroidal ectopic thymus masquerades as focal lymphocytic aggregates

Thyroid sections were examined using several techniques in the course of the experiments (2.2.22). Macroscopically there were no thyroids that appeared enlarged. Immunized group 1 thyroids were mounted in paraffin as a pair and sections cut through the entire block. Thyroid follicular structure was frequently disrupted by the brittle nature of the colloid (Figure 2.22.A). Commenting on subtle changes such as thyrocyte height was not possible using 5μm slices as the section was a composite of more than one thyrocyte. No intrathyroidal lymphocytic infiltrates were present. However, in the absence of a murine histology atlas to illustrate normal parathyroid structure, a descriptive text reporting the parathyroid to be composed of clear, intermediate and darkly stained cells initially meant the structures seen in Figure 2.22.B-E, were discounted as being normal parathyroid. This was supported by the presence of similar structures in non-immunized and non-primed transfer recipients (Figure 2.23.B-F). The darkly stained cells were always encapsulated with the parathyroid gland but occasionally, depending on orientation and slice depth, the darkly stained cells could appear to be alone within the thyroid follicles, but further sectioning could always trace their origin adjacent to the parathyroid gland.

With the problems of colloid fracturing in paraffin the subsequent splenocyte transfer group had thyroids prepared for semi-thin and cryostat histology. The preservation of structure in semi-thin was understandably greater than cryostat sections and the absence of lymphocytic infiltrates meant no ICC characterisation was carried out. From semi-thin sections normal thyroid histology was seen to comprise follicular size and thyrocyte depth heterogeneity with occasional apical budding and colloid endocytosis (Figure 2.24.A-B). The ability to recognise clear, intermediate and darkly stained cells in parathyroids was straightforward with excellent resolution of microvilli present in the parathyroid cysts (Figure 2.24.C-D). Again, discrete clusters of darkly stained, large nucleated cells adjacent to normal parathyroid were present in non-primed recipients and largely disregarded. The capsule did not stain well with toluidine blue in comparison to H&E.

Group 2 immunized mice also showed no intrathyroidal infiltrates and a normal range of heterogeneous follicles. Individual mast cells were seen occasionally resident within connective tissue adjacent and within thyroids with no greater frequency between immunized and control mice.

While reviewing the histology and comparing it to that published previously it became apparent the parathyroid associated cells were present in models from both locations [158; 165; 185]. The clusters were characterised previously as primarily being T-cells $CD3^+$, $Il\text{-}2^+$ and B-cells. From our initial impression the parathyroid associated cells were not exclusively present in immunized mice hinting towards an anatomical rather than pathological finding. Further literature searching reminded us of the possibility of ectopic thymus adjacent to the parathyroid gland [191; 192].

To further understand the distribution and incidence of ectopic thymus in control and immunized mice, available sections were re-examined and remaining blocks cut with closer 100-150μm intervals. In the absence of TSHR immunity in the splenocyte transfer group only non-primed recipients were sectioned further to serve as controls. From the more detailed sections a wide range of thyroid/parathyroid/thymic appearances were seen ranging from extensive and extra thyroidal (Figure 2.25.A-B) to a more intrathyroidal location (Figure 2.26.A-D). Mostly the parathyroid and thymus was separated by a thin layer of connective tissue but occasionally was seen as a paired structure (Figure 2.25.C-D). The level of the section produced some artefacts underlining the importance of multiple sections at frequent intervals. When at the tip of a parathyroid some parathyroid cells could extend between follicles mimicking an infiltrate but further sections confirm the cells' parathyroid origins (Figure 2.25.E). Similarly a small piece of medullary thymic tissue could be difficult to distinguish from parathyroid, but the presence of murine equivalents of Hassal bodies and clustering of lymphocytes around venules aided the histological diagnosis along with further sections (Figure 2.26.A-D). Cortical thymus had a more uniform appearance with densely packed, dark stained cells with large nuclei (Figure 2.24.E-F, Figure 2.25.A-B). Another occasional appearance was the thymus gradually faded towards the edge of the gland, became less well defined and developed an atrophic appearance with vacuolated adipocytes (Figure 2.26.E-F). This may represent involution of the thymus, an age related process, whereby replacement with fibroadipose tissue occurs. Overall, the appearance, size and orientation of the ectopic thymus were highly variable.

It was not always possible to detect parathyroid in the sections (Table 2-7). Lacking awareness of the need to cut 100-150μm sections at the outset is the most likely cause of this. When cutting plastic sections the smaller the area cut, the greater the performance and durability of the glass knife, as a result, extensive trimming of tissue around the thyroid

was performed to such an extent that a thymus the size of that in Figure 2.25.A-B may inadvertently be removed along with the parathyroid. Due to pairing of the parathyroid with ectopic thymus in all cases, if the parathyroid was not seen it is probable that thymus could be missed and we may be unintentionally under-reporting the incidence of ectopic parathyroid thymus.

In order to determine if TSHR immunization influenced the number of mice with ectopic thymus they were grouped as, TSHR immunized (GI, ECD, MBL, MBB, GIL and GIB) or non-immunized (non-immunized and FNP), 13/26 and 6/9 mice, respectively, have thymus present and the difference was not significant ($p=0.46$, Fisher's exact). Returning to blocks previously sectioned without having frequent uniform sections cut made attempts to estimate volumes by image analysis unworkable.

Table 2-7 Proportion of mice with histologically detectable parathyroid and thymic tissue

	Parathyroid detected	Parathyroid and thymus
Non-immunized	2/2 (100%)	2/2 (100%)
FNP	7/7 (100%)	4/7 (57%)
GI	3/5 (60%)	3/5 (60%)
ECD	1/4 (25%)	1/4 (25%)
MBL	3/4 (75%)	2/4 (50%)
MBB	3/3 (100%)	2/3 (60%)
GIL	4/5 (80%)	2/5 (40%)
GIB	4/5 (80%)	3/5 (60%)

2.3.10 Orbital connective tissue and fat do not demonstrate inflammatory changes. Artefactual muscle contraction exaggerates normal muscle fibre separation

No significant macroscopic changes were present in terms of proptosis, orbital fat expansion or extraocular muscle hypertrophy. For group 1 (GI and ECD) and control mice, paraffin sections were prepared. Normal ocular muscle in cross-section had areas where connective tissue was common between muscle fibres corresponding to the singly

innervated orbital muscle layers (Figure 2.27.A). In none of these areas did PAS positive material accumulate suggesting no abnormal glycosaminoglycan deposition (Figure 2.27.C). No lymphocytic infiltration was present in any immunized mice. Artefactual separation of fibres due to fracturing of the section could also be seen similar to that occurring with the thyroid colloid (Figure 2.27.B).

For group 2 (GIL, GIB, MBL and MBB) and splenocyte recipients plastic sections were prepared. In splenocyte transfer recipients and control mice, ocular muscle with a packed appearance towards the centre of the largest part of the sample, were the multiply innervated global muscle fibres (Figure 2.28.A). Adjacent orbital layer muscle fibres had areas of contracted, buckled myofibrils routinely. Buckling deformed the connective tissue and could give rise to the false impression of oedema. Similar changes were present in group 2 immunized mice with sections of myofibrils appearing normal adjacent to segments with contraction bands and knots without any evidence of inflammatory infiltrate (Figure 2.28.C/D/E). Elsewhere, striated muscle attached to the thyroid usually appeared tightly packed but contraction and buckling could similarly be seen at the edge of the specimen demonstrating the changes were not restricted to the ocular muscles (Figure 2.28.E). The normal connective tissue separation of orbital muscle fibres could be exaggerated further by crease artifacts that developed when insufficient temperature was used to dehydrate the section onto the slides (Figure 2.28.B).

In summary, the ocular muscles from immunized, transfer and control groups had no evidence of hypertrophy, inflammatory infiltrate, glycosaminoglycan deposition and a false impression of oedema could occur due to muscle contraction. Orbital fat appearances were similar in control and immunized animals. Organised lobules of fat were bordered by connective tissue within which scatterings of mast cells were resident with no lymphocytic accumulations present (Figure 2.27.E). Sporadic multi-vacuolated adipocytes were found within areas of connective tissue in control and immunized mice representing the normal background of adipogenesis (Figure 2.27.D).

Figure legends

Figure 2.22 Thyroid sections from Group 1 immunized mice

A. Normal thyroid follicles found adjacent to muscle and cartilage. Colloid had a brittle nature tending to cause fractures across follicles. [GI 1R, paraffin, H&E, x10].
B-C. Darkly stained thymocytes separated from parathyroid cells by a parathyroid cyst. [B-ECD 0, C-GI 3R, paraffin, H&E, x10].
D-E. Ectopic thymus sizes varied significantly in relation to the parathyroid gland. [D-GI 2B, E-GI 0, paraffin, H&E, x10 and x20 respectively].

Figure 2.23 Non-immunized and non-primed recipient thyroid sections.

A. Normal thyroid follicles of non-immunized control. [C3, cryostat, tol. blue, x10].
B. Darkly stained more compact cells representing thymocytes could be distinguished from paler stained less tightly packed parathyroid cells. [C2, cryostat, tol. blue, x10].
C-D. Cutting sections through an entire thyroid lobe allowed for an appreciation of how the tail of the thymus in D could be misinterpreted as a focal lymphoid aggregate when not viewed with its adjacent parathyroid gland in C. [C1, cryostat, tol. blue, x10].
E-F. Cryostat sections did not preserve structure well, these consecutively cut sections show areas difficult to distinguish parathyroid or thymic origin. Contrast these images with 2.12.4.C-D from plastic sections in which ultrastructure is well conserved. [BNP male 2B, cryostat, tol.blue-E, H&E-F].

Figure 2.24 Splenocyte transfer recipient thyroid sections.

A. Thyrocyte depth varied significantly within follicles irrespective of immunization or splenocyte transfer. Similarly, follicular heterogeneity was a normal feature. [FNP female 1R, LR white, tol.blue, x40].
B. Occasional follicles with active apical thyrocyte endocytosis (arrowed) were normal features, no more common in immunized or control thyroid glands. [FGI female 1R, LR white, tol.blue, x20].
C. Parathyroid glands were composed of clear (C), intermediate (I) and darkly (D) stained cells. A bundle of neural tissue (N) is seen adjacent to this thyroid. [FNP male 1B, LR white, tol.blue, x10].
D. Parathyroid cysts are remnants of the ultimobranchial vesicle with microvilli lining their cavities. [FGI female 1R, LR white, tol.blue, x20].
E-F. Ectopic cortical thymus present in non-primed recipient, densely packed large nucleated thymocytes. [FNP male 2R, LR white, tol.blue, x10-20].

Figure 2.25 Immunized group 2 thyroid sections, varying thymic and parathyroid appearances.

A-B. Ectopic thymus (T) could be large but was always seen closely associated with parathyroid tissue (P). [MBB 0, LR white, tol.blue, x4-10].
C-D. Thymus and parathyroid could be found separated by a capsule and connective tissue (C) or form a single structure (D). Thymus can have a medullary appearance with large, pale staining cells (C) and a cortical appearance with densely packed dark cells (D) [GIB 1R (C), GIL 1B (D), LR white, tol.blue, x10].
E. When at the tip of a parathyroid (P), sectioning artefact could give the impression of being an intrathyroidal infiltrate but located adjacent to the cyst (C) and thymus (T) were

useful indicators of parathyroid tissue (confirmed by further sectioning) [GIB 0, LR white, tol.blue, x10].

Figure 2.26 Immunised group 2 and splenocyte recipient thyroid sections.

A-D. A small edge of medullary thymus could be difficult to distinguish from parathyroid in a single section (A). The larger pale staining cells of the medulla contrasted with the smaller, denser cells clustered around the small venule, likely to be mature thymocytes (B). Murine Hassal bodies (HB) were smaller then human equivalents and contain less keratin but further aid the detection of thymus. Further into the section it becomes easier to differentiate between parathyroid and thymus (D). Mast cells (MC) were seen individually, mostly in their normal location, the connective tissue septae, but occasionally in parathyroid tissue (B). [GIL 1R, LR white, tol.blue, x10 A/C, x20 B, x40 C].
E-F. This thin strip of thymus gradually faded towards the edge of the gland, became less well defined and developed an atrophic appearance with adipocytes. This may represent thymic involution and replacement by fibroadipose tissue an age related change [FNP male 1B, LR white, tol.blue, x10].

Figure 2.27 Orbital histology from immunized group 1 and non-immunized mice.

A. Normal ocular muscle in cross-section showed connective tissue intervening muscle bundles. [C 2, paraffin, H&E, x10].
B. Ocular muscle showing an artifactual separation of fibres due to fracturing of the section. No lymphocytic infiltration developed in any immunized mice. [GI 2R, paraffin, H&E, x10].
C. No accumulation of PAS positive mucopolysaccharides developed between ocular muscles (M) or connective tissue of immunized group 1. [GI 2R, paraffin, PAS, x10].
D. Sporadic multi-vacuolated adipocytes were found within areas of connective tissue in control and immunized mice representing the normal background of adipogenesis. [FNP 1R, LR white, tol.blue, x10].
E. Mast cells were normal residents in the connective tissue adjacent to lobules of orbital fat in control and immunized mice, no lymphocytic accumulations were present. [MBL 1R, LR white, tol.blue, x10].

Figure 2.28 Striated muscle from immunized group 2 and splenocyte recipients.

A-B. Ocular muscle with a packed appearance represents the global muscle layers (A). Adjacent sections of orbital muscle layers had buckled muscle fibres caused by contraction, the connective tissue spaces between them exaggerated in this section by crease artifact. [FNP 2R, LR white, tol.blue, x10].
C. Ocular muscles of immunized mice show similar contraction with no evidence of inflammatory changes.
D. Myofibrils have normal appearances (N) alongside knots (K) and areas of dense contraction bands (CB) [GIB 2R, LR white, tol.blue, x10].
E. On cross-section contraction bands are less evident [GIB 1B, LR white, tol.blue, x10].
F. Striated muscle attached to the thyroid usually appeared tightly packed but contractions could also be seen, tending to be at the edge of the specimen, indicating the changes were not restricted to the ocular muscles. [FNP male 1B, LR white, tol.blue, x10].

Figure 2.22 Immunized Group 1 thyroid histology

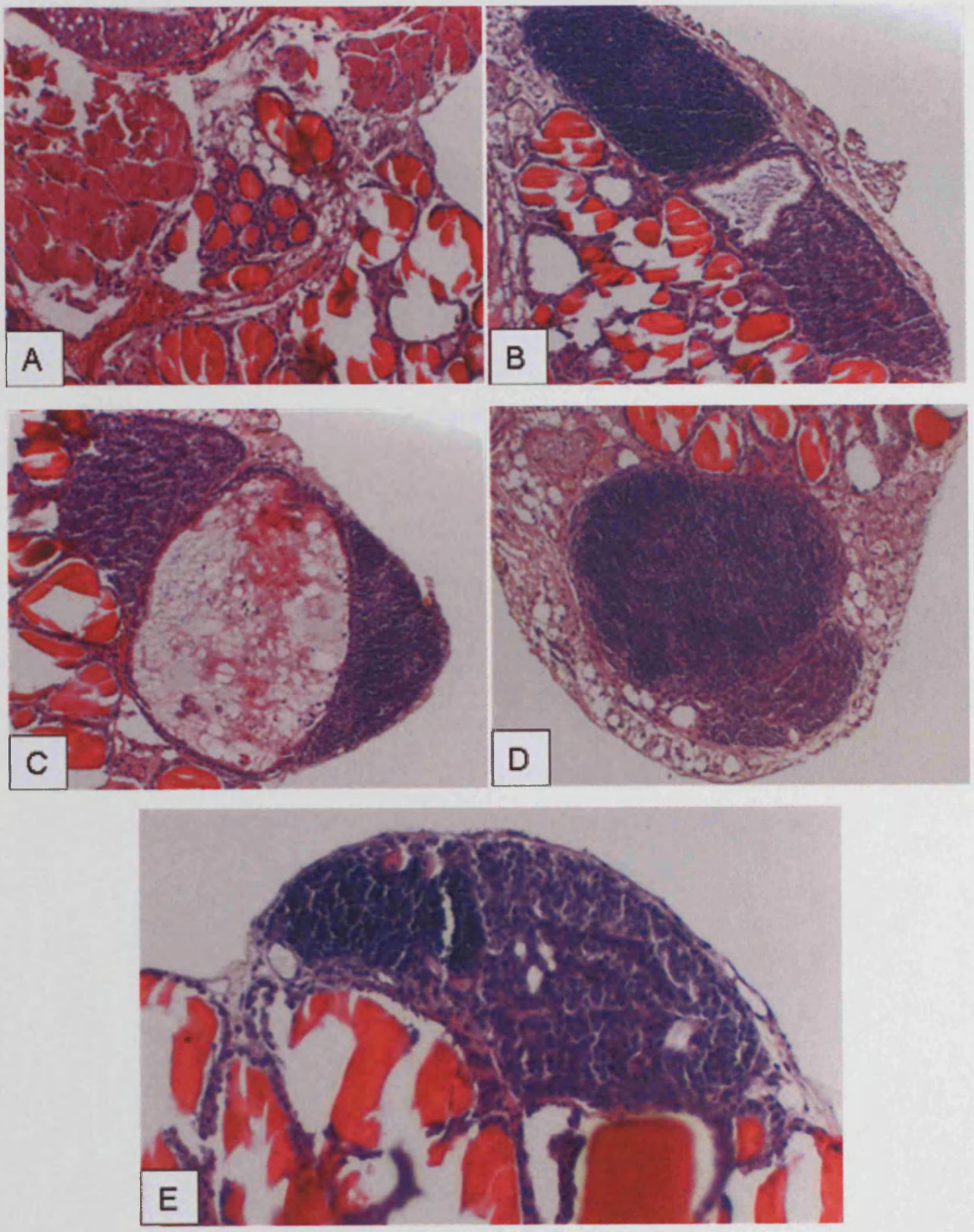

Figure 2.23 Non-immunized and non-primed recipient thyroid sections

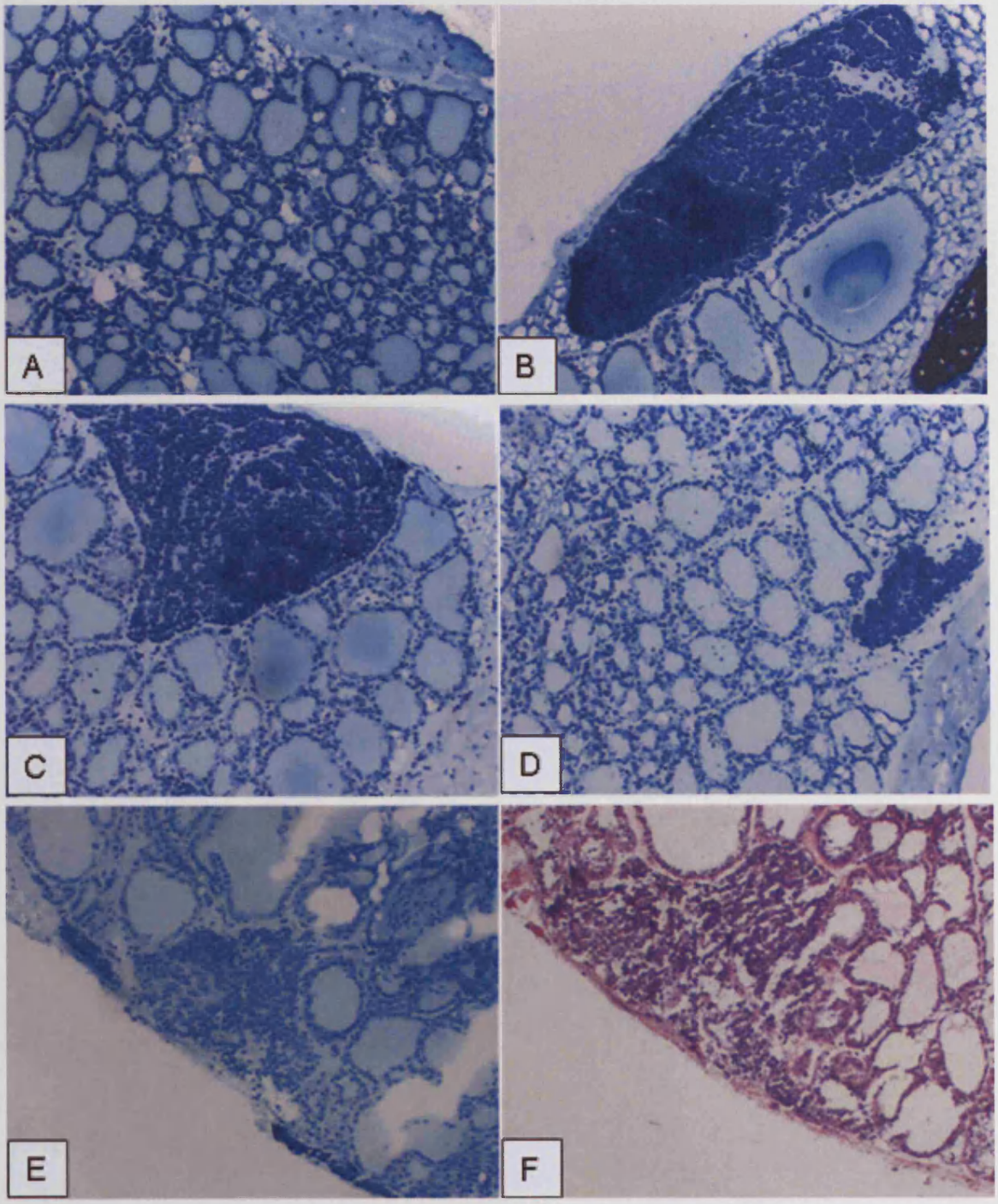

Figure 2.24 Splenocyte transfer recipient thyroid sections

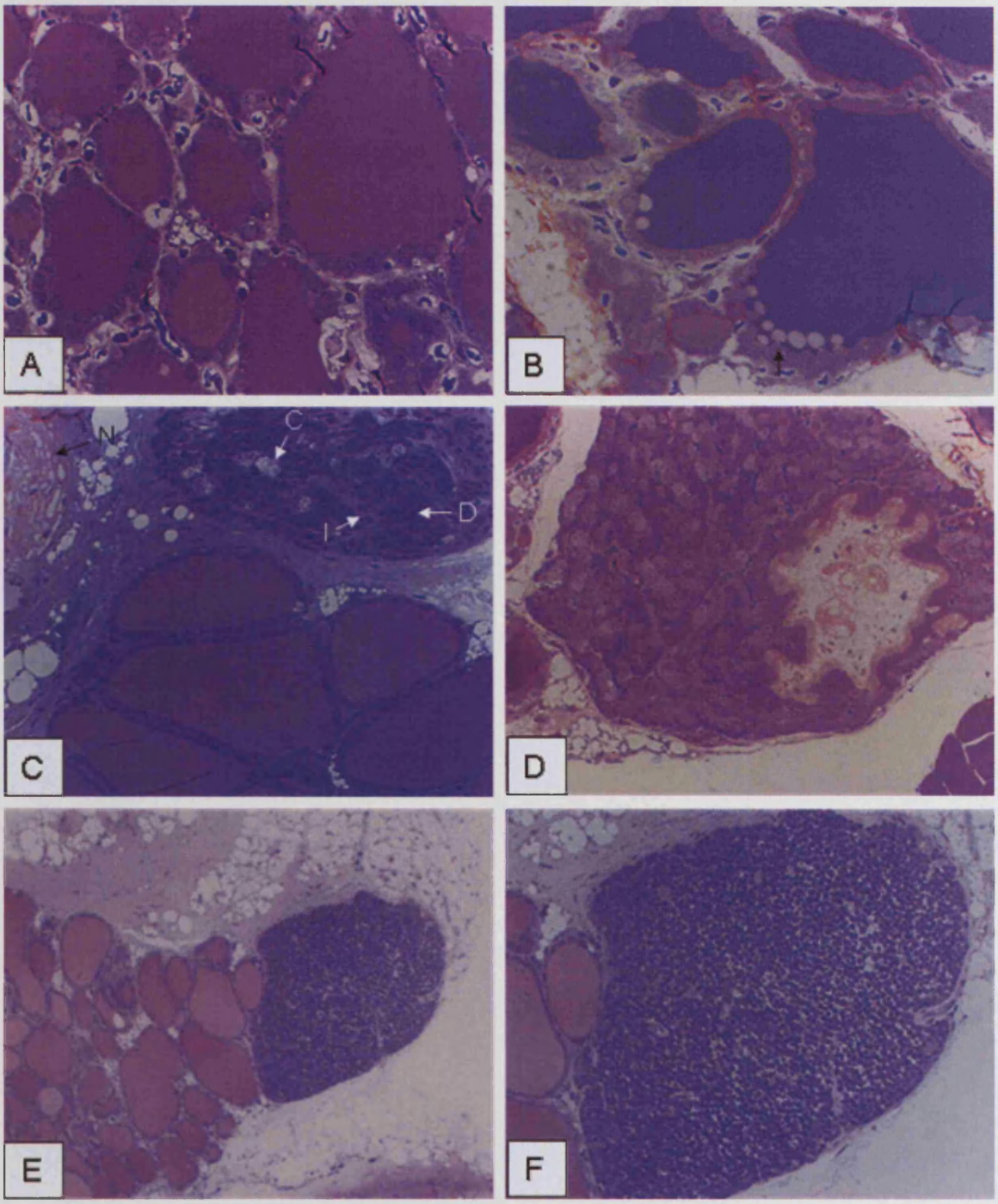

Figure 2.25 Immunized group 2 thyroid sections, varying thymic and parathyroid appearances

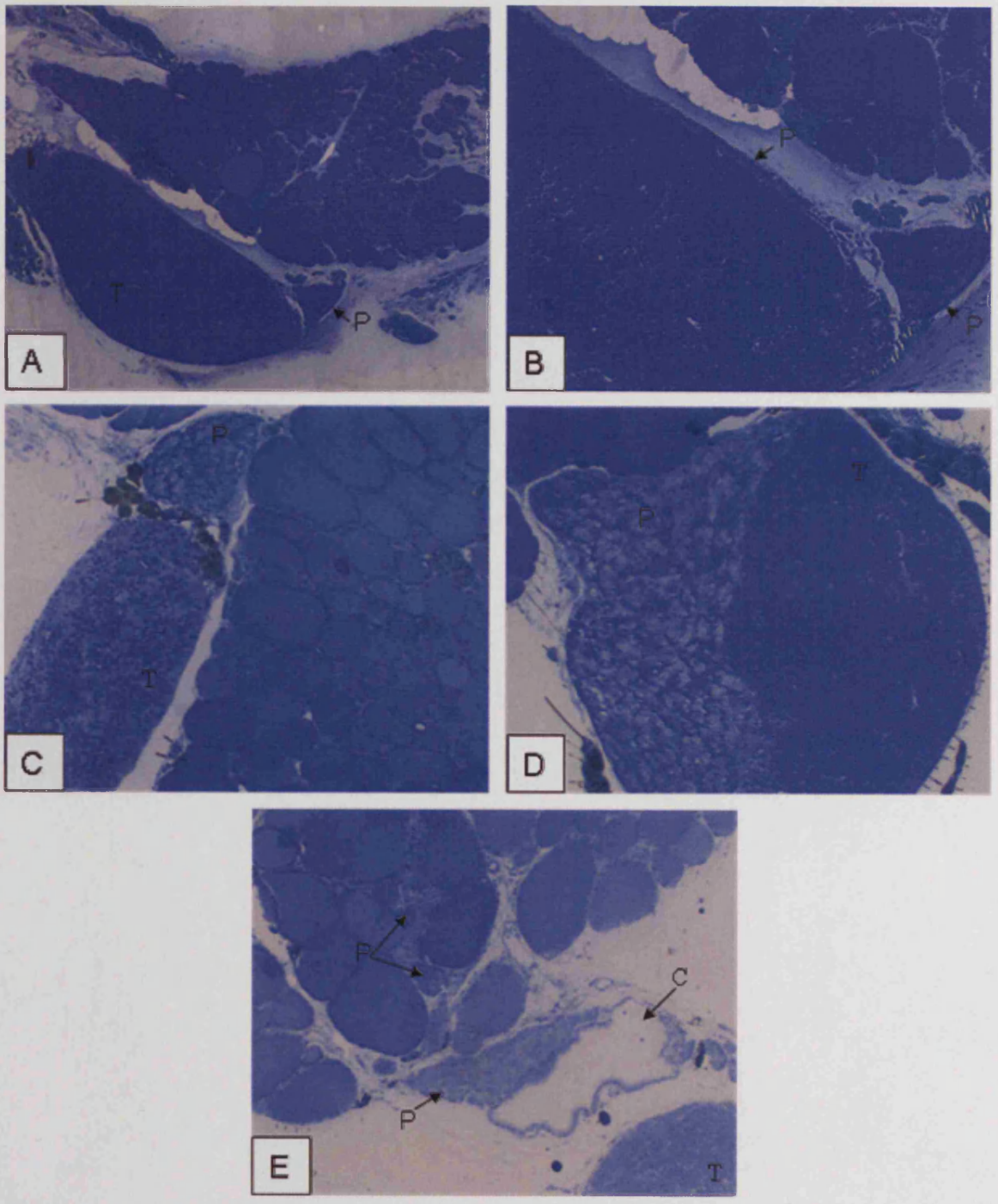

Figure 2.26 Immunized group 2 and splenocyte recipient thyroid sections

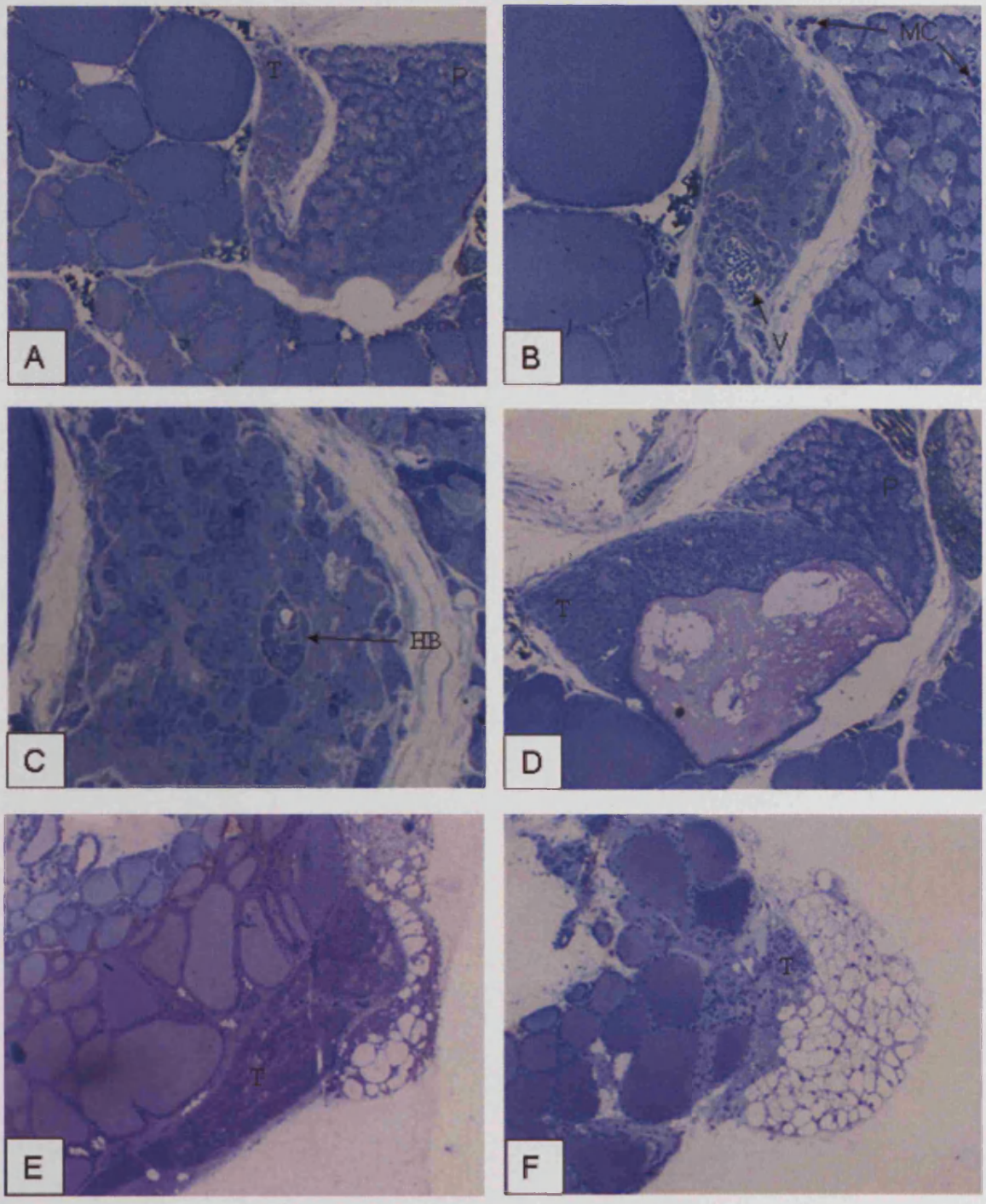

Figure 2.27 Orbital histology from immunized group 1 and non-immunized mice

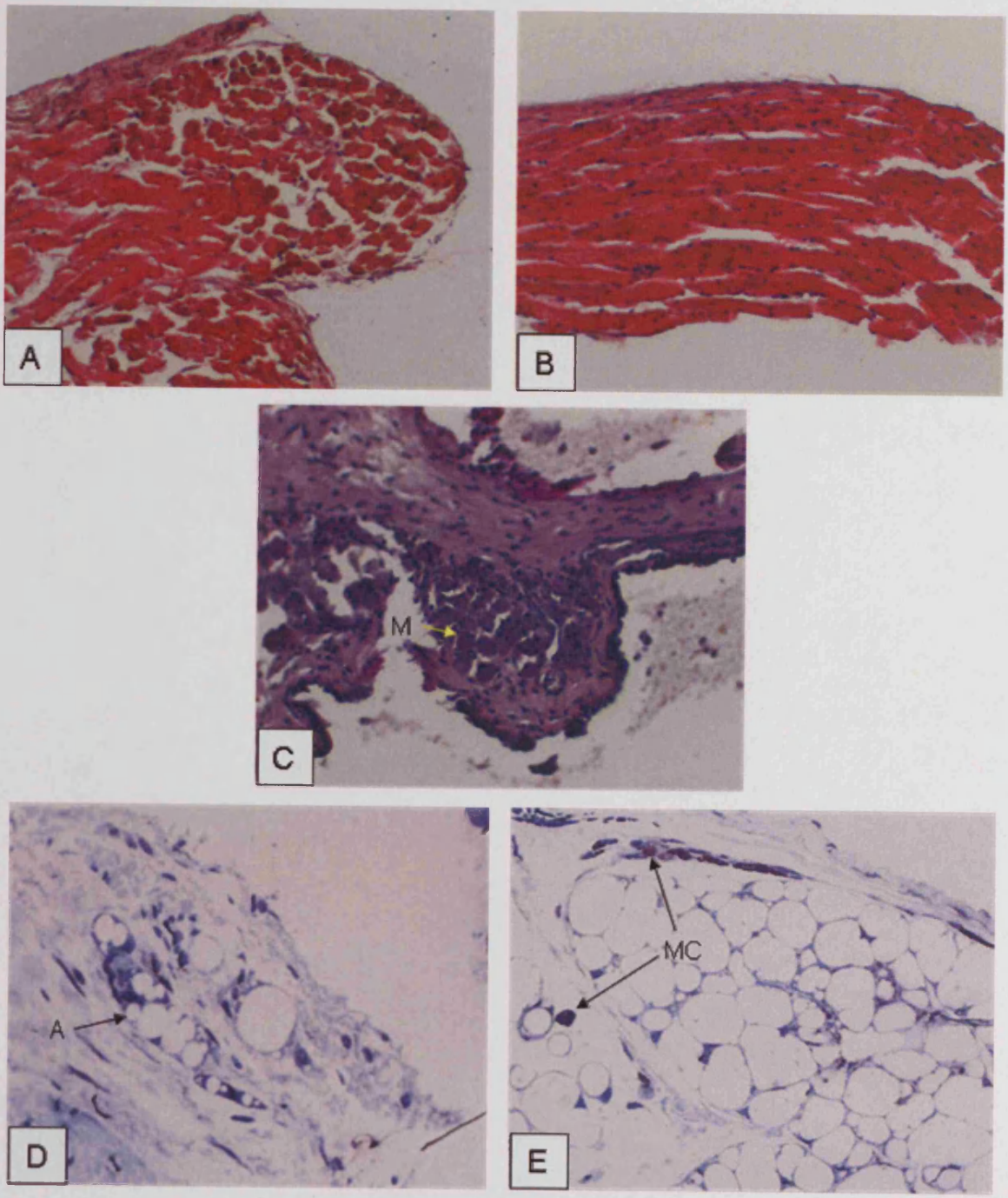

Figure 2.28 Striated muscle from immunized group 2 and splenocyte recipients

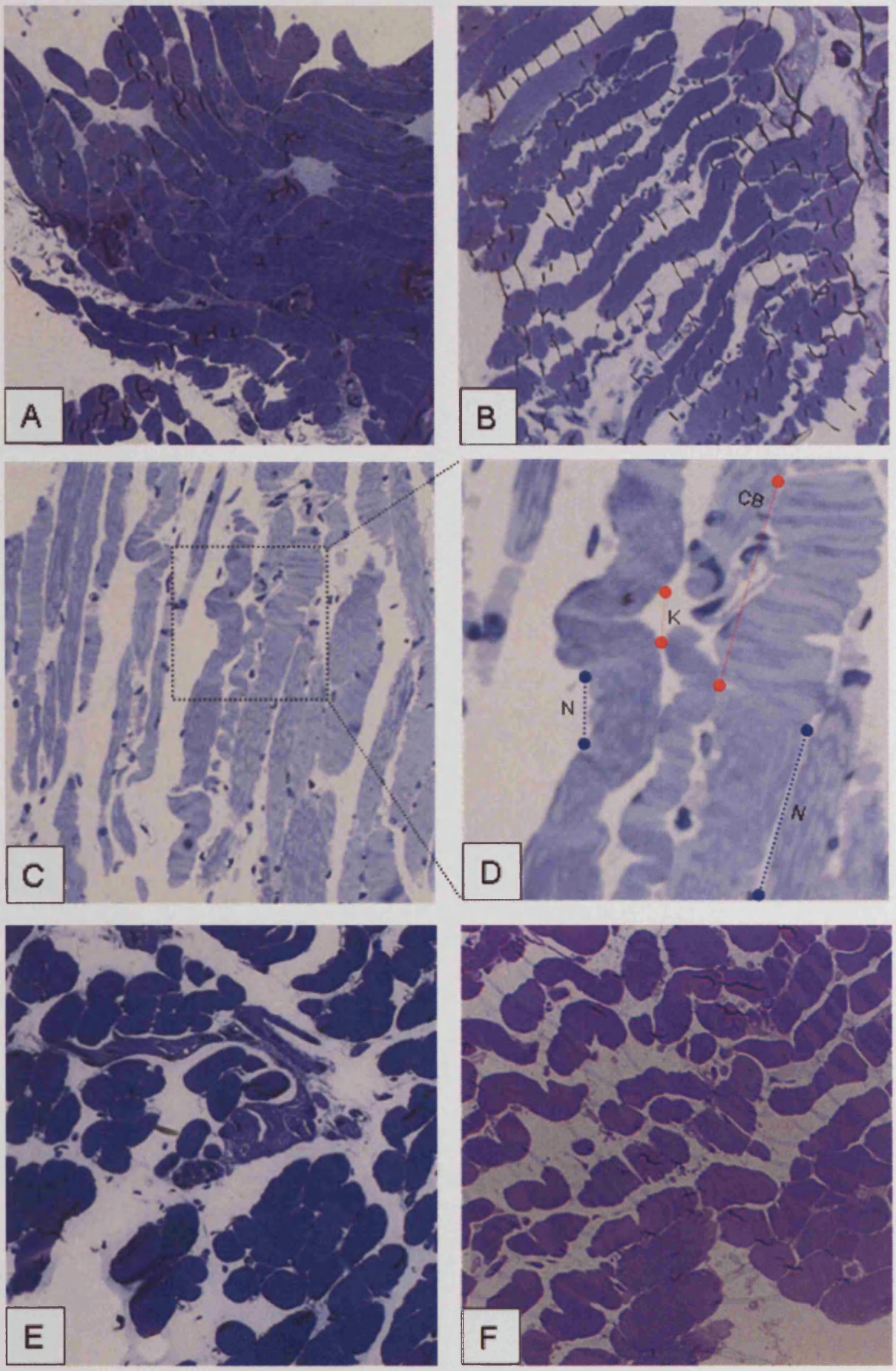

Figure 2.29 Embryological origin of thyroid, parathyroid and thymus

A. Formation of organ primordia within branchial pouches.
B. Ventral descent of organs to normal resting sites.
(Adapted from [193])

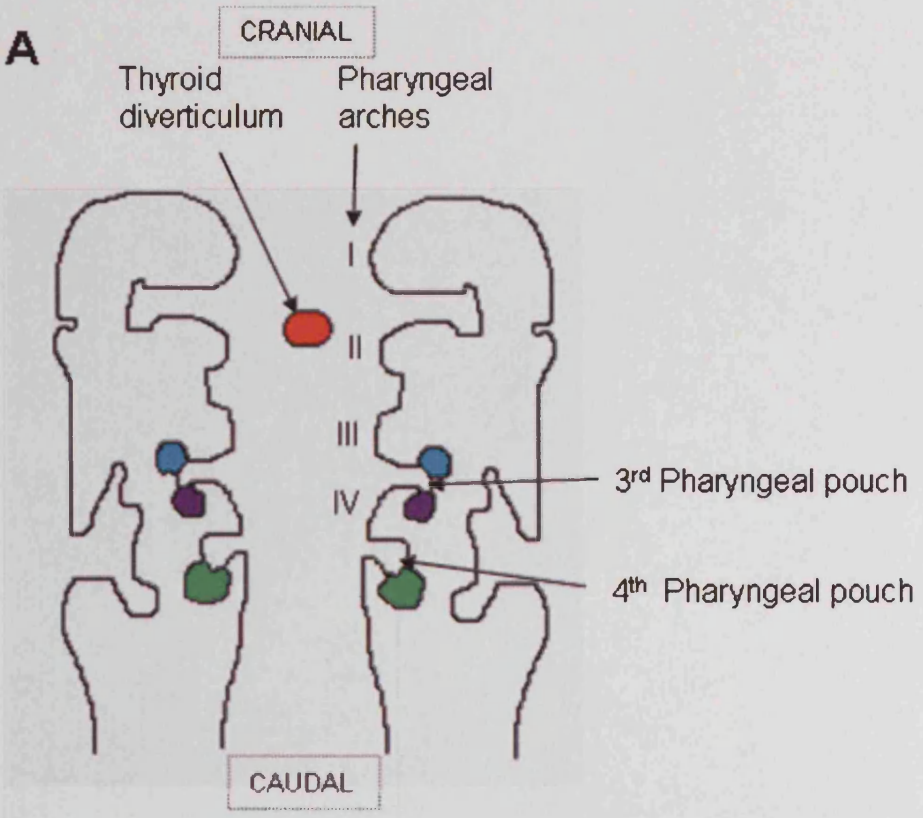

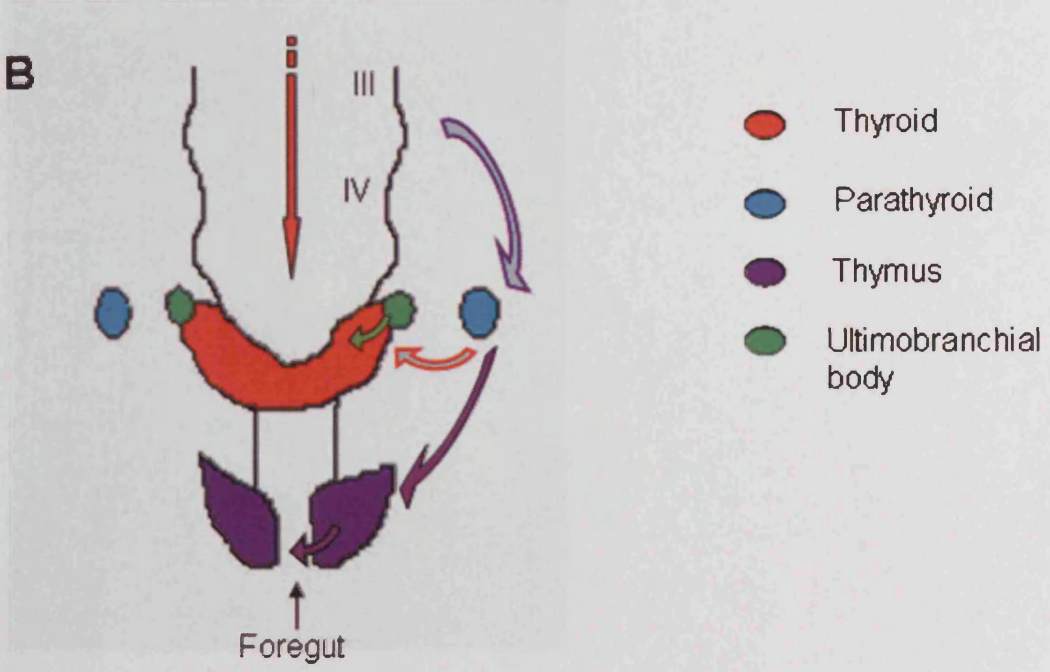

Table 2-8 Individual results of immunized group 1 females

Immunized group 1 females	Anti-ecd/mbp ELISA OD	Anti-TSHR Flow 'D'	TSAB SI	TBII %	T4 µg/100ml
GI 0	0.67	0.84	1.5	108	10.5
GI 1R	0.39	0.52	2	93	9.4
GI 2R	1	0.8	13.7	32	6.5
GI 3R	0.48	0.72	2.1	70	8.8
GI 2B	0.48	0.41	1.3	57	-
ECD 0	1.89	0.9	2.9	27	-
ECD 1R	1.79	0.81	21.5	102	8
ECD 2R	1.85	0.82	1.6	87	8.8
ECD 1B	2.59	0.66	0.4	85	8.5

Table 2-9 Individual results of local female single splenocyte transfer recipients

Single transfer female local	Anti-ecd/mbp ELISA OD	Anti-TSHR Flow 'D'	TSAB SI	TBII %	T4 µg/100ml
BGI 0	0.655	0.1	0.7	120	6.3
BGI 1R	0.386	0.06	0.8	130	5.6
BGI 2R	0.3385	0.13	1	144	6.1
BGI 1B	0.364	0.07	1.1	115	8.5
BGI 2B	0.2845	0.09	0.8	139	12
BECD 0	0.2615	0.12	1.1	120	7.5
BECD1R	0.3805	0.1	1.3	116	6.3
BECD2R	0.369	0.14	1.8	104	6
BECD1B	0.305	0.29	0.9	123	5.2
BECD2B	0.3845	0.16	1.1	110	5.7
BNP 1R	0.64	0.09	0.8	79	4.3
BNP 2R	0.6605	0.16	1	115	3.3
BNP 1B	0.4635	0.11	1	115	8.5
BNP 2B	0.6755	0.17	0.9	104	5.4

Table 2-10 Individual results of local male single splenocyte transfer recipients

Single transfer male local	Anti-ecd/mbp ELISA OD	Anti-TSHR Flow 'D'	TSAB SI	TBII %	T4 µg/100ml
BGI 0	0.1745	0.1	1.4	97	4.7
BGI 1R	0.1955	0.12	1.5	102	3.3
BGI 2R	0.2205	0.1	0.9	90	2.2
BGI 1B	0.272	0.14	1.1	87	9.8
BGI 2B	0.2545	0.29 (!)	0.8	106	2.9
BECD1R	0.152	0.44 (!)	0.9	71	2.7
BECD2R	0.2975	0.16	1.1	39	2.4
BECD1B	0.201	0.08	1	79	2.4
BECD2B	0.265	0.31	1.4	115	2.5
BNP 1R	0.476	0.2	0.9	76	3.7
BNP 2R	0.483	0.06	0.6	91	5.5
BNP 1B	0.6295	0.6	0.6	93	6.6
BNP 2B	0.438	0.3	0.5	81	5.3

(!) bias of D value calculation indicating a left shift but not positive result

Table 2-11 Individual results of French female single and double splenocyte transfer recipients

Single transfer female French	Anti-ecd/mbp ELISA OD	Anti-TSHR Flow 'D'	TSAB SI	TBII %	T4 µg/100ml
FGI 0	0.392	0.06	0.6	129	4.8
FGI 1R	0.277	0.07	0.6	86	4.6
FGI 2R	0.366	0.27	0.7	54	4.6
FGI 3R	0.345	0.18	0.7	121	4.9
FECD 0	0.355	0.11	0.8	74	4.5
FECD1R	0.5575	0.31	1	167	7.3
FECD2R	0.7525	0.1	1.3	116	5.6
FECD3R	0.511	0.14	1.2	64	3.9
FNP1R	0.424	0.44	0.7	68	10.6
FNP1B	0.434	0.21	0.6	53	3.5
FNP2B	0.3955	0.02	0.8	104	4.8
Control 1	-	-	1	101	4.2
Control 2	-	-	1	126	3.4
Female double transfer French					
FGI 1B	-	0.04	0.8	76	4.8
FGI 2B	-	0.62	0.7	68	4.7
FGI 3B	-	0.31	0.8	75	4.2
FECD1B	-	0.24	0.9	88	5.8
FECD2B	-	0.18	0.6	88	5.1
FECD3B	-	0.18	1.1	72	4.6

Table 2-12 Individual results of French male single and double splenocyte transfer recipients

Male single transfer French	Anti-ecd/mbp ELISA OD	Anti-TSHR Flow 'D'	TSAB SI	TBII %	T4 µg/100ml
FGI 0	0.5535	0.06	1.4	126	4.5
FGI 1R	0.358	0.23	1.4	253	5.6
FGI 2R	0.345	0.11	2	233	4.7
FGI 3R	0.3535	0.22	0.6	49	5.7
FECD 0	0.508	0.06	0.9	202	3.9
FECD1R	0.3155	0.12	0.8	137	8
FECD2R	0.5335	0.36	1.4	225	10.5
FECD3R	0.385	0.12	1	192	10.1
FNP 1R	0.2635	0.15	1	122	9.1
FNP 2R	0.326	0.05	1.8	140	8.2
FNP 1B	0.438	0.2	1.6	75	4.2
FNP 2B	0.4265	0.2	1	45	4.4
Control 1	-	-	1	101	2.8
Control 2	-	-	1	94	4.0
Male Double Transfer French					
FGI 1B	-	0.28	0.8	108	5.1
FGI 2B	-	0.05	0.9	93	2.5
FGI 3B	-	0.17	0.9	-	4.4
FECD1B	-	0.09	0.9	112	4.5
FECD3B	-	0.10	1	113	6

Table 2-13 Individual results of immunized group 2 females

Immunised group 2 females	Anti-TSHR Flow 'D'	TSAB SI	TBII %	T4 µg/100ml
GIL 0	0.17	0.8	125	4.3
GIL 1R	0.08	0.7	102	4.1
GIL 2R	0.07	0.1	112	4.3
GIL 1B	0.6	0.9	110	4.2
GIL 2B	0.24	1	137	2.7
GIB 0	0.42	1.1	90	4
GIB 1R	0.57	1.2	95	4.7
GIB 2R	0.75	1.1	120	4.4
GIB 1B	0.82	1	126	4.9
GIB 2B	0.72	1.4	125	3.5
ECDL 0	0.8	0.8	103	3.5
ECDL 1R	0.99	0.9	116	3.9
ECDL 2R	0.84	0.8	145	4.1
ECDL 1B	0.8	0.8	139	4
ECDB 0	0.89	0.9	121	2.6
ECDB 1R	0.87	0.7	141	4.3
ECDB 1B	0.82	0.8	124	-
ECDB 2B	0.93	1.1	132	2.4

2.4. Discussion

Outside of Belgium there has been little success in using human TSHR DNA or protein vaccination to reproduce thyroiditis or ophthalmopathy in mice. In view of the reported model having the highest incidence of TSHR induced thyroiditis we aimed to independently confirm the findings and extend knowledge of the model by replicating conditions used previously as closely as possible. Instead, we find no evidence of thyroiditis and ophthalmopathy and discuss our experimental findings, limitations and possible improvements.

Immunized group 1 and 2 largely share a high incidence of forming anti-TSHR IgG but the presence of limited TSAB and TBII activity and elevated T4 values is exclusive to group 1. An instant impression might be that the first group behaves like the outbred strain NMRI Graves' model whereas group 2 has no inhibiting/stimulating antibodies induced by TSHR immunization. However in group 1, T4 and TSAB do not correlate (ρ= -0.635, p=0.126, Pearson), questioning the finding. Positive TSAB in group 1 could be artefactual, the result of not using an IgG fraction, as seen in two female mice immunized with MBP alone [158]. With the wide range of assays used and the need for repeats, the volume of serum available was limited and insufficient for an IgG fraction. The potential loss of sensitivity using whole serum is an issue if a small proportion of mice are false positives. However, BALB/c do produce TSAB [94; 194] and our original assay not being fully optimized for TSAB may be lacking in sensitivity. More reliable future TSAB measurement would use a modified TSAB selective working buffer [190].

Initially in the reported adoptive transfer model of thyroiditis, naïve recipients had no transfer of IgG antibody response to; ECD/MBP, CD4+ enriched cells or non-primed cells, when assessed by ECD/MBP ELISA after 16 days [185]. When this was repeated in subsequent experiments up to 12 weeks after transfer, ODs ranging from 0.4-1.2 were reported as positive [182]. From the ECD/MBP ELISA results of the single transfer group, reactivity to the ECD/MBP was unable to be transferred to the local colony. In contrast, 6/16 French recipients had ODs between 0.5-0.75 that were considered positive against controls and 5/16 of these received ECD/MBP primed cells. If the response were from a residual ECD/MBP contaminant during the in vitro priming step one might expect more of the pcDNA3-TSHR primed recipients to also be positive. ECD/MBP reactivity did not correlate with the negative flow anti-TSHR results (ρ=0.07, p=0.796), but there is a

suggestion that limited transfer is occurring in the main from ECD/MBP primed splenocytes.

Modifying environmental conditions had no effect on the high incidence of anti-TSHR IgG detected by flow cytometry in the ECD/MBP immunized groups. In the pcDNA3-TSHR group, environment modifications lead to higher numbers of mice with anti-TSHR. This is at odds with the fact that the entire pcDNA3-TSHR first immunized group developed anti-TSHR while housed in local conditions. Subtle differences exist between the first and second groups that may be significant. On importation, the second immunization group was established on local feed, water and bedding for a period of three weeks. This resulted in their immunization being delayed to 9 weeks in comparison to the first group who were immunized at 6 weeks. Environment modifications were made at the time of immunization for the second group, the mice were exposed to a difference in dietary iodine, a factor thought to alter the susceptibility to thyroiditis in several animal models (reviewed [195]). In the autoimmune prone BB rat, the increased incidence of spontaneous "thyroiditis" with higher dietary iodine, is carefully re-described as being "thyroid associated lymphoid tissue" given its high degree of organisation similar to secondary lymphoid organs and absence of follicular destruction [196; 197; 198]. However in NOD-H-2^{h4} mice the term "thyroiditis" is used to describe the increased spontaneous infiltration seen in line with raised iodine [160]. The local feed (RM1, SDS) has 1mg/kg iodine while the feed used in Brussels (RN-01, Carfil) has 4.5mg/kg. An enriched iodine diet can be induced using water with iodine at 6.5 mg/litre, not far off the 4.5mg/kg used in the feed [199]. Mice on average will drink 3-7 mls of water per day and eat 3-4 g of feed. In order to confirm the high iodine diet is ingested requires measurement of urinary iodine at 50-100 μg/day (normal levels 7 μg/day). Additionally, the drinking water iodine concentrations should be determined given approximately equal volumes of feed and water is ingested.

Wishing not to overdraw the role of iodine or environmental processes an alternative explanation can be given. Flow histograms for ECD/MBP mice were from the fourth immunization point (9 weeks) and were all positive for anti-TSHR. At this time 1/5 locally treated and 2/5 environment modified pcDNA3-TSHR immunized mice were positive. The pcDNA3-TSHR flow histograms illustrated (figure 2.6.1&7) are from five weeks later (14 weeks), at time of sacrifice, when there has been an increase in the environment modified group to 5/5 and no increase in the locally treated. This, along with the ECD/MBP ELISA

results (figure 2.5.1) confirm a slower antibody response to the genetic immunization and is slightly later than reported previously when most mice were positive at 11 weeks [165]. This paper shows that cardiotoxin pretreatment brings forward the anti-TSHR response by several weeks in comparison to the vector in sucrose. We were unable to use this adjuvant and the pcDNA3-TSHR mice from group 1 and 2 mice were kept in identical conditions and only differ by a 3 week delay in the immunization, the apparent lack of anti-TSHR in the environment modified group could be due to them still evolving an anti-TSHR response and the statistically significant difference may represent a type 1 error. The high incidence of anti-TSHR induced in pcDNA3-TSHR immunized mice 11/15 (groups 1 and 2) is slightly at odds with other reports using plasmid DNA vaccination [167; 169]. This may be a sampling effect due to antibodies measured at an earlier time point in these studies, strain and environment variation.

While the flow detection of anti-TSHR would seem highly specific it produced positive results from two non-primed recipients. Occasionally when using GPI based flow cytometry to detect anti-TSHR IgG and IgA in humans there are normal individuals who demonstrate binding of TSHR who are otherwise TBII and TSAB negative [34]. One out of eleven mice receiving a double splenocyte transfer was positive for anti-TSHR, it is likely this represents a similarly non-specific event.

There were slightly lower T4 values in the protein immunized mice of the second group. It is noteworthy to mention the overall worse morbidity in protein immunized mice noticed in the first immunized group (2.2.10). This deteriorated in the second group when the pertussis vaccine had to be substituted for the toxin. Mortality rates rose with 3/10 mice dying within 3 days of an immunization. The mice were lost following different immunizations, one lost at second, third and fourth points, with no mice dying following any genetic immunizations. The changes in T4 may be related to a non-thyroidal illness related to the adjuvant.

Examining the cytokine profiles of splenocytes proposed to transfer thyroiditis we see no significant differences in the major TH1 and 2 cytokines irrespective of method of stimulation or environment in which the mice are raised. However, cryotherapy adversely affects proliferative and cytokine responses of most splenocytes [200; 201] and the very low levels of cytokines produced by these thawed splenocytes differ from those used fresh in other studies on TSHR induced murine Graves' disease [167; 168]. Given the very low

responses of thawed splenocytes, their capacity to transfer disease may similarly be affected and it would be interesting to track them in vivo. The homing of H^3-thymidine labeled splenocytes to the lungs in a transfer model of viral respiratory infection illustrates a possible technique that could clarify further attempts to transfer thyroiditis to naïve recipients [202]. Ex vivo splenocytes, without freezing, would ideally be transferred and examined for cytokine/proliferation responses in future studies.

The presence of ectopic thymus in parathyroids/thyroids has been detected in several mammals; dogs, cats, guinea pigs, bats, mice, rats, baboons and humans [191; 192; 203; 204; 205; 206] and conversely, ectopic parathyroid can be found in the thymus [207]. In the cat the almost constant appearance of the anomaly was referred to as the "*internal thymic lobule of the thyreoid*" [208]. Discussion on the origins initially centred on a IV pharyngeal pouch structure but included suggestions that the thymic tissue within the thyroid may be related to thyrocyte transformation [191], but embryological studies demonstrate this to be a developmental anomaly. The murine third pharyngeal endodermal pouch produces a parathyroid from a small dorsal segment and thymus from a larger ventral segment. This situation only exists in mammals with all other higher vertebrates forming parathyroid ventrally and thymus dorsally [209]. At 11 days gestation the parathyroid primordium appears in the third pharyngeal pouch roughly at the same time as the equivalent area in the cranial portion of the fourth pouch degenerates (Figure 2.14.A). This region in other mammals forms the superior parathyroid and its degeneration explains the presence of only two parathyroids in mice compared with four in humans. At the end of day 11 the branchial complex is separating from its ecto/endodermal membrane origin with the parathyroid anlage at its cranial portion connected to the caudal thymic anlage. Thymic ectoderm is destined to form the medulla, endoderm the cortex and by 12½ days the two complexes are no longer distinct following invasion of blood vessels and lymphoblasts. It is also at this time the fourth branchial pouch derived ultimobranchial vesicle reduces to form a small epithelial nodule that may persist (figure 2.12.1.B/C). By day 13, thymus and parathyroid separate or can remain connected by a thin cord of cells, they migrate ventrally to meet the thyroid and during day 14 the parathyroid should remain with the thyroid while the thymus continues its ventral descent (figure 2.14.B). It is at this point a fragment of thymic tissue can remain attached to parathyroid and incorporated into the thyroid on days 14 and 15 [210]. We find this to be a common anomaly amongst BALB/c in agreement with others [192; 204]. Misinterpretation as focal lymphoid infiltrates, in both BALB/c and NOD mice, can arise due to variation in appearances of medullary and cortical thymus. Serial

sections tracing the full extent of any such areas and their association to the parathyroid gland should be available when proposing any histological evidence of focal thyroiditis.

Incidence of ectopic thymus in BALB/c thyroids approaches 100%, is often unilateral and is sometimes seen only as a collection of lymphocytes rather like those in Figure 2.12.3.F (personal communication from Thelma Dunn quoted in [204]). Given such a high incidence, one can speculate on the likely presence of mutations/polymorphisms or possibly common environmental factors acting to produce such a frequent anomaly in the inbred BALB/c. In looking for reasons for the failure of thymus and parathyroid separation during embryological descent, clues are given by previous experiments. During early thymic development, prothymocytes are attracted to the thymic anlage by embryonic chemokines; stromal cell-derived factor 1 (SDF-1), secondary lymphoid tissue chemokine (SLC) and thymus-expressed chemokine (TECK). Absence of TECK and SDF-1 in the nude mouse thymic anlage cause prothymocytes to home to the parathyroid anlage, resulting in an abnormal thymus [211]. In another model, insufficient retinoic acid synthesis caused a generalised pharyngeal pouch maldevelopment that is lethal and resembles the human DiGeorge syndrome [212]. The formation of the pharyngeal arches is largely fashioned by neural crest cells and gene defects in; *Hoxa3, Pax-1, EYA-1, GCM2* and *FOXn1* are important in parathyroid and thymus development [193; 213; 214]. Ectopic thymus develops in two mutants; heterozygous, $Hoxa3^{+/-}Pax1^{-/-}$ and homozygous $Pax9^{-/-}$, due to delayed separation from the pharynx, however the resultant ectopic thymus is hypoplastic and not thyroid associated in contrast with the BALB/c we have examined [215; 216].

While we were unable to give volumetric estimates of ectopic thymus or make any comment on whether TSHR immunization influences this, we would report a wide range in the sizes of ectopic thymus present. It leads us to review previous reports linking the thyroid and thymus. Factors influencing the thymus to cause hypertrophy include TSH and thyroxine [217; 218]. An enriched iodine diet produced a transiently increased incidence of thyroid associated ectopic thymic tissue in Wistar rats after 3-6 weeks and occurs alongside lowered anti-colloid antibodies [199]. In an unrelated model, a possibly immunosuppressive role is hinted at in null 1α hydroxylase mice that have enlarged parathyroid lymphoid tissue (morphologically ectopic thymus) had a reduced $CD4^+$ and $CD8^+$ peripheral lymphocyte count [219]. Meanwhile in humans the role of an enlarged thymus and benefits of it's excision in Graves' disease has been considered to have varying degrees of success for many years and remind us of an alternative cause of a

breathless thyrotoxic patient [220; 221; 222]. The presence of thymic medullary lymphoid follicles in patients with Graves' differ subtly from those of other patients with autoimmunity; myasthenia gravis, rheumatoid arthritis and systemic lupus erythematosus and are rarely found in non toxic nodular goitre or after parenteral immunization [223; 224]. The role of such follicles in myasthenia gravis is the expansion and affinity maturation of B-cell clones (reviewed in [225]). Thymectomy for thymoma has shown only moderate clinical benefits in myasthenia gravis [226], an explanation for this may be the persistence of ectopic thymic tissue such as that associated with the thyroid [227]. In any case, the enlarged thymus in Graves' disease patients has been shown to reduce in volume and density following antithyroid treatment in parallel with reduced anti-thyroid and anti-TSHR antibodies [224; 228]. The latter group also detected TSHR mRNA and protein in normal thymus. A further Graves' related effect is thymocytes have been shown to proliferate in response to immunoglobulins from a patient with Graves' and an enlarged thymus [229]. Altogether with the more recent report of structures within thymic epithelium that resemble thyroid follicles and contain thyroglobulin [230], give a sense of the thymus being another possible extrathyroidal autoimmune target rather than a bystander to the generalised thyrotoxicosis. However, it remains that reduction in thymus size on treatment with antithyroid therapy, like the improved thyroiditis itself, could be due to a drug related immunosuppression or to normalization of the thyrotoxicosis [231], but in all probability, results from a combination of both. None of the models utilizing TSHR as an antigen have so far examined the possible thyroid and thymus relationship and it would seem worthy of further investigation.

Improved techniques characterising thyroiditis such as whole thyroid flow cytometry are an interesting and essential part of future investigations promising a more quantifiable index of cellular infiltrates and possibly distinguishing them from ectopic thymus [232]. Identifying some of the thymocytes could be done, as suggested, by identifying double positive $CD4^+$ and $CD8^+$ cells but more markers would be required to identify the significant proportion of mature thymocytes that are singly $CD4^+$ or $CD8^+$ and the progenitor thymocytes that are pre-TCR expression [233].

Noteworthy fixation artefacts were present in the parathyroid and ocular muscles. Firstly, the apparent light, intermediate and darkly stained parathyroid cells were originally thought to represent the level of secretory activity of these cells. It has since been shown to be due to the level of cellular disorganization caused by incomplete immersion fixation

[234]. Disintegration of organelle membranes produced pale stained cells with intermediate forms, while well preserved cells stained darkly. The heterogeneous staining could be corrected either by perfusion fixation or altering buffer properties, but for our purposes of parathyroid identification the artifact is a useful aid to recognition. Secondly, was the appearance of irregular spaces between ocular and some skeletal muscles, suggestive of oedema. During routine preparation ocular muscles were excised from the common tendinous insertion at the orbital apex and then from the globe, involving a significant degree of manipulation for a delicate tissue prior to fixation. While stretched in vivo they measured approximately 3.5mm but when cut, rapidly contract to less than 1.5mm, their size prevented us fixing them stretched. Classically packed skeletal muscle appearances were seen in those attached to the trachea and thyroid, muscle contraction was only present at the edge of these specimens. Skeletal muscle differs significantly in organisation and molecular constituents to the highly specialized ocular muscles, the appearance of packed ocular muscle corresponded to the global muscle layer (reviewed and references in [235; 236]). Adjacent ocular muscles organised into smaller bundles with more connective tissue intervening were the orbital layers and here the contraction artefact produced an irregular redistribution of the connective tissue that might be interpreted as oedema. An awareness of the anatomical variations within ocular muscles is important especially when compounded by artefacts of contraction and hyper-contraction [237]. These changes could be reduced by perfusion fixation, but would restrict onward use of the spleen or thyroids to histology. Alternatively, excising the globe en bloc is possible, leaving the muscles attached to annulus of Zinn, splinted by the optic nerve, then fixed before excising and embedding. The larger size might be sectioned more efficiently in paraffin blocks rather than plastic sections. The process of, fixation after manipulation, that produces contraction artefacts is the same as that used in the BALB/c and NMRI models, contraction artifacts are present in these papers illustrations but are not commented on.

The concept of how delayed the evolution of anti-TSHR to pcDNA3-TSHR has not been emphasized by experiments comparing this method to far more robust immunizations in which co-stimulation enhance the immune response [167; 169]. Techniques using TSHR immunization with co-stimulation are more reliable in raising TSAB, causing thyrocyte hypertrophy and infrequently in older mice, lymphocytic infiltration [170; 171; 172; 173]. Dendritic cells are thought to be important at an early stage of thyroiditis. They are present in significant numbers in normal thyroids, regulate growth and function of thyrocytes, express TSHR and can be used to induce experimental thyroiditis [175; 232; 238; 239]. As an

aside, pertussis toxin used as an adjuvant for TH2 responses in experimental Graves' disease in BALB/c [172] is shown to promote TH1 inflammatory responses via dendritic cells in another organ specific autoimmune BALB\c model, experimental autoimmune uveitis [240]. The advancing complexity of models is inevitable and the importance of inbred and out-bred strains is likewise essential. The newer Graves' models currently do not distinguish an immune infiltrate that is a strain dependent response to thyrocyte/dendritic cell proliferation secondary to TSHR stimulation by TSAB, from a targeted anti-TSHR T cell mediated response. Inclusion of controls receiving recombinant TSH might resolve this. Clarifying existing models is particularly pertinent given the recent description of another stimulating antibody, directed towards IGF-1, indicating a more widespread loss of tolerance occurring in Graves' disease that will likely need to be incorporated into our model systems [42].

In general terms it has been established that DNA vaccination is characterised by strong cell mediated immune responses and significantly weaker antibody responses in comparison to protein based vaccinations with adjuvant, so our model actually performs as predicted once the ectopic thymus red herring is removed [241]. This skew in antibody response may be related to the increased CD4/CD8 ratio present in protein immunized mice. If we are to pursue the potential of TSHR DNA based vaccination inducing TSAB, thyroid hyperplasia and thyroiditis, attempts to strengthen antigenicity need exploring and murine TSHR may make a more logical target to induce thyroiditis [174]. The addition of conventional aluminium adjuvants to DNA vaccination has been shown to greatly increase antibody responses and may be a start point [242]. Additionally, raising cell mediated immune responses has been engineered by Fas mediated apoptotic death of cells expressing antigen [243]. There followed an increase in antigen uptake by antigen presenting cells, elaboration of TH-1 cytokines and enhanced antigen specific cytotoxic T-lymphocytes beyond that seen with a standard pcDNA3 vector. The co-expression of antigen and mutant caspase apoptotic proteins can induce apoptosis while antigen expression is not interfered with [244]. This has particular interest because the adjuvant activity enhanced B-cell as well as T-cell responses and this approach can incorporate gene gun delivery to amplify TH-2 responses [245]. DNA-TSHR immunization requires adjuvants in future attempts to model Graves' ophthalmopathy.

3 Increasing TSHR activation in differentiated orbital preadipocytes has variable effects on lipid accumulation

3.1 Introduction

3.1.1 Extrathyroidal thyrotropin receptor expression in fat

Proposing the TSHR to be an antigen in Graves' ophthalmopathy required evidence of orbital expression. Extrathyroidal expression of TSHR was first suggested by White and Engel who reported, as an aside, a low level lipolytic effect of TSH on rat epididymal adipose cells that was less potent than adrenocorticotrophic hormone (ACTH) [246]. This work was confirmed and developed further in the same cell types in rats and guinea pigs in which TSH also increased oxygen consumption, glucose utilization, release of free fatty acids and could be substituted for by LATS [247; 248; 249; 250]. Following this, some years later, the presence of TSHR in orbital fat had been implied by TSH binding and cAMP production from retro-orbital membranes of both humans and guinea pigs [251; 252]. In humans, membranes were from connective tissue and fat cells but in guinea pigs the main target for TSH binding was the membranes of the Harderian gland which is absent in humans. Another group, using similar techniques of examining membrane preparations, did not demonstrate TSH binding to human orbital fat but supported its presence in guinea pigs [253].

Elsewhere evidence of functional extrathyroidal TSHR expression is in neonates in whom TSH is the main stimulus for lipolysis but the effect decreases by childhood and further into adulthood, at which time catecholamine effects predominate [254]. Again the TSHR ligand, TSH, could be substituted for by TSAB and lipolysis reciprocally blocked by TBAB [255]. Despite the reduced TSHR expression in adult adipocytes, the thyroid axis still affects fat stores whereby thyrotoxicosis causes lipolysis by an indirect effect, increasing adipocyte β2-adrenoreceptors expression and their cAMP production [256]. The apparent change in TSH sensitivity from infant to adult may reflect the reduction in preadipocytes and preponderance of adipocytes comprising the adult fat organ.

Following cloning of the human TSHR it became possible to investigate the presence of extrathyroidal mRNA transcripts [81; 257]. Initially it was detected in whole orbital tissues of

Graves' ophthalmopathy patients and non-thyroid autoimmune individuals but attempts to identify the cell type did not include orbital fat [258]. A TSHR variant transcript was detected in extraocular muscles and, to a lesser extent, orbital fibroblasts and fat, but the protein was non-functional for signalling, lacking the required trans-membrane segment [259]. Similarly, from cultured orbital fibroblasts extracellular TSHR mRNA was reproducibly detected [260; 261]. These qualitative techniques are vulnerable to illegitimate transcription, unlike northern blotting and in situ hybridisation that eventually confirmed TSHR mRNA in orbital fat of Graves' ophthalmopathy patients [178; 262; 263].

Fibroblasts were the focus of a large proportion of ophthalmopathy research until 1996 when preadipocyte 3T3-L1 cells were the first non-thyroidal cell line shown to have inducible TSHR expression on differentiation [264]. The same group demonstrated rat preadipocytes also express TSHR on differentiation [265]. Shortly after, the capacity of a small proportion of human orbital preadipocytes to undergo differentiation in vitro was reported [50]. In common with the 3T3-L1 and rat preadipocytes, orbital preadipocyte differentiation induced TSHR expression [266]. Subdividing the orbital contents into preadipocytes and adipocytes demonstrated a functional TSHR only in adipocytes or differentiating preadipocytes but not from undifferentiated preadipocytes [179]. TSHR expression seems therefore to be a marker of adipocyte differentiation. Furthermore, the detection of TSHR mRNA in Graves' patients orbital and cervical fat ex vivo by sensitive quantitative real-time PCR, would imply an active adipogenic process that is not exclusive to the orbit [177] and is commented on in early histological reports [9].

3.1.2 TSHR expression and signalling in differentiated preadipocytes

The expression of functional TSHR on differentiated preadipocytes has been demonstrated but how this might relate to the pathogenesis of Graves' ophthalmopathy first requires investigation of the effects of TSH on preadipocytes in reproducible cellular models.

From their initial cloning of rat TSHR from epididymal fat [267], Onaya's group went on to examine TSHR expression and signalling in rat and murine preadipocytes and compared it to the well characterised thyroid FRTL-5 cell line. Initially they demonstrated TSHR expression and TSH dependent cAMP production in differentiated but not undifferentiated 3T3-L1[264]. TSHR mRNA expression started around day 5, peaked on day 7, coinciding

with lipid accumulation. In keeping with this, TSH (10-100mU) stimulated cAMP production started on day 7 and increased on days 9 and 11. Expression required dexamethasone and IBMX in the first three days. From day 4, insulin alone could induce TSHR expression whereas dexamethasone and IBMX alone could not. When the culture was continued from day 4 with all three agents (insulin/dexamethasone/IBMX) lipid accumulated but cells did not express TSHR. An insulin response element is present in the promoter region of the TSHR gene (downstream of TTF-1). In subsequent experiments TSH was shown to reduce TSHR expression in differentiated 3T3-L1 in a cAMP dependent manner that continued from 1-4 hours[268]. This was different to the initial transient increase in cAMP seen in FRTL-5 cells, in addition, adipocytes lacked TTF-1, it was concluded that different CRE like activity in the TSHR promoter occurred in the two cell types. Further work suggested that differentiation resulted in reduced suppression of interaction between two promoters, the CRE like element and an Ets-binding motif that are present upstream of the TSHR gene, that after differentiation can act synergistically[269]. Considering the three main transcription factors identified in adipogenesis; C/EBPα, ADD1 and PPARγ, the TSHR promoter lacks both the CCAAT and E-box binding sites of C/EBPα and ADD1 respectively. PPARγ2 dimerises with RXRα and binds to DR-1, half its binding site corresponds to the CRE like element, giving a possible link with the main adipogenic transcription factors and TSHR gene expression.

Other factors influencing preadipocyte differentiation and TSHR expression include possible effects from cytokines and TSH. The inflammatory cytokines TNFα, hTGFβ$_1$ and IFNγ, reduce lipid accumulation, terminal markers of differentiation (LPL, aP2), TSH dependent cAMP production and TSHR expression in rat preadipocytes [270]. Despite widely different mechanisms of cell signalling the cytokines had a common negative effect on adipogenesis. In differentiating rat preadipocytes, TSH resulted in an increase in proliferation in a dose dependent fashion and did not decrease apoptosis[271]. (These effects occurred in the first 5 days of differentiation which is curious given the expression of TSHR mRNA in 3T3-L1 only appeared at 5 days [264]). The terminal marker LPL was decreased by TSH alongside reduced lipid vacuole size and number. Prolonged incubation with TSH rendered the differentiating preadipocytes incapable of developing lipid droplet formation. However, when stimulating cAMP directly using forskolin or dibutyryl cAMP almost the opposite was seen. Cell numbers were decreased by high levels of dibutyryl cAMP and LPL mRNA expression increased slightly. These effects may be due to other

signalling pathways being activated by TSH or by the transient rise in cAMP produced by TSH signalling contrasted with the continuous stimulation of forskolin and dibutyryl cAMP. One such alternative pathway that has been demonstrated in 3T3-L1, human orbital and abdominal differentiated preadipocytes is TSH activation of p70 S6 kinase via phosphoinositol 3-kinase[272; 273]. cAMP may in fact only have a very short window of effect in the expression of terminal markers as seen in differentiating 3T3-L1 cells[274]. In this model, cAMP increases aP2 expression by effects on a negative element in the promoter but only in confluent preadipocytes, it has no effect on proliferating or differentiated cells. In contrast, differentiated 3T3-F442A cells show a marked reduction in LPL and glycerophosphate dehydrogenase in response to forskolin[275]. From the illustrated variability of cAMP effects on lipid metabolism it is apparent that the pleiotropic nature is determined by cell and differentiation specific events.

3.1.3 Cell lines and retroviral transduction

Human orbital preadipocytes can be derived from collagenase digests or from explant cultures of orbital fat biopsies [276]. Given the difficulties of small numbers of surgical specimens and slower growth rates of human primary cells we also selected cell lines that have adipogenic potential, 3T3-L1, HC C1 and MG63. 3T3-L1 cells are a well characterised preadipocyte murine cell have already been discussed. MG63 cells are from a human osteosarcoma cell line that despite their osteoblastic potential can be switched to adipocytes accumulating lipid, expressing PPARγ and aP2 when cultured in rabbit serum [277]. HC C1 is a recently established human osteoblastic cell line from a bone marrow aspirate with osteoblastic and adipogenic potential depending on culture conditions [278].

Introducing standard vectors into cells often produce transient expression of the gene of interest. Retroviral vectors incorporate into the host genome and result in a permanent transduction for prolonged gene expression rather than a temporary transfection. A retroviral construct is engineered with the gene of interest downstream of a promoter. The retroviral construct then requires further modification by the addition of matrix, capsid and nucleoproteins (*gag*), reverse transcriptase and integrase (*pol*) and the protein envelope (*env*) to form complete viral particles that can penetrate cells. Lacking the coding regions (*gag*, *pol* and *env*) pLNSX constructs, once packaged, are capable of only one round of infection, so-called "replication incompetent retroviruses". It has been previously

demonstrated pLNSX vectors containing activating mutant forms of TSHR have varying effects on function and cellular proliferation when examined in COS-7, human thyrocytes and FRTL-5 cells [89]. The basal cAMP levels of the L629F and M453T mutants were similar when examined in COS 7, whereas in FRTL-5 the highest constitutive cAMP levels were in M453T transduced cells with L629F having less[89] . In addition, in a case with germline M453T mutation, possible proptosis was reported [279]. These two mutations could potentially influence preadipocytes with a medium and high level constitutive cAMP effect in an attempt to reproduce the sustained stimulation brought about by the action of TSAB or TSH.

3.1.4 Aims: to investigate the effects of TSHR activation on adipogenesis using gain-of-function TSHR mutations

1. To develop a modified explant preadipocyte harvesting method from small surgical specimens.
2. To determine the effects of elevated cAMP from gain-of-function TSHR mutations on the proliferation and differentiation of preadipocytes.

This work outlines a method of harvesting primary orbital preadipocytes from small human orbital fat samples modified from a previously described technique [276].
Human primary orbital preadipocytes from Graves' ophthalmopathy and normal individuals, 3T3-L1, HC C1 and MG63 cells were transduced with retroviral vectors expressing activating mutant forms of TSHR. The different levels of constitutive cAMP production induced by the mutant TSHRs were assessed on cell proliferation before differentiation. The transduced cells and controls were then differentiated to determine effects on lipid accumulation. From previous research we hypothesize cAMP from TSHR might have lipolytic effects. Conversely, given the orbital fat proliferation seen in Graves' ophthalmopathy, TSHR activation may also have a proadipogenic role.

3.2 Materials and Methods

3.2.1 Preadipocyte explant cultures

Human orbital fat samples were obtained with informed consent according to LREC approval (information sheet and consent, app.B). Graves' tissue was retrieved at the time of orbital decompression surgery or during routine lid surgery where fat removal was beneficial to patient outcome, such as a fat blepharoplasty. Unlike fat samples derived from abdominal surgery, orbital fat samples were small (0.25-1.25ml). Collagenase digest resulted in low yields of preadipocytes so, as an alternative, undigested fat explants were used. This allowed repeated harvesting of preadipocytes from the explants for several months.

Samples were transported from theatre on damp swabs or gauze and washed twice in DMEM/HAMS/10% FCS in a tissue culture hood (Microflow biological safety cabinet). The explants were cut into small pieces (~2-3mm) using sterile blades in 60mm petri dishes containing 3ml of red blood cell lysis buffer. The samples were always divided between at least two dishes, preferably three, to allow continued preadipocyte harvesting in remaining dishes if mould/yeast infections overtook individual culture dishes. The explants were evenly spread, 5-10mm apart, on a 60mm petri dish that had been pre-wet with 1.4 ml of medium. Fluid volumes were important, too much and the explants floated off, too little and the dish would occasionally dry out. Explants were allowed 2-3 days to attach, then the medium was changed gently to remove any remaining erythrocytes and replaced with 1.5-2.0ml. If explants floated off, the volume was reduced back to 1.4 ml and allowed a further 3 days to attach before changing the medium again.

These primary cultures required daily reviews where possible and in the event of a single mould colony growing, unaffected explants could be thoroughly rinsed in fresh medium, replanted on a new dish and cultures could frequently be continued without regrowth. Usually after 4-6 weeks the base of the dishes would be approaching confluence, explants were transferred to new dishes and the cycle repeated. Adherent preadipocytes were washed with HBSS (app.B) and then detached with 350µl of trypsin (containing 500µM

EDTA/EGTA, cell lines did not require this addition). Cells were washed twice in 5ml of fresh medium, transferred to freezing mix, stored and thawed when required as in 2.2.11. The longest this cycle was repeated was 9 months. The most significant factor influencing duration of culture was the yeast and mould infections of these relatively slow growing cells. The explants gradually diminished in size, but however small, if one could transfer and get them to attach by reducing the volume to 1-1.5ml, it would continue to seed cells onto the dish. In total 11 samples from Graves' ophthalmopathy patients and 10 from patients undergoing other eyelid procedures were collected and stored (patient summaries in app.B).

3.2.2 Transformation of competent cells with retroviral constructs

Activating mutant TSHRs had previously been subcloned from an initial pSVL vector into the retroviral pLNSX vector [89]. Amplification of these constructs required transformation of JM109 competent cells (Promega). pLNSX plasmids (gi:208844) containing the following constructs were transformed; L629F[280], M453T[279], V656F, Del 613-621[281], C672Y, V509A[282], wild type (WT) TSHR and neo.

Competent cells were thawed on ice for 5 minutes, 200µl were added and mixed with 1ng of each pLNSX construct in tubes chilled on ice and incubated for 30 minutes. Cells were then heat shocked at 42 C (Clifton water bath) for 90 seconds to facilitate DNA entry, allowed to recover for 2 minutes on ice, before adding 800µl of SOC (app.B) and incubating at 37 C in an orbital shaker for one hour. The cell suspension, 100µl, was then streaked onto an LB agar plate (app.B) and incubated overnight at 37 C.

3.2.3 Small and large scale plasmid preparation

Following successful transformation, confirmation of the plasmid construct and creation of a glycerol stock was required. In a small scale plasmid DNA preparation, a single colony was picked from the agar plate, inoculated into 5ml LB broth (app.A) and incubated overnight in an orbital shaker at 37C. One and a half millilitres of the overnight culture was centrifuged at 8000g (Mikro 22R) for 1 minute. The supernatant was aspirated and the pellet vortex washed in 1ml of SET (app.B), repeat centrifuged, aspirated and the pellet

resuspended in 150µl of SET. Five microlitres of 10mg/ml DNAse free RNAse A (app.B) was added, vortexed, lysed with 350µl of lysis buffer (app.B), inverted five times and left to stand on ice for 5 minutes. The lysis reaction was stopped with 250µl of sodium acetate (app.B), inverted five times, left on ice for 30 minutes and then centrifuged at 8000g, 4 C for 30 minutes. The supernatant was transferred to a new tube with an equal volume of isopropanol and the DNA pelleted by centrifuging at 8000g, 20C for 30 minutes. The pellet was washed twice in ethanol (70% made up in TE app.A), air dried and redissolved in 20µl of TE. Two-three micrograms of DNA was restriction digested with BstEII to generate two fragments, 4 and 4.4kb in size, from WT and mutant TSHR plasmids (app.B). The products were run on a 1% agarose gel (section 2.2.8) to confirm transformation.

For the glycerol stock; 500µl of overnight culture was added to 500µl of glycerol in a 1.5ml eppendorf, inverted ten times and stored at -80 C. These stocks were used for maxipreps (section 2.2.6) to generate large quantities of DNA for transfection of the packaging cells.

3.2.4 Transfection of ϕNX packaging cells with pLNSX-TSHR constructs

The phoenix (ϕNX) packaging cells provided a transient transfection method to create high titres of complete virus particles containing pLNSX constructs [283] and were handled in a class 2 biosafety facility observing established guidelines (app.B). Selection was possible through the resistance gene for geneticin.

ϕNX cells were maintained in DMEM with 10% heat inactivated FCS. When 70-80% confluent, they were detached with a single slap to the flask and plated at 1 x 10^6 cells in a 35mm petri dish and transfected at 50-60% confluence. For each plate a transfection solution was prepared with 5µg of plasmid DNA (WT/neo/629/453) and 50µl of 2.5M $CaCl_2$, made up to 500µl with distilled water. This solution was transferred to a 5 ml polypropylene tube and while air was bubbled through an automatic pipette, 500µl of 2 x HEPES (app.B) was added dropwise. The solution was left to stand for 20 minutes at 37 C and once a white precipitate had formed, it was added to the ϕNX cells. Five minutes before the addition of the transfection solution, 25µM chloroquine (Sigma) was added to the cells. The transfection incubation was continued for 16 hours at 37 C, after which, the

transfection solution was gently removed and replaced with fresh medium. Retroviral supernatants were harvested at 32 C, collected at 24, 48 and 72 hour timepoints after transfection and stored in sealed bags at -80 C.

3.2.5 Retroviral transduction of preadipocytes

A group of preadipocyte cells were selected to create an in vitro model to study the effects of increased TSHR stimulation on adipogenesis. Cells were maintained in appropriate media; murine 3T3-L1[284] (DMEM/CS 10%), human preadipocytes (DMEM/HAMS/ FCS 10%), human osteo/adipoprogenitor MG63 [277](DMEM/FCS 10%) and HCC1[278] (MEM/FCS 10%), all at 37 C in 5% CO_2. Retroviral uptake and insertion of reverse transcribed cDNA into the cellular genome resulted in permanent transduction. The expression of TSHR variants were under the control of the SV 40 late promoter from the pLNSX.

Cells were plated when at 60-80% confluence, 3T3-L1, MG63, HCC1 ($1x10^5$ cells/35mm well) and human preadipocytes IL, HM, GC ($5x10^3$ cells/35mm well). After 1 day the cell lines were at subconfluent readiness and were incubated in fresh medium containing hexadimethrine bromide (polybrene, 8μg/ml) for 1 hour at 37 C (the primary cells seeded at lower densities and slower in growth required up to 6 days). Meanwhile, retroviral supernatants containing pLNSX-WT/neo/629/453 were thawed and filtered through a pre-rinsed 0.45μm filter and polybrene (8μg/ml) added. The wells were aspirated and 1ml of retroviral supernatant was added to duplicates/triplicates of each cell type, incubated for 3 hours at 37 C, followed by the addition of fresh medium. Geneticin selection was commenced 3 days later and continued. As colonies expanded they were transferred firstly to T25 and then T75 flasks and when confluent subdivided and frozen (2.2.11). Preadipocytes were examined by phase contrast microscopy throughout expansion.

3.2.6 RNA extraction and reverse transcription

Following expansion of the transduced 3T3-L1, MG63 and HCC1 colonies, RNA was extracted and reverse transcribed to cDNA in the first step to detect TSHR mRNA. Given the slow growth the primary preadipocytes, these cells were reserved for other

experiments. However the same retroviral supernatants were used to transduce the primaries and the MG63 and HCC1 cells.

To confluent 35mm wells, 1ml of Trizol (Invitrogen) was added, aspirated and re-pipetted three times and transferred to RNAse free 1.5ml eppendorf tubes. Two hundred microlitres of chloroform was added, vortexed, incubated at room temperature for 2 minutes and centrifuged for 15 minutes, 4 C, at 12,000g. The clear aqueous layer was removed, taking care not to disturb the interface and transferred to a new tube. RNA was precipitated in 500µl of isopropanol, mixed, incubated at room temperature for 10 minutes and the RNA pelleted by centrifugation for 10 minutes, 4 C, at 12,000g. The supernatant was removed, the RNA washed in 1ml of ethanol (75%) and centrifuged for 5 minutes, 4 C, at 7,500g. The supernatant was removed, the pellet air-dried and resuspended in 13µl of TE.

The RNA was then heated to 65 C for 5 minutes (QBT2 hotplate, Grant instruments) and 3µl used to measure 260/280nm ODs to estimate RNA concentration (2.2.7). One to two micrograms of RNA was made up to a volume of 10µl in DEPC water, heated to 65 C for 10 minutes and 10µl of RT master mix (app.B) was added. The RNA was reverse transcribed (1½ hours, 37 C), enzyme denatured (10 minutes, 95 C) and returned to hold (4C) in a thermal cycler (Genius, Techne). The cDNA was stored at -20 C.

3.2.7 PCR amplification of cDNA and PEG precipitation

PCR amplification of reverse transcribed cDNA was followed by PEG precipitation to purify the cDNA before direct sequencing. The human TSHR was amplified from transduced murine 3T3-L1 cells using TSHR primers (pair A, Table 3-1) that crossed exon 7 to 9 prior to sequencing (TSHR mRNA; human (gi:4507700) and murine (gi:6755896)) . These primers were selected because they specifically amplified human TSHR but not murine TSHR. Murine β-actin was amplified using primer pair B to confirm the presence of murine cDNA.

PCR reactions were then performed on 3T3-L1, MG63 and HCC1 using human TSHR primers (Table 3-1) to different regions of exon 10: C (WT and 453) and D (629). (PCR reactions and programs were carried out as shown in app.B). Resulting cDNAs were added to equal volumes of polyethylene glycol (PEG) and left standing for 10 minutes.

Precipitated DNA was then centrifuged for 30 minutes at 12,000g, the supernatant decanted and discarded and the pellet washed with 500µl ethanol 70%. Following another centrifugation, 10 minutes at 12,000g and supernatant aspiration, the pellet was air dried for 10 minutes in a 40 C oven before finally re-suspending in 100µl of distilled water. Confirmation of the purified product was shown using agarose gel electrophoresis (2.2.8).

Table 3-1 TSHR PCR primers

	Forward	Reverse	Amplicon
A	CAA TGG GAC AAA GCT GGA TG	TCT GAT TTT CTT CTG ATT CTT	287bp
B	TGT GAT GGT GGG AAT GGG TCA	TTT GAT GTC ACG CAC GAT TTC C	514bp
C	AAA AAC CCC CAG GAA GAG AC	GTC CAT GGG CAG GCA GAT AC	609bp
D	ACT GTC TTT GCA AGC GAG TT	GAT GCC AAA CTT GCT GAG TAG G	594bp

3.2.8 Direct DNA sequencing of RV transduced 3T3-L1, HCC1 and MG63 cells

Forward and reverse strands of purified hTSHR were amplified and then sequenced using a Dye Rhodamine Terminator kit. Firstly, 10µl single strand PCR reactions were performed (app.B) followed by precipitation in sodium acetate (3M, pH5.2). One microlitre of sodium acetate was added to the 10µl PCR product with 30µl 100% ethanol, vortexed and precipitated for 10 minutes. Then re-centrifugation, 12,000g for 30 minutes, supernatant discarded, the pellet washed in 500µl 70% ethanol before centrifuging 12,000g for 10 minutes, supernatant discarded and finally air-drying the pellet. The dye labelled cDNA was then analysed on an ABI automatic sequencer.

3.2.9 Cell proliferation and counting

Transduced and non-transduced cell proliferation was determined by direct cell counting of trypsinised cells in a Coulter counter (Beckman Coulter), following 3 and 5 days of growth in 3T3-L1 and HC C1, 3 days in MG 63, and 7 days in primary preadipocytes.

Sub-confluent cultures were trypsinised and counted in a haemocytometer chamber and after washing were resuspended to give 2 x 10^4 cells/ml. One millitre was added to six-well plates (Costar) allowing triplicate determinations for day 3, and day 5 when required, and the plate tilted gently to cover well bottoms. This initial seeding density, 2 x 10^4 cells/well, ensured the five day growth was not post confluent. After the required growth period, cells were detached, washed and resuspended in 500µl of Isoton (Beckman Coulter) and counted in a coulter counter. Cell numbers were reported as a percent relative to non-transduced cells.

3.2.10 cAMP accumulation and measurement by RIA

Basal and stimulated cAMP levels were measured in all transduced and non-transduced cells. Basal cAMP levels were recorded after a four hour incubation with the phosphodiesterase inhibitor isobutylmethylxanthine (IBMX). In addition cells were stimulated with TSH and the adenylate cyclase stimulator, forskolin.

Six well plates were loaded with each cell type at 4 x 10^4 cell/well and left in their respective standard media for 24 hours at which time 70% confluence was usually achieved. Into all wells fresh medium containing 250mM IBMX was added with duplicates for basal (IBMX), 1 and 10 mU of TSH and 10µM forskolin. After a four hour incubation cAMP was extracted in 500µl/well of hydrochloric acid (0.1N) and samples speedvac dried overnight before storing at -80 C. The cAMP levels were determined in a radioimmunoassay with sensitivity to below 5 fM and were carried out by Dr M Ludgate [285]. One well was used to determine cellular protein levels to normalise for differences in cellular proliferation. The trichloroacetic acid precipitation method was used for protein estimation (2.2.3).

3.2.11 TSHR immunocytochemistry

Cells were allowed to attach to coverslips placed in 6-well plates overnight. They were then rinsed with PBS and fixed with ice-cold acetone for 5 seconds. Endogenous peroxidase was inhibited with 0.025% periodic acid and rinsed with PBS-T-gelatine (PGT, app.B) for 5 minutes. A Vectastatin Elite ABC kit (Vector Labs) was used for the

following protocol (www.vectorlabs.com/data/descriptions/pdf/PK7200.pdf). Samples were blocked in diluted horse serum for 10 minutes, followed by an avidin/biotin blocking step and washing with PGT. Primary antibodies were diluted 1:100 and incubated for 90 minutes followed by 3, 5 minute washes with PGT. The negative control omitted the primary antibody. The secondary antibody incubation was for 30 minutes with biotinylated anti-mouse IgG followed by 2, 5 minute washes with PGT. Avidin/biotin crosslinking required 5 minutes incubation with the ABC reagent and was washed twice for 2 minutes with PGT. Antibody/biotin/avidin/ peroxidase complexes were visualised with the chromogen diaminobenzidine tetrahydrochloride (DAB) 0.001% and hydrogen peroxide 0.01% in PBS for 2-3 minutes and washed in PGT twice for 10 minutes. Counter staining with haematoxylin required 30 seconds, a tap water wash, dehydration in 100% alcohol twice, fixed in xylene twice and then mounted with DPX (Sigma-Aldrich) onto microscope slides. Images were captured using a Zeiss digital charge coupled device (Axiocam).

3.2.12 Lipid staining

Following differentiation or when assessment of lipid content was required oil red-O (ORO) staining was performed. Stock solution of ORO was diluted 3:2 with distilled water, mixed, allowed to stand for 15 minutes and then filtered before using. Cells mounted on coverslips were fixed in 60% isopropanol for 1 minute, stained with ORO for 15 minutes and washed 3-4 times in 60% isopropanol. Cells were counterstained with haematoxylin for 1-2 minutes, fixed in 60% isopropanol for 1 minute and then mounted in glycerol. The average percentage, from two coverslips, of cells containing lipid inclusions used a 10 x 10 eyepiece mounted graticule in a 10 times field of magnification and averaged ten continuous non-adjacent sampled areas per coverslip.

3.2.13 Preadipocyte differentiation

The full differentiating conditions for 3T3-L1 cells were in DMEM medium containing 10% fetal bovine serum (FBS), 10mg/ml insulin, 0.2mg/ml dexamethasone and 0.5 mM IBMX for 3 days (Sigma). After which, cells were kept in DMEM containing 10% FBS and 10mg/ml insulin and re-fed on alternate days [264]. Human preadipocytes were

differentiated in medium consisting of DMEM: F-12 (1:1) supplemented with 3% FCS, 160 mM insulin, 1 μM dexamethasone, and for the first 3 days only, 1 μM pioglitazone and 250 μM IBMX (modified from [286]). Cultures were maintained in this medium for 14 days. Cell percentages containing lipid were determined as above (3.2.12).

3.2.14 Nile red flow cytometry for lipid accumulation

The high level of ORO staining in post confluent undifferentiated 3T3-L1 made it difficult to distinguish differences between the differentiation methods. Nile red is a fluorescent lipophyllic dye that is highly selective for lipid vesicles in cells. It has been used in flow cytometry to quantify proportions of differentiated orbital preadipocyte populations accumulating lipid [286].

3T3-L1 transduced and non transduced cells were treated as above with either the full differentiating or non-differentiating protocol. Cells were detached with 5mM EGTA/EDTA in PBS/BSA (section 2.2.15), fixed in 0.5% paraformaldehyde and then stained in 0.1μg/ml Nile red for 10 minutes. Stained cells were washed and resuspended in PBS/BSA and fluorescence (530-610nm) measured in the FL2 channel FACScan cytometer. Forward and side scatter plots were generated to gate out non viable cells. Gated plots with forward scatter on the x axis and FL2 on the y were examined for a right shift with larger cells staining with lipid.

3.2.15 Statistical analysis

Means were compared non-parametrically by Kruskal Wallis and post hoc by Dunns multiple comparison test and parametrically by ANOVA with post hoc TUKEY HSD using software as in 2.2.23.

3.3 Results

3.3.1 Explants shrink in long term culture but can exert a positive effect on adjacent cell lipid content

During the long term explant cultures it was possible to harvest preadipocytes every 6-8 weeks for as long as 9 months. During this time explants decreased in size with lipid accumulating on the surface of the media suggesting lipolysis. Additionally, lipid filled preadipocytes would cluster, adjacent, beneath, and at the end of thin strands of connective tissue remaining following explant contraction (Figure 3.1.A and B). These vacuoles were visible by contrast microscopic examination and lipid confirmed by oil red-O staining (Figure 3.1.C). Once present, the vacuolated cells seemed to persist and a cluster of cells could often be recognised unaltered until the cells were harvested. These appearances could be modified. Adding excess media, detaching the explants and not allowing them to reattach and continuing the culture for two weeks reduced the numbers of cells staining with lipid (Figure 3.2.B). If the explant was completely removed from the well for the same length of time (2 weeks) the cells assumed a uniform fibroblastic appearance with no lipid (Figure 3.2.C). Another recognisable feature was the further away from the attached explant the fewer cells were found to contain lipid, but still contained vacuoles (Figure 3.2.D). Therefore, both the presence and proximity to the explant seemed to alter the cell monolayer. The florid appearances seen in Figure 3.1 were infrequent, but developed in some of both the Graves' and normal tissue samples.

Figure legends

Figure 3.1 Fat explants

A. Some fat explants, whether from Graves' orbits or normal orbits, had vacuolated cells adjacent to them. These cells, once present did not appear to alter in morphology. (Insert shows the proximity of vacuolated cells to the explant (dark shadow, bottom edge)). [PSM, contrast microscopic image, x10 insert and x40 main].
B. Vacuolated cells can gather at the edge of thin strands of connective tissue that remained after the explants had contracted. [PSM, contrast microscope x40].
C. Vacuolated cells contain lipid. [PSM, oil red-O x40].

Figure 3.2 Fat explants

A. Rounded lipid containing cells present, beneath and adjacent to undisturbed explants. [PSM, or-O x40].
B. Detaching the explants and allowing them to float in the media above the cell monolayer for two weeks reduced lipid containing cells number and volume. [PSM, or-O x20].
C. Removing the explants from the cell monolayer for the same period resulted in cells with a uniform fibroblastic appearance and no lipid inclusions. [PSM, or-O x20].
D. Some cell clusters could be identified away from explants that by altering the condenser on the microscope, have numerous small vacuoles but only faint traces of lipid staining. The florid lipid filled morphology was only a feature of cells adjacent to or beneath explants as in A. [PSM, or-O x40].

Figure 3.1 Fat explants

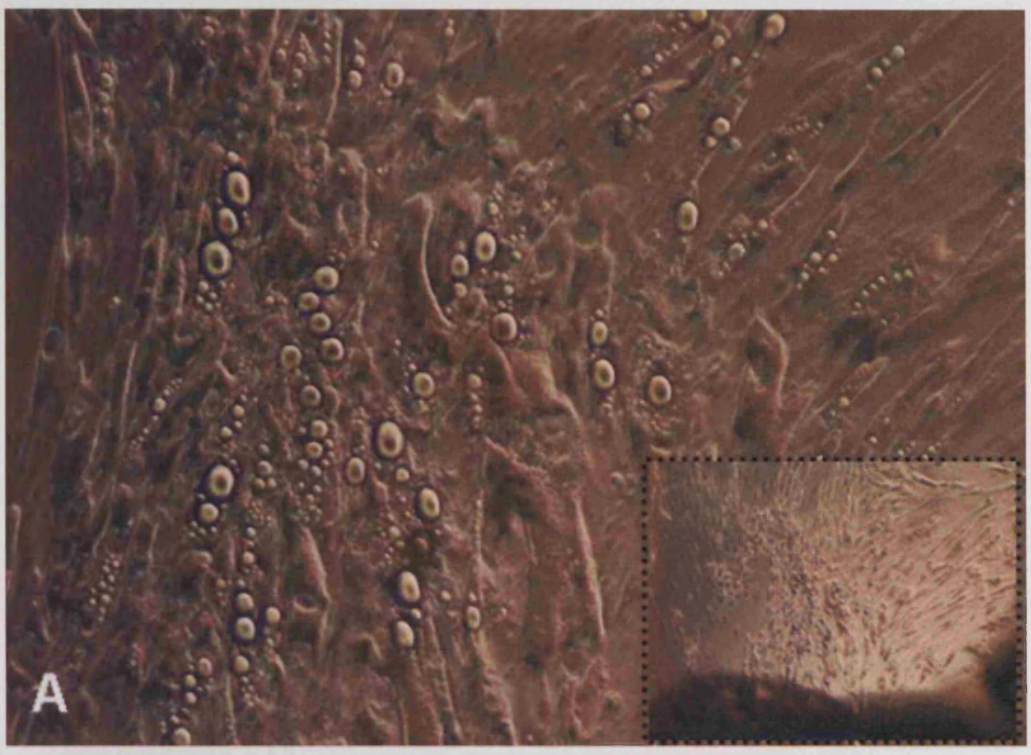

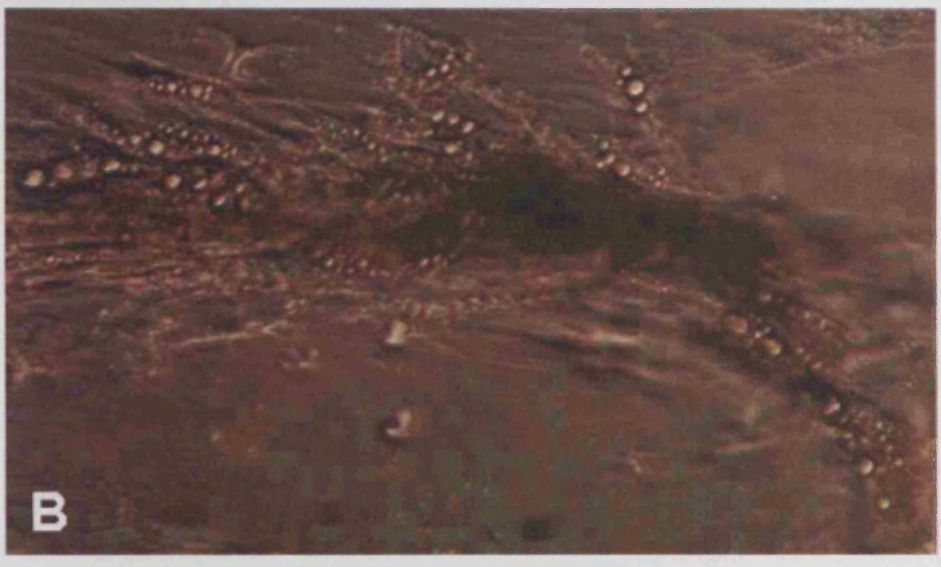

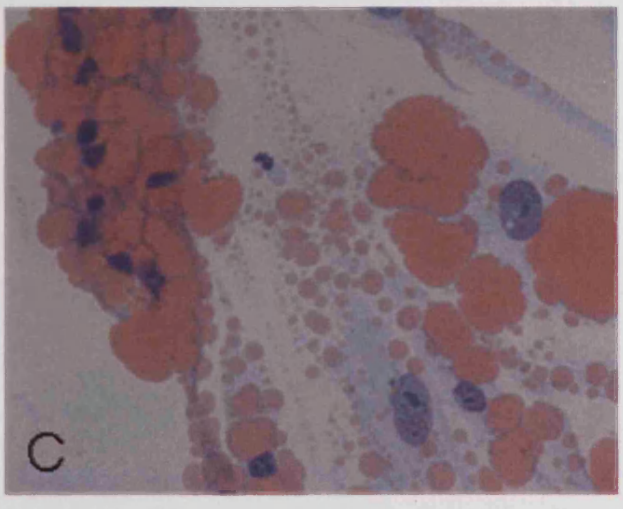

Figure 3.2 Fat explants

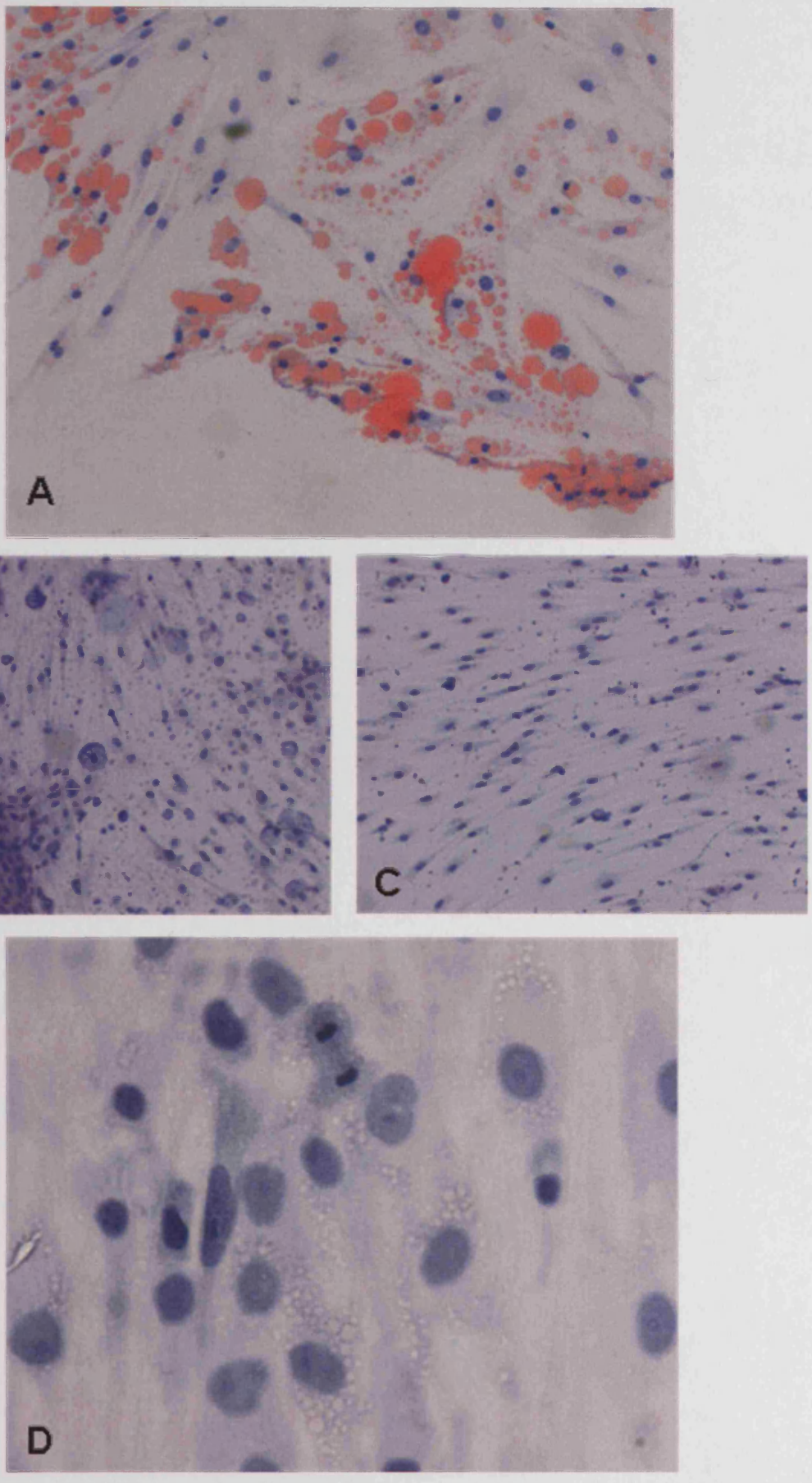

3.3.2 Competent cells were transformed with pLNSX constructs and sequencing confirmed mutant forms of TSHR

JM109 cells were transformed with pLNSX constructs and transformation was confirmed by endonuclease restriction with BstEII (Figure 3.3), transformed cells were used for maxipreps. The purified DNA was packaged into complete viral particles by ϕNX packaging cells and supernatants collected for transduction of preadipocytes. To confirm retroviral transduction of preadipocytes, direct DNA sequencing was performed after G418 antibiotic selection. Forward and reverse strands of mRNA were shown to contain the appropriate nucleotides. Methionine to threonine substitution occurs from an ATG-ACG mutation at point 453 and leucine to phenylalanine occurs at point 629 from a TTG-TTT mutation (Figure 3.4).

Figure 3.3 Restriction digest of pLNSX-TSHR transformed cells

BstEII restriction of pLNSX transformed cells. WT and mutant TSHR cut (long arrow) to produce 4 and 4.4kb fragments. (Unrestricted plasmids-short arrows. pLNSX neo has only one BstEII restriction site and is linearized).

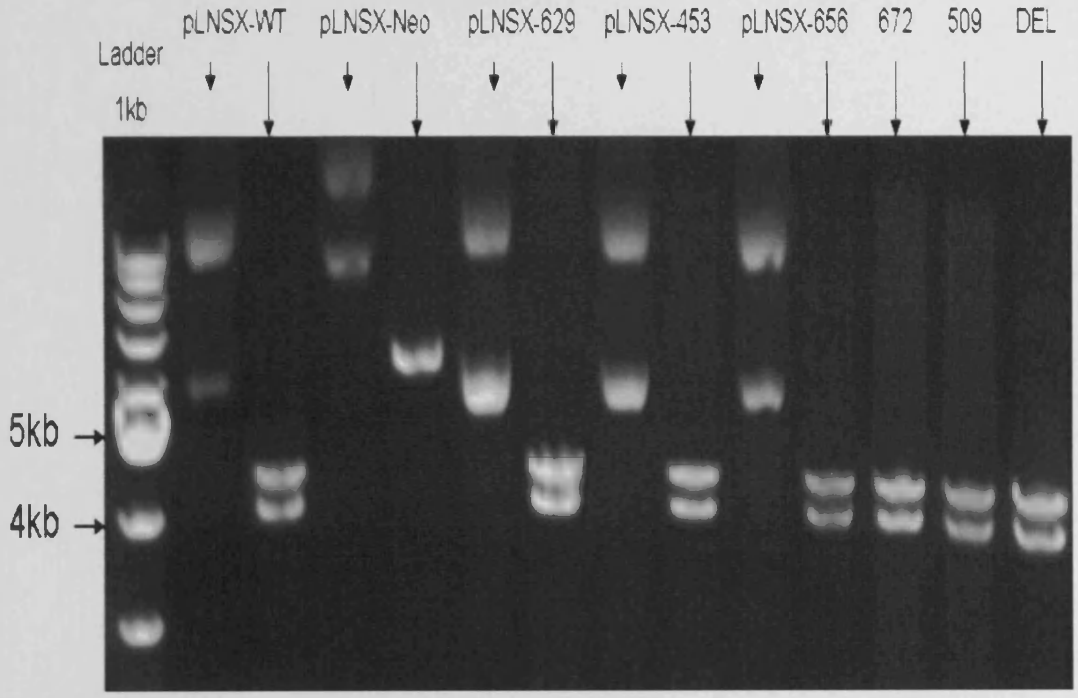

Figure 3.4.DNA sequencing of transduced cells

Transduction of preadipocytes with TSHR was confirmed by direct sequencing. Electropherograms showing peak dye fluorescence of PCR amplified cDNA, nucleotides are shown from pLNSX transduced HC C1 cells. The M453T mutation results from an ATG to ACG point nucleotide substitution and the L629F results from a TTG to TTT mutation.

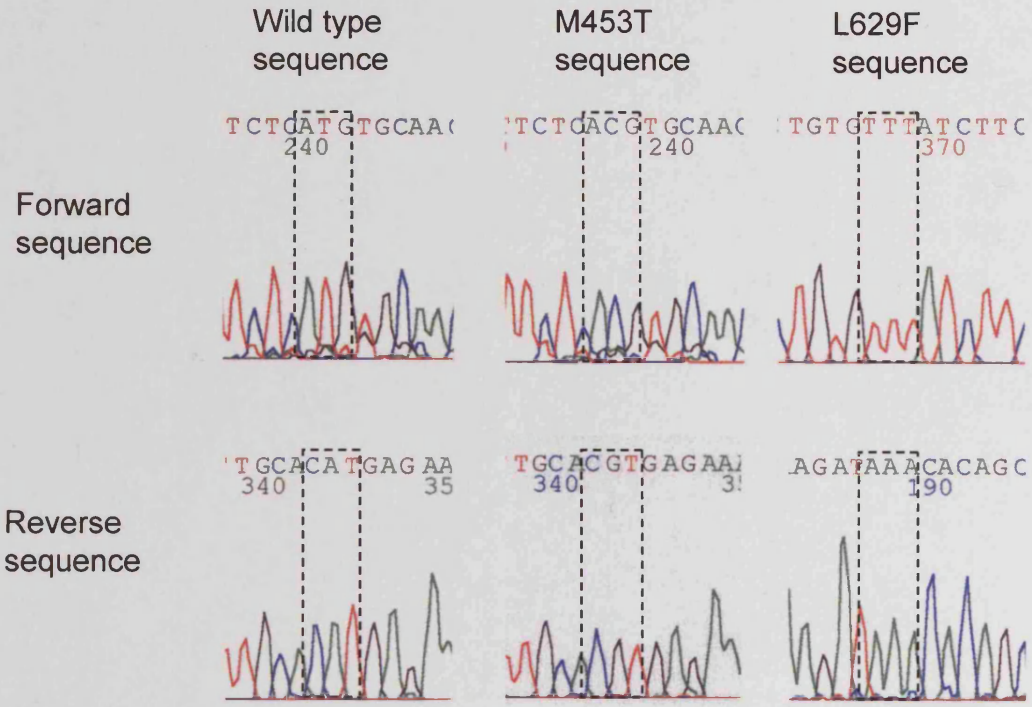

G418 selection of cells transduced with the WT, M453T and L629F resulted in the appearance of resistant colonies. However the neo retroviral supernatants did not generate antibiotic resistant cells. Consequently non-transduced and pLNSXWT cells served as control for comparison with the mutant transduced cells.

3.3.3 Varying effects on cell proliferation are seen in transduced cells, inhibition predominates in human preadipocytes with activating TSHR mutations

A range of effects on cell proliferation were seen on the transduced cells (Table 3-2). Cells were initially examined after 3 days growth, stimulation developed in 3T3-L1, inhibition in HCC1 and human primaries and no apparent effect on MG63 when compared to non-transduced cells. Further experiments looked at proliferation over 3 and 5 days in 3T3-L1 and HCC1 cells.

Firstly 3T3-L1 stimulation, significant differences were present between the cell types ($p<0.0005$ KW, Figure 3.5). At both 3 and 5 days, L629F showed increased cell numbers relative to non transduced cells (190% ($p<0.001$)- 158% ($p<0.05$)(Dunn post hoc)). However, at 5 days WT cells proliferated significantly relative to non transduced cells (150%, $p<0.05$) and at no time was L629F proliferation significantly greater than WT. M453T cells proliferation of 121% was not significantly greater than WT or non transduced cells at either time point.

In HCC1 cells, some inhibition was present in transduced cells on both days ($p<0.0124$-$p<0.001$ (KW), Figure 3.6). Significant WT inhibition was seen at 3 and 5 days (83%($p<0.01$)-58%($p<0.001$). Inhibition of L629F and M453T was minor and only significant in M453T at 5 days (70%, $p<0.01$). At no timepoint was there a significant difference between WT, M453T and L629F transduced cells.

Before transduction the differences in proliferation rates between cell lines and primary preadipocytes was already profound. After transduction, cell lines would require flask passages 2-3 times/week while primary preadipocytes would be passaged once in 3-6 weeks, particularly longer in those cells transduced with activating mutations. Accumulating enough cells for other experiments at these growth rates made studying the primary preadipocytes a lengthy procedure. The reduced proliferation rate required experiments lasting 7 days. Graves' orbital preadipocytes showed reduced proliferation in transduced cells relative to non transduced ($p<0.0001$(ANOVA), Figure 3.8). Reduced WT (77%, $p=0.064$) was not significant while both L629F (67%, $p=0.009$) and M453T (34%, $p<0.0001$) were significant, relative to non-transduced. M453T proliferation was significantly less than WT ($p=0.002$) and L629F ($p=0.012$), but L629F and WT did not differ significantly.

Normal orbital preadipocytes showed reduced proliferation in all transduced cells relative to non transduced at three days ($p=0.0036$(KW), Figure 3.9). The severely reduced proliferation in growth of the M453T transduced cells was such that despite several colonies resistant to G418 selection, even after 4 months of growth, insufficient cells grew to allow any experiments to be performed. The only significant reduction between the groups of cells was between non-transduced and L629F (38%, $p<0.05$).

In MG63 differences in proliferation effects were seen (p=0.002 (KW), Figure 3.7). Relative to non-transduced, WT (84%) showed inhibition while L629F (114%) and M453T (113%) proliferated slightly, no differences were significant. However there was apparent stimulation when comparing.WT to both L629F ($p<0.01$) and M453T ($p<0.05$).

Table 3-2 Transduced vs normal cell proliferation rates

Proliferation percentage calculated by: numbers of transduced/ non-transduced cells expressed as a percentage (non-transduced shown as 100%). Mean and standard error of mean are recorded. (* $p<0.05$ relative to non-transduced. # $p<0.05$ relative to WT).

	Non-transduced	pLNSX WT	pLNSX 629	pLNSX 453
3T3-L1: 3 days (n=12)	100 (1.9)	133.9 (8.7)	190.5 (11.6) *	121.9 (15.3)
5 days	100 (0.8)	150.0 (9.3) *	158.6 (18.6) *	121.4 (11.9)
HC C1: 3 days (n=15)	100 (0.7)	82.8 (4.4) *	95.9 (6.5)	92.7 (2.9)
5 days	100 (0.6)	57.9 (5.7) *	79.5 (6.2)	70.2 (4.8) *
MG 63 (n=6)	100 (2.7)	84.3 (5.0)	114.3 (1.3) #	113.8 (6.2) #
Non GO (n=3)	100 (9.9)	62.9 (4.0) *	38.3 (1.3) *	-
GO (n=3)	100 (7.9)	77.2 (5.1)	66.5 (4.1) *	34.4 (2.6) *#

Figure 3.5 Proliferation of 3T3-L1 cells

Cell proliferation of transduced 3T3-L1 cells relative to non-transduced. Significant proliferation is shown in L629F transduced cells but also WT (Dunn post hoc).

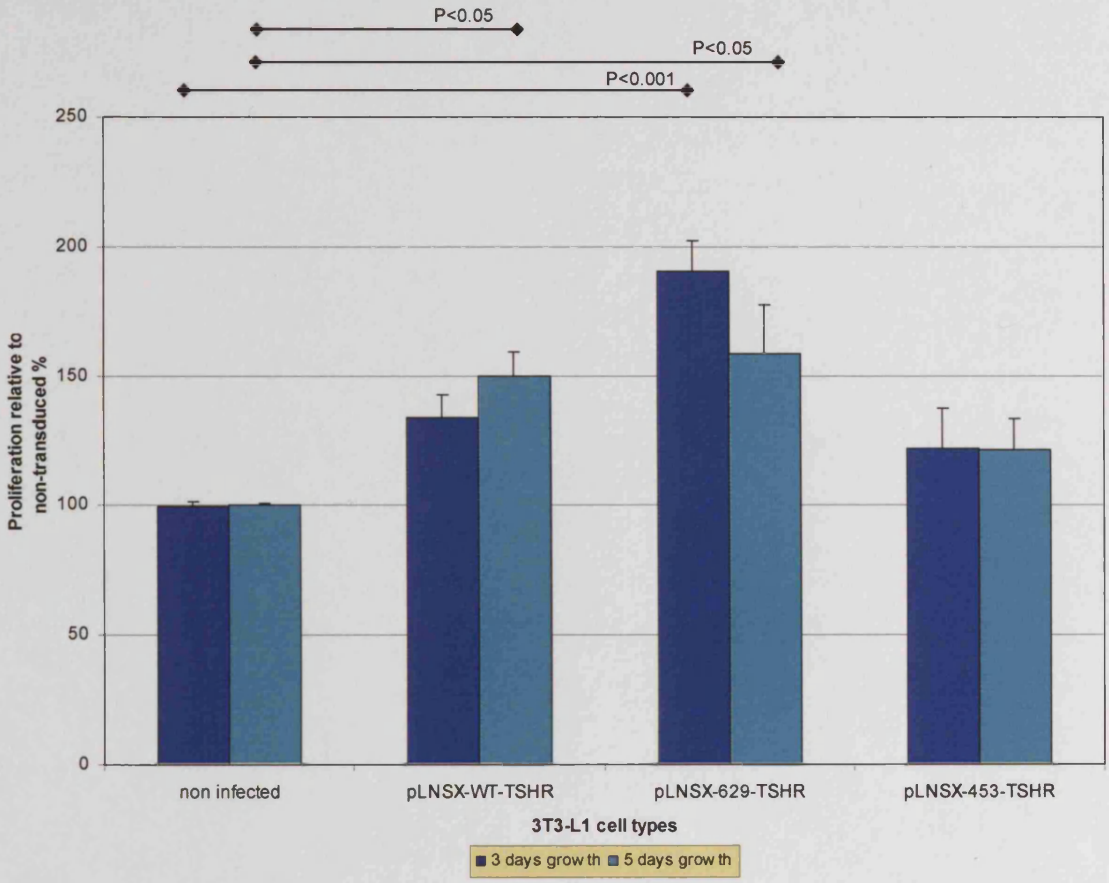

Figure 3.6 Proliferation of HC C1 cells

Cell proliferation in HC C1 cells is reduced in WT while only minor effects are seen on L629F and M453T cells that are greater at 5 days.

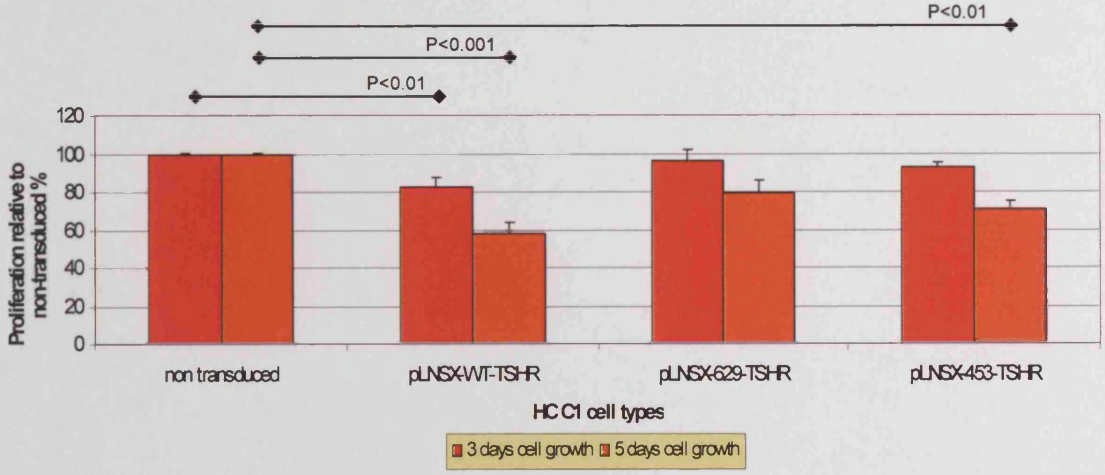

Figure 3.7 Proliferation in MG63 cells

Proliferation in MG63 cells showed minor reduction in WT numbers and minor proliferation with L629F and M453T but changes were not significant at three days relative to non transduced cells. With these opposite effects, significance was seen between the inhibited WT and the proliferating L629F and the M453T.

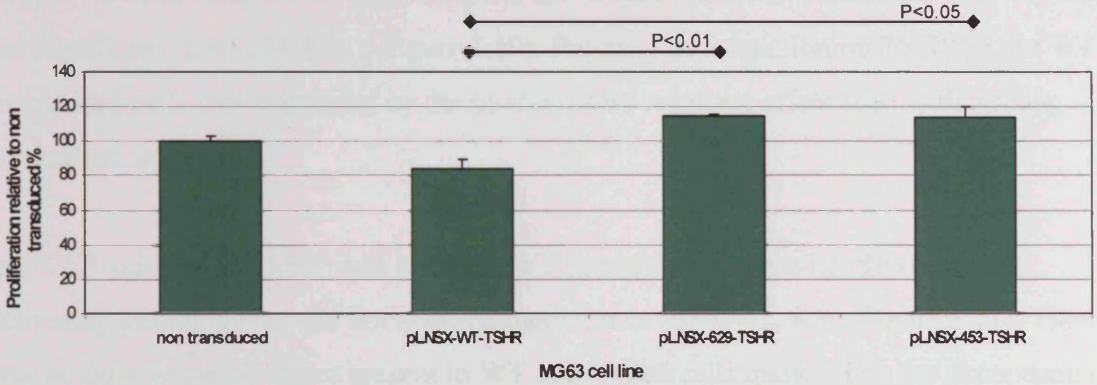

Figure 3.8 Proliferation in Graves' orbital preadipocytes

Graves' orbital preadipocytes showed reduced proliferation in all transduced cells relative to non transduced at seven days and was significant in L629F and M453T. M453T proliferation was significantly less than than WT and L629F, but L629F and WT did not differ significantly.

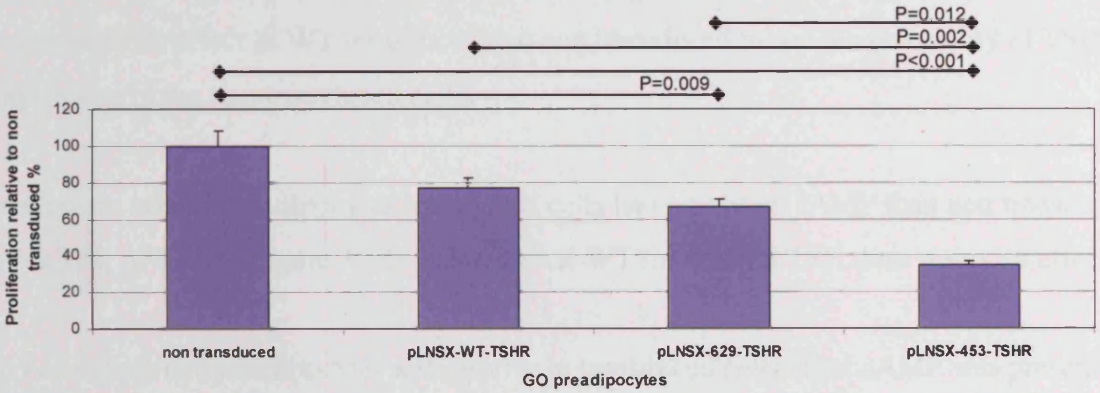

Figure 3.9 Proliferation in normal orbital preadipocytes

Normal orbital preadipocytes showed reduced proliferation in all transduced cells relative to non transduced at seven days and was significant in L629F. L629F and WT did not differ significantly. Proliferation in the M453T cells was so profound that insufficient cell numbers could be collected for experimentation.

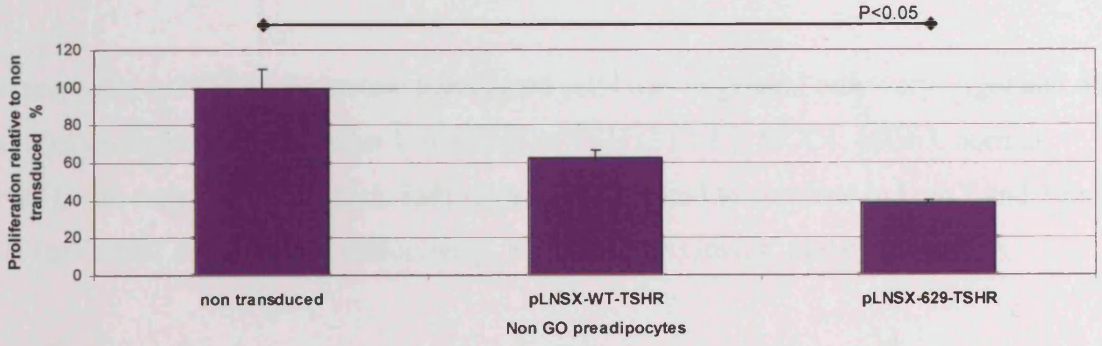

3.3.4 Basal cAMP production can be elevated by transduction with activating TSHR mutations. M453T generates more basal cAMP than L629F

In 3T3-L1 cells basal cAMP showed some low level increase in transduced cells but was not significant (p=0.174(KW), Figure 3.10). Presence of a functioning TSHR in the WT transduced cells was suggested by the positive dose response effect seen with a rising concentration of TSH.

In HCC1 cells basal cAMP was raised in WT transduced but not L629F or M453T activating mutations but did not achieve significance (p=0.342, KW, Figure 3.11). There was no dose response effect present in WT transduced cells questioning the expression of receptor in these cells while there was a slight rise at 1mU TSH in the M453T transduced cells.

In the MG63 cells, transduced cells had less basal cAMP than non transduced (p=0.01, KW, but none were significant with post hoc testing, Figure 3.12). The presence of a dose response TSH effect in WT transduced and non transduced raised the possibility of TSHR expression in the non transduced cells.

In Grave's orbital preadipocytes transduced cells had less basal cAMP than non transduced (p=0.328, ANOVA, Figure 3.13) and a normal WT transduced TSH dose response effect.

In normal orbital preadipocytes a slight rise in transduced cells basal cAMP was present (p=0.102, KW, Figure 3.14) and a normal WT transduced TSH dose response effect.

The predicted basal rise of cAMP of activating mutations above non transduced cells was present in only 3T3-L1 and normal orbital preadipocytes. However it is noteworthy that in all cell types L629F basal levels are lower than M453T.

The response to TSH in the mutant transduced cells was in general only very slight and did not achieve significance in either 1 or 10mU of TSH (3T3-L1, HCC1, MG63, normal orbital). The only group in which TSH signalling appeared to continue in both 1 and 10mU TSH ($p<0.0001$ and p=0.007 respectively, KW) was the Graves' preadipocytes.

Figure 3.10 cAMP production by 3T3-L1 cells

Basal cAMP production in 3T3-L1 cells is slightly elevated by activating mutants L629F and M453T. There is an expected dose response effect of increasing TSH concentration on the WT transduced cells. Forskolin activates cAMP in all cell types. (N=2, hence no error bars).

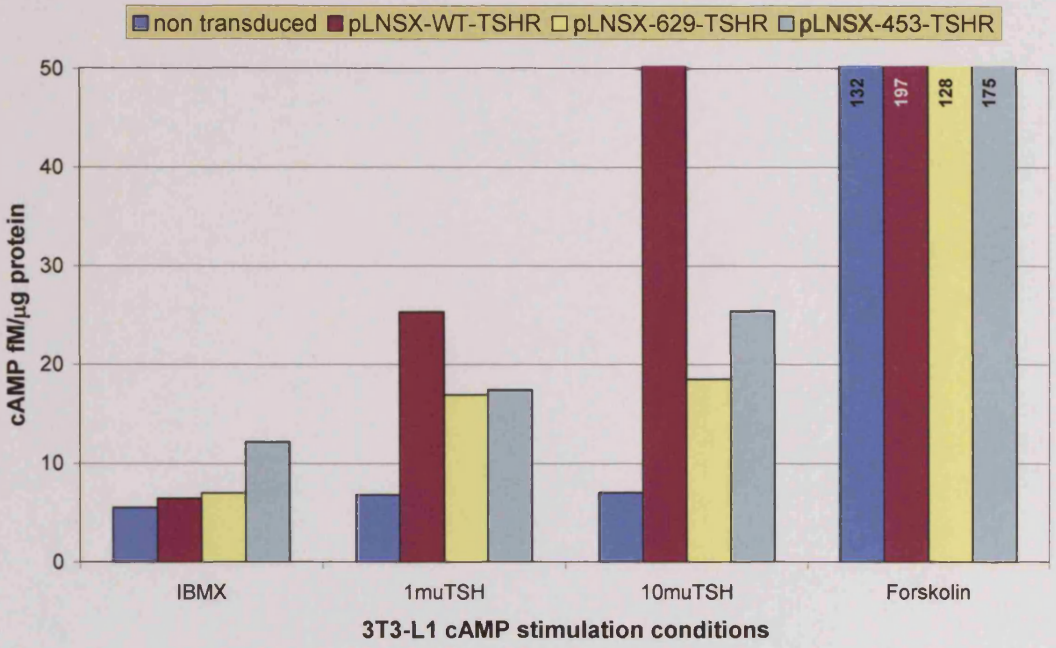

Figure 3.11 cAMP production by HCC1 cells

HCC1 cells cAMP production shows no elevation by the activating mutants and lacks a dose response effect from the WT transduced cells. (N=2, hence no error bars).

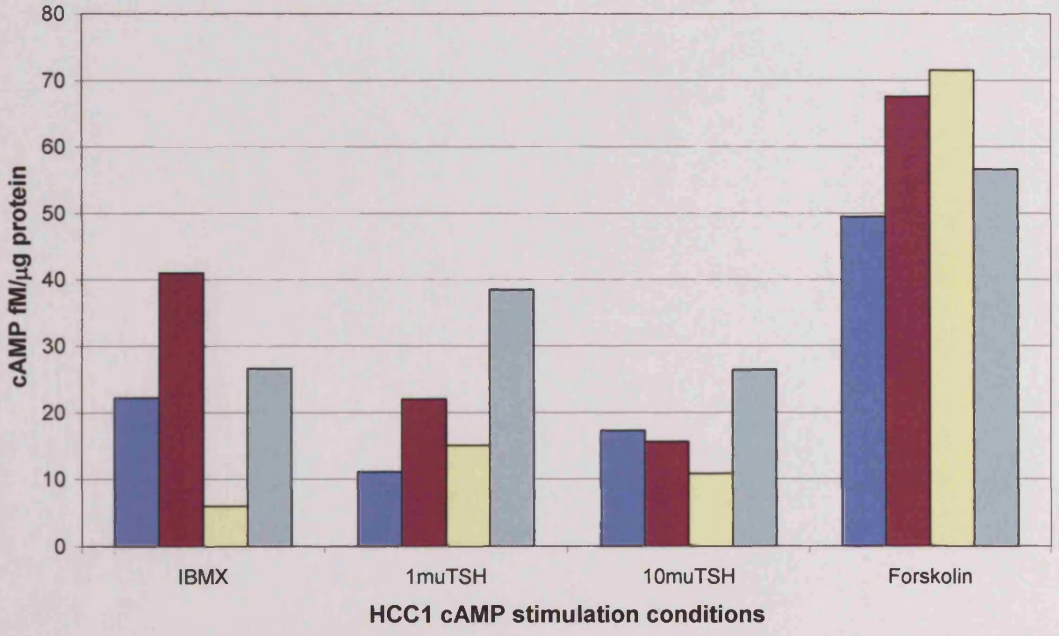

Figure 3.12 cAMP production by MG63 cells

MG63 cells show no increase in basal cAMP in the transduced cells. The TSH dose response effect is seen in both WT transduced and non transduced cells suggesting functional TSHR in these cells. Low response to forskolin may suggest a phosphodiesterase insensitive to IBMX. (N=2, hence no error bars).

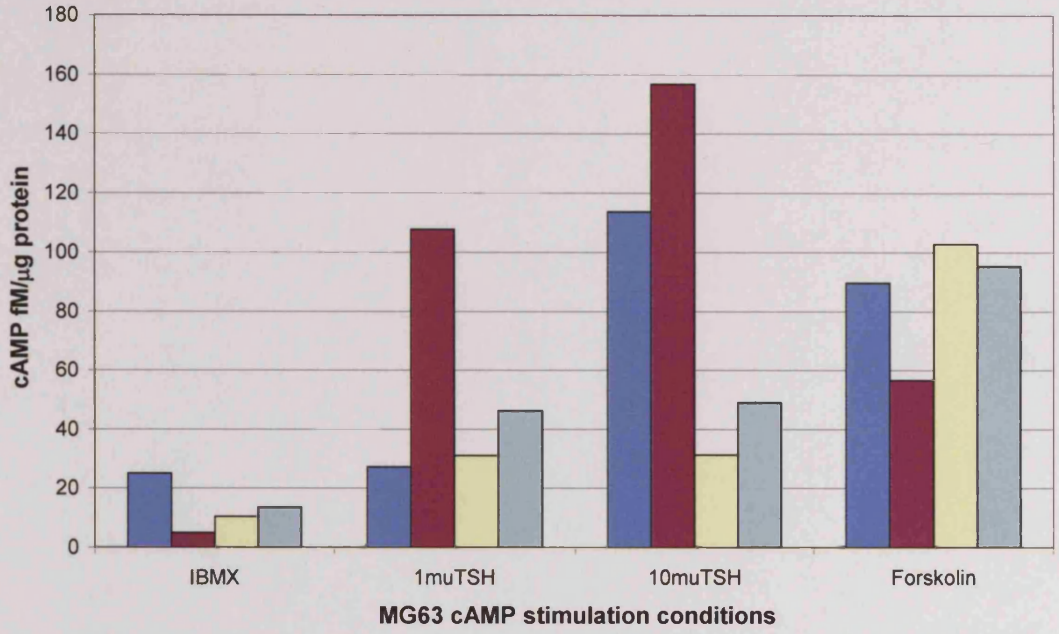

Figure 3.13 cAMP production by Graves' orbital preadipocytes

Graves' orbital preadipocytes showed no increase in basal cAMP in transduced cells. WT transduced cells showed the expected dose response effect while both mutant forms appear to respond to TSH stimulation. (N=4)

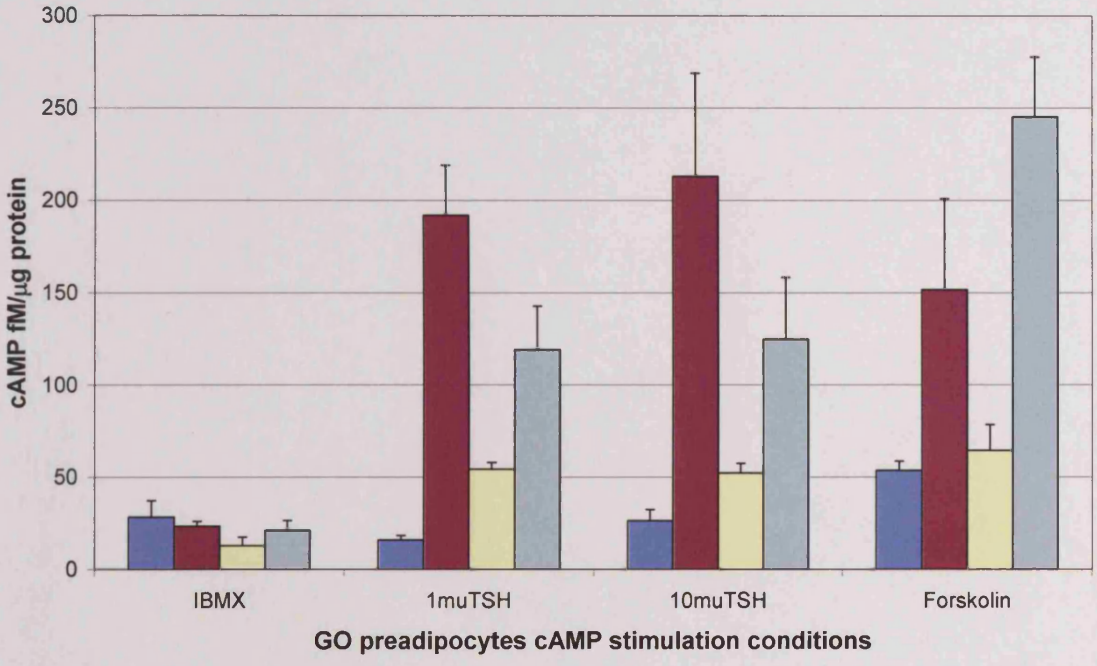

Figure 3.14 cAMP production by normal orbital preadipocytes

Normal orbital preadipocytes show an increase in basal cAMP in transduced cells along with the expected TSH dose response effect in the WT transduced cells. Response to forskolin is low in WT and L629F cells.

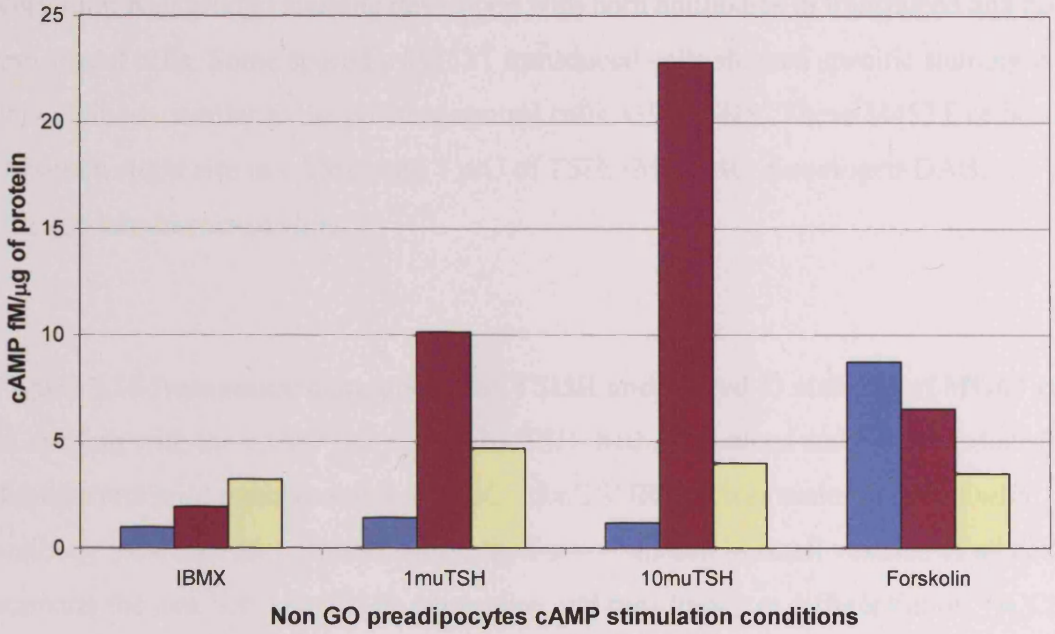

3.3.5 HCC1 cells did not uniformly express TSHR, while transduced and non transduced MG63 cells express TSHR and accumulate lipid

ICC for TSHR on HCC1 cells showed some sporadic staining using antibody 3G4 (and 23.1) of M453T transduced cells that also showed a mild rise in cAMP on stimulation with 1mU of TSH (Figure 3.15). Other cell types exhibited background staining in keeping with absence of dose response effects to TSH in cAMP production (Figure 3.11).

ICC for TSHR on the MG63 cells showed transduced and non transduced cells both expressed low levels of the receptor including the sulphated form (Figure 3.16). This is consistent with the increased levels of cAMP seen by stimulating these cells with TSH (Figure 3.12). In keeping with differentiating preadipocytes expressing TSHR, almost universally, MG63 cells accumulate small lipid vesicles in transduced and non transduced cells. No HCC1 cells accumulated lipid. With the expression of both TSHR and lipid in the MG63 cell line it would suggest they are further along the pathway from preadipocytes to adipocyte than the other preadipocytes examined here.

Figure legends

Figure 3.15 Immunocytochemistry for TSHR on HCC1 cells

Very faint background staining developed with both antibodies in transduced and non transduced cells. Some sporadic M453T transduced cells showed specific staining with 3G4 antibody similar to the positive control cells, GPI-TSHR. These M453T cells also showed a slight rise in cAMP with 1 mU of TSH. (Mag.x40, chromogen-DAB, counterstain-haematoxylin).

Figure 3.16 Immunocytochemistry for TSHR and oil red-O staining of MG63 cells

In keeping with the cAMP rise caused by TSH, both transduced and non transduced cells demonstrate mild positive staining by ICC for TSHR that was easier to detect with antibody 3G4 than 23.1. Additionally, lipid accumulation in small vesicles of all cell types supports the link between TSHR expression and preadipocytes differentiation. (ICC; mag.x40, chromogen-DAB, counterstain-haematoxylin. Lipid; mag.x20, oil red-O, counterstain-haematoxylin).

Figure 3.15 Immunocytochemistry for TSHR on HCC1

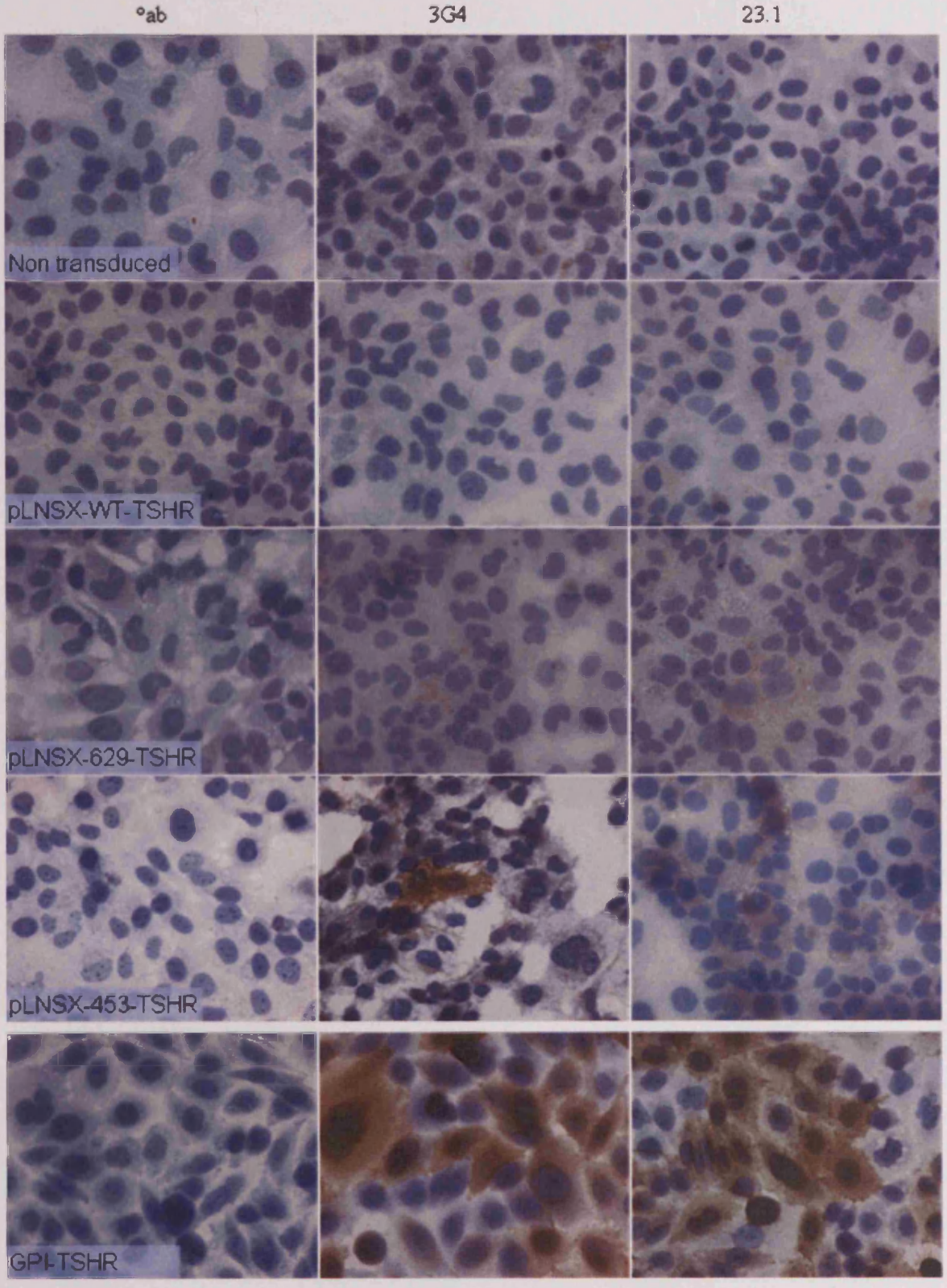

Figure 3.16 Immunocytochemistry for TSHR and oil red-O staining on MG63

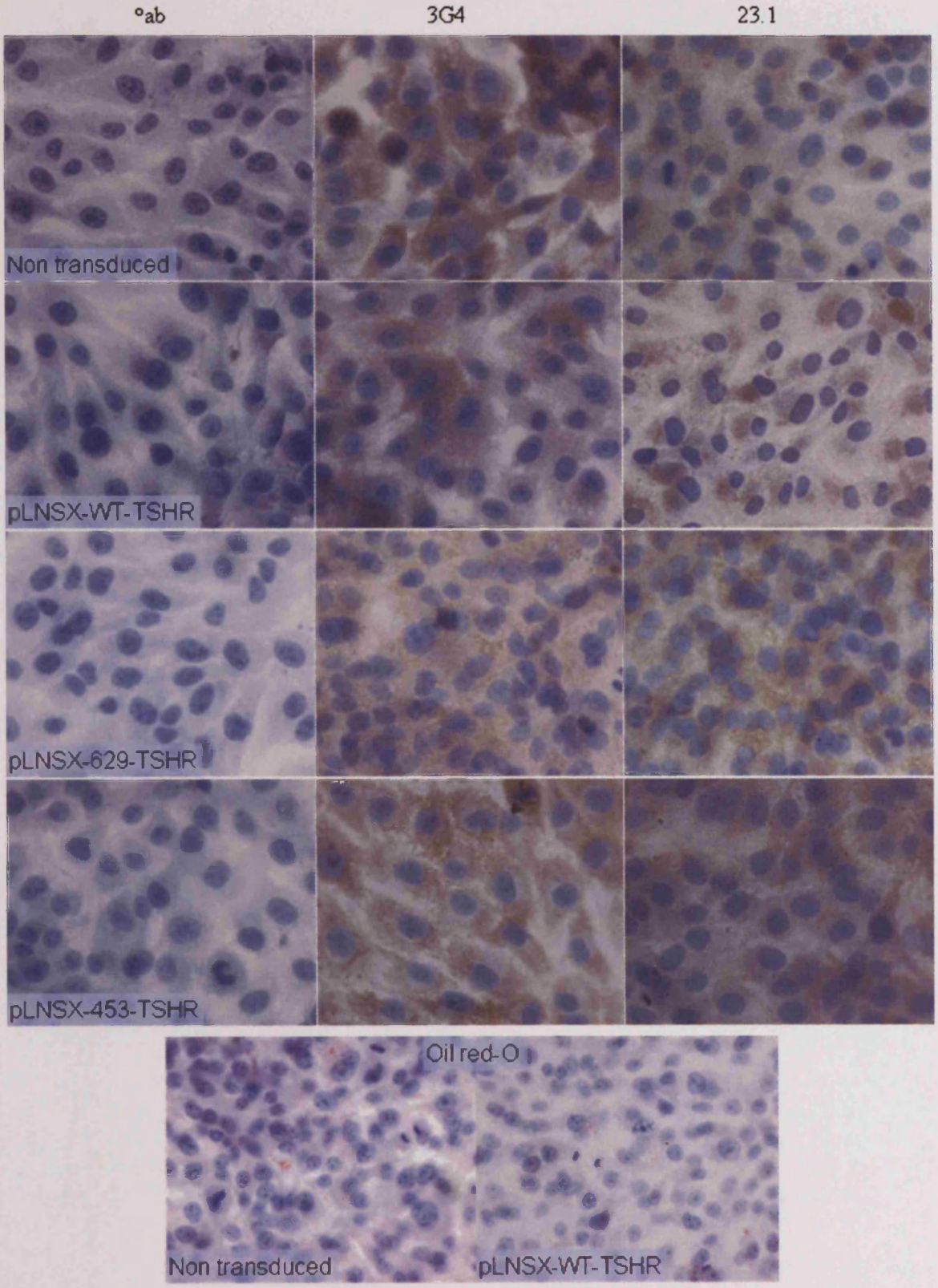

3.3.6 Cell proliferation inhibition has contrasting effects on lipid accumulation in primary preadipocytes

Activating TSHR transduction produced no spontaneous lipid accumulation within the normally passaged cultures of 3T3-L1, HCC1, normal and Graves' orbital preadipocytes. As mentioned previously non transduced MG63 cells accumulate lipid with no discernable effects of transduction when assessed by ORO staining.

In differentiating conditions both transduced and non-transduced 3T3-L1 cells accumulate small lipid vacuoles spontaneously after growth arrest at confluence that occurred early in the 14 day culture. Quantification by visible lipid accumulation could not detect variations in differentiation in the 3T3-L1 cells transduced with activating mutations. For both 3T3-L1 and MG63 lipid assessment by this means lacked sensitivity. Flow cytometry using Nile red was carried out on differentiated, undifferentiated, transduced and non transduced 3T3-L1. This demonstrated the same problem in that all cells would take up Nile red and fluoresce just as they had done for ORO (Figure 3.17). Other fat cell markers such as mRNA for PPARγ, aP2 or triglyceride would be required to further assess cellular differentiation.

Figure 3.17 Nile red flow cytometry in 3T3-L1 cells

Undifferentiated (open histogram) and differentiated (filled histogram) 3T3-L1 cells universally accumulate variable sized lipid vacuoles after reaching confluence. Without the lipophyllic nile red stain, fluorescence is less than 10^2 for both groups of cells. Fluorescence increases equally with nile red in both groups confirming the finding with oil red-O that all 3T3-L1 cells accumulate lipid in these conditions.

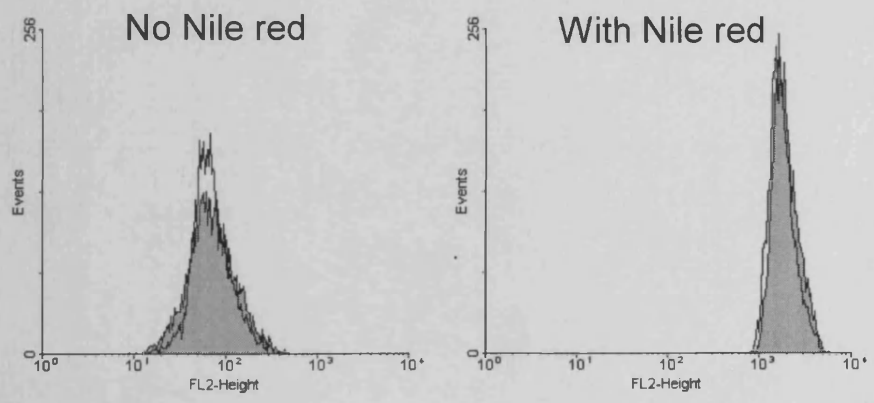

In human preadipocytes no lipid accumulation was seen in the non-differentiating conditions. PPARγ induced differentiation showed significant variation between the lipid accumulation of transduced cells from a Graves' orbit relative to non transduced ($p<0.0001$, KW), WT (44%), L629F (445%) and M453T (0%) (Figure 3.18). Post hoc testing did not identify significant differences between the groups because of the small sample size and inability to repeat experiments with the slowly proliferating cells. Similarly in the transduced normal orbital preadipocytes, lipid accumulation was significantly different ($p<0.0001$, KW), WT (225%) and L629F (0%) but no significant differences were present between transduced and non-transduced cells. There appeared to be a biphasic pattern of lipid accumulation in relation to cell proliferation in human primary preadipocytes. In transduced cells with a moderate reduction in proliferation (~65% relative to non-transduced) there was an increase in lipid accumulation, Graves' L629F (444%) and normal WT (225%). In contrast, in cells whose proliferation was inhibited the greatest (~30%), despite morphological changes characteristic of adipogenesis, cell clustering and rounding up of the normally slender fibroblast, no lipid accumulation developed in either Graves' M453T or normal L629F (Figure 3.19). In the normal orbital, L629F, the failure of lipid accumulation and greatest reduction in proliferation also coincides with the cell type with the highest basal cAMP.

Figure 3.18 Lipid accumulation in primary preadipocytes varies in transduced cells

In normal orbital preadipocytes, WT transduced cells accumulate more lipid than non transduced and L629F don't accumulate any lipid. In Graves' preadipocytes there are also variations. The cell types that don't accumulate any lipid (non GO L629F and GO M453T). (N=2)

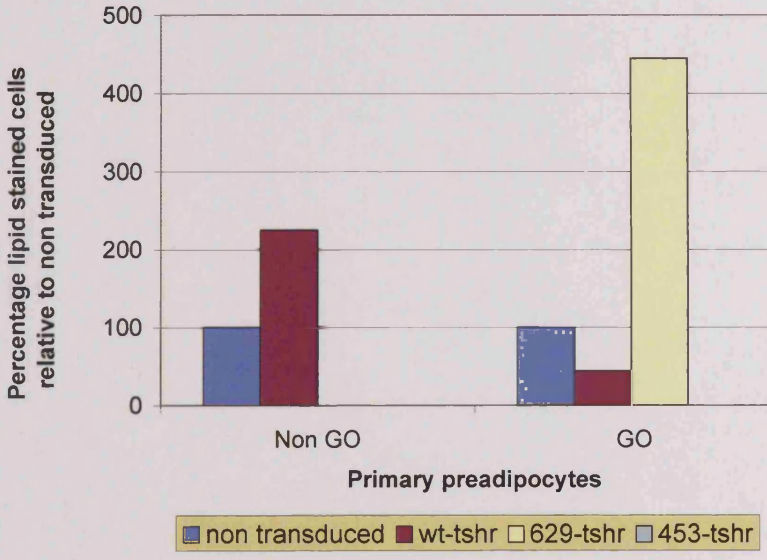

Figure 3.19 Lipid accumulation in Graves' orbital preadipocytes

Discrete cells developed lipid containing vacuoles when differentiated in the presence of PPARγ agonist apart from those whose proliferation was inhibited the greatest, M453T (upper panel). Differentiated cells also tend to cluster and alter shape becoming rounded and lose the slender fibroblastic appearance of their undifferentiated counterparts (lower panel).

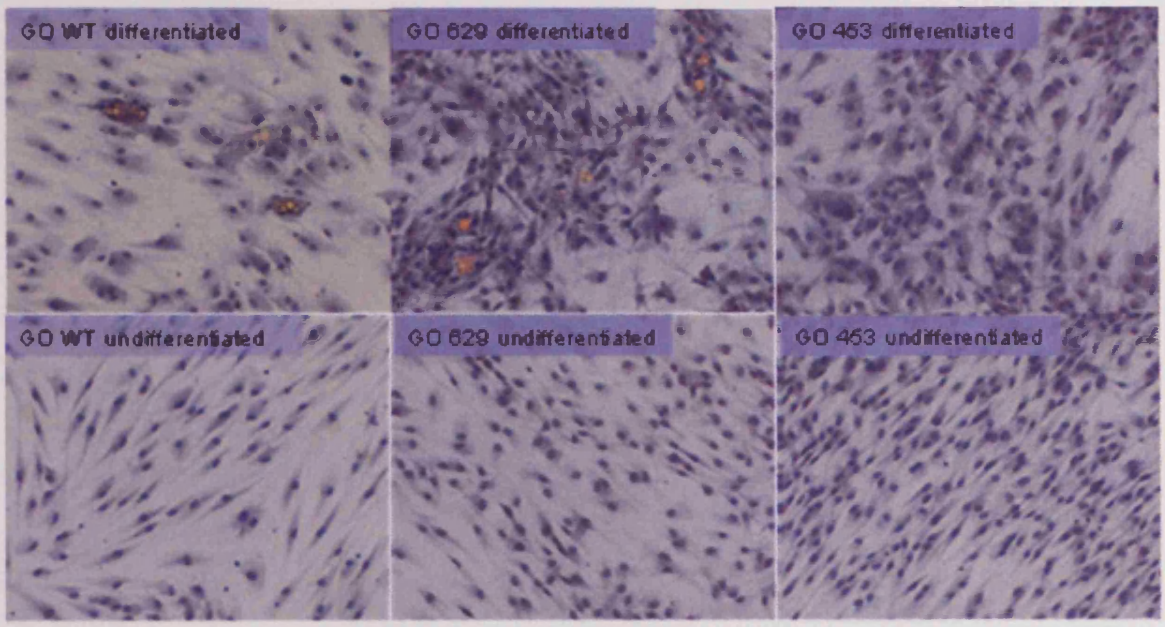

3.4 Discussion

Orbital fat is scarce for investigators to come by and highly passaged preadipocytes lose their ability to differentiate. Standard practise for explant cultures is to discard the explant after sufficient cells have gathered and then to continue monolayer cultures to expand cell numbers [276]. Modifying the culture by removing the explant and allowing them to reattach, we were able to harvest first passage preadipocytes for many months from the same explants. Fat explants in long term culture reduced progressively in size, liberated lipid into the medium and away from the explants themselves, underwent morphological changes to that of a fibroblast. These changes were consistent with adipocyte dedifferentiation. A time course study of explanted fat showed changes occur within the first 48 hours[287]. The medium of explants developed increased, TNFα, anaerobic glycolysis and lipolysis. There was also a rapid reduction in expression of adipocyte specific genes; hormone sensitive lipase, lipoprotein lipase and PPARγ2. These changes could be reduced by agents that elevate cAMP (IBMX/forskolin). In our experience, despite the explants' dedifferentiation and inexorable shrinkage, outgrowth of cells continued undiminished with the rate-limiting factor for culture duration always being mould infection.

In some cultures, cells adjacent to explants accumulated lipid and maintained vacuoles that did not appear to dedifferentiate over 6-8 weeks of culture. This morphology did not persist when explants were removed. This raises interesting possibilities that explants either; maintain the morphology of partially dedifferentiated adipocytes that have migrated onto the plate or that preadipocytes are being differentiated and maintained by paracrine factors present in the explant. The fact that fat conditioned medium (fat floating in the medium) does not maintain the phenotype might suggest soluble factors alone are insufficient and that either cell contact or extracellular matrix are important. Two preadipocyte surface receptors that may be involved with this paracrine action; leukaemia inhibitory factor (LIF) receptor and prostacyclin receptor, have proadipogenic effects via both C/EBPs[288; 289]. However, both LIF and prostacyclin are secreted by preadipocytes and not adipocytes. LIF signals via the extracellular signal related kinase (ERK) pathway, prostacylin by cAMP production and both have a common downstream effector, cAMP responsive element binding protein/activated transcription factor 1 (CREB/ATF1)[290].

Returning to our primary aim of examining adipogenesis in the presence of elevated cAMP using gain-of-function TSHR mutations, perhaps the clearest effects were demonstrated in the normal orbital preadipocytes. We show increased basal cAMP, significant inhibition of undifferentiated preadipocyte proliferation and reduced lipid accumulation despite morphological changes suggestive of differentiation. The inhibition in the M453T transduced cells was so profound that from the initial colonies sufficient cells never accumulated to be studied. This inhibitory trend on proliferation was also seen in the Grave's orbital preadipocytes and HCC1 cells. This reduced proliferation is in keeping with the effects seen in NIH3T3 cells expressing activated $G_{\alpha s}$ [291]. The cAMP stimulation activated protein kinase A (PKA), inhibited Ras proliferative signalling and arrested fibroblasts in G_1.

Different effects were seen on the cell proliferation of transduced 3T3-L1 cells. A moderate rise in basal cAMP induced by the L629F mutation was accompanied by an increase in cell proliferation at 3 days but after 5 days the WT/L629F transduced cells were all shown to proliferate significantly relative to non-transduced. However, the increase in cell numbers is affected by cell density and this is particularly an issue with the rapidly proliferating 3T3-L1 cells[271], whereby the number of L629F cells may have been inhibited by approaching confluence after 5 days of culture and the data at 3 days may be more representative. Similarly in MG63 cells proliferation was seen with L629F and M453T above that of WT but not above non transduced cells. These seemingly opposite effects occurring in the cell types are likely to be due to different cell specific cAMP signalling and recruitment of pathways such as mitogen-activated protein kinase (MAPK) among others (reviewed in [292; 293]). Uncommonly cells proliferate in the presence of cAMP (thyroid/pituitary) as did the transduced 3T3-L1 and MG63. Additional similarities: 3T3-L1 readily differentiate into adipocytes that express TSHR and MG63 cells already express TSHR and accumulate lipid. (The MG63 cell line has previously been shown to express TSHR[294] and our ICC and cAMP data support these findings). More commonly cAMP has inhibitory effects on cell growth as in the transduced human preadipocytes and HCC1 cells, as mentioned above, similar to the effects seen in NIH3T3 cells expressing activated $G_{\alpha s}$ [291]. Alternatively other pathways such as the inositol phosphate-diacylglycerol cascade have also been shown to be activated by mutant forms of TSHR [295] and the $G_{\beta\gamma}$ protein subunits may be signalling [296].

In differentiated normal preadipocytes a slight rise in basal cAMP increased lipid accumulation, higher levels completely inhibited lipid accumulation in what appeared to be differentiated cells. From these studies it is unclear whether this represents variation in cAMP induced lipolysis or altered adipocyte differentiation. During differentiation cAMP elicits a pro-adipogenic effect first described in 1976 using IBMX and PGF2α [297]. Elevation of cAMP by IBMX rapidly reduces the differentiation suppressing Wnt10b [298]. CREB activation alone was shown to be sufficient to induce adipogenesis in 3T3-L1[131] and CREB induced the important PPARγ co-activator, PGC-1α gene expression [299]. Alternatively the lipolytic potential of cAMP has long been described (1970), whereby cAMP activated protein kinase increases lipase activity [300]. Adrenergic induced cAMP elevation causes translocation of hormone sensitive lipase from the cytosol to the membranes of lipid vesicles prior to the release of glycerol [301]. However the changes of apparent adipocyte morphology without the lipid vacuole formation has been seen previously, reported in 1981, in the presence of prolonged elevation of cAMP during adipocyte differentiation [302]. The altered morphology was probably due to reduction in actin (amongst other proteins). The lipid accumulation was reduced due to decreases in key lipogenic enzymes (fatty acid synthase, malic acid and glycerophosphate dehydrogenase) and was not as a result of increased lipolysis.

Similarly in differentiated Graves' orbital preadipocytes a slight reduction in proliferation was seen in line with increased lipid accumulation whereas greater inhibition of proliferation completely stopped visible lipid accumulation. However, proportional changes in basal cAMP were not detected and this maybe due to sampling error. We would have predicted that all cells transduced with L629F and M453T would have had basal increases in cAMP. This was not the case; one possible explanation is the presence of a phosphodiesterase insensitive to IBMX. Alternatively we measured basal increase cAMP after four hours, similar to that used for FRTL-5[89] cells, but longer than the 30 minutes used by other groups for 3T3-L1 [264]. With the action of multiple different phosphodiesterases terminating cAMP signalling, time course studies of cAMP kinetics would ideally be undertaken for each cell type to understand possible variation in cAMP levels developing in the transduced cells.

An impression of the negative effects of TSHR activation on lipid accumulation in human preadipocytes is given by our experiments. The impact of TSHR activation in 3T3-L1 is not evident from our experiments. A much shorter differentiation time is required for

murine and rat preadipocytes (7-9 days) than human (15-20 days). Our experiments allowed both to proceed for 14 days. In rat preadipocytes lipid accumulates in 85% of cells after 5 days and increases to greater than 90% at 9 days [271]. Direct cell counting of ORO stained cells was our only method to assess adipogenesis, other groups include estimation of lipid vacuole size [270]. Difficulties counting large numbers of lipid staining 3T3-L1 cells manually lead us to Nile red staining with flow cytometric counting. This confirmed what we found with direct cell counting but may be of use when smaller proportions of the cells populations accumulate lipid as in human preadipocytes. Conversely ORO could miss cells (fig 3.1.2.D) that have possibly undergone lipolysis whose vacuoles do not stain. Relying on lipid staining to measure adipogenesis is insufficient and additional parameters such as glycerol, free fatty acids or markers of terminal differentiation (LPL, PPARγ, ACRP30) would be supportive of adipogenesis in future work.

The use of pLNSX-WT cellular transduction with activating mutations was effective in the main in inducing a TSH dose response elevating cAMP (apart from HCC1 cells). TSH dose response effects from mutant expressing cells were generally low in all cell types but the Graves' orbital preadipocytes. TSH signalling was maintained in these cells in both pharmacological concentrations (1 and 10mU). It has been shown both in vitro and in vivo that activating mutations are often poorly expressed at the surface of cells contrasting with the high surface expression of TSHR in Graves' disease [280; 295; 303]. It is a curious finding in Graves' disease that in spite of continual receptor stimulation by TSAB the normal inducible cAMP early repressor mechanism of down-regulation of TSHR does not occur [304]. It would seem similarly uncharacteristic that mutant forms of TSHR are readily signalling in preadipocytes derived from a Graves' patient and one can only speculate on possible causes of both these processes.

How then might TSHR activation via TSAB have a proadipogenic role in Graves' ophthalmopathy? From our work we see that a moderate reduction in cell proliferation seen with a parallel moderate increase in cAMP results in enhanced adipogenesis, underlining the already well established role of elevated cAMP in preadipocyte differentiation. Higher levels of cAMP induced by activating mutations reduce lipid accumulation possibly due to reduced expression of lipogenic enzymes, rather than inducing lipolysis. Our model is not faithful to the physiological pattern of TSHR expression in adipogenesis because it is continually driven by the retroviral SV40 promoter. Differentiating preadipocytes express TSHR from day 5 onwards and as lipid is

already accumulating by day 7, TSHR expression is peaking in 3T3-L1 cells. Ideally we would investigate TSHR activation following this pattern using inducible vectors/TSAB monclonals. Additionally we need to determine the TSHR expression pattern accurately in human primaries to be able to replicate the experiments. TSAB or TSH would seem to have a relatively brief period in which it could affect adipogenesis given TSHR expression in mature adipocytes is low. It is currently questionable that TSHR on preadipocytes signal greatly given the in vitro TSH concentrations (10-100mU) required to do so are above normal physiological levels. However TSAB could be a supra-physiological stimulus or have higher affinities for TSHR on differentiating preadipocytes. It is also interesting that of all our transduced cells, the Graves' ophthalmopathy patient had the clearest dose responsive TSH signalling. Is it possible that the normal mechanism of TSHR down-regulation seen in thyrocytes is impaired in Graves' disease and ophthalmopathy? Does this promote later stages of adipocyte differentiation producing cells whose volumes once lipid laden is vast compared to its precursor cell? Clarifying our understanding of these very basic models is necessary before we can extrapolate to the complexity of orbital cells and cytokines present in Graves' ophthalmopathy. Had TSHR activation resulted in proadipogenic effects like those seen with PPARγ agonists a case for a direct role in adipogenesis could have easily been argued. However, our model needs to be adapted to more closely follow the pattern of TSHR expression in adipogenesis to answer our question. If a role for TSHR activation in adipogenesis cannot be identified perhaps more direct effects are exerted either towards vascular structures or immune cells to cause orbital congestion in Graves' ophthalmopathy.

4 Characterisation of the alterations in tear composition in smokers and patients with Graves' ophthalmopathy

4.1 Introduction

4.1.1 Effects of smoking on Graves' ophthalmopathy

Smoking has been identified as an environmental factor that may promote ophthalmopathy in Graves' disease patients (reviewed in[60; 305; 306]). Smoking effects are immediate, linked to current, not lifetime smoking patterns and Graves' disease smokers are more likely to develop ocular motility disturbance and proptosis [307]. A cohort of newly diagnosed Graves' disease patients showed smokers had a 1:3 fold increase in symptomatic ophthalmopathy with objective measurements of proptosis and diplopia being 2.6 and 3.1 times more common respectively. One possible mechanism investigated, smoking induced hypoxia, showed orbital fibroblasts (but not dermal fibroblasts) produced increased glycosaminoglycans on stimulation with TNFα, INFγ and IL-1 in vitro, compared with normal oxygen tension [308]. Both Graves' ophthalmopathy patients and healthy smoking female controls have elevated levels of antibodies to HSP72, but antibodies do not correlate with severity, suggesting a marker of autoimmune susceptibility rather than a disease specific marker [309]. Cigarette smoke constituents, tar and nicotine, in the presence of INFγ, promote expression of HLA-DR in orbital fibroblasts [310]. The enhanced antigen presentation in smokers could increase their susceptibility. Mast cells exposed to cigarette smoke in vitro release several cytokines including IL-4, 5, 10 and 13 and TNFα and are thought to have pro-allergic effects [311]. IL-4 and 13 induce class switching to IgE and while Graves' ophthalmopathy is not an allergic disease, TNFα is a major cytokine implicated in several aspects of pathogenesis [312]. Smoking not only modifies the presentation of disease but also prolongs recovery in terms of soft tissue swelling and ocular motility when treated with steroid and radiotherapy for moderate (CAS 2-6) Graves' ophthalmopathy [313].

4.1.2 Tear film and content abnormalities in Graves' ophthalmopathy

Dry, burning, watery eyes are some of the most widely experienced symptoms of Graves' ophthalmopathy patients. Reduced tear break up times (TBUT) are common in Graves'

ophthalmopathy[314] but the causes are many. These symptoms can be contributed to by factors that increase corneal exposure and tear evaporation: vertical palpebral aperture, proptosis, blink rate, lagophthalmos and lid lag. Tear osmolarity is commonly elevated in Graves' ophthalmopathy associated with greater palpebral apertures and higher blink rates [315]. Blink related micro-trauma is a process explaining the pathogenesis of superior limbic keratoconjunctivitis (SLK) seen in Graves' ophthalmopathy [316]. Alterations in lubricity and blinking result in a spiral of changes that damage tarsal and bulbar conjunctiva and corneal epithelium and in turn continue the tear film disruption and high blink rates. The volume of tears in Graves' ophthalmopathy has been shown recently to be decreased and correlates with an increase in ocular surface damage [317].

Lacrimal gland involvement in Graves' ophthalmopathy was first reported in 1935 [318] and radiological evidence came with advances in CT imaging in the early 1980's [319]. Increased activity within the lacrimal gland has also been highlighted by radiolabelled gallium and somatostatin [320; 321]. Interestingly the gallium scan[320] detected increased uptake in thyroid, thymus and lacrimal gland, all of which express TSHR and can be enlarged in Graves' ophthalmopathy [228; 317]. Examining the products of lacrimal secretion would therefore seem worthwhile, however, conjunctival vessel transudate, goblet cells and mucosal associated lymphoid tissue also contribute to tears. Protein analysis of tears using PAGE has shown reductions in lysozyme, lactoferrin and lipocalin in patients with longstanding severe infiltrative ophthalmopathy and attributed to lacrimal gland dysfunction [322]. Using HPLC separation of tear proteins, 5 peaks were observed, increases in IgA or protein G peak were obtained in 28% of Graves' ophthalmopathy samples [323]. IgA antibodies have been shown in Graves' disease directed towards thyroglobulin, microsomes and TSHR [34; 324]. The endomysium and perimysium of Graves' ophthalmopathy ocular muscles (not orbital fat), in longstanding or severe disease, exhibits staining for IgA_1 [325].The unknown protein G eluted between lactoferrin (80kD) and lysozyme (14kD) and was elevated in 20% of Graves' ophthalmopathy patients [323]. No link could be drawn between the NOSPECS classification of the patients and their tear protein profile. The same group reported an increased IgA:lysozyme ratio in 33% of Graves' ophthalmopathy patients, especially those with long-standing disease [326]. Searching through a reference 2D gel map [327] for a tear protein between 80-14kD identifies firstly; zinc-α_2-glycoprotein (ZAG), several isoforms present between 44-50kD and secondly; an abundant n-terminal sequence blocked protein of 67kD (this most likely represents albumin, 66-69 kDa).

Apart from the previously discussed causes of tear film disturbance, two further radio-iodine related causes are also noteworthy. An initial report showed radio-iodine is secreted in tears [328] and subsequently a prospective study has demonstrated ocular dryness with a sicca like dry mouth in a quarter and a third (respectively) of patients receiving radio-iodine therapy [329]. The effect is mostly transient but can persist past three years and is an additional factor that compounds Graves' ophthalmopathy patients' tear film problems. Conversely epiphora can occur due to radio-iodine induced naso-lacrimal obstruction [330].

4.1.3 Tear thyrotropin stimulator in smokers and Graves' patients

Availability of GO orbital adipose and connective tissues is restricted to that obtained from invasive surgery, often when disease is inactive. A non-invasive method to evaluate immune and endocrine mediators present in active disease was sought. TRAb activity has previously been demonstrated in saliva from patients with Graves', Hashitoxicosis and Hashimoto's thyroiditis and found to be higher than TRAB activity in serum [331]. Given the above outlined changes in tear film proteins and lacrimal gland inflammation; tears were assessed for thyrotropin receptor stimulating activity (TSHR-SA) and protein changes that may occur in conjunctival/lacrimal secretion as a result of orbital disease.

The principle of using bioassays to detect TSAB by measuring cAMP is well established [332]. Refining the assay demonstrated increased sensitivity for TSAB in lower salt assay conditions, loss of sensitivity in normal salt concentration did not occur with TSH [333]. While these low salt conditions are not physiological their use is widely accepted. Another variation on the TSAB bioassay was co-expressing the human TSHR and a cAMP responsive luciferase reporter in CHO cells that allowed the replacement of cAMP estimation with radioimmunoassay by light output in a luminometer [188]. Previous work within the department (S. Gullu, B. Mazzi and S. Rajapaska) measured TSHR-SA in tears using the cAMP luciferase reporter based assay described in 2.2.17 [188]. Results showed that 9/25 (36%) smokers, 7/51 (14%) Graves' disease patients and 13/47 (28%) Graves' ophthalmopathy patients had tear TSHR-SA above the 97th centile of non-smokers tears. To calculate specific TSHR-SA the stimulation index (S.I.) of 'zulu' cells (not expressing TSHR) was subtracted from the S.I. of 'lulu' cells (expressing TSHR) and values obtained (mean ± S.D. of each group) of normal non smokers (NNS, 0.15±0.52), normal smokers (NS, 0.35±1.09), Graves' disease (GD, 0.71±1.83) and Graves' ophthalmopathy

(0.73±1.29). The reference normal baseline group (NNS) had a 97th centile S.I. of 0.85. From this data, 'specific' TSHR-SA was present in the tears from approximately 25% NS, 32% GD and 41% GO patients.

TSHR-SA was assessed in the tears from 7 Hashimoto's thyroiditis patients (all female, age 28-62). A specific TSHR-SA was present in 2/7, both of whom were smokers.

Apart from tears, the luminescent assay was also applied to investigate the TSHR-SA of; Viscotears, a common ocular lubricant (carbomer, Novartis, 10% vol/vol in SFM), lysozyme (0.002 to 20μM), lactoferrin (recombinant and biochemically purified, Sigma, 0.001 to 10 μM), mast cell tryptase (0.002 to 20 μM) and of trypsin (0.01% vol/vol in SFM). Neither Viscotears nor lysozyme caused any TSHR-SA luciferase activity.

TSHR can be activated by the proteolytic cleavage of trypsin [334]. Trypsin (0.01% vol/vol) caused a modest TSHR-SA response (4-fold increase) after 10 minutes incubation and this persisted at 30 minutes incubation. A smaller response (2-fold increase) was also obtained using the 'zulu' cell line indicating the presence of receptors, which can be activated by proteolysis, endogenous to the parent CHO cell line. A second experiment demonstrated that the effects disappeared when the cells were incubated with trypsin for 60 or 120 minutes.

To examine proteins present in tears, pools from the various patient groups were analysed using silver-stained gels. A consistent observation was an increased vol/vol protein content in the tears from GO patients and smokers. This was accompanied by the presence of additional bands in the 30 to 40kD molecular weight range.

4.1.4 Aims: Further characterisation of the alterations in tear composition in smokers and patients with Graves' ophthalmopathy

1. To measure TSHR-SA in serum free and salt free conditions to determine whether activity is enhanced as in the case for TSAB.
2. To determine if a correlation exists between the TSHR-SA in tears, smoking, circulating thyrotropin stimulating antibodies and Graves' ophthalmopathy disease activity.
3. To identify a group of 30-40kD proteins in the tears of smokers and Graves' ophthalmopathy patients.

4.2 Methods

4.2.1 Patient recruitment

Three groups of individuals were recruited, these comprised 9 normal non-smokers (7 female, 2 male, age range 24-50); 8 normal smokers (7 female, 1 male, age range 24-60) and a group of 38 patients with Graves' ophthalmopathy (32 female, 6 male, age range 18-73) with ophthalmopathy clinical activity scores (CAS [22]) ranging from (0-9). Clinical data, tears and serum were collected and informed consent obtained in accordance with local research ethic committee approval (Bro Taf). Clinical data included age, sex, CAS, sum of proptosis (exophthalmometry readings from both eyes), orbital radiotherapy, steroid treatment (current, previous, none), radio-iodine treatment, carbimazole therapy, TSH, T4, T3, serum TSAB and tear TSHR-SA (in serum free and salt free conditions).

4.2.2 Tear collection and storage

Reflex tears were collected from both eyes using Shirmer strips placed at the outer canthus of un-anaesthetised eyes using gloved hands for 5 minutes. No prior administration of dilation or staining agents had occurred. Strips were removed using forceps and placed into 0.5ml Eppendorf tubes and caps sealed to prevent evaporation. To extract tears from the tubes, the base of the collecting tube was pierced with a 25G needle, the tube placed into a 1.5ml Eppendorf tube and then centrifuged at 3000g, 4 C for 5 minutes. Tubes were sealed, labelled and stored at -80 C until used.

4.2.3 Thyrotropin receptor stimulation assay

Both tear samples and serum were assayed using the TSHR luciferase assay as described in section 2.2.17 with the following modifications for the tear assay. 5µl of tears were analysed in triplicate in 45µl of both salt free and serum free buffer (app. A). Serum was assayed with 10µl serum in 90µl of buffer (i.e. both 10%vol/vol). The stimulation index of nine normal patients' tears and serum in the two buffers was used to generate a 97th centile cut-off, above which tear TSHR-SA and serum TSAB were considered positive. The assay

sensitivities were monitored by running a TSH standard in serum free medium (0.1/1/10mU) and a TSAB standard in salt free buffer (0.025/0.25/1U).

4.2.4 SDS-PAGE Analysis of Tear proteins

Tears from normal non-smokers (NNS), normal smokers (NS), GD patients (GD) and GO patients (GO) were pooled, usually in these four separate groups. Each sample of pooled tears was boiled with an equal volume of 2 x loading buffer (10% β-mercaptoethanol; 4% SDS; 0.125M Tris; 20% glycerol; 10% bromophenol blue) and 50μl per lane loaded onto 10% SDS-polyacrylamide gels. Electrophoresis was carried out as in section 2.2.4, followed by silver staining, according to the manufacturer's instructions (Biorad) or electroblotted to PVDF membranes for western analysis as in section 2.2.5. The blots were probed with a 1:500 dilution of rabbit polyclonal antibody to ZAG (H-123, Santa Cruz) for 1 hour. Detection used an anti-rabbit IgG-horse radish peroxidase (HRP) conjugate (1:5000, room temperature for 1 hour Amersham Biosciences) and was visualised by enhanced chemiluminescence (ECL Plus, Amersham Biosciences).

Tear proteins have also been stained after electrophoresis using SYPRO Ruby (Invitrogen) by a collaborator (Dr Catherine Winder, Department of Chemistry, UMIST). The following samples were examined; Graves' ophthalmopathy smokers (TSHR-SA negative), smokers (TSHR-SA positive), Graves' ophthalmopathy non-smokers (TSHR-SA negative), smokers (TSHR-SA negative), normal non-smokers and Graves' ophthalmopathy smokers (same sample used in lane 4 of Figure 4.3, TSHR-SA activity not assessed). The gel (Figure 4.5) was imaged using Gene tools analysis software (Syngene) to estimate molecular weight and optical density (OD). Four bands were measured roughly between 30-40kD to correspond with the four bands of similar molecular weight excised from the silver gel. The first two lanes 32kD bands were not measured by the software making comparison of this band not possible in all samples. A simple ratio between the three bands was made by dividing the optical density of the band by the optical density of the 28kD band.

4.2.5 MALDI-TOF Mass Spectrometry of Tear Proteins

Following silver staining, proteins of approximately 43, 41, 38 and 33kd were cut from the gel using a scalpel and stored at -80°C until analysis. The following steps were carried out by Dr Mike Morton (Department of Medical Biochemistry, UWCM). Bands were cut into small pieces (~1x1mm cubes) with a clean scalpel. After 2-3 washes with water the silver-stained gels were destained with a freshly prepared, 50:50 mixture of 30mM potassium ferricyanide and 100mM sodium thiosulphate. The clear gels were incubated with 200mM ammonium bicarbonate (20min), washed with water, dehydrated with acetonitrile and dried in a vacuum centrifuge. The dried gel plugs were reduced in 10mM dithiothreitol (DTT) in 100mM ammonium bicarbonate and incubated at 56°C for 45 minutes. The gel plugs were cooled to room temperature, the DTT removed and alkylated with 55mM iodoacetamide (IAA) in100mM ammonium bicarbonate at room temperature in the dark for 30 minutes. The IAA was removed; the gel plugs washed twice with 50:50 acetonitrile/100mM ammonium bicarbonate and then dried in a vacuum centrifuge. The gel plugs were rehydrated in a freshly prepared and chilled digestion buffer containing 50mM ammonium bicarbonate and 12.5ng/µl sequencing grade trypsin at 4°C. After 45 minutes on ice any remaining digestion buffer was removed and replaced with sufficient 50mM ammonium bicarbonate (~20µl) to keep the gel pieces wet during overnight incubation at 37°C. Peptides were extracted from the gel by incubation with 25mM ammonium bicarbonate (20µl) for 10 minutes, without removing the supernatant the same volume of acetonitrile was added and incubation continued for a further 10 minutes. The supernatant was recovered and the peptides further extracted from the gels by two similar extractions with 5% formic acid and acetonitrile. All extracts were pooled, dried in a vacuum centrifuge and redissolved in 5% formic acid (10µl).

The peptide solutions were then purified and concentrated in U-C18 ZipTips (Millipore) using the manufacturers protocol for wetting, equilibration, bonding and washing and peptides eluted directly onto the MALDI target with the matrix solution (saturated solution of α-cyano-4-hydroxycinnamic acid in 50:50 acetonitrile/0.2% triflouroacetic acid (TFA), diluted 1:5 with 60:40 acetonitrile/0.2%TFA).

Peptide mass fingerprinting was carried out using a Bruker Reflex III MALDI-TOF mass spectrometer in the reflectron mode. All mass spectra were externally calibrated with a peptide mixture containing Angiotensin I and II, Substance P, Bombesin, ACTH (1-17 and

18-39) and Somatostatin. Mascot software (Matrix Science, London, UK) was used for searching the NCBInr database using monoisotopic mass values for each peptide mass spectrum. Protein identity was based on a MOWSE score with a ρ significant value of <0.05 within the Mascot software.

4.3 Results

4.3.1 Tear TSHR-SA does not show increased stimulation in salt free buffer unlike serum TSAB

The 97th centile for tear TSHRA stimulation index in salt free conditions was 1.14 and in serum free conditions 1.65. (All clinical and biochemical parameters are tabulated in appendix B "Clinical data Graves' ophthalmopathy patients chapter 4"). There was sufficient tear sample to perform triplicates in serum free conditions on 38 patients and salt free in 30 patients, all patients were tested for TSAB in both conditions, stimulation indicies are illustrated in Figure 4.1 and Figure 4.2.

Tear TSHR-SA was present in 4/8 smokers and 13/38 Grave's ophthalmopathy patients in serum free conditions, the difference in proportions was not statistically significant (Table 4-1). In Graves' ophthalmopathy, positive serum TSAB increased significantly from 8/38 in serum free conditions to 32/38 in salt free buffer (McNemar $p<0.001$, Figure 4.2). Serum TSAB was not detected in smokers in either condition. In contrast, rather than increasing in salt free buffer, positive tear TSHR-SA in smokers decreased from 4/8 to 1/8 ($p=0.2$), and was not greatly altered in Graves' ophthalmopathy patients from 13/38 to 9/30 ($p=0.7$), when in serum free and salt free buffer, respectively (Table 4-1).

Table 4-1 Measurement of TSAB and TSHR-SA

Number of patients detected to have TSHR stimulating activity in tears and serum in different assay conditions. (Serum free medium (SFM) and salt-free buffer (SFB) from normal non-smokers (NNS), normal smokers (NS) and patients with Graves' ophthalmopathy (GO)).

	Tear TSHR-SA		Serum TSAB	
	SFM	SFB	SFM	SFB
NNS	0/9 (0%)	1/8 (12.5%)	0/9 (0%)	0/9 (0%)
NS	4/8 (50%)	1/7 (14%)	0/8 (0%)	0/8 (0%)
GO	13/38 (34%)	9/30 (30%)	8/38 (21%)	32/38 (84%)

Figure 4.1 TSHR-SA (Tears) in salt free buffer and serum free medium

Representative samples of Smokers and Graves' ophthalmopathy patients tears show tear TSHR-SA of comparable levels in salt free and serum free buffer. (S- smokers. G- Graves' ophthalmopathy patients. Colour matched dotted line represents normal cut off of each assay).

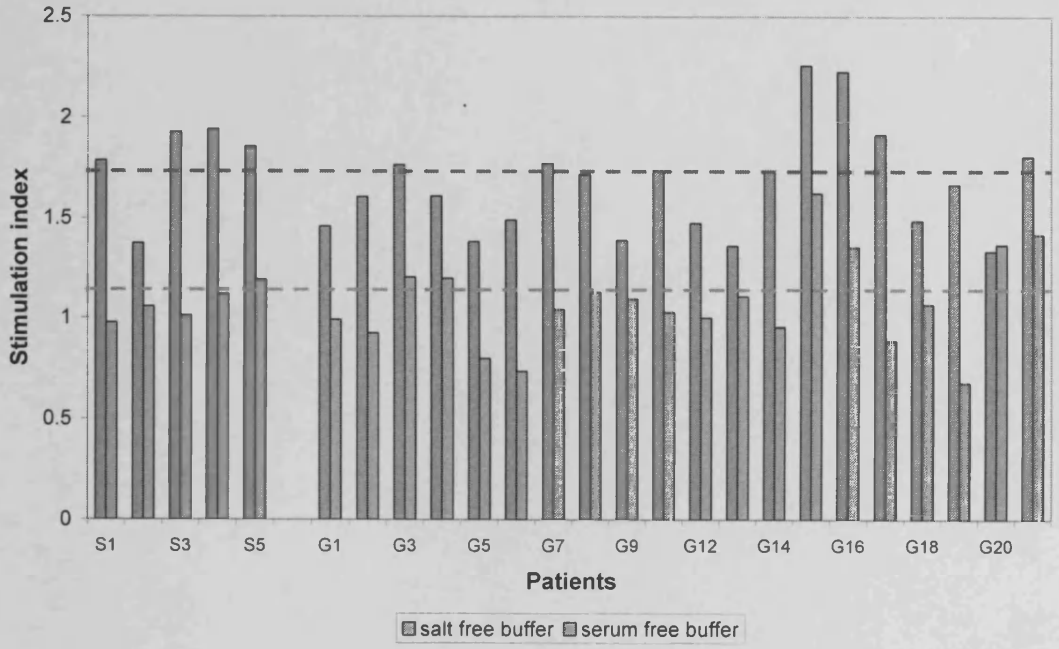

Figure 4.2 TSAB (Serum) in salt free buffer and serum free medium

Graves' ophthalmopathy patients serum shows TSAB activity greater in salt free buffer compared to serum free. (Dotted line represents normal cut off of both assays).

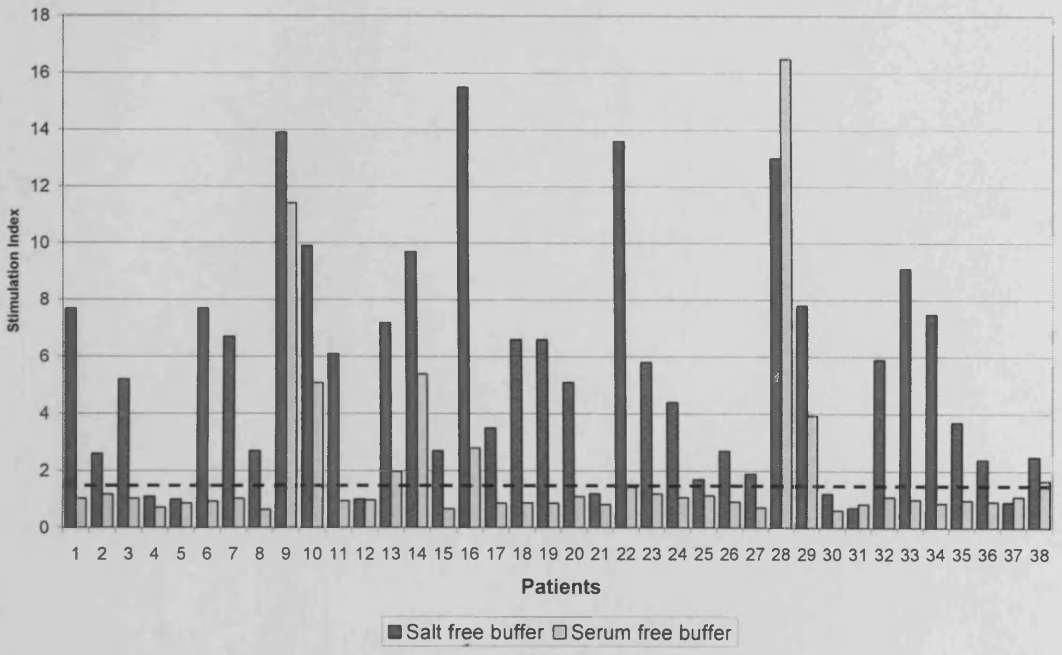

Correlations between serum TSAB, tear TSHR-SA and other linear variables; CAS, TSH, T4, T3, proptosis and age were tested (Spearman). Tear TSHR-SA tested in both buffers did not correlate with each other or with serum TSAB activity. Serum TSAB in serum free medium correlated with salt free buffer (rho=0.61, $p<0.0001$). CAS showed a positive correlation with serum TSAB in salt free buffer (rho=0.41, p=0.01) but not in serum free media. CAS did not correlate with tear TSHR-SA in either buffer. However, some would consider the CAS not to be a truly linear variable. We therefore grouped patients into those with active ophthalmopathy (CAS>3) and inactive (CAS<3) and compared mean tear TSHR-SA with smokers and non-smokers, both assay conditions were examined statistically (ANOVA) and no differences were found. Serum TSAB when grouped in this manner showed no significant difference between active and inactive Graves' ophthalmopathy but both were significantly higher than smokers (active p=0.018, inactive $p<0.0001$) and non-smokers (active p=0.016, inactive $p<0.0001$) in salt free buffer. Serum TSAB in serum free medium showed no difference between groups. The apparent aberration between the positive correlation of CAS and serum TSAB and the failure of patients with active disease to have higher serum TSAB, may be caused by uneven sampling skewing distributions. The most frequent CAS was 3 (n=11), just below the threshold for active disease and only 7 out of the 38 patients had CAS greater than 3.

Mean tear TSHR-SA and serum TSAB showed no significant differences in either buffer when the Graves' ophthalmopathy patients were grouped into; smokers/ non-smokers and patients with and without the following treatments; carbimazole, radio-iodine, orbital radiotherapy, thyroidectomy, steroids.

TSH was negatively correlated with tear TSHR-SA in salt free buffer (rho=-0.36, p=0.048) but not in serum free medium. However given TSHR-SA in salt free buffer had a very narrow range (SI.0.7-1.6) the strength of this correlation is questionable. TSH was not correlated with serum TSAB in either buffer. As expected, TSH levels had negative correlation with serum T4 (rho=-0.64, $p<0.0001$) and T3 (rho=-0.51, p=0.04). Similarly, T4 and T3 correlated positively (rho=0.61, p=0.012). Age and proptosis did not correlate with any other variables.

Further experiments were performed by Dr Marian Ludgate using 5 pooled TSHR-SA positive Graves' ophthalmopathy tear samples in SFM and in the presence of a thyrotropin receptor blocking antibody (TBAB) or normal human serum (both at 5, 10 and 20%

vol/vol). There was no difference in activity in the pooled tears in the presence of the TBAB compared with the normal human serum.

4.3.2 Tear zinc-α_2-glycoproteins are present in different proportions from Graves' ophthalmopathy patients but does not show tear TSHR-SA

Increased banding was demonstrated on silver gels in the 30-40kD range along with increased vol/vol protein content in smokers and Graves' ophthalmopathy patients (Figure 4.3). Given the tear 2D reference map suggested ZAG is around this size, western blotting was used to detect ZAG in pooled normal and Graves' ophthalmopathy patients. ZAG appears to be a highly abundant protein with nearly equal densitometry in normal non-smokers and Graves' ophthalmopathy patients (Figure 4.4). However this is a sensitive technique and titration experiments using lower concentrations of primary antibody were not carried out.

SYPRO-Ruby staining of tear proteins was performed by a collaborator (Dr Catherine Winder, Department of Chemistry, UMIST). The following samples were examined; Graves' ophthalmopathy smokers (TSHR-SA negative), smokers (TSHR-SA positive), Graves' ophthalmopathy non-smokers (TSHR-SA negative), smokers (TSHR-SA negative), normal non-smokers and Graves' ophthalmopathy smokers (same sample used in lane 4 of Figure 4.3). The gel (Figure 4.5) was imaged using Gene tools analysis software (Syngene) to estimate molecular weight and optical density (OD). Four bands were measured roughly between 30-40kD to correspond with the four bands of similar molecular weight excised from the silver gel (Table 4-2). The 32kD bands of the first two lanes were not measured by the software so comparisons were not possible. Graves' ophthalmopathy patients (lane 1&3) have similar ODs for, 42, 39 and 28kD proteins and the average ratio was 2.7:2.7:1 (42:39:28 kD). The total protein in these two samples is greater than a sample collected by previous investigators of Graves' ophthalmopathy tears (lane 6) and differs also in the ratio 2.1:1.1:1. The smokers (lane 2&4) have differences between all three bands and the average ratio of the two groups was 3.7:2.1:1. The normal non-smoker tears had very similar OD readings to the previously collected GO tear sample and identical ratios 2.1:1.1:1. Whereas most samples show a reduction in OD from the 42kD to the 39kD band, the more recent Graves' ophthalmopathy samples did not.

Figure 4.3 Silver stained gel of tear proteins

Increased banding in 30-40kD region of Graves ophthalmopathy and smokers tears is shown. Gel bands excised for MALDI-TOF protein analysis.

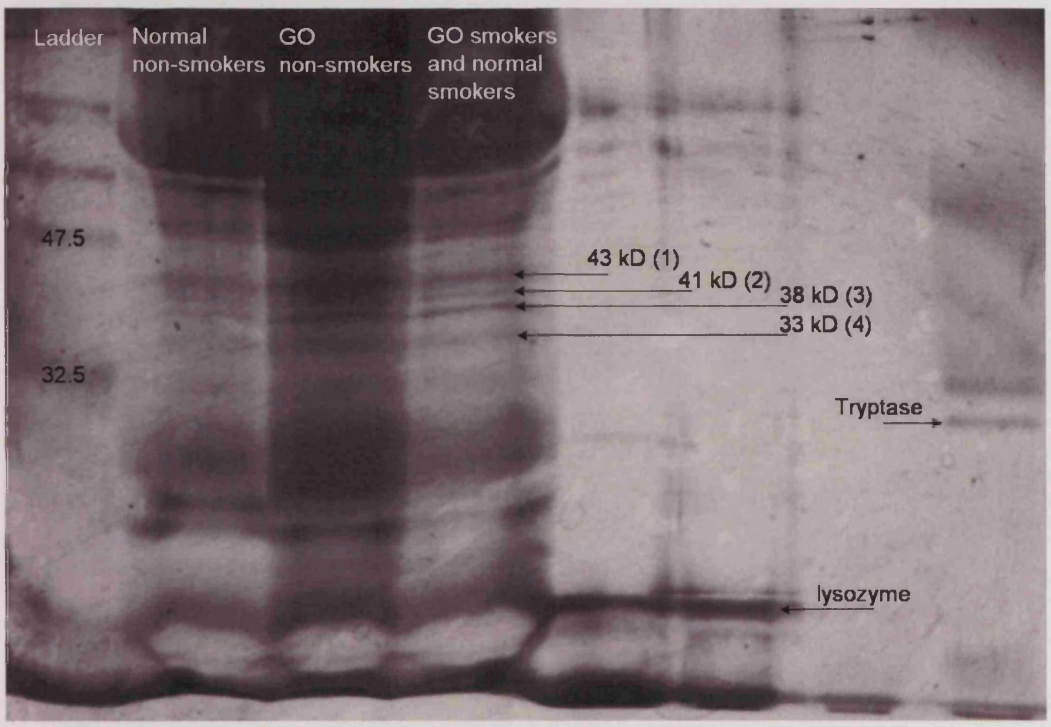

Figure 4.4 Western blot for tear ZAG

The Western blot is overlaid onto gel with molecular weight markers. Lane; 1, normal non-smokers, 2, molecular weight markers, 3, Graves' patients, 4, rainbow molecular weight markers.

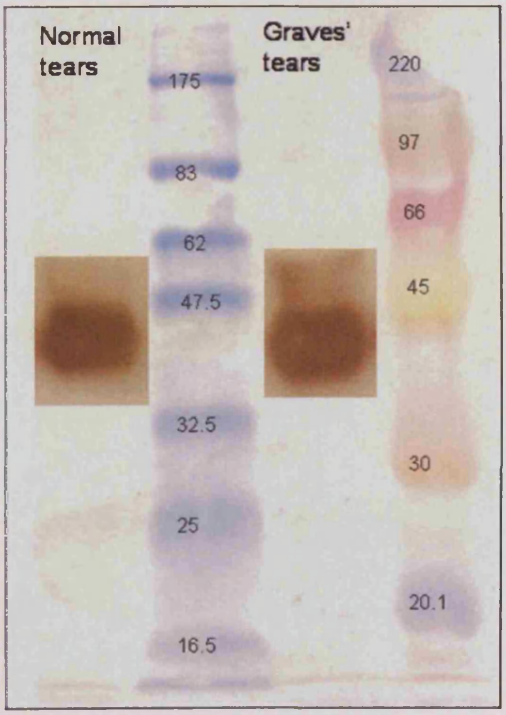

Figure 4.5 SYPRO Ruby stained tear proteins

Lane1, Graves' ophthalmopathy smokers (TSHR-SA negative). Lane 2, smokers (TSHR-SA positive). Lane 3, Graves' ophthalmopathy non-smokers (TSHR-SA negative). Lane 4, smokers (TSHR-SA negative). Lane 5, normal non-smokers. Lane 6, Graves' ophthalmopathy smokers (same sample as lane 4 Figure 4.3).

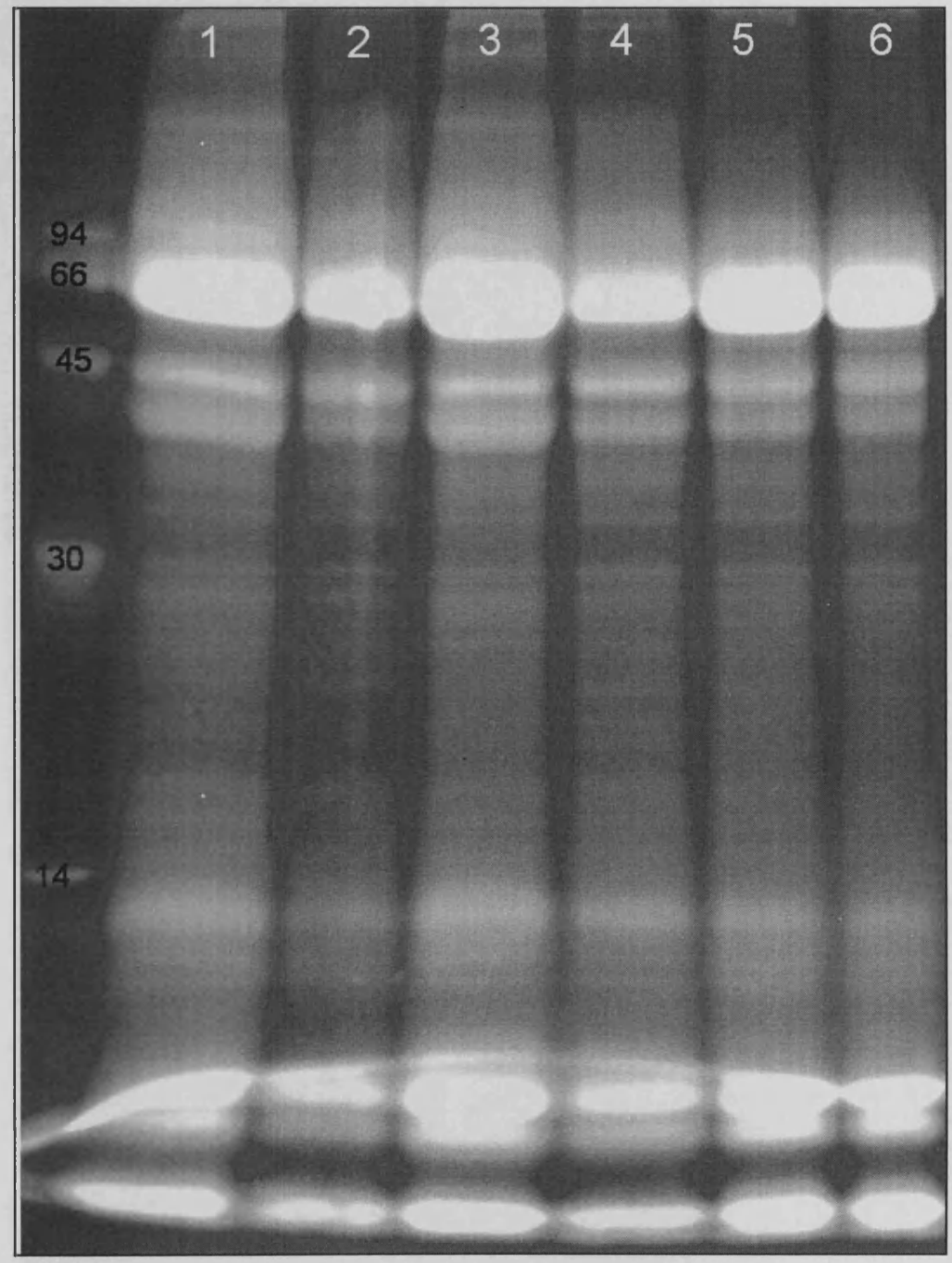

Table 4-2 Tear proteins stained with SYPRO-Ruby

Data from gel in Figure 4.5 showing molecular weight and optical density. In brackets is the ratio of optical density relative to that of the 28kD protein. Negative and positive refer to TSHR-SA. Sample six was included to compare staining in the previous silver stained gel and TSHR-SA was not measured in this sample.

kD	GO smoker negative 1	Smoker positive 2	GO non smoker negative 3	Smoker negative 4	Normal non smoker 5	GO smoker 6
42	60.5 (2.9)	50.8 (3.1)	56.9 (2.5)	69.5 (4.3)	48.4 (2.1)	44.1 (2.1)
39	56.7 (2.8)	28.9 (1.8)	59.5 (2.6)	38.1 (2.4)	25.0 (1.1)	22.0 (1.1)
32	nr	nr	9.7 (0.4)	7.6 (0.5)	11.2 (0.5)	11.4 (0.6)
28	20.6 (1)	16.4 (1)	23.0(1)	16.1 (1)	23.5 (1)	20.5 (1)

Table 4-3 MALDI-TOF peptide analysis of tears

Protein bands (30-40kD) excised following SDS-PAGE of tears from normal non-smokers, patients with GO and a pool of GO smokers and normal smokers were analysed by MALDI-TOF. (ZAG, zinc-α-2-glycoprotein; numbers indicate probability ($p<0.05$) based on Mowse score; Neb, nebulin; Hypothet. protein, hypothetical protein KIAA0542. In addition, the mast cell tryptase band was recognised with a significant Mowse score of 101).

	Normal non-smokers	GO	GO smokers and smokers
1	Nothing detected	ZAG, 129	ZAG, 164
2	Neb, 76 Hypothet. protein,	Nothing detected	ZAG, 84
3	Lactoferrin, 84	Lactoferrin, 78	Lactoferrin, 93
4	Nothing detected	Lactoferrin, 70	Lactoferrin, 86

The four bands excised in the 30 to 40kD region from each of the 3 tear-containing lanes and a band containing mast cell tryptase from the adjacent lane were analysed by MALDI-TOF (Figure 4.3). The 4 bands were zinc-α-2-glycoprotein (the two at higher Mr) and lactoferrin (the two lower Mr bands). The results of the analysis are summarised in Table 4-3. The results suggest the proteins in Graves' ophthalmopathy patients present in similar proportions (2.7:2.7:1) are ZAG:ZAG:lactoferrin.

In order to test ZAG for TSHR-SA, a colleague, Martin Bullock (Department of Endocrinology, UWCM) purified his–tagged human ZAG from A293 cells provided by Dr. Laura Hale (Duke University). The purified ZAG and the conditioned medium of the A293 cells were tested in the luciferase assay but neither displayed TSHR-SA.

4.4 Discussion

To summarise work carried out previously and in this study; we have identified differences in the bioactivity and composition of Graves' ophthalmopathy patients' tears, which are similar to those observed in normal smokers, when compared with non-smokers.

There are several indications to suggest that tear TSHR-SA is not an antibody. The activity was detected in almost one third of 'healthy' smokers, yet in the small group (n=8) examined, none had serum TSAB. TSHR-SA was not affected by the presence of human serum containing TBAB. Furthermore the optimal conditions for the tear stimulating activity are physiological, unlike the salt-free assay buffer preferred by TSAB. If not an antibody, could it be a protease? The bioassay we have used is able to demonstrate TSHR activation by trypsin. However the kinetics of this response, which peaks at 30 minutes, differs from those of TSHR-SA. This may be due to differences in concentration. A proportion of the activity we have detected in tears is due to activation of Gsα coupled receptors, other than the TSHR, which are endogenously expressed by the parent CHO cell line. The maximum stimulation index obtained using the zulu cell line was 4.5 (range 1.1 to 4.5), contrasting with the lulu cells expressing the TSHR, which produced stimulation indices ranging from 1.1 to 21.1 (Additional experiments by Dr Ludgate).

The tear gels stained by SYPRO-ruby (Dr Catherine Winder) show variation in protein content of pooled samples from Graves' ophthalmopathy patients, smokers and normals and in general protein content would seem higher in keeping with other studies [317]. Extrapolating protein quantity by gel densitometry is an in-exact process and the need for confirmation with other quantitative tests is clear but only possible after identification of the exact proteins has been made. The results hint at the differences present in the ratios of the various proteins that may underlie disease processes rather than simply tear osmolarity changes. Proteins present in tears are extensively modified; fragmentation, truncation, glycosylation, phosphorylation, are all changes that alter protein function. Subtle changes in the isoforms of the proteins may underlie the pathological processes and resolution of such changes might only be possible with narrow pH gradients on 2D gels or other techniques such as combined HPLC/electrospray ionisation/mass spectrometry where both peptide types and quantification are possible [335].

While total protein content of tears in normal individuals does not alter much day to day, serum albumin and immunoglobulin levels can fluctuate whereas regulated tear proteins (lysozyme, lactoferrin) seem fairly constant [336]. In dry eye lactoferrin levels are reduced [337]. By optical densitometry, levels of the 28kD lactoferrin fragment were similar in our samples. Lactoferrin is an iron binding protein having pleiotropic effects, including anti-inflammatory and anti-microbial [338]. Lactoferrin is able to bind glycosaminoglycans [339] and has been found to have both protease [340] and protease inhibitor activities [341]. Apart from preventing infection of the ocular surface, lactoferrin in tears has been suggested to have a role in reducing the formation of free radicals [342]. Tear lactoferrin has been reported previously at 83 and 78kD, major and minor forms, but others were also present; 64, 60, 57 and 52kD, the shift to smaller isoforms was repeated when iron ions were added to tears [343]. We have detected the protein at considerably lower molecular weight but consistent with fragments of the larger forms. Elsewhere, nasal lavage fluid of normal subjects contains a 39kD fragment of lactoferrin [344]. Components of cigarette smoke have been shown to increase proteolysis of lactoferrin [345], which can also be cleaved by cathepsins, a process that reduces its anti-microbial activity [346]. Neutrophil elastase has also been shown to cleave lactoferrin in the lungs of cystic fibrosis patients [347]. Neutrophils and their elastase are commonly found in conjunctiva, particularly at night [348]. Proteolytic cleavage of major forms of lactoferrin seems the most likely source of our fragment and could explain the reduced lactoferrin reported previously [322]. Measurement of all forms of lactoferrin and their biological activity would be required to understand whether smoking or Graves' ophthalmopathy has an effect.

Our initial tear gels suggested normals contained lower total proteins and the bands 30-40kD were virtually absent. This contrasts with the later samples visualised by SYPRO-Ruby stained gels and the western showing abundant ZAG (~40kD) in normal tears. Similarly elsewhere, tear gels from normals show prominent Coomasie blue stained proteins in the 30-40kD region [336]. The apparent disparity between the protein contents of our early and late sampling could be due to a number of factors including sampling methods by different investigators and protein degradation in the older samples.

We have identified by MALDI-TOF (Dr Mike Morton) and western, the higher molecular weight bands as ZAG. It is therefore a common tear protein but receives little interest, searching PubMed for the two terms (zinc-alpha-2 glycoprotein, tears) returns only two articles [327; 349]. The purification of human ZAG was described in 1961 [350]. ZAG is a 41kD

protein present in plasma, saliva and tears with a high similarity to the extra-cellular domain of the MHC class I α chain, its natural ligand may be a polyunsaturated fatty acid and it possibly has a role in lipid homeostasis [351; 352]. ZAG has an identical amino acid sequence to lipid mobilising factor, responsible for the cachexia seen in some cancers and produces lipolysis in-vitro and in-vivo via a β3-adrenoreceptor cAMP dependent mechanism [353; 354]. MALDI-MS has detected 5-7 ZAG isoforms 35-40.5kD in mass due to variable glycosylation and differences in scialic acid content [354]. Tear sialic acid has been detected previously [355] and its presence attributed to an unknown glycoprotein, that we would now suggest to be ZAG. This number of ZAG isoforms detected in tears by 2DGE is similar to another study [327], our 1DGE could only resolve 2 bands of ZAG from Graves' ophthalmopathy patients and smokers. A recent study found that the plasma of smokers contains a higher proportion of aberrantly glycated proteins compared with non-smokers due to nornicoteine [356]. The precise function of ZAG in tears and other biological fluids is unclear but it has recently been shown to be expressed by adipocytes [337]. Whether the increased ZAG in Graves' ophthalmopathy tears is derived from lacrimal gland secretion or possibly related to vascular leakage from congested orbits with fat hypertrophy is not known.

We have, in line with our specified aims, identified the proteins present in tears between 30-40kD, however, studying the SYPRO-ruby gel shows numerous proteins below 10kD in size and initial MALDI-TOF characterisation of these low molecular weight proteins has been partially examined elsewhere [357]. There are no correlations between serum TSAB, tear TSHR-SA and smoking in Graves' ophthalmopathy. Serum TSAB in salt free buffer correlates with CAS as shown previously [358] but our sample sets are too uneven to support this fully. Graves' ophthalmopathy tears contain a unique ZAG protein profile of unknown significance.

5 In vivo and ex vivo investigation of a possible role for adiponectin in orbital adipogenesis

5.1 Introduction

5.1.1 Adiponectin, an insulin sensitising adipokine

As discussed in the introduction appreciation of the active metabolic role adipose tissue plays, particularly in obesity and diabetes, has become of great interest given the increased incidence of these two diseases [359]. Insulin signalling is central to lipid homeostasis with resistin having a negative effect and adiponectin having a positive effect on insulin sensitivity [360; 361]. Adiponectin has become the accepted name for a protein previously identified by several terms including: adipocyte complement-related protein 30kD (ACRP30), adipoQ (murine form), adipose most abundant gene transcript 1 (apM1) and gelatine-binding protein 28kd (GBP28) (reviewed [362]). Sequence homology and a C-terminal complement factor C1q-like globular domain add adiponectin to a family of proteins including human type VIII and X collagens, precerebellin and hibernation-regulated proteins (hib 20, 25 and 27) [363]. The locus for adiponectin is 3q27 and produces a protein containing 247 amino acids (aa); signal peptide (17aa), highly conserved N terminus (1-44aa), remaining collagen domain (45-109aa) and a globular domain (110-247aa). Secreted protein is present as low molecular weight trimer dimers and high molecular forms such as hexamers, dodecamers and 18 mers. Adiponectin is present in human plasma between 5-30nM and therefore with such high levels present receptors were predicted to have low affinity binding. The adiponectin receptors have recently been cloned and two main isoforms characterised, adipoR1 (widely expressed but mainly skeletal muscle) and adipoR2 (mainly liver), whose actions are mediated via AMP kinase and PPARα ligands [364]. The receptors have seven transmembrane segments but are not G-protein receptors and are orientated oppositely with the C terminus externally and the N terminus internally. AdipoR2 is the receptor for full length adiponectin while adipoR1 has high affinity for a globular domain fragment that may be produced in small amounts by complement cascade activation or leukocyte elastase [365; 366]. Adipocyte adiponectin gene expression has sterol regulatory sites within its promoter for the transcription factor ADD/SREBP, an important factor during the initiation of adipogenesis [367].

Recombinant adiponectin has been shown in vivo to decrease glucose production by increasing hepatic sensitivity and is mirrored in vitro by hepatocyte culture results [360; 368]. In humans, dietary restriction of calories elevated adiponectin and type 2 diabetic patients (insulin insensitive) have lower adiponectin levels than non-diabetic controls [369]. Elevation of circulating adiponectin can be achieved by thiazolidinedione treatment which improves insulin sensitivity [370]. Adiponectin knockout mice showed increasing insulin resistance from heterozygous to homozygous forms and were more susceptible to atherogenic insult [371]. The globular head domain of adiponectin, when cleaved, caused glucose lowering by increased muscle fatty acid oxidation but this form is present in small amounts in human plasma [365]. However, the globular domain has been shown to improve insulin resistance more effectively than full length adiponectin [372]. Murine transgenics expressing the globular domain of adiponectin when crossed with leptin deficient ob/ob mice showed increased insulin responses to glucose and improved insulin resistance but did not improve obesity [373]. The same adiponectin transgenic mice when crossed with atherosclerosis model, apoE-deficient mice, produced an improvement in atherosclerosis. Adiponectin may reduce inflammation in endothelial cells by disruption of cAMP-PKA, NF-κB pathways [374].

5.1.2 Transgenic elevation of full length adiponectin improves insulin sensitivity

A group at the Albert Einstein College of Medicine (AECOM) showed that secretion of adiponectin could be enhanced by the expression of a truncated form of adiponectin lacking Gly-X-Y repeats in the collagenous domain [375]. Adiponectin initially formed as trimers, then pairs of trimers and finally the tertiary protein structure contained 12-18 subunits. The effect of the truncated adiponectin was thought to be post-transcriptional, with a maximal effect around three hours, increasing secretion by reducing a normal process of internal degradation. Conversely, adding Gly-X-Y repeats to the collagenous domain decreased adiponectin secretion. A transgenic model based on the truncated adiponectin developed serum levels of normal oligomeric adiponectin three times that of its wild type controls and was secreted from fat pads, none of the truncated form was secreted. The most successful transgene promoter was the fat specific aP2, the more ubiquitously expressed CMV promoter founder lines were difficult to propagate due to infertility. The pre-existing sexual dimorphism of females having 2-3 times the circulating adiponectin compared to males was conserved in the transgenic mice. Transgenic elevation

of adiponectin did not alter levels of; TNFα, glucocorticoids, growth hormone or leptin, but prolactin levels were doubled in the transgenic mice. In wild type mice prolactin decreases adiponectin levels and might represent a counter regulatory mechanism to lower adiponectin in the transgenic mice. Female transgenic mice displayed higher rates of triglyceride and fatty acid clearance with increased lipoprotein lipase activity. Increased hepatic insulin sensitivity was found in transgenic mice prior to and after, increases in fat mass. Similarly, glucose clearance was achieved at lower levels of insulin in transgenic mice.

5.1.3 Elevated adiponectin causes selective fat pad proliferation

A characteristic phenotype developed midlife in the transgenic mice with large interscapular and intraconal orbital fat pads but was only present when circulating adiponectin had been elevated by transgene expression. Percentage fat mass determined by tritiated water distribution showed increases in females but not males relative to wild type. The changes in fat mass were not obviously due to changes in food intake, 24hr energy expenditure or respiratory quotients. Macroscopic and microscopic appearances of the interscapular fat pads were in keeping with brown fat but the transgenic adipocytes tended to contain less lipid vacuoles. Brown fat is known to secrete adiponectin and resistin [376]. The proptotic changes within the orbits of the mice were investigated as part of this thesis and are described in the results (5.3.2).

Proptosis caused by fat expansion and de novo adipogenesis is, in part, a pathology we see in Graves' ophthalmopathy. We hypothesized, given preadipocyte differentiation increases TSHR expression, the profound increases in fat pads of the adiponectin transgenic mice might lead to a break in tolerance to TSHR and the transgenic mice may have developed an inflammatory eye disease akin to Graves' ophthalmopathy. Furthermore in humans the elevation of circulating adiponectin by thiazolidinediones [370] has been implicated in the relapse of a patient with Graves' ophthalmopathy commenced on pioglitazone [377] and also has also been reported to cause proptosis in a patient without Graves' disease or ophthalmopathy on roziglitazone [378]. Consequently adiponectin levels may influence Graves' ophthalmopathy activity.

5.1.4 Aims:

1. To investigate whether the proptosis of the transgenic mice is caused by expansion of the orbital fat, ocular muscles and oedema. (A macroscopic, microscopic and MRI study).
2. To determine whether the transgenic mice have developed a Graves'-like disease by measuring antibodies to the TSHR
3. To measure adiponectin levels in patients with Graves' disease and ophthalmopathy with varying severity to establish if any correlations exist.

5.2 Methods

5.2.1 Thyroxine and thyrotropin receptor antibody determination

Serum from FVB mice was collected and frozen by our collaborators at AECOM and transported to the UK; wild-type females (n=10), transgenic females (n=8), over-ovulated wild-type females (n=3), over-ovulated transgenic females (n=3), wild-type males (n=9) and one transgenic male. Serum was assayed for thyroxine, TSAB and TBII as in sections 2.2.16-18. Serum assay for TSHR antibodies by flow was carried out as in 2.2.15, with the modification of using CHO cells with and without the human TSHR. We then compared the histograms using Kolmogorov Smirnof statistics to obtain a 'd' value. TSH was measured by our collaborators.

5.2.2 Histology and electron microscopy

Orbital samples were set in fixation fluid after excision of the entire orbit and eyelid skin (exenteration) prior to transportation to Cardiff. On arrival, samples were further dissected to remove the skin and Harderian gland before macroscopic photography. Samples were then mounted in plastic for light microscopy as in section 2.2.22. Electron microscopy was carried out on some specimens by Dr Chris von Rhuland, Department of Medical Microscopy.

5.2.3 Orbital MRI

The MRI facility is a purely experimental setup for imaging and spectroscopy and has not been used previously for murine imaging, to gain experience of the equipment we used BALB/c mice to develop the following methods and sequence protocols. Imaging was carried out under the supervision of Dr Bill Stewart (Medical Physics, UWCM).

A 1.2 Tesla, 17cm bore, superconducting magnet, associated imaging electronics, radio frequency generator and detectors (Surrey Medical Imaging Systems) were integrated at the system level by the Department of Medical Physics, UWCM. A miniature 2.5cm radio-frequency (RF) coil was designed in-house. T1 weighted images were generated on a 32

row greyscale matrix of 256x256 with a slice thickness of 1.5mm but some 0.75mm images were also acquired. Switching between X, Y and Z detectors required additional scan sequences for axial, coronal and saggital images. The miniaturisation of the RF coil resulted in each sequence of images generating four slices for analysis. Mice were sacrificed by CO_2 (cervical dislocation was avoided to prevent orbital haemorrhage) and transferred to the MRI lab. Positioning within the coil was aided by wrapping the mice in cling film, a brief sequence, 4-8 minutes duration, was then run to confirm correct positioning within the field and adjusted as necessary to reduce artefacts of rotation and poor symmetry. Each adjustment required disconnection of the RF cables and extracting the RF coil from the centre of the magnet bore. Departmental guidelines regarding the safety of high magnetic fields were observed. The full imaging sequence acquisition was 25-45 minutes. Two wild-type FVB and two age matched transgenic mice were transferred from AECOM and studied by MRI. Fat explants were taken from the mice after MRI and cultured as in chapter 3.

5.2.4 Plasma adiponectin measurement

A small sample of patients with Graves' disease, Hashimoto's and controls were tested for adiponectin in a pilot study. Plasma was transferred at -80C to Dr Terry Combs (AECOM) for the Western blot assay. Briefly, 3µl of serum was separated by SDS-PAGE (12%), transferred to nitrocellulose, blots exposed to ^{125}I-labelled rabbit antibody against murine adiponectin and analysed by densitometry against standards of known adiponectin concentration [370].

Initial results suggesting an elevation in circulating adiponectin lead us to examine levels in Graves' ophthalmopathy patients (n=36) and compare them to a group of thyrotoxic patients with toxic multinodular goitre (TMNG, n=13). Data and serum gathered from the ophthalmopathy patients was in accordance with local research ethic committee approval (Bro Taf). Clinical data included age, sex, CAS, body mass index, sum of proptosis (exophthalmometry readings from both eyes), orbital radiotherapy, orbital decompression surgery, steroid treatment (current, previous, none), radio-iodine treatment, carbimazole therapy, TSH, T4, T3 and serum TSAB. Statistical analysis was carried out as in 2.2.23.

5.3 Results

5.3.1 TSHR antibodies are not induced by adiponectin over-expression. FVB mice hypothyroidism is not altered by adiponectin over-expression

From ten female and nine male wild type mice centiles were established for normal ranges of the antibody and thyroxine assays. TSHR by flow had a 97th centile "d" cutoff value of 0.34, TBII had a 3rd centile value of 69%, TSAB had a stimulation index 97th centile of 1.15 and thyroxine had a 97th centile of 3.3μg/dl and a third centile of 1.9μg/dl.

No TSHR antibodies were detected by flow cytometry or inhibition of TSH binding (Table 5-1). Low level increases in TSAB were only present in some older mice; 2/3 16 month female transgenic (SI=1.5 and 1.28), 1/3 11 month female over-ovulated (SI=1.27) and the one male 16 month transgenic (SI=1.27). None of these mice had a reciprocal elevation in thyroxine. Thyroxine levels were normal, all between the 97th and 3rd centiles, in all FVB mice tested, irrespective of transgene presence. The average thyroxine levels of FVB was nearly half that of BALB/c tested in chapter 2. No significant differences in TSHR antibodies or thyrotropin were detected between the groups (ANOVA).

Table 5-1 TRAbs, Thyroxine and TSH results from FVB mice

Thyrotropin receptor antibodies (IgG by flow, TBII and TSAB), thyroxine and TSH results from FVB; wild type, transgenic and over-ovulated (OV) female and male mice (mean in bold, standard deviation or standard error of the mean (sem) in faint).

	TSHR IgG ("d")	TBII (%)	TSAB (SI)	T4 (μg/dl)	TSH (mU/ml)
Wild type female n=10	**0.23** 0.05	**99.3** 13.1	**1.0** 0.1	**2.4** 0.47	**4.3** 0.4 sem
Transgenic female n=8	**0.28** 0.09	**104** 9.04	**1.07** 0.34	**2.36** 0.5	**4.5** 0.5 sem
Wild type female OV n=3	**0.24** 0.14	**91.3** 1.53	**1.11** 0.15	**2.16** 0.15	-
Transgenic female OV n=3	**0.29** 0.08	**91** 2.65	**0.98** 0.04	**2.47** 0.16	-
Wild type male n=9	**0.29** 0.04	**79** 7.35	**0.91** 0.18	**2.69** 0.44	-
Transgenic male n=1	0.24	91	1.87	2.4	-

5.3.2 Elevated adiponectin induces intraconal fat pad proliferation causing proptosis and phthisis

The phenotype of middle aged (8 months) wild type and transgenic FVB mice are shown in Figure 5.1.1. The hypertrophied interscapular fat pad gave a rounded, hunched appearance in the transgenic and the apparently larger eye is caused by the proptosis, the globe sizes are not altered. The wild type eye (8 months) in Figure 5.1.2 shows the normal macroscopic appearance after exenteration: the globe and muscles are shrouded by Harderian gland, ocular muscles taper away from the globe meeting at the peak of the cone with the optic nerve, the uvea is unpigmented in these albino mice giving the translucent appearance. Incising the muscle cone and removing the fat showed the retracted bundles of severed ocular muscles and the remaining stump of optic nerve (Figure 5.1.3). The 8 month transgenic globe in Figure 5.1.4 has the harderian gland reflected to the right. The muscle cone was unopened and the muscle fibres were distended by fat from within, an individual muscle was separated into multiple fibres by the expansion of fat, adjacent to it an unsplit ocular muscle was spread broadly without splitting. The cornea remained clear. At the orbital apex the tendinous ring insertion of the ocular muscles was dilated with fat prolapsing through it. The entry point for the central retinal artery was through the tendinous ring. Chronic exposure keratopathy due to proptosis ultimately ulcerated the corneas of older mice as illustrated by Figure 5.1.5 (20 months, transgenic). Globe perforation would follow but sight loss would probably already have occurred due to retinal artery occlusion. The intraconal fat would continue to prolapse between the straps of ocular muscles. Once perforated, end stage phthisical shrinkage of the globe developed (Figure 5.1.6), and the intraconal fat advanced over the scarred remnant. The microscopic appearance of phthsis; globe contraction, corneal and retinal disruption with a central fibrotic process is shown in Figure 5.1.7. F. These disfiguring changes resulted in a decision by the vets to sacrifice the mice at 12 months before the onset of corneal ulceration, treatment by tarsorrhaphy or enucleation was not thought to be viable.

Histological preparation required chloroform extraction to remove the large amount of saturated lipid present. Two main morphologies were seen in the orbital fat although a spectrum between the two was present. The type most commonly found in transgenic mice had adipocytes composed of large single lipid spaces remaining with a few unsaturated lipid droplets (Figure 5.1.7. A). Cytoplasm was diminished to a thin tracing around the cell wall and nuclei. The appearances were in keeping with white adipose tissue with a storage

function but electron microscopy from AECOM showed the presence of mitochondria in keeping with brown fat. The other fat morphology differed clearly (Figure 5.1.7. B), adipocytes had larger areas of cytoplasm, the nuclei had more densely stained heterochromatin. The lipid vacuoles were smaller and multiple and unsaturated lipid droplets formed in the cytoplasm. More blood vessels were scattered throughout the tissue. These appearances were interpreted to be consistent with either brown fat or sites of active adipogenesis. No inflammatory cellular infiltrates were present in any fat samples examined.

Ocular muscles were neatly organised in wild type and transgenic animals (Figure 5.1.7. A-B). Muscle fibres contained numerous pale staining mitochondria similar to those seen in chapter 2. In ocular muscles split by intraconal fat expansion the myofibrils were distended and vacuolated (Figure 5.1.7. C). Using electron microscopy the vacuolations were identified as swollen mitochondria with disruption of internal cristae (Figure 5.1.8. A-B). Degeneration of light and dark bands was widespread and sarcomere length was increased (Figure 5.1.8. C). In the connective tissue between the muscles, no normal blood vessels were demonstrated and nerve tissue showed degeneration (Figure 5.1.8. D-F). These changes most likely represent an ischaemic process resulting from mechanical distension and compression caused by the fat volume expansion.

A small number of thyroids were examined and both wild type thyroids and transgenic thyroids contained a normal range of thyroid follicular heterogeneity (Figure 5.1.9. A-B). The older of the two transgenic mice had a focal small mononuclear cell infiltrate present between the follicles (Figure 5.1.9. C-D). There were no signs of follicular destruction or hypertrophy. Further sectioning did not identify any associated ectopic thymus attached to the infiltrate. While dissecting out thyroids it was apparent there was an increase in fat throughout the head and necks of the transgenic mice indicating fat hypertrophy was not just confined to the orbit and interscapular pads.

Figure legends

Figure 5.1 Macroscopy and histology of adiponectin transgenic mice

5.1.1. Phenotype of female wild type and transgenic FVB mice aged 8 months. Large interscapular fat pad developing in transgenic animal.
5.1.2-3. Exenteration specimens from female 8 month FVB showing normal anatomy of globe, ocular muscles, harderian gland and intraconal fat.
5.1.4. Female 8 month transgenic animal with intraconal fat hypertrophy and splitting of ocular muscles.
5.1.5. Female 20 month transgenic, proptosis had resulted in corneal exposure and ulceration.
5.1.6. Female 20 month transgenic, following on from corneal ulceration, globe perforation concludes with phthisis.
5.1.7. A-B. Orbital fat pads from both wild type and transgenic animals comprised two main morphologies: A, large adipocytes with minimal cytoplasm and a solitary lipid vacuolated area and B, cells with greater cytoplasmic content and multiple lipid vacuoles. No inflammatory cell clusters were noted. [8 month transgenic, LR white, tol. Blue, x40].
5.1.7. C-E. Ocular muscles were normal in wild type (C, x40) and transgenic mice (D, x40), containing the normal appearance of multiple pale areas of mitochondria. Abnormalities were seen in the mitochondria of muscles split by fat proliferation (E, x100).
5.1.7. F. A phthisical eye with highly disorganised cornea, retina and a central fibrotic process (x10).
5.1.8. A-C. Mitochondria from mechanically distorted ocular muscles (5.1.4) show swelling and degeneration of cristae (A,B). In some muscle fibres the dark and light bands degenerated and sarcomere length had increased. [Transmission EM, x500-1000].
5.1.8. D-F Connective tissue between muscle fibres (5.1.4) is similarly disorganised and no blood vessels could be identified (D). Degenerative nerves could be detected by the preservation of external myelin structure (E-F). [Transmission EM, x1000-2000].
5.1.9 Normal thyroid follicular heterogeneity was present in transgenic (A) and wild type (B) mice. In a 20 month female transgenic mouse a mononuclear cell infiltrate was present but no signs of follicular destruction were evident (C, D). [x10-40].

Figure 5.2 Magnetic resonance imaging of murine orbits

5.2.1. A-B MRI machine (A) and surface coil (B), department of medical physics UHW.
5.2.1. C-E T1 weighted images of BALB/c heads, section showing coronal (A), saggital (B) and axial (C) 1.5mm slices through globes.
5.2.1. F-H Increasing resolution by decreasing thickness to 0.75mm slice could define retro-orbital structures of muscles and optic nerve. Scan duration improved signal to noise ratio and image quality; 16 minutes (F), 32 minutes (G) and 44 minutes (H).
5.2.1. I-K For orientation, normal sequence progression demonstrated in BALB/c, starting with the lowest on left (I) to highest on right (K). BALB/c mice orbits contained minimal retro-orbital fat irrespective of age.
5.2.2. A-B Age matched, 8 months, orbital MRI of wild type FVB (A) and transgenic (B) mice showing high signal (white) retro-orbital tissue on T1 in keeping with fat present in transgenic but not wild type FVB.
5.2.2. C-D 20 month wild type (C) mice accumulate considerable retro-orbital fat with age. 20 month transgenic (D) mice develop phthisis and the orbits are filled with fat.

Figure 1.1

Figure 1.2

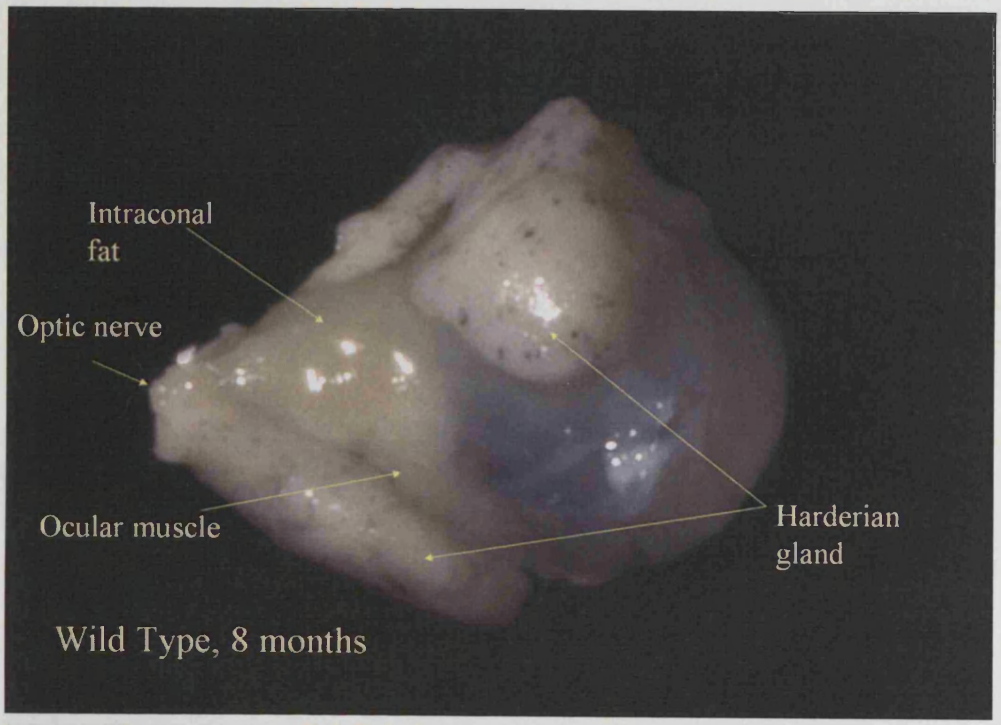

Figure 1.3

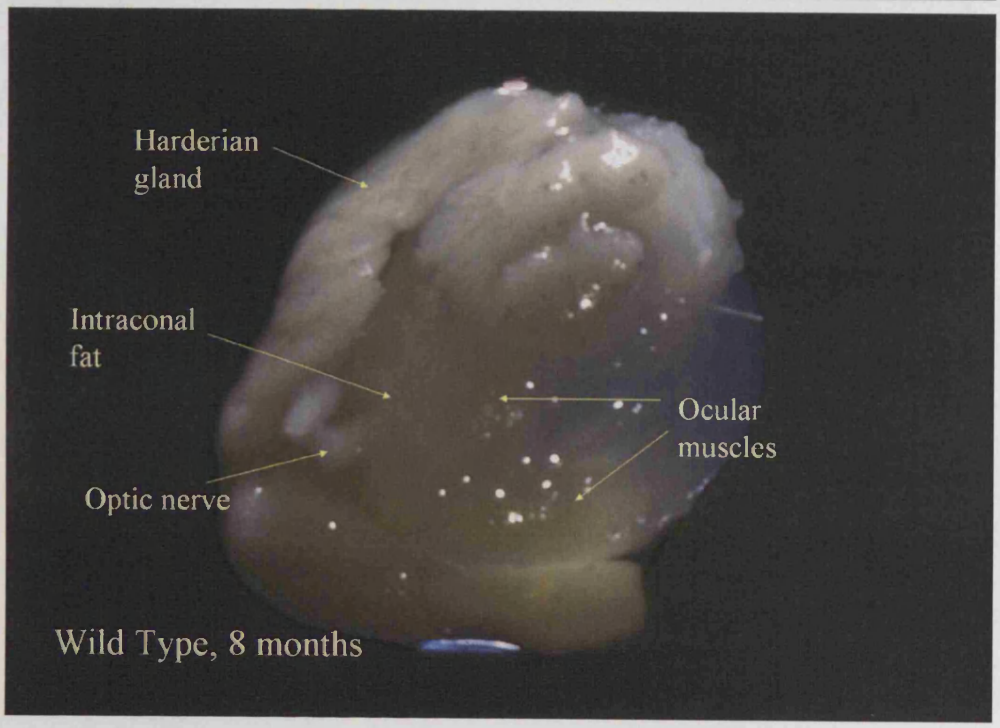

Figure 1.4

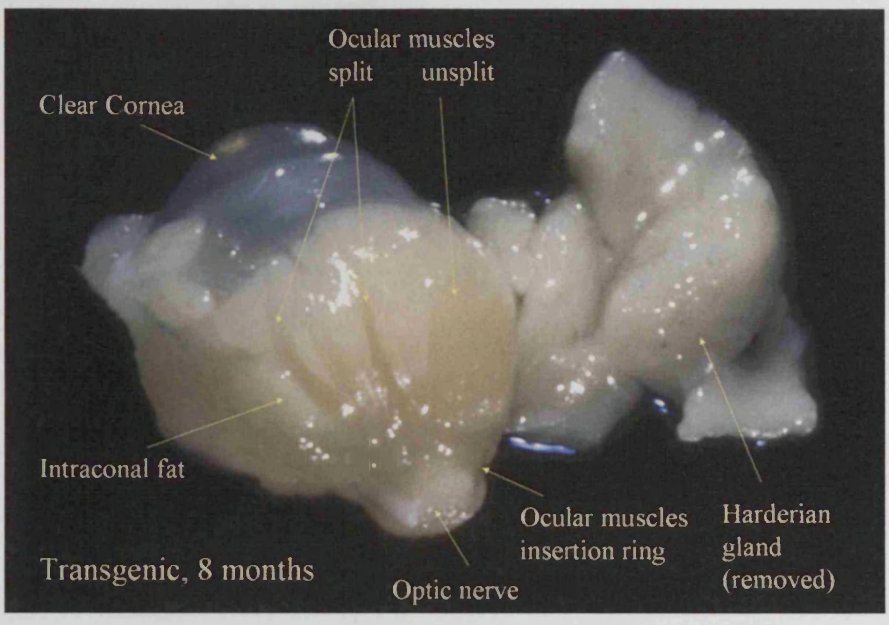

Figure 1.5

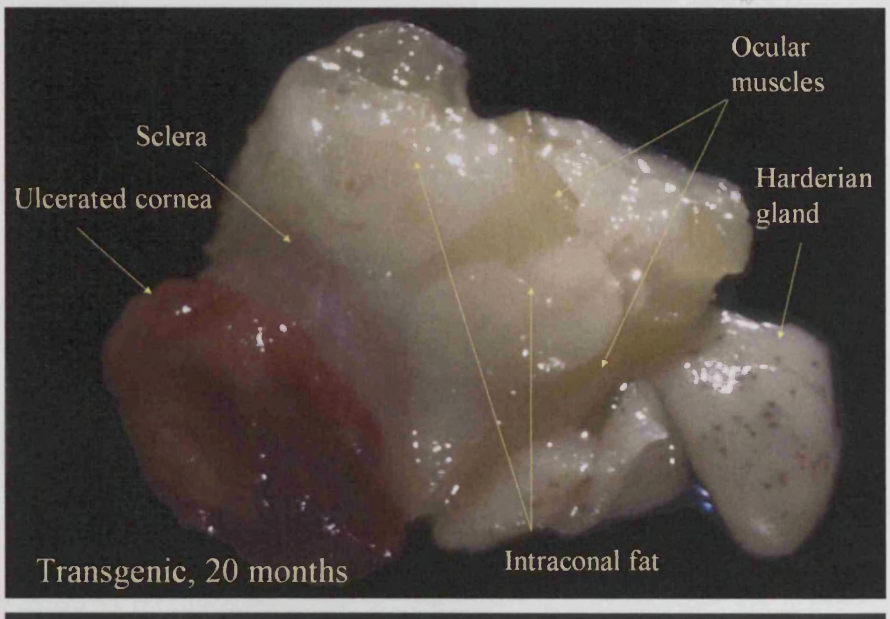

Figure 1.6

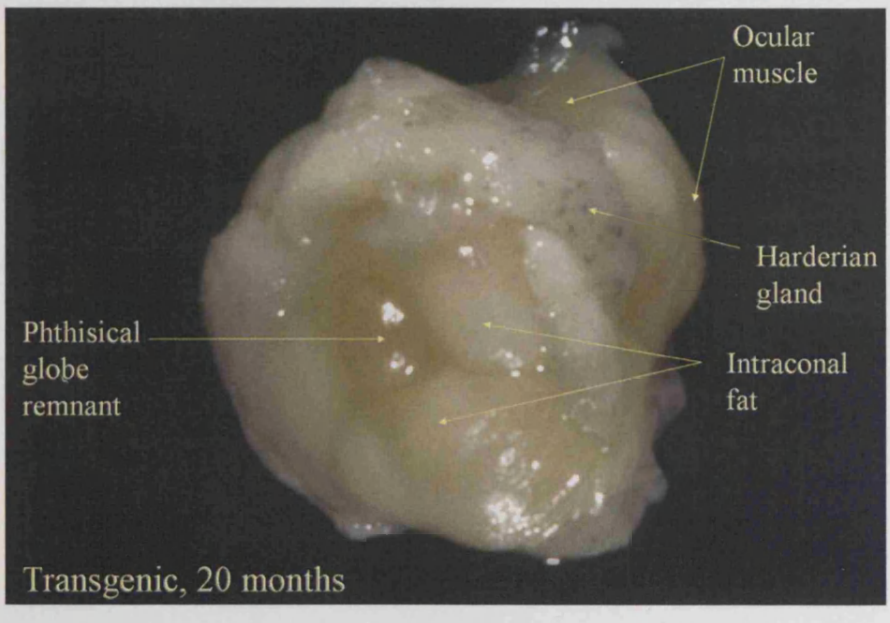

Figure 5.1.7

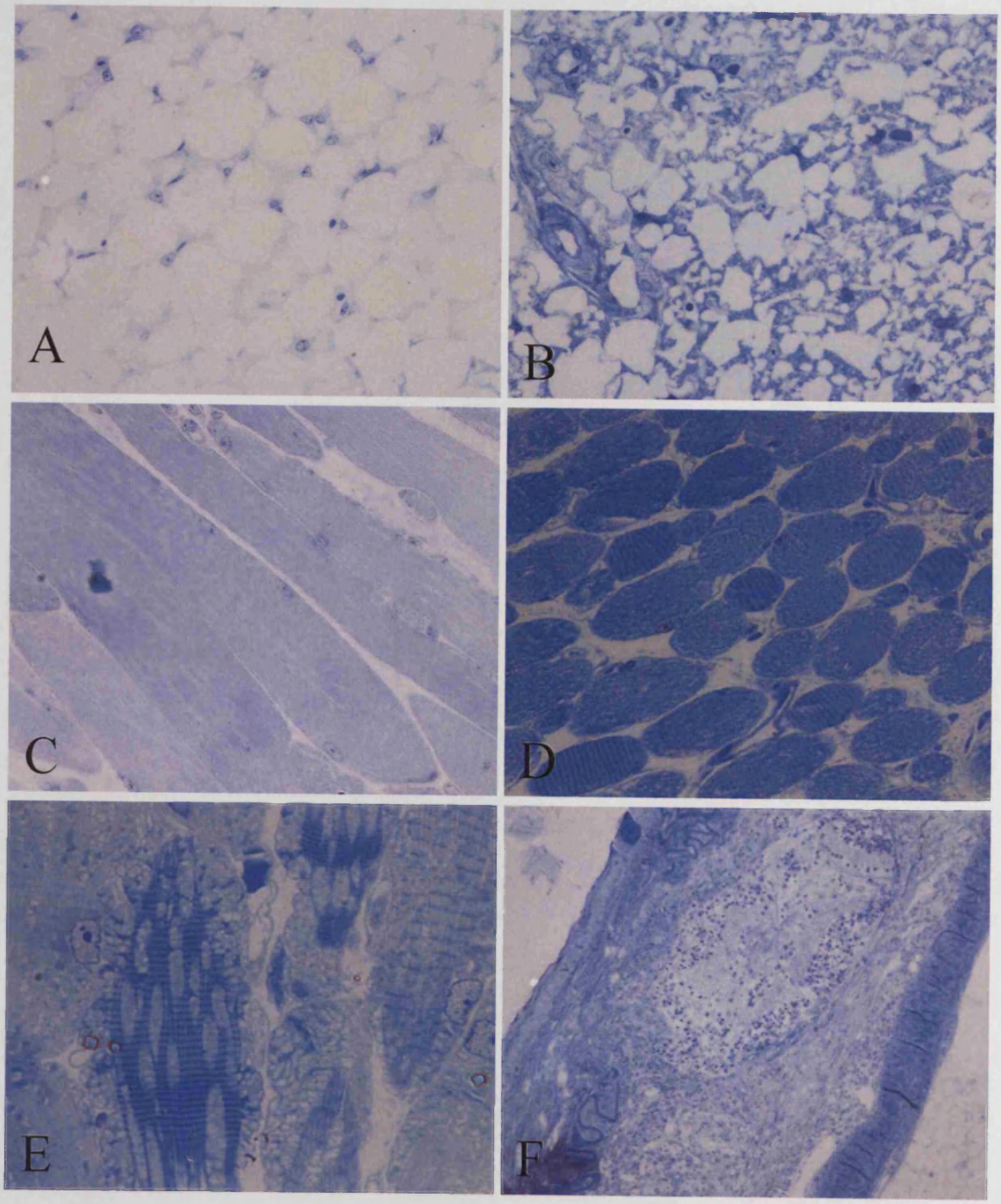

Figure 5.1.8

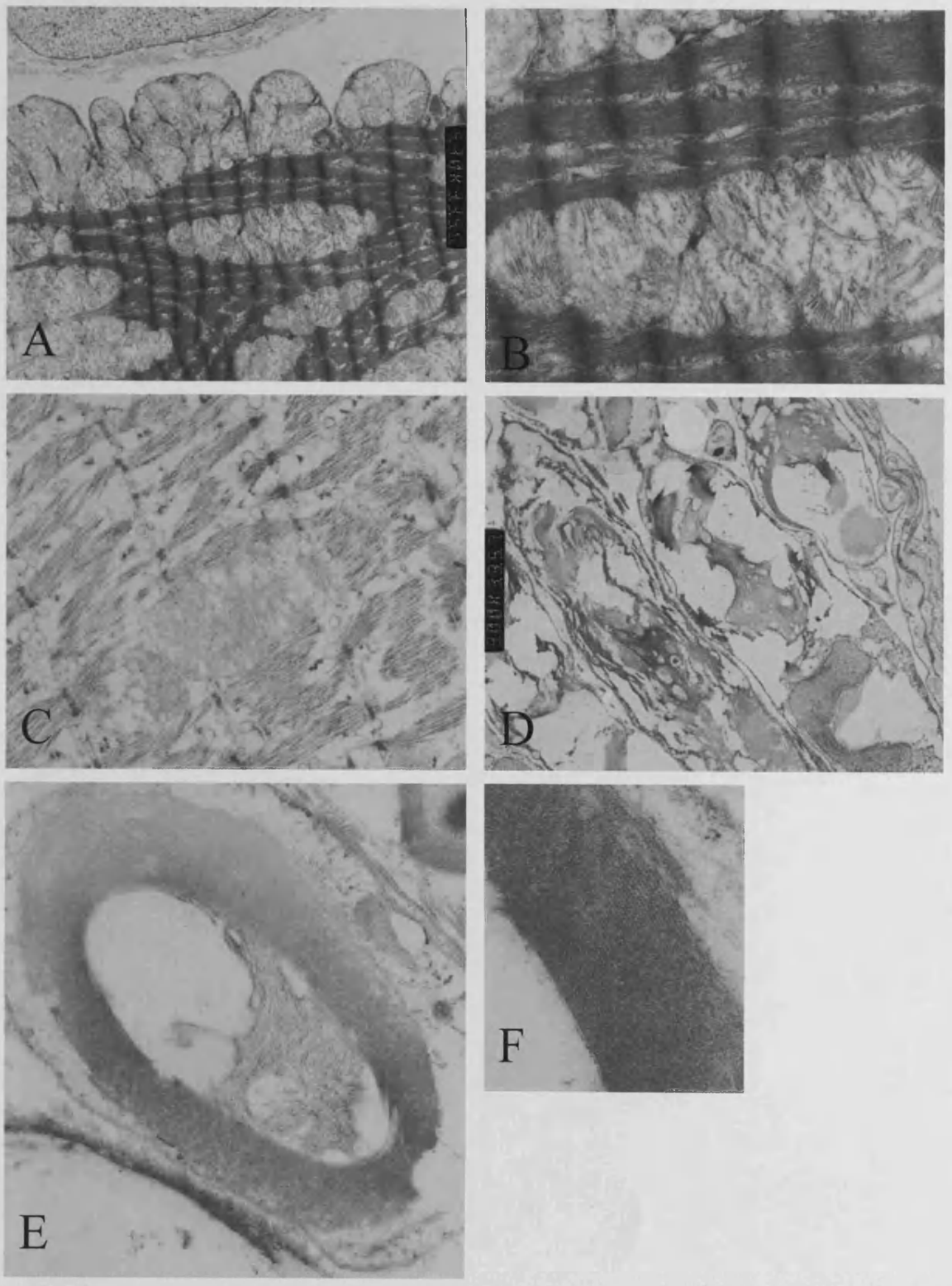

Figure 5.1.9

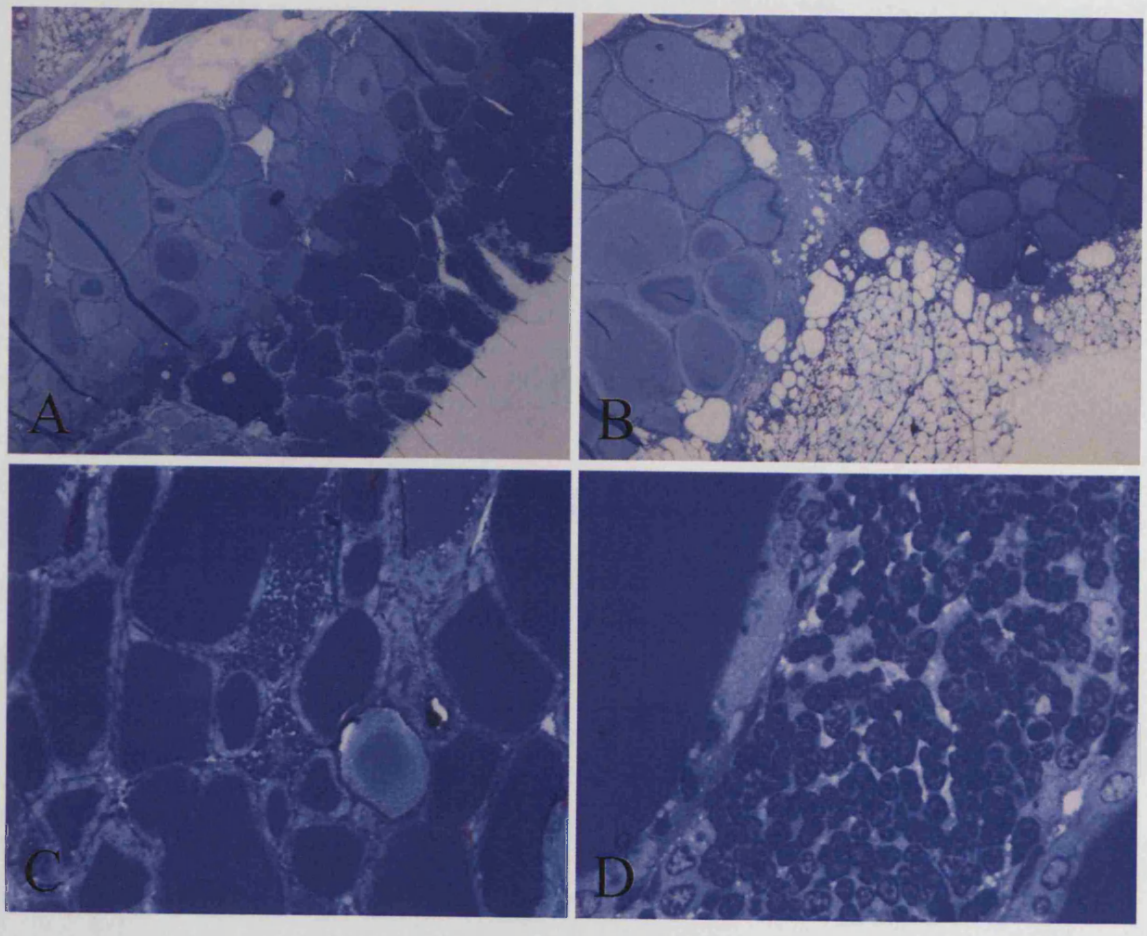

Figure 5.2.1

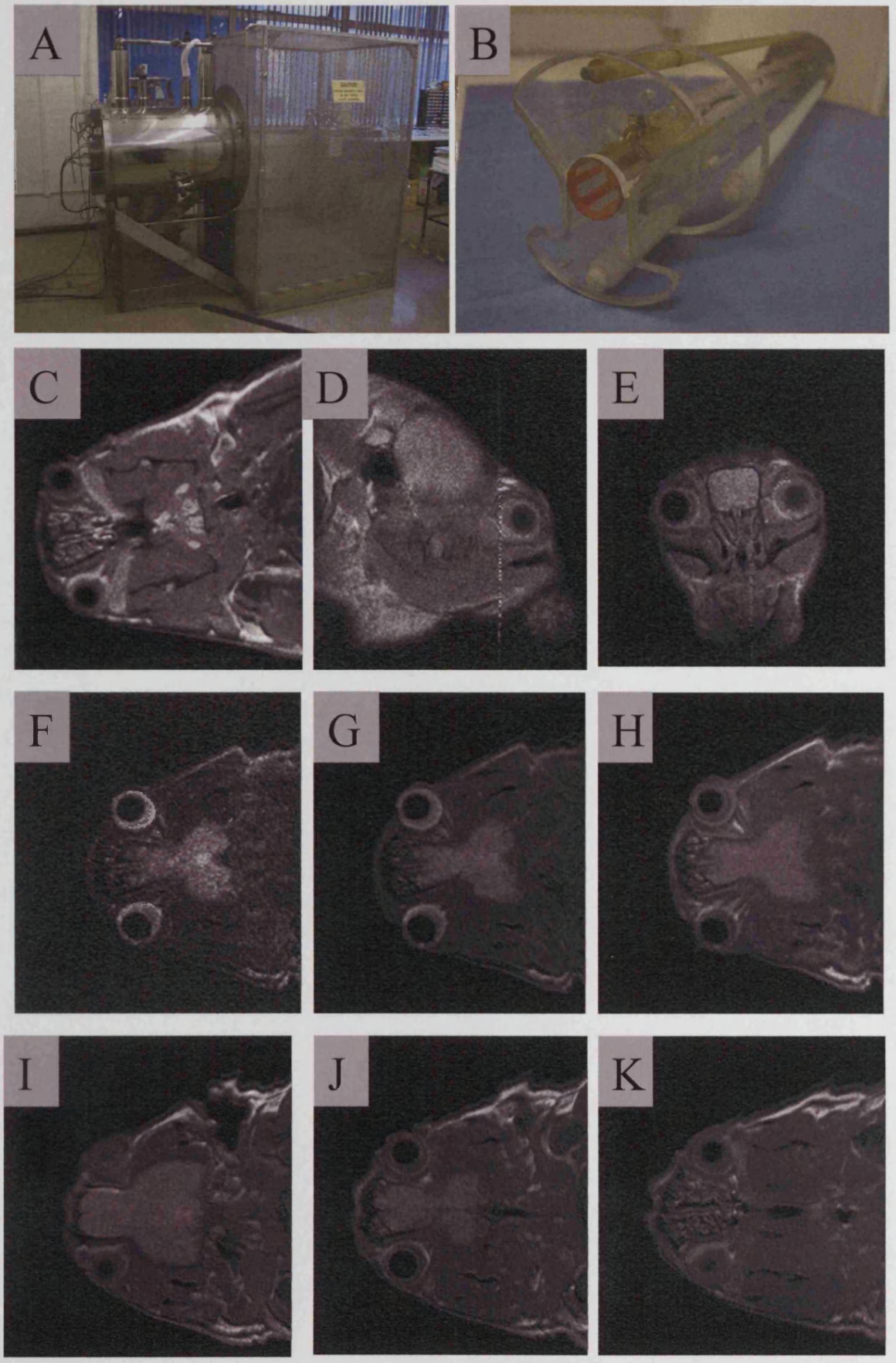

Figure 5.2.2

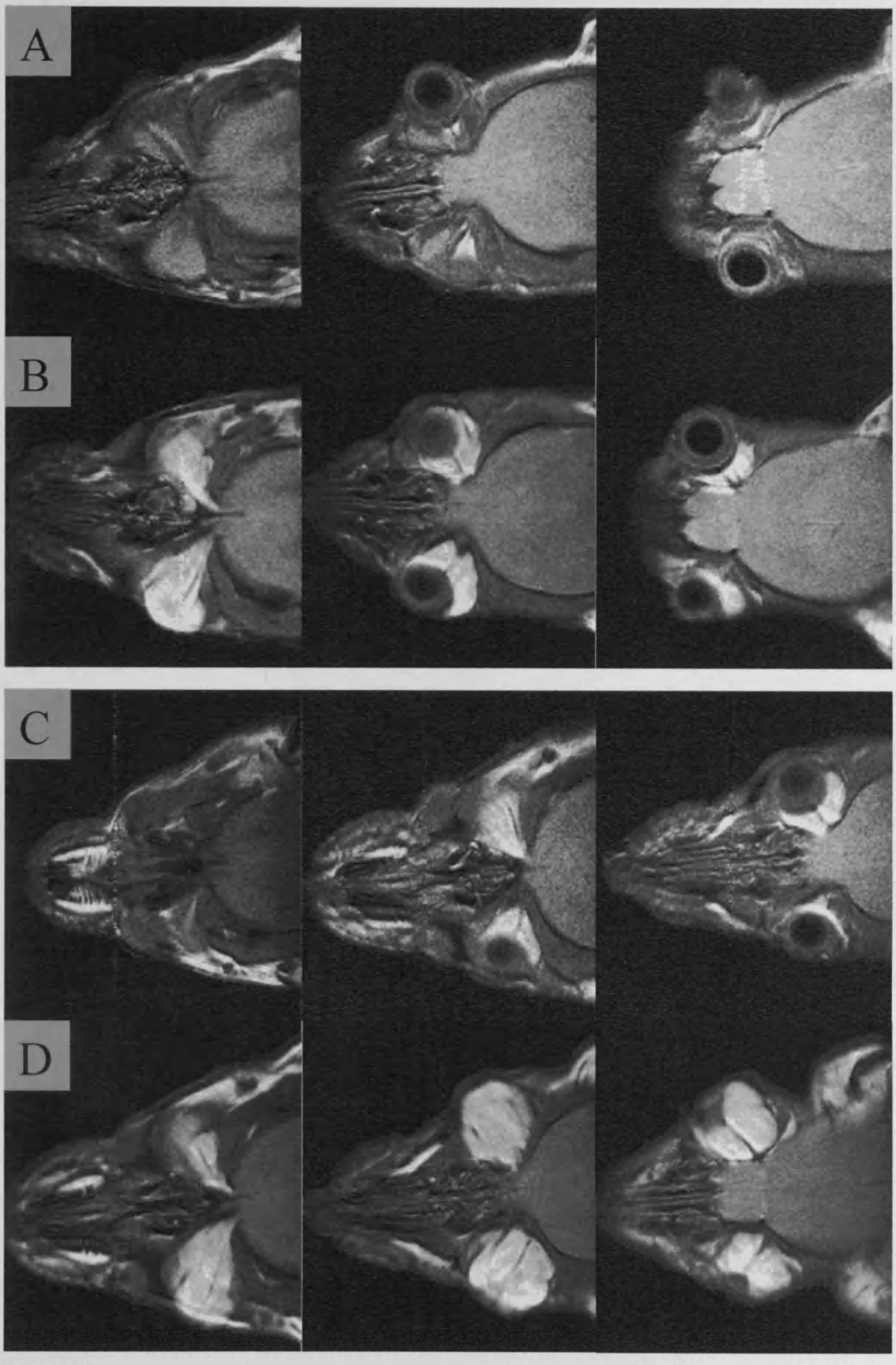

5.3.3 Orbital fat pads can be imaged using MRI and demonstrates differences between adiponectin transgenic, wild-type FVB and BALB/c

The experimental MRI facility did not have an established protocol for scanning small animals but did have some miniature surface coils that could be adapted for such usage (Figure 5.2.1. A-B). Initial imaging experience used BALB/c mice to determine a working protocol. Images could be acquired in axial, transverse and coronal planes and once positioned correctly, retro-orbital contents could be demonstrated most effectively using coronal slices (Figure 5.2.1. C-E). A slice thickness of 1.5mm was routinely used but by altering RF gain it was possible to increase resolution down to 0.75mm slices giving detailed images of ocular muscles and optic nerves. Decreasing the slice thickness greatly diminished the signal:noise ratio and very long imaging times (45 minutes to get sufficient signal) were required as the magnetic field could not be increased above 1.2 Tesla (Figure 5.1.9. F-H). During this time the temperature within the bore of the MRI would rise considerably, this along with the inaccessible nature of the long bore made initial plans of performing imaging on live anaesthetized mice not feasible. Additionally, even small respiratory movements of anaesthetized mice over a prolonged period of scanning could induce a movement artifact that might render the image useless. Attempts to generate a fat suppression sequence like the STIR useful in Graves' ophthalmopathy produced images with distorted anatomy despite scan times in excess of 55minutes. High field experimental MRIs with magnets up to 9-10 Tesla might reduce scan times but can induce tissue changes at high field strengths.

At the outset, the high resolution imaging (0.75mm slice) was planned to examine the Graves' ophthalmopathy model using gadolinium tagged antibodies but in the absence of any orbital pathology we gathered images of normal BALB/c orbits that contain little or no retro-orbital fat irrespective of age (Figure 5.2.1. I-K). The large orbital fat pads in the transgenic FVB mice could be imaged with 1.5mm slices and an image time of around 25 minutes. However, allowing for between 2 and 4 positioning scans with adjustment it could take 90 minutes to achieve satisfactory scans. Images from an 8 month old transgenic mouse showed the high signal (white=fat) tissue accumulating in the retro-orbital space contrasting with minimal fat in the wild type (Figure 5.2.2. A-B). With advancing age (20 months) the transgenic mouse had bilateral phthisis and became enveloped by the proliferating fat pad. Its 20 month wild type counterpart had a normal

globe but did accumulate orbital fat similar in volume to the 8 month transgenic mouse and much greater than that seen in BALB/c.

After imaging, orbital fat pads were excised and explant cultures attempted as in section 3.2.1. Only one of the transgenic samples developed any adherent cells. These cells initially had a fibroblastic appearance but rapidly developed multiple lipid droplets, similar to cells in a differentiation protocol and in less than three weeks the cells gradually all lost contact and no further cells attached to the surface.

5.3.4 Wide individual ranges of circulating adiponectin exist in Graves' ophthalmopathy patients and are inversely correlated with body mass index but not other clinical indices

In the small pilot experiment adiponectin levels in the Graves' group averaged 65.9μg/ml (sem=5.9, n=14), Hashimoto's 39.4 μg/ml (sem=3.93, n=5) and controls 35.4μg/ml (sem=3.53, n=5). Differences between the groups were significant (Kruskall Wallis p=0.0022) and post hoc testing showed significance only between Graves' and normals (Dunn $p<0.01$).

In the second larger group, Graves' ophthalmopathy patients had mean adiponectin levels of 118.4μg/ml (sem 11.3, n=37) compared to 127.6μg/ml (sem= 6.7, n=13) in the TMNG group. The difference was not significant (unpaired t test p=0.464). For reference we had samples from another study used in the same assay comprising 10 females in early pregnancy that had mean adiponectin of 109.4μg/ml (sem=7.4), no significant difference was present between the three groups (ANOVA). The difference in values between the pilot study and the second cohort are large and possibly due to inter-assay variation as a result of having to use densitometry as an end point of the western. Out of age, CAS, proptosis, TSH, T4, T3, TSAB, BMI, the only factors to be correlated with adiponectin were BMI (Spearman rho=-0.51, p=0.005) and TSAB (rho=0.33, p=0.045). When adiponectin levels are adjusted for BMI no new correlations were revealed. Comparing mean adiponectin in smokers/non smokers and patients with and without the following treatments; carbimazole, radio-iodine, orbital radiotherapy, thyroidectomy, steroid treatment, did not show any significant differences. As expected there is a slight sexual dimorphism present, with female Graves' ophthalmopathy patients having higher mean

adiponectin 126.3μg/ml (n=27) compared to men 97.3μg/ml (n=10) (unpaired t, p=0.08). Repeating the correlations excluding males only alters the adiponectin/BMI correlation slightly (rho= -0.492, p=0.011) and revealed no new correlations. Considering the females that underwent orbital decompression, as a marker of severity of disfigurement and dysfunction, they had a higher mean adiponectin of 144.4μg/ml (n=7, median=173) compared to those not requiring surgery 119.5μg/ml (n=20, median=122). The difference was not significant (Welch's, p=0.21). The numbers of males undergoing decompression was too small for meaningful analysis. Three patients had adiponectin sampled twice; the first had adiponectin measured 10 months apart (134 and 133μg/ml), the second 3 months apart (28 and 47μg/ml) and the third four months apart (118 and114μg/ml), suggesting from this small sample that adiponectin levels do not fluctuate much.

5.4 Discussion

Transgenic elevation of adiponectin in FVB mice induced orbital adipocyte fat pads to enlarge. The cells contained within were larger, with single lipid vacuoles more like white adipose tissue, but contained increased mitochondria, in comparison to the more mixed appearance of the smaller wild type fat pads. These in vivo changes are in agreement with in vitro work using lentivirus driven adiponectin over-expression in 3T3-L1 cells [379]. Adiponectin over-expression lead to more rapid cellular lipid accumulation with larger lipid droplets, increased mRNA expression of C/EBPα and PPARγ and decreased levels of adiponectin receptor mRNA. Adiponectin over-expression accelerated growth by increasing cell numbers entering G1/S transition.

Attempting to culture preadipocytes from orbital fat pads of adiponectin transgenic mice was largely unsuccessful, this is disappointing given brown fat explants are thought to maintain a more normal phenotype of the cells mitochondria [380]. The single plate that did attach may have similarities to the 3T3-L1 with adiponectin over-expression. Ex vivo adiponectin transgenic cells rapidly transformed from fibroblast like cells to lipid containing cells and then detached from the plates. Mature adipocytes are known to be poorly adherent. A feature of some human fat explants is the accumulation of lipid in the cells that have attached to the culture plates adjacent to and maintained by the explants as described in section 3.3.1. The adiponectin explants may represent an extreme form of that seen in human explants. Given the behaviour of the transgenic explant preadipocytes and the adiponectin over-expressing 3T3-L1 it is tempting to speculate that endogenously produced adiponectin may be an autocrine factor in the lipid accumulation in human explants.

Our initial pilot data on circulating adiponectin suggested Graves' patients had significantly higher levels than normal subjects. This may simply relate to the lower BMI induced by thyrotoxicosis but adiponectin levels generally fluctuate only slightly [381] and levels may be set by adiponectin polymorphisms or mutations as seen in some patients with the metabolic syndrome [382]. One study is in agreement with our findings of thyrotoxic patients adiponectin levels being elevated, but curiously the negative correlation with BMI was lost in thyrotoxics but remained negatively correlated in control patients [383]. Additionally T3, T4 and TRAb correlated with adiponectin. Given the small sample size of both our Hashimoto's and normals our result would need to be validated with a larger

sample and otherwise should be considered as open to bias. However it interested us sufficiently to study adiponectin levels in Graves' ophthalmopathy patients in which we found no difference between patients with a non-autoimmune cause of thyrotoxicosis, TMNG. Both groups had large ranges; Graves' ophthalmopathy (28-180μg/ml) and TMNG (51-192μg/ml). Adiponectin does not correlate with factors routinely measured in assessing Graves' ophthalmopathy but this may be due to our inability to estimate the parameter it may influence, orbital fat volumes. Given proptosis correlates more closely to orbital fat volumes than muscle changes [384] more attention could be made of this when orbital imaging is performed. Our cohort's showed a low level correlation between TSAB and adiponectin in keeping with the above study [383]. It is interesting that female patients undergoing orbital decompression had slightly higher mean adiponectin levels than those not requiring surgery, median values were very different but sample sizes were not equal. We found adiponectin levels did not greatly alter in patients over time periods as long as a year, this is in agreement with other work demonstrating this once changes in BMI had been taken into consideration [381]. Improved understanding of receptors and the various circulating forms of adiponectin along with more accurate adiponectin ELISA/RIA's, combined with orbital volumetric imaging may help to determine if adiponectin levels skew the degree of muscle or fat hypertrophy in Graves' ophthalmopathy.

In a small study examining several adipocytokines, thyrotoxic patients with lower body mass index had lower adiponectin levels than the higher body mass index hypothyroid patients [385]. This is opposite to the negative correlation of BMI and adiponectin seen in weight loss [369] and in our cohort of Graves' ophthalmopathy patients. There also existed a sexual dimorphism with females having higher adiponectin than males seen in our cohort and by other investigators [385]. The seemingly paradoxical situation of hypothyroid patients (higher body mass/higher TSH/lower T4/higher adiponectin/female biased sexual dimorphism) is reminiscent of some of the changes in the adiponectin transgenic mice. How much of the changes in the transgenic mice that are solely due to adiponectin elevation is unknown. As mentioned in the introduction, transgenic mice had elevation of prolactin, a hormone primarily known for its role in the proliferation of glandular and adipose breast tissue in lactation. Prolactin receptor knockout mice, particulary females, have lower fat mass than their wild type counterparts [386]. In FVB wild type mice prolactin decreases adiponectin levels and may represent a counter regulatory mechanism to lower adiponectin in the transgenic mice. Alternatively, murine breast adipocytes secrete extra-pituitary prolactin [387], in the adiponectin transgenics, breast tissue might be the source of

the increased circulating prolactin and it would be worthwhile determining if either interscapular or orbital fat expressed the prolactin receptor.

Another factor that may be contributing to the changes seen in the FVB transgenics is their thyroid status. The two different mouse strains, FVB [375] and C57BL/6 [373], in which adiponectin has been elevated by transgenic modification have resulted in different phenotypes in terms of fat proliferation but similar capacity to improve insulin resistance. Is this difference due to the former having the natural adiponectin molecule and the latter the globular domain? As shown by the orbital MRI wild type FVB mice spontaneously accumulate orbital fat with age unlike BALB\c. The FVB phenotype would thus seem to be accentuated by the adiponectin transgene. Average T4 concentrations were lower in FVB (2.36μg/dl) than in C57BL/6 (4.6μg/dl) and while average TSH levels were similar, a very wide range was present in the FVB strain [388]. Out of all mice tested [388]; CD-1, C57BL/6, SWR/J, NOD SCID, the FVB had the lowest T4 and highest TSH and could be considered as a hypothyroid strain relative to most other mice. As mentioned in the introduction, CD-1 mice given a short course of TZDs accumulate interscapular brown fat [128]. It would be interesting to examine the effects on fat mass a prolonged course would have on both CD-1 and FVB strains in terms of their contrasting thyroid status. Similarly the C57BL/6 adiponectin transgenics were only examined between 2 and 5 months and might also develop fat mass alteration in later life. Profound changes in body mass associated with congenital hypothyroidism are now largely confined to ancient literature since routine infant hypothyroid screening was introduced. "Fat masses in the necks of cretins" were identified as similar in phenotype to the hibernating glands of hedgehogs in 1909 by Shattock [389]. The infant fat pads were seen to occupy the posterior triangle of the neck, dip beneath the clavicles and could be traced extending over the infraspinal muscles and to the lowest angle of the scapula. Treatment with thyroid extract lead to disappearance of the fat pads. These observations were describing brown fat and the supraclavicular pad can also swell slightly in adults with hypothyroidism, these facts lead Doniach to hypothesize that TSH stimulated brown fat in 1975 [390]. Initially detected in guinea pig brown fat, the role of TSHR was unclear [391]. Hypothyroidism was shown to selectively elevate adenyl cyclase type III indirectly via adrenergic stimulation [392]. When later studied in rat brown adipocytes TSH was found to stimulate cAMP in a dose dependent fashion and TSHR mRNA was inhibited by TSH stimulation, similar to the situation seen in thyrocyte cell lines [393]. TSH stimulation lead to increased type II iodothyronine deiodinase and uncoupling protein (UCP)-1 mRNA. T3 is required for

optimal expression of UCP-1 and this is achieved by conversion of T4 by locally transcribed type II iodothyronine deiodinase. UCP-1 is responsible for thermogenesis and is located on the inner mitochondrial membrane. However the levels of TSH required to achieve this were 10 times that required to stimulate thyroid cells. We performed a pioglitazone induced differentiation experiment on 9 patients orbital preadipocytes, extracted RNA and attempted to measure UCP-1 levels after 7 and 14 days but only detected house-keeper and no UCP-1 (data not shown). The experiment was hampered by the lack of a positive UCP-1 control. Dr Ludgate has subsequently demonstrated UCP-1 [394] present in differentiated orbital preadipocytes in keeping with others findings [395]. White adipose tissue is known to contain small amounts of brown adipose specific UCP-1 [396]. Whether the fat proliferation in Graves' ophthalmopathy contains alterations in brown and white cell number is not known but understanding the biology might offer more selective therapy as our current treatment, steroids, can cause orbital fat proliferation [397]. Differences in fat accumulation are illustrated by our MRI findings both between strains and between transgenically modified animals. Newer scanners offer increased resolution, shorter scan times and software to measure volume, all features that would allow in vivo detection of changes in fat.

In summary, the fat mass increase of the adiponectin transgenic mouse is in keeping with in vitro changes seen in 3T3-L1 cells, but additional factors including TSH and prolactin may also have effects that are specific to the FVB strain. In particular, wild type FVB appear to spontaneously accumulate orbital fat with advancing age in excess of age matched of BALB/c. Generalised orbital, interscapular and neck fat proliferation does not in turn lead to a widespread break in tolerance to TSHR. Although some low level TSAB activity was detected, this was only present in older animals and did not alter thyroxine levels. Advances in understanding adiponectin biology are ongoing, it probably has effects on fat directly and indirectly by altering muscle and liver function where its' receptors are highly expressed. Adiponectin is demonstrated to be a robust pro-adipogenic adipokine with transgenic over-expression, this would seem at odds with higher levels of adiponectin seen in people with lower BMI's. However, in the physiological setting of lower BMI, adipose tissue probably aims to restore fat mass by increased adiponectin secretion and conversely decrease fat mass with low level secretion in obesity. Patients seem to have relatively constant levels of adiponectin and whether this alters fat proliferation in Graves' ophthalmopathy remains unanswered but given the multifactoral nature of the disease is worthy of further investigation.

6 General discussion

This thesis reports a series of in vivo and in vitro models used to examine tissue remodeling in Graves' ophthalmopathy. The first model demonstrates a recurring problem of reproducibility and re-evaluates findings present in terms of thyroiditis and ophthalmopathy. The presence of a focal thyroiditis needs to be distinguished from the frequent developmental anomaly of ectopic thymic tissue, but is interesting in itself, given that thymic enlargement is seen in Graves' disease. The normal contraction artefacts in muscle histology require considerable experience to distinguish them from pathological changes and would be best avoided entirely by the outlined dissection and fixation techniques. From this work, there has been a re-evaluation of previously proposed models of Graves' ophthalmopathy in BALB/c and NMRI mice. It remains that we are without a reproducible model for Graves' ophthalmopathy.

In chapter three a moderate reduction in cell proliferation, following a moderate rise in basal cAMP, results in enhanced adipogenesis. Higher levels of cAMP prevented any lipid accumulation, but morphological changes of rounding were not affected. Work by other groups suggests this is due to reduced expression of lipogenic enzymes, rather than inducing lipolysis [302]. Our model fails to follow the temporal pattern of TSHR expression in adipogenesis because it is driven by a viral promoter and cAMP signalling is continuous. Normally, lipid is already accumulating by the time TSHR expression is peaking in 3T3-L1 cells (7 days) and TSHR mRNA was not present before day 5 [264]. We need to characterise the pattern of TSHR expression in human primaries fully (and in any other cell line used) and then reproduce this using inducible vectors controlling the activating TSHR mutants. TSAB or TSH would seem to have a relatively brief period to affect adipogenesis given TSHR expression in mature adipocytes is low. TSHR on preadipocytes are possibly non-functional in a normal physiological range, they require high TSH concentrations (10-100mU) for cAMP signalling. However, TSAB might have higher binding affinities, above the level of TSH, for TSHR on differentiating preadipocytes. If TSHR activation has a direct effect on adipocyte differentiation we would expect it to be in the middle or late stages and this is what this work has guided us to. TSHR activation might act in tandem with other recently identified factors such as antibodies that stimulate IGF-1 receptor [42]. We find no clear evidence to support a role for TSHR stimulation in adipogenesis from our study.

We have further characterised a TSHR stimulating factor present in tears and concluded its behaviour does not follow that of TSAB. While examining the tears of smokers and Graves' ophthalmopathy patients we were able to identify a prominent protein that had initially appeared to present in lower concentrations in non-smokers. This was not evident in later samples but a profile of ZAG expression was present that seemed to be different in smokers compared with Graves' ophthalmopathy patients and non-smokers. This agrees with a recent publication demonstrating increased proteins in smokers tears, with the region between 25 and 40kD being most discriminatory [398]. The full complexity of the protein profiles would require considerable further work using 2DGE or other techniques that allow peptides to be identified and quantified. The role of ZAG in the tear film is not known and its' role in lipid mobilisation in cachexia is all that is currently understood. Future studies might also investigate the time course e.g. tear composition whilst smoking at varying intervals and passive smoking. From our studies we cannot identify a specific protein to cause TSHR stimulation in tears and cannot rule out a non-specific ionic effect caused by an increased protein concentration in tears.

The final experimental chapter hints at a possible synergistic effect of an abundant adipocytokine, adiponectin and TSH in the proliferation of fat. Adiponectin transgenic elevation resulted in profound fat accumulation in vivo [375] and similar in vitro [379] changes have been demonstrated by others. What this probably tells us is adiponectin gene expression is lipogenic but might also suggest that the secreted protein may also be lipogenic or adipogenic. The FVB mice stand apart from other strains of mice in terms of their relatively hypothyroid status and accumulation of orbital fat, even in wild type mice. Transgenic adiponectin elevation in another more euthyroid strain did not induce fat proliferation at the ages studied [373]. Fat proliferation seen in congenital hypothyroidism [389] has some similarities with that of the transgenic FVB mice, again hinting at a proadipogenic effect of elevated TSH. However these effects seem very different to those of activating TSHR mutants that appear to reduce fat mass, but the kinetics of cAMP signalling is presumably very different in ligand/receptor interactions compared to a constitutively active receptor as seen in our in vitro model. While we found wide ranges of circulating adiponectin in Graves' ophthalmopathy, levels within the orbit may be more important and others have shown increases in adiponectin mRNA in Graves' ophthalmopathy adipose tissue [399; 400]. If adiponectin has an autocrine proadipogenic effect, heightened by orbital congestion, it could be a key step in the perpetuation of a chronic disease process triggered by TSHR activation by either TSAB or TSH.

Future work on modelled ophthalmopathy may require heightened antigenicity; techniques utilizing adjuvants and apoptosis have been discussed in chapter 2. More recently, activation of Toll-like receptors, either with direct agonists or heat killed gram positive and negative bacteria, have been shown to be effective in increasing virally induced type-1 diabetes [401]. However, no similar virally or bacterial induced in vivo model is available for Graves' disease but this would be another method to increase immune responses and add support to the importance of infection and the innate immune system. In this context, a recent abstract reported higher and more persistent induced TSAB in mice housed in a conventional animal unit compared with a pathogen free facility [402]. As reviewed in chapter 2, there are several reproducible models of Graves' disease whereby TSAB are induced in which it would also be interesting to increase immune responses [173; 175]. Low level and sporadic lymphocytic infiltration is already present in these models. The roles of these infiltrates is unknown, are they simply non-specific responses of thyrocytes and local dendritic cells (both expressing TSHR) that are relentlessly stimulated by TSAB, a type of wound response, rather than a TCR/TSHR specific interaction? Our interpretation and further investigation of animal models are important tools in understanding Graves' disease and ophthalmopathy.

If TSHR is not proadipogenic then we possibly need to explore how preadipocytes could act as APCs, does differentiation induce co-stimulatory signals such as CD-40 or HLA II [52]? Understanding the basic models is necessary before we can add into the equation the full range of orbital cells and cytokines present in Graves' ophthalmopathy. This in vitro model needs to replicate the pattern of TSHR expression and this might more faithfully test over-stimulation that mimics the action of TSAB. From our findings of reduced lipid accumulation in cells transduced with activating mutations that cause greatest inhibition of proliferation we investigated for possible similar effects on body composition of germline TSHR mutations. One patient has been examined in preliminary work, a euthyroid 8-year-old girl harbouring the activating TSHR V597L. She had weight and height below the 0.4th centile compared with 3 siblings and parents who were between the 9-25th centiles. Measurement of body composition using dual energy X-ray absorptiometry demonstrated that she had reduced body fat (19.1% of total body weight) compared to her unaffected 11-year-old twin sisters (22.1 & 25.4%) and 13-year-old sister (23.3%). The reduced height and fat mass observed could possibly be attributed to prolonged thyrotoxicosis. Graves' thyrotoxicosis can cause significant lowering of body cell mass while increasing

extracellular water content, changes that normalise after euthyroidism is established [403]. Fat mass is reduced in males with Graves' disease but is not significantly altered in women [404]. Not only fat mass is affected but bone density is also reduced in thyrotoxic Graves' patients and this improves with normalised thyroid function but might not reach levels of unaffected control patients [405; 406]. Improvement in bone density correlates with reduced TSAB levels but whether this is an epiphenomenon or a TSHR mediated effect on bone is unclear. As demonstrated by us and others previously [294], MG63 osteoblastic cells express TSHR but the importance of TSHR has only recently been demonstrated in bone metabolism [407]. Halving TSHR expression impaired osteoblast and osteoclast formation resulting in osteoporosis and localised osteosclerosis.

Clinical outcomes in Graves' ophthalmopathy have improved considerably in the fifty years intervening since Duke-Elder's 1952 text book in which patients were still being enucleated due to lack of understanding of the condition. Improvements have come mainly from re-establishing euthyroidism, immunosuppression and surgery. Further understanding the underlying pathogenesis requires ongoing co-operation and funding between clinicians and scientists.

7 References

1. Weetman, A. & McGregor, A. (1994). Autoimmune thyroid disease: further developments in our understanding. *Endocr Rev* 15, 788-830.
2. Rees Smith, B., McLachlan, S. & Furmaniak, J. (1988). Autoantibodies to the thyrotropin receptor. *Endocr Rev* 9, 106-121.
3. Paschke, R. & Ludgate, M. (1997). The thyrotropin receptor in thyroid diseases. *N Engl J Med* 337, 1675-81.
4. Perros, P. & Kendall-Taylor, P. (1995). Thyroid-Associated Ophthalmopathy - Pathogenesis and clinical management. *Baillieres Clin Endocrinol Metab* 9, 115-35.
5. Heufelder, A., Weetman, A., Ludgate, M. & Bahn, R. (2000). Pathogenesis of Graves' ophthalmopathy. In *Recent developments in Graves' ophthalmopathy* (Prummel, M., Wiersinga, W. & Mourits, M., eds.), pp. 15-37. Kluwer Academic publishers, Boston/Dordrecht/London.
6. Parry, C. (1825). Collections from unpublished medical writings., Vol. ii, pp. 111, London.
7. Graves, R. (1835). *London Med Surg J* 173, lecture xii.
8. Basedow, C. (1840). *f. d. ges. Heilk* xiv, 197-220.
9. Duke-Elder, S. (1952). Orbital involvement in general disease. Endocrine disorders. In *Text Book of Ophthalmology.* (Duke-Elder, S., ed.), Vol. V, pp. 5478-5507. Henry Kimpton, London.
10. Brooks, B. (1922). Pathologic changes in muscle as a result of disturbances of circulation; an experimental study of Volkman's ischaemic paralysis. *Arch Surg* 5, 188-216.
11. Stallard, H. (1936). A case of "exophthalmic ophthalmoplegia with thyrotoxicosis". *Br J Ophthalmol* 20, 612-619.
12. Elisei, R., Weightman, D., Kendall-Taylor, P., Vassart, G. & Ludgate, M. (1993). Muscle Autoantigens In Thyroid-Associated Ophthalmopathy - The Limits of Molecular-Genetics. *J Endocr Invest* 16, 533-40.
13. Ahmann, A., Baker, J., Jr, Weetman, A., Wartofsky, L., Nutman, T. & Burman, K. (1987). Antibodies to porcine eye muscle in patients with Graves' ophthalmopathy: identification of serum immunoglobulins directed against unique determinants by immunoblotting and enzyme-linked immunosorbent assay. *J Clin Endocrinol Metab* 64, 454-460.
14. Gunji, K., De Bellis, A., Kubota, S., Swanson, J., Wengrowicz, S., Cochran, B., Ackrell, B. A. C., Salvi, M., Bellastella, A., Bizzarro, A., Sinisi, A. A. & Wall, J. R. (1999). Serum Antibodies against the Flavoprotein Subunit of Succinate Dehydrogenase Are Sensitive Markers of Eye Muscle Autoimmunity in Patients with Graves' Hyperthyroidism. *J Clin Endocrinol Metab* 84, 1255-1262.
15. Bednarczuk, T., Stolarski, C., Pawlik, E., Slon, M., Rowinski, M., Kubota, S., Hiromatsu, Y., Bartoszewicz, Z., Wall, J. & Nauman, J. (1999). Autoantibodies reactive with extracellular matrix proteins in patients with thyroid-associated ophthalmopathy. *Thyroid* 9, 289-95.
16. Dong, Q., Ludgate, M. & Vassart, G. (1991). Cloning and sequencing of a novel 64-kDa autoantigen recognized by patients with autoimmune thyroid disease. *J Clin Endocrinol Metab* 72, 1375-1381.
17. Bahn, R., Gorman, C., Johnson, C. & Smith, T. (1989). Presence of antibodies in the sera of patients with Graves' disease recognizing a 23 kilodalton fibroblast protein. *J Clin Endocrinol Metab* 69, 622-628.
18. Tallstedt, L. & Norberg, R. (1988). Immunohistochemical staining of normal and Graves' extraocular muscle. *Invest. Ophthalmol. Vis. Sci.* 29, 175-184.
19. Heufelder, A. & Bahn, R. (1992). Graves' immunoglobulins and cytokines stimulate the expression of intercellular adhesion molecule-1 (ICAM-1) in cultured Graves' orbital fibroblasts. *Eur J Clin Invest* 22, 529-37.
20. Ludgate, M., Swillens, S., Mercken, L. & Vassart, G. (1986). Homology between thyroglobulin and acetylcholinesterase: an explanation for pathogenesis of Graves' ophthalmopathy? *Lancet* 2, 219-20.
21. Ludgate, M., Dong, Q., Pa, D., Zakut, H., Taylor, P., Vassart, G. & Soreq, H. (1989). Definition, At The Molecular-Level, Of A Thyroglobulin Acetylcholinesterase Shared Epitope - Study Of Its Pathophysiological Significance In Patients With Graves Ophthalmopathy. *Autoimmunity.* 3, 167-76.
22. Mourits, M., Prummel, M. F., Wiersinga, W. M. & Koornneef, L. (1997). Clinical activity score as a guide in the management of patients with Graves' ophthalmopathy. *Clinical Endocrinology* 47, 9-14.
23. Gerding, M., van der Meer, J., Broenink, M., Bakker, O., Wiersinga, W. & Prummel, M. (2000). Association of thyrotrophin receptor antibodies with the clinical features of Graves' ophthalmopathy. *Clin Endocrinol* 52, 267-71.

24. Davies, T. (2000). Causes of thyrotoxicosis. In *Werner and Ingbar's the thyroid. A fundamental and clinical text.* 8 edit. (Braverman, L. & Utiger, R., eds.), pp. 519-530. Lippincott, Williams and Wilkins, Philadelphia.
25. Coles, A., Wing, M., Smith, S., Coraddu, F., Greer, S., Taylor, C., Weetman, A., Hale, G., Chatterjee, V., Waldmann, H. & Compston, A. (1999). Pulsed monoclonal antibody treatment and autoimmune thyroid disease in multiple sclerosis. *Lancet.* 354, 1691-5.
26. Okumura, M., Hidaka, Y., Kuroda, S., Takeoka, K., Tada, H. & Amino, N. (1997). Increased Serum Concentration of Soluble CD30 in Patients with Graves' Disease and Hashimoto's Thyroiditis. *J Clin Endocrinol Metab* 82, 1757-1760.
27. Del Prete, G., De Carli, M., D'Elios, M., Daniel, K., Almerigogna, F., Alderson, M., Smith, C., Thomas, E. & Romagnani, S. (1995). CD30-mediated signaling promotes the development of human T helper type 2-like T cells. *J. Exp. Med.* 182, 1655-1661.
28. Yang, D., Hiromatsu, Y., Hoshino, T., Inoue, Y., Itoh, K. & Nonaka, K. (1999). Dominant infiltration of Th1-type CD4+ T cells at the retrobulbar space of patients with thyroid associated ophthalmopathy. *Thyroid* 9, 305-9.
29. Aniszewski, J. P., Valyasevi, R. W. & Bahn, R. S. (2000). Relationship between Disease Duration and Predominant Orbital T Cell Subset in Graves' Ophthalmopathy. *J Clin Endocrinol Metab* 85, 776-780.
30. Hiromatsu, Y., Yang, D., Bednarczuk, T., Miyake, I., Nonaka, K. & Inoue, Y. (2000). Cytokine Profiles in Eye Muscle Tissue and Orbital Fat Tissue from Patients with Thyroid-Associated Ophthalmopathy. *J Clin Endocrinol Metab* 85, 1194-1199.
31. Smith, T. J. & Parikh, S. J. (1999). HMC-1 Mast Cells Activate Human Orbital Fibroblasts in Coculture: Evidence for Up-Regulation of Prostaglandin E2 and Hyaluronan Synthesis. *Endocrinology* 140, 3518-3525.
32. Sato, A., Takemura, Y., Yamada, T., Ohtsuka, H., Sakai, H., Miyahara, Y., Aizawa, T., Terao, A., Onuma, S., Junen, K., Kanamori, A., Nakamura, Y., Tejima, E., Ito, Y. & Kamijo, K. (1999). A Possible Role of Immunoglobulin E in Patients with Hyperthyroid Graves' Disease. *J Clin Endocrinol Metab* 84, 3602-3605.
33. Yamada, T., Sato, A., Aizawa, T., Ootsuka, H., Miyahara, Y., Sakai, H., Terao, A., Onuma, S., Ito, Y., Kanamori, A., Nakamura, Y. & Tejima, E. (1998). An elevation of stem cell factor in patients with hyperthyroid Graves' disease. *Thyroid.* 8, 499-504.
34. Metcalfe, R., Jordan, N., Watson, P., Gullu, S., Wiltshire, M., Crisp, M., Evans, C., Weetman, A. & Ludgate, M. (2002). Demonstration of Immunoglobulin G, A, and E Autoantibodies to the Human Thyrotropin Receptor Using Flow Cytometry. *J Clin Endocrinol Metab* 87, 1754-1761.
35. Gauchat, J., Henchoz, S., Mazzei, G., Aubry, J., Brunner, T., Blasey, H., Life, P., Talabot, D., Flores-Romo, L. & Thompson, J. (1993). Induction of human IgE synthesis in B cells by mast cells and basophils. *Nature* 365, 340-3.
36. Trautmann, A., Krohne, G., Brocker, E.-B. & Klein, C. E. (1998). Human Mast Cells Augment Fibroblast Proliferation by Heterotypic Cell-Cell Adhesion and Action of IL-4. *J Immunol* 160, 5053-5057.
37. Heufelder, A. & Bahn, R. (1993). Detection and localisation of cytokine immunoreactivity in retro-ocular connective tissue in Graves' ophthalmopathy. *Eur J Clin Invest* 23, 10-17.
38. Villanueva, R., Inzerillo, A., Tomer, Y., Barbesino, G., Meltzer, M., Concepcion, E., Greenberg, D., MacLaren, N., Sun, Z., Zhang, D., Tucci, S. & Davies, T. (2000). Limited genetic susceptibility to severe Graves' ophthalmopathy: no role for CTLA-4 but evidence for an environmental etiology. *Thyroid.* 10.
39. Heufelder, A. & Bahn, R. (1993). Elevated expression in situ of selectin and immunoglobulin superfamily type adhesion molecules in retroocular connective tissues from patients with Graves' ophthalmopathy. *Clin Exp Immunol* 91, 381-9.
40. Pappa, A., Calder, V., Ajjan, R., Fells, P., Ludgate, M., Weetman, A. & Lightman, S. (1997). Analysis of extraocular muscle-infiltrating T cells in thyroid-associated ophthalmopathy (TAO). *Clin Exp Immunol* 109, 362-9.
41. Sciaky, D., Brazer, W., Center, D. M., Cruikshank, W. W. & Smith, T. J. (2000). Cultured Human Fibroblasts Express Constitutive IL-16 mRNA: Cytokine Induction of Active IL-16 Protein Synthesis Through a Caspase-3-Dependent Mechanism. *J Immunol* 164, 3806-3814.
42. Pritchard, J., Han, R., Horst, N., Cruikshank, W. W. & Smith, T. J. (2003). Immunoglobulin Activation of T Cell Chemoattractant Expression in Fibroblasts from Patients with Graves' Disease Is Mediated Through the Insulin-Like Growth Factor I Receptor Pathway. *J Immunol* 170, 6348-6354.
43. Sempowski, G. D., Rozenblit, J., Smith, T. J. & Phipps, R. P. (1998). Human orbital fibroblasts are activated through CD40 to induce proinflammatory cytokine production. *Am J Physiol Cell Physiol* 274, C707-714.

44. Elner, V., Burnstine, M., Kunkel, S., Strieter, R. & SG., E. (1998). Interleukin-8 and monocyte chemotactic protein-1 gene expression and protein production by human orbital fibroblasts. *Ophthal Plast Reconstr Surg* 14, 119-25.
45. Hiromatsu, Y., Tanaka, K., Ishisaka, N., Kamachi, J., Kuroki, T., Hoshino, T., Inoue, Y., Wall, J. & Nonaka, K. (1995). Human histocompatibility leukocyte antigen-DR and heat shock protein-70 expression in eye muscle tissue in thyroid-associated ophthalmopathy. *J Clin Endocrinol Metab* 80, 685-691.
46. Heufelder, A., Smith, T., Gorman, C. & Bahn, R. (1991). Increased induction of HLA-DR by interferon-gamma in cultured fibroblasts derived from patients with Graves' ophthalmopathy and pretibial dermopathy. *J Clin Endocrinol Metab* 73, 307-313.
47. Heufelder, A., Wenzel, B., Gorman, C. & Bahn, R. (1991). Detection, cellular localization, and modulation of heat shock proteins in cultured fibroblasts from patients with extrathyroidal manifestations of Graves' disease. *J Clin Endocrinol Metab* 73, 739-745.
48. Smith, T., Bahn, R., Gorman, C. & Cheavens, M. (1991). Stimulation of glycosaminoglycan accumulation by interferon gamma in cultured human retroocular fibroblasts. *J Clin Endocrinol Metab* 72, 1169-71.
49. Wang, H.-S., Cao, H. J., Winn, V. D., Rezanka, L. J., Frobert, Y., Evans, C. H., Sciaky, D., Young, D. A. & Smith, T. J. (1996). Leukoregulin Induction of Prostaglandin-Endoperoxide H Synthase-2 in Human Orbital Fibroblasts. An in vitro model for connective tissue inflammation. *J. Biol. Chem.* 271, 22718-22728.
50. Sorisky, A., Pardasani, D., Gagnon, A. & Smith, T. (1996). Evidence of adipocyte differentiation in human orbital fibroblasts in primary culture. *J Clin Endocrinol Metab* 81, 3428-3431.
51. Cao, H., Wang, H., Zhang, Y., Lin, H., Phipps, R. & Smith, T. (1998). Activation of Human Orbital Fibroblasts through CD40 Engagement Results in a Dramatic Induction of Hyaluronan Synthesis and Prostaglandin Endoperoxide H Synthase-2 Expression. Insights into potential pathogenic mechanisms of Thyroid Associated Ophthalmopathy. *J. Biol. Chem.* 273, 29615-29625.
52. Feldon, S. E., Park, D. J. J., O'Loughlin, C. W., Nguyen, V. T., Landskroner-Eiger, S., Chang, D., Thatcher, T. H. & Phipps, R. P. (2005). Autologous T-Lymphocytes Stimulate Proliferation of Orbital Fibroblasts Derived from Patients with Graves' Ophthalmopathy. *Invest. Ophthalmol. Vis. Sci.* 46, 3913-3921.
53. Smith, T. (2001). Participation of orbital fibroblasts in the inflammation of Graves' ophthalmopathy. In *Thyroid Eye Disease. Endocrine Updates 14.* (RS, B., ed.), pp. 83-98. Kluwer Academic.
54. Smith, T., Sempowski, G., Wang, H., Del Vecchio, P., Lippe, S. & Phipps, R. (1995). Evidence for cellular heterogeneity in primary cultures of human orbital fibroblasts. *J Clin Endocrinol Metab* 80, 2620-2625.
55. Phipps, R., Penney, D., Keng, P., Quill, H., Paxhia, A., Derdak, S. & Felch, M. (1989). Characterisation of two major populations of lung fibroblasts: Distinguishing Morphology and discordant display of Thy-1 and Class II MHC. *Am J Respir Cell Mol Biol* 1, 65-74.
56. Sempowski, G., Beckman, M., Derdak, S. & Phipps, R. (1994). Subsets of murine fibroblasts express membrane bound and soluble IL-4 receptors. *J Immunol* 152, 3606-14.
57. Derdak, S., Penney, D., Keng, P., Felch, M., Brown, D. & Phipps, R. (1992). Differential collagen and fibronectin production by Thy-1 positive and negative lung fibroblast subpopulations. *Am J Physiol Cell Physiol* 263, 283-90.
58. Koumas, L., Smith, T. J., Feldon, S., Blumberg, N. & Phipps, R. P. (2003). Thy-1 Expression in Human Fibroblast Subsets Defines Myofibroblastic or Lipofibroblastic Phenotypes. *Am J Pathol* 163, 1291-1300.
59. Wetzel, A., Chavakis, T., Preissner, K. T., Sticherling, M., Haustein, U.-F., Anderegg, U. & Saalbach, A. (2004). Human Thy-1 (CD90) on Activated Endothelial Cells Is a Counterreceptor for the Leukocyte Integrin Mac-1 (CD11b/CD18). *J Immunol* 172, 3850-3859.
60. Ludgate, M. & Baker, G. (2002). Unlocking the immunological mechanisms of orbital inflammation in thyroid eye disease. *Clin Exp Immunol* 127, 193-198.
61. Prabhakar, B. S., Bahn, R. S. & Smith, T. J. (2003). Current Perspective on the Pathogenesis of Graves' Disease and Ophthalmopathy. *Endocr Rev* 24, 802-835.
62. Nussey, S. & Whitehead, S. (2001). The thyroid gland. In *Endocrinology an integrated approach.* (Nussey, S. & Whitehead, S., eds.). Bios Scientific Publishers, Oxford.
63. Carrasco, N. (2000). Thyroid Hormone Synthesis. In *Werner and Ingbar's The Thyroid, A fundamental and clinical text.* 8th edition edit. (Braverman, L. & Utiger, R., eds.), pp. 53-61.
64. Grossmann, M., Weintraub, B. & Szkudlinski, M. (1997). Novel insights into the molecular mechanisms of human thyrotropin action: structural, physiological, and therapeutic implications for the glycoprotein hormone family. *Endocrine Reviews.* 18, 476-501.
65. Rapoport, B., Chazenbalk, G. D., Jaume, J. C. & McLachlan, S. M. (1998). The Thyrotropin (TSH)-Releasing Hormone Receptor: Interaction with TSH and Autoantibodies. *Endocr Rev* 19, 673-716.

66. Marinissen, M. & Gutkind, J. (2001). G-protein-coupled receptors and signaling networks: emerging paradigms. *Trends in Pharmacological Sciences.* 22, 368-76.
67. Davies, T. F., Ando, T., Lin, R.-Y., Tomer, Y. & Latif, R. (2005). Thyrotropin receptor-associated diseases: from adenomata to Graves disease. *J. Clin. Invest.* 115, 1972-1983.
68. Kyewski, B. & Klein, L. (2006). A Central Role for Central Tolerance. *Annu Rev Immunol.*
69. Kamradt, T. & Mitchison, N. (2001). Tolerance and autoimmunity. *New England Journal of Medicine.* 344, 655-64.
70. Saoudi, A., Seddon, B., Fowell, D. & Mason, D. (1996). The Thymus Contains a High Frequency of Cells that Prevent Autoimmune Diabetes on Transfer into Prediabetic Recipients. *J. Exp. Med.* 184, 2393-2398.
71. Seddon, B. & Mason, D. (1999). Regulatory T Cells in the Control of Autoimmunity: the Essential Role of Transforming Growth Factor beta and Interleukin 4 in the Prevention of Autoimmune Thyroiditis in Rats by Peripheral CD4+CD45RC- Cells and CD4+CD8- Thymocytes. *J. Exp. Med.* 189, 279-288.
72. Seddon, B. & Mason, D. (1999). Peripheral Autoantigen Induces Regulatory T Cells that Prevent Autoimmunity. *J. Exp. Med.* 189, 877-882.
73. Volpe, R. (1993). T lymphocyte dysfunction is important in the pathogenesis of autoimmune thyroid disease: a perspective. *Thyroid* 3, 345-352.
74. Irvine, S. & Irvine, A. (1952). Lens induced uveitis and glaucoma. *Am J Ophthalmol* 35, 177-86.
75. Weiss, M., Ingbar, S., Winblad, S. & Kasper, D. (1983). Demonstration of a saturable binding site for thyrotropin in Yersinia enterocolitica. *Science* 219, 1331-3.
76. Tomer, Y. & Davies, T. (1993). Infection, thyroid disease, and autoimmunity. *Endocr Rev* 14, 107-120.
77. Tomer, Y. & Davies, T. F. (2003). Searching for the Autoimmune Thyroid Disease Susceptibility Genes: From Gene Mapping to Gene Function. *Endocr Rev* 24, 694-717.
78. Brix, T. H., Kyvik, K. O., Christensen, K. & Hegedus, L. (2001). Evidence for a Major Role of Heredity in Graves' Disease: A Population-Based Study of Two Danish Twin Cohorts. *J Clin Endocrinol Metab* 86, 930-934.
79. Winsa, B., Adami, H., Bergstrom, R., Gamstedt, A., Dahlberg, P., Adamson, U., Jansson, R. & A., K. (1991). Stressful life events and Graves' disease. *Lancet.* 338, 1475-9.
80. Kajita, Y., Rickards, C., Buckland, P., Howell, R. & Rees Smith, B. (1985). Analysis of thyrotropin receptors by photoaffinity labeling. Orientation of receptor subunits in the cell membrane. *Biochem. J* 227.
81. Libert, F., Lefort, A., Gerard, C., Parmentier, M., Perret, J., Ludgate, M., Dumont, J. & Vassart, G. (1989). Cloning, sequencing and expression of the human thyrotropin (TSH) receptor: evidence for binding of autoantibodies. *Biochem Biophys Res Commun.* 165, 1250-5.
82. Loosfelt, H., Pichon, C., Jolivet, A., Misrahi, M., Caillou, B., Jamous, M., Vannier, B. & Milgrom, E. (1992). Two-Subunit Structure of the Human Thyrotropin Receptor. *PNAS* 89, 3765-3769.
83. Wadsworth, H., Chazenbalk, G., Nagayama, Y., Russo, D. & Rapoport, B. (1990). An insertion in the human thyrotropin receptor critical for high affinity hormone binding. *Science*, 1423-1425.
84. Latif, R., Graves, P. & Davies, T. F. (2002). Ligand-dependent Inhibition of Oligomerization at the Human Thyrotropin Receptor. *J. Biol. Chem.* 277, 45059-45067.
85. Vassart, G., Pardo, L. & Costagliola, S. (2004). A molecular dissection of the glycoprotein hormone receptors. *Biochem. Sci* 29.
86. Refetoff, S. (2003). Resistance to thyrotropin. *J. Endocrinol. Invest.* 26, 770-779.
87. Xie, J., Pannain, S., Pohlenz, J., Weiss, R. E., Moltz, K., Morlot, M., Asteria, C., Persani, L., Beck-Peccoz, P., Parma, J., Vassart, G. & Refetoff, S. (1997). Resistance to Thyrotropin (TSH) in Three Families Is not Associated with Mutations in the TSH Receptor or TSH. *J Clin Endocrinol Metab* 82, 3933-3940.
88. Farid, N., Kascur, V. & Balazs, C. (2000). The human thyrotropin receptor is highly mutable: a review of gain-of-function mutations. *Eur J Endocrinol* 143, 25-30.
89. Fuhrer, D., Lewis, M. D., Alkhafaji, F., Starkey, K., Paschke, R., Wynford-Thomas, D., Eggo, M. & Ludgate, M. (2003). Biological Activity of Activating Thyroid-Stimulating Hormone Receptor Mutants Depends on the Cellular Context. *Endocrinology* 144, 4018-4030.
90. Adams, D. & Purves, H. (1956). Abnormal Responses in the Assay of Thyrotropin. :. *Proceedings of the University of Otago Medical School.* 34, 11.
91. Shewring, G. & Rees Smith, B. (1982). An improved radioreceptor assay for TSH receptor antibodies. *Clin Endocrinol* 17, 409-17.
92. Rose, N., Rasooly, L., Saboori, A. & Burek, C. (1999). Linking iodine with autoimmune thyroiditis. *Environ Health Perspect.* 107, 749-52.

93. Perret, J., Ludgate, M., Liebert, F., Gerad, C., Dumont, J., Vassart, G. & Parmentier, M. (1990). Stable expression of the human TSH receptor in CHO cells and characterisation of differentially expressing clones. *Biochem Biophys Res Commun* 171, 1044-1050.
94. Sanders, J., Jeffreys, J., Depraetere, H., Richards, T., Evans, M., Kiddie, A., Brereton, K., Groenen, M., Oda, Y., Furmaniak, J. & Rees Smith, B. (2002). Thyroid-Stimulating Monoclonal Antibodies. *Thyroid* 12, 1043-1050.
95. Konishi, J., Iida, Y., Kasagi, K., Ikekubo, K., Kuma, K. & Torizuka, K. (1982). Adipocyte-TSH-receptor-related antibodies in Graves' disease detected by immunoprecipitation. *Endocrinol Jpn* 29, 219-26.
96. Rosen, E. D., Walkey, C. J., Puigserver, P. & Spiegelman, B. M. (2000). Transcriptional regulation of adipogenesis. *Genes Dev.* 14, 1293-1307.
97. Deslex, S., Negrel, R., Vannier, C., Etienne, J. & Ailhaud, G. (1987). Differentiation of human adipocyte precursors in a chemically defined serum-free medium. *Int J Obes.* 11, 19-27.
98. Prins, J. & O'Rahilly, S. (1997). Regulation of adipose cell number in man. *Clin Sci (Lond).* 92, 3-11.
99. Berg, J., Tymoczko, J. & Stryer, L. (2002). *Biochemistry*, W. H. Freeman and Co., New York.
100. Considine, R. V., Sinha, M. K., Heiman, M. L., Kriauciunas, A., Stephens, T. W., Nyce, M. R., Ohannesian, J. P., Marco, C. C., McKee, L. J., Bauer, T. L. & Caro, J. F. (1996). Serum Immunoreactive-Leptin Concentrations in Normal-Weight and Obese Humans. *N Engl J Med* 334, 292-295.
101. Zhang, Y., Proenca, R., Maffei, M., Barone, M., Leopold, L. & Friedman, J. M. (1994). Positional cloning of the mouse obese gene and its human homologue. *Nature* 372, 425-432.
102. Montague, C., Farooqi, I., Whitehead, J., Soos, M., Rau, H., Wareham, N., Sewter, C., Digby, J., Mohammed, S., Hurst, J., Cheetham, C., Earley, A., Barnett, A., Prins, J. & O'Rahilly, S. (1997). Congenital leptin deficiency is associated with severe early-onset obesity in humans. *Nature* 387, 903–908.
103. Kern, P., Saghizadeh, M., Ong, J., Bosch, R., Deem, R. & Simsolo, R. (1995). The expression of tumor necrosis factor in human adipose tissue. Regulation by obesity, weight loss, and relationship to lipoprotein lipase. *J Clin Invest.* 95, 2111-9.
104. Hotamisligil, G., Shargill, N. & Spiegelman, B. (1993). Adipose expression of tumor necrosis factor-alpha: direct role in obesity-linked insulin resistance. *Science.* 259, 87-91.
105. Mohamed-Ali, V., Goodrick, S., Rawesh, A., Katz, D. R., Miles, J. M., Yudkin, J. S., Klein, S. & Coppack, S. W. (1997). Subcutaneous Adipose Tissue Releases Interleukin-6, But Not Tumor Necrosis Factor-α, in Vivo. *J Clin Endocrinol Metab* 82, 4196-4200.
106. Vozarova, B., Weyer, C., Hanson, K., Tataranni, P. A., Bogardus, C. & Pratley, R. E. (2001). Circulating Interleukin-6 in Relation to Adiposity, Insulin Action, and Insulin Secretion. *Obes Res* 9, 414-417.
107. Bastard, J.-P., Jardel, C., Bruckert, E., Blondy, P., Capeau, J., Laville, M., Vidal, H. & Hainque, B. (2000). Elevated Levels of Interleukin 6 Are Reduced in Serum and Subcutaneous Adipose Tissue of Obese Women after Weight Loss. *J Clin Endocrinol Metab* 85, 3338-3342.
108. Steppan, C. & Lazar, M. (2002). Resistin and obesity-associated insulin resistance. *Trends Endocrinol Metab.* 13, 18–23.
109. Pittas, A. G., Joseph, N. A. & Greenberg, A. S. (2004). Adipocytokines and Insulin Resistance. *J Clin Endocrinol Metab* 89, 447-452.
110. Wright, J. & Hausman, G. (1990). Monoclonal antibodies against cell surface antigens expressed during porcine adipocyte differentiation. *Int J Obes.* 14, 395-409.
111. Taylor, S. & Jones, P. (1979). Multiple new phenotypes induced in 10T1/2 and 3T3 cells treated with 5-azacytidine. *Cell.* 17, 771-9.
112. Green, H. & Kehinde, O. (1974). Sublines of mouse 3T3 cells that accumulate lipid. *Cell* 1.
113. Chen, N., Hausman, G. & Wright, J. (1996). Influence of thyroxine in vivo on preadipocyte development and insulin-like growth factor-I and IGF binding protein secretion in fetal stromal vascular cell cultures. *Obes Res.* 4, 357-66.
114. Altiok, S., Xu, M. & Spiegelman, B. M. (1997). PPARγ induces cell cycle withdrawal: inhibition of E2F/DP DNA-binding activity via down-regulation of PP2A. *Genes Dev.* 11, 1987-1998.
115. Higgins, C., Chatterjee, S. & Cherington, V. (1996). The block of adipocyte differentiation by a C-terminally truncated, but not by full-length, simian virus 40 large tumor antigen is dependent on an intact retinoblastoma susceptibility protein family binding domain. *J. Virol.* 70, 745-752.
116. Tontonoz, P., Hu, E., Devine, J., Beale, E. & Spiegelman, B. (1995). PPAR γ 2 regulates adipose expression of the phosphoenolpyruvate carboxykinase gene. *Mol. Cell. Biol.* 15, 351-357.
117. Lehmann, J. M., Moore, L. B., Smith-Oliver, T. A., Wilkison, W. O., Willson, T. M. & Kliewer, S. A. (1995). An Antidiabetic Thiazolidinedione Is a High Affinity Ligand for Peroxisome Proliferator-activated Receptor. *J. Biol. Chem.* 270, 12953-12956.

118. Kliewer, S. A., Sundseth, S. S., Jones, S. A., Brown, P. J., Wisely, G. B., Koble, C. S., Devchand, P., Wahli, W., Willson, T. M., Lenhard, J. M. & Lehmann, J. M. (1997). Fatty acids and eicosanoids regulate gene expression through direct interactions with peroxisome proliferator-activated receptors alpha and gamma. *PNAS* 94, 4318-4323.
119. Kliewer, S., Lenhard, J., Willson, T., Patel, I., Morris, D. & Lehmann, J. (1995). A prostaglandin J2 metabolite binds peroxisome proliferator-activated receptor gamma and promotes adipocyte differentiation. *Cell.* 83, 813-9.
120. Hu, E., Tontonoz, P. & Spiegelman, B. (1995). Transdifferentiation of Myoblasts by the Adipogenic Transcription Factors PPARγ and C/EBPα. *PNAS* 92, 9856-9860.
121. Yeh, W., Cao, Z., Classon, M. & McKnight, S. (1995). Cascade regulation of terminal adipocyte differentiation by three members of the C/EBP family of leucine zipper proteins. *Genes & Dev* 15, 168-181.
122. Lin, F. & Lane, M. (1992). Antisense CCAAT/enhancer-binding protein RNA suppresses coordinate gene expression and triglyceride accumulation during differentiation of 3T3- L1 preadipocytes. *Genes Dev.* 6, 533-544.
123. Lin, F. & Lane, M. (1994). CCAAT/Enhancer Binding Protein α is Sufficient to Initiate the 3T3-L1 Adipocyte Differentiation Program. *PNAS* 91, 8757-8761.
124. Yokoyama, C., Wang, X., Briggs, M., Admon, A., Wu, J., Hua, X., Goldstein, J. & Brown, M. (1993). SREBP-1, a basic-helix-loop-helix-leucine zipper protein that controls transcription of the low density lipoprotein receptor gene. *Cell* 75:, 187-197.
125. Tontonoz, P., Kim, J., Graves, R. & Spiegelman, B. (1993). ADD1: a novel helix-loop-helix transcription factor associated with adipocyte determination and differentiation. *Mol. Cell. Biol.* 13, 4753-4759.
126. Kim, J. & Spiegelman, B. (1996). ADD1/SREBP1 promotes adipocyte differentiation and gene expression linked to fatty acid metabolism. *Genes Dev.* 10, 1096-1107.
127. Kim, J. B., Wright, H. M., Wright, M. & Spiegelman, B. M. (1998). ADD1/SREBP1 activates PPARgamma through the production of endogenous ligand. *PNAS* 95, 4333-4337.
128. Tai, T.-A. C., Jennermann, C., Brown, K. K., Oliver, B. B., MacGinnitie, M. A., Wilkison, W. O., Brown, H. R., Lehmann, J. M., Kliewer, S. A., Morris, D. C. & Graves, R. A. (1996). Activation of the Nuclear Receptor Peroxisome Proliferator-activated Receptor gamma Promotes Brown Adipocyte Differentiation. *J. Biol. Chem.* 271, 29909-29914.
129. Weetman, A., McGregor, A., Ludgate, M., Beck, L., Mills, P., Lazarus, J. & Hall, R. (1983). Cyclosporin improves Graves' ophthalmopathy. *Lancet.* 2, 486-9.
130. Ho, I.-C., Kim, J. H.-J., Rooney, J. W., Spiegelman, B. M. & Glimcher, L. H. (1998). A potential role for the nuclear factor of activated T cells family of transcriptional regulatory proteins in adipogenesis. *PNAS* 95, 15537-15541.
131. Reusch, J. E. B., Colton, L. A. & Klemm, D. J. (2000). CREB Activation Induces Adipogenesis in 3T3-L1 Cells. *Mol. Cell. Biol.* 20, 1008-1020.
132. Reusch, J. E. B. & Klemm, D. J. (2002). Inhibition of cAMP-response Element-binding Protein Activity Decreases Protein Kinase B/Akt Expression in 3T3-L1 Adipocytes and Induces Apoptosis. *J. Biol. Chem.* 277, 1426-1432.
133. Leo, C. & Chen, J. (2000). The SRC family of nuclear receptor coactivators. *Gene.* 245, 1-11.
134. Yao, T.-P., Ku, G., Zhou, N., Scully, R. & Livingston, D. M. (1996). The nuclear hormone receptor coactivator SRC-1 is a specific target of p300. *PNAS* 93, 10626-10631.
135. Puigserver, P., Adelmant, G., Wu, Z., Fan, M., Xu, J., O'Malley, B. & Spiegelman, B. M. (1999). Activation of PPAR Coactivator-1 Through Transcription Factor Docking. *Science* 286, 1368-1371.
136. Ludgate, M. & Baker, G. (2001). Animal models of Graves' ophthalmopathy. In *Thyroid Eye Disease* (Bahn, R., ed.), pp. 67-81. Kluwer Academic Publishers, Boston/Dordecht/London.
137. Schockaert, J. (1932). Hyperplasia of the thyroid and exophthalmos from treatment with anterior pituitary in young duck. *Proc Soc Exp Biol Med* 29, 306-308.
138. Marine, D., Spence, A. & Cipra, A. (1932). Production of goitre and exophthalmos in rabbits by administration of cyanide. *Proc Soc Exp Biol Med* 29, 822-823.
139. Smelser, G. (1936). Experimental production of exophthalmos resembling that found in Graves' disease. *Proc Soc Exp Biol Med* 35, 128-130.
140. Paulson, D. (1937). Experimental exophthalmos in the guinea pig. *Proc Soc Exp Biol Med* 36, 604-605.
141. Dobyns, B. (1945). The influence of thyroidectomy on the prominence of the eyes in the guinea pig and man. *Surg Gynecol Obstet* 80, 526-533.
142. Winand, R. J. & Kohn, L. D. (1970). Relationships of Thyrotropin to Exophthalmic-producing Substance. PURIFICATION OF HOMOGENEOUS GLYCOPROTEINS CONTAINING BOTH ACTIVITIES FROM [3H]-LABELED PITUITARY EXTRACTS. *J. Biol. Chem.* 245, 967-975.

143. Kohn, L. D. & Winand, R. J. (1975). Structure of an exophthalmos-producing factor derived from thyrotropin by partial pepsin digestion. *J. Biol. Chem.* 250, 6503-6508.
144. Winand, R. & Kohn, L. (1973). Retrobulbar modifications in experimental exophthalmos: the effect of thyrotropin and an exophthalmos producing substance derived from thyrotropin on the SO4 incorporation and glycosaminoglycan content of Harderian glands. *Endocrinology* 93, 670-680.
145. Valk, T., Taylor, R., Jr & Barker, S. (1975). Production and measurement of exophthalmos-producing factor in guinea pigs. *Endocrinology* 96, 151-159.
146. Vladutiu, A. & Rose, N. (1971). Autoimmune murine thyroiditis relation to histocompatibility (H-2) type. *Science* 174, 1137-1139.
147. Maron, R., Zerubavel, R., Friedman, A. & Cohen, I. (1983). T lymphocyte line specific for thyroglobulin produces or vaccinates against autoimmune thyroiditis in mice. *J Immunol* 131, 2316-2322.
148. Romball, C. & Weigle, W. (1987). Transfer of experimental autoimmune thyroiditis with T cell clones. *J Immunol* 138, 1092-1098.
149. Hutchings, P., Cooke, A., Dawe, K., Champion, B., Geysen, M., Valerio, R. & Roitt, I. (1992). A thyroxine-containing peptide can induce murine experimental autoimmune thyroiditis. *J. Exp. Med.* 175, 869-872.
150. Dobyns, B., Wright, A. & Wilson, L. (1961). Assay of exophthalmic producing substance in the serum of patients with progressive ophthalmopathy. *J Clin Endocrinol Metab* 21, 648-662.
151. Endo, T., Ohmori, M., Ikeda, M. & Onaya, T. (1991). Rabbit antibodies toward extracellular loops of the membrane spanning region of human thyrotropin receptor possess thyroid stimulating activities. *Biochem Biophys Res Commun.* 181, 1035-1041.
152. Endo, T., Ohmori, M., Ikeda, M. & Onaya, T. (1991). Thyroid stimulating activity of rabbit antibodies toward the human thyrotropin receptor peptide. *Biochem Biophys Res Commun.* 177, 145-150.
153. Ohmori, M., Endo, T. & Onaya, T. (1991). Development of chicken antibodies toward the human thyrotropin receptor peptides and their bioactivities. *Biochem Biophys Res Commun.* 174, 399-403.
154. Sakata, S., Ogawa, T., Matsui, I., Manshouri, T. & Atassi, M. (1992). Biological activities of rabbit antibodies against synthetic human thyrotropin receptor peptides representing thyrotropin binding regions. *Biochem Biophys Res Commun.* 182, 1369-1975.
155. Marion, S., Braun, J. M., Ropars, A., Kohn, L. D. & Charreire, J. (1994). Induction of Autoimmunity by Immunization of Mice with Human Thyrotropin Receptor. *Cellular Immunology* 158, 329-341.
156. Costagliola, S., Alcalde, L., Ruf, J., Vassart, G. & Ludgate, M. (1994). Overexpression of the extracellular domain of the thyrotrophin receptor in bacteria; production of thyrotrophin-binding inhibiting immunoglobulins. *J Mol Endocrinol* 13, 11-21.
157. Costagliola, S., Alcalde, L., Tonacchera, M., Ruf, J., Vassart, G. & Ludgate, M. (1994). Induction of Thyrotropin Receptor (TSH-R) Autoantibodies and Thyroiditis in Mice Immunized with the Recombinant TSH-R. *Biochemical and Biophysical Research Communications* 199, 1027-1034.
158. Costagliola, S., Many, M., Stalmans-Falys, M., Tonacchera, M., Vassart, G. & Ludgate, M. (1994). Recombinant thyrotropin receptor and the induction of autoimmune thyroid disease in BALB/c mice: a new animal model. *Endocrinology* 135, 2150-2159.
159. Costagliola, S., Many, M., Stalmans-Falys, M., Vassart, G. & Ludgate, M. (1995). The autoimmune response induced by immunising female mice with recombinant human thyrotropin receptor varies with the genetic background. *Mol Cell Endocrinol* 115, 199-206.
160. Rasooly, L., Burek, C. & Rose, N. (1996). Iodine-induced autoimmune thyroiditis in NOD-H-2h4 mice. *Clin Immunol Immunopathol.* 81, 287-297.
161. Wagle, N., Dallas, J., Seetharamaiah, G., Fan, J., Desai, R., Memar, O., Rajaraman, S. & Prabhakar, B. (1994). Induction of hyperthyroxinemia in BALB/C but not in several other strains of mice. *Autoimmunity.* 18, 103-112.
162. Vlase, H., Weiss, M., Graves, P. & Davies, T. (1998). Characterization of the murine immune response to the murine TSH receptor ectodomain: induction of hypothyroidism and TSH receptor antibodies. *Clin Exp Immunol* 113, 111-118.
163. Dupuis, M., Denis-Mize, K., Woo, C., Goldbeck, C., Selby, M. J., Chen, M., Otten, G. R., Ulmer, J. B., Donnelly, J. J., Ott, G. & McDonald, D. M. (2000). Distribution of DNA Vaccines Determines Their Immunogenicity After Intramuscular Injection in Mice. *J Immunol* 165, 2850-2858.
164. Fu, T., Ulmer, J., Caulfield, M., Deck, R., Friedman, A., Wang, S., Liu, X., Donnelly, J. & Liu, M. (1997). Priming of cytotoxic T lymphocytes by DNA vaccines: requirement for professional antigen presenting cells and evidence for antigen transfer from myocytes. *Mol Med* 3, 362-371.
165. Costagliola, S., Rodien, P., Many, M.-C., Ludgate, M. & Vassart, G. (1998). Genetic Immunization Against the Human Thyrotropin Receptor Causes Thyroiditis and Allows Production of Monoclonal Antibodies Recognizing the Native Receptor. *J Immunol* 160, 1458-1465.

166. Costagliola, S., Many, M.-C., Denef, J.-F., Pohlenz, J., Refetoff, S. & Vassart, G. (2000). Genetic immunization of outbred mice with thyrotropin receptor cDNA provides a model of Graves' disease. *J. Clin. Invest.* 105, 803-811.
167. Pichurin, P., Yan, X.-M., Farilla, L., Guo, J., Chazenbalk, G. D., Rapoport, B. & McLachlan, S. M. (2001). Naked TSH Receptor DNA Vaccination: A TH1 T Cell Response in Which Interferon-{gamma} Production, Rather than Antibody, Dominates the Immune Response in Mice. *Endocrinology* 142, 3530-3536.
168. Pichurin, P., Pichurina, O., Chazenbalk, G. D., Paras, C., Chen, C.-R., Rapoport, B. & McLachlan, S. M. (2002). Immune Deviation Away from Th1 in Interferon-{gamma} Knockout Mice Does Not Enhance TSH Receptor Antibody Production after Naked DNA Vaccination. *Endocrinology* 143, 1182-1189.
169. Rao, P. V., Watson, P. F., Weetman, A. P., Carayanniotis, G. & Banga, J. P. (2003). Contrasting Activities of Thyrotropin Receptor Antibodies in Experimental Models of Graves' Disease Induced by Injection of Transfected Fibroblasts or Deoxyribonucleic Acid Vaccination. *Endocrinology* 144, 260-266.
170. Nagayama, Y., Kita-Furuyama, M., Ando, T., Nakao, K., Mizuguchi, H., Hayakawa, T., Eguchi, K. & Niwa, M. (2002). A Novel Murine Model of Graves' Hyperthyroidism with Intramuscular Injection of Adenovirus Expressing the Thyrotropin Receptor. *J Immunol* 168, 2789-2794.
171. Shimojo, N., Kohno, Y., Yamaguchi, K.-i., Kikuoka, S.-i., Hoshioka, A., Niimi, H., Hirai, A., Tamura, Y., Saito, Y., Kohn, L. D. & Tahara, K. (1996). Induction of Graves-like disease in mice by immunization with fibroblasts transfected with the thyrotropin receptor and a class II molecule. *PNAS* 93, 11074-11079.
172. Kita, M., Ahmad, L., Marians, R. C., Vlase, H., Unger, P., Graves, P. N. & Davies, T. F. (1999). Regulation and Transfer of a Murine Model of Thyrotropin Receptor Antibody Mediated Graves' Disease. *Endocrinology* 140, 1392-1398.
173. Ando, T., Imaizumi, M., Graves, P., Unger, P. & Davies, T. F. (2003). Induction of Thyroid-Stimulating Hormone Receptor Autoimmunity in Hamsters. *Endocrinology* 144, 671-680.
174. Kaithamana, S., Fan, J., Osuga, Y., Liang, S.-G. & Prabhakar, B. S. (1999). Induction of Experimental Autoimmune Graves' Disease in BALB/c Mice. *J Immunol* 163, 5157-5164.
175. Kita-Furuyama, M., Nagayama, Y., Pichurin, P., McClachlan, S., Rapoport, B. & Eguichi, K. (2003). Dendritic cells infected with adenovirus expressing the thyrotrophin receptor induce Graves' hyperthyroidism in BALB/c mice. *Clin Exp Immunol* 131, 234-240.
176. Spitzweg, C., Joba, W., Hunt, N. & Heufelder, A. (1997). Analysis of human thyrotropin receptor gene expression and immunoreactivity in human orbital tissue. *Eur J Endocrinol* 136, 599-607.
177. Starkey, K., Janezic, A., Jones, G., Jordan, N., Baker, G. & Ludgate, M. (2003). Adipose thyrotrophin receptor expression is elevated in Graves' and thyroid eye diseases ex vivo and indicates adipogenesis in progress in vivo. *J Mol Endocrinol* 30, 369-80.
178. Crisp, M., Lane, C., Halliwell, M., Wynford-Thomas, D. & Ludgate, M. (1997). Thyrotropin receptor transcripts in human adipose tissue. *J Clin Endocrinol Metab* 82, 2003-5.
179. Crisp, M., Starkey, K. J., Lane, C., Ham, J. & Ludgate, M. (2000). Adipogenesis in Thyroid Eye Disease. *Invest. Ophthalmol. Vis. Sci.* 41, 3249-3255.
180. Bahn, R. S., Dutton, C. M., Natt, N., Joba, W., Spitzweg, C. & Heufelder, A. E. (1998). Thyrotropin Receptor Expression in Graves' Orbital Adipose/Connective Tissues: Potential Autoantigen in Graves' Ophthalmopathy. *J Clin Endocrinol Metab* 83, 998-1002.
181. Valyasevi, R. W., Harteneck, D. A., Dutton, C. M. & Bahn, R. S. (2002). Stimulation of Adipogenesis, Peroxisome Proliferator-Activated Receptor-{gamma} (PPAR{gamma}), and Thyrotropin Receptor by PPAR{gamma} Agonist in Human Orbital Preadipocyte Fibroblasts. *J Clin Endocrinol Metab* 87, 2352-2358.
182. Many, M.-C., Costagliola, S., Detrait, M., Denef, J.-F., Vassart, G. & Ludgate, M. (1999). Development of an Animal Model of Autoimmune Thyroid Eye Disease. *J Immunol* 162, 4966-4974.
183. Yamada, M., Li, A., West, K., Chang, C. & Wall, J. (2002). Experimental model for ophthalmopathy in BALB/c and outbred (CD-1) mice genetically immunized with G2s and the thyrotropin receptor. *Autoimmunity.* 35, 403-413.
184. Saber, E., McDonnell, J., Zimmermann, K., Yugar, J. & Feldon, S. (1996). Extraocular muscle changes in experimental orbital venous stasis: some similarities to Graves' orbitopathy. *Graefes Arch Clin Exp Ophthalmol.* 234, 331-6.
185. Costagliola, S., Many, M., Stalmans-Falys, M., Vassart, G. & Ludgate, M. (1996). Transfer of thyroiditis, with syngeneic spleen cells sensitized with the human thyrotropin receptor, to naive BALB/c and NOD mice. *Endocrinology* 137, 4637-4643.

186. Filetti, S., Foti, D., Costante, G. & Rapoport, B. (1991). Recombinant human thyrotropin (TSH) receptor in a radioreceptor assay for the measurement of TSH receptor autoantibodies. *J Clin Endocrinol Metab* 72, 1096-1101.
187. Ludgate, M., Perret, J., Parmentier, M., Gerard, C., Libert, F., Dumont, J. E. & Vassart, G. (1990). Use of the recombinant human thyrotropin receptor (TSH-R) expressed in mammalian cell lines to assay TSH-R autoantibodies. *Molecular and Cellular Endocrinology* 73, R13-R18.
188. Evans, C., Morgenthaler, N. G., Lee, S., Llewellyn, D. H., Clifton-Bligh, R., John, R., Lazarus, J. H., Chatterjee, V. K. K. & Ludgate, M. (1999). Development of a Luminescent Bioassay for Thyroid Stimulating Antibodies. *J Clin Endocrinol Metab* 84, 374-377.
189. Pala, P., Hussell, T. & Openshaw, P. (2000). Flow cytometric measurement of intracellular cytokines. *J Immunol Methods* 243, 107-124.
190. Jordan, N. (2002). Molecular Characterisation of Thyroid Dysfunction. PhD, University of Wales College of Medicine.
191. De Winiwarter, H. (1926). Foyers thymiques chez la souris. *C.R. de la Soc.de biol.* 100, 433-35.
192. Dunn, T. B., Moloney, J. B., Green, A. W. & Arnold, B. (1961). Pathogenesis of a virus induced leukaemia in mice. *J Natl Cancer Institute* 26, 189-221.
193. Manley, N. & Capecchi, M. (1995). The role of Hoxa-3 in mouse thymus and thyroid development. *Development* 121, 1989-2003.
194. Costagliola, S., Franssen, J. D. F., Bonomi, M., Urizar, E., Willnich, M., Bergmann, A. & Vassart, G. (2002). Generation of a mouse monoclonal TSH receptor antibody with stimulating activity. *Biochemical and Biophysical Research Communications* 299, 891-896.
195. Ruwhof, C. & Drexhage, H. (2001). Iodine and thyroid autoimmune disease in animal models. *Thyroid* 11, 427-436.
196. Allen, E., Appel, M. & Braverman, L. (1986). The effect of iodide ingestion on the development of spontaneous lymphocytic thyroiditis in the diabetes-prone BB/W rat. *Endocrinology.* 118, 1977-1981.
197. Voorby, H., Kabel, P., de Haan, M., Jeucken, P., van der Gaag, R., de Baets, M. & Drexhage, H. (1990). Dendritic cells and class II MHC expression on thyrocytes during the autoimmune thyroid disease of the BB rat. *Clin Immunol Immunopathol.* 55, 9-22.
198. Mooij, P., de Wit, H. & Drexhage, H. (1993). An excess of dietary iodine accelerates the development of a thyroid-associated lymphoid tissue in autoimmune prone BB rats. *Clin Immunol Immunopathol.* 69, 189-198.
199. Mooij, P., de Wit, H. & Drexhage, H. (1994). A high iodine intake in Wistar rats results in the development of a thyroid-associated ectopic thymic tissue and is accompanied by a low thyroid autoimmune reactivity. *Immunology* 81, 309-16.
200. Symes, M., Riddell, A. & Hill, R. (1968). A human spleen cell bank. *Lancet* 1, 1052-1053.
201. Schmidt-Wolf, I., Aihara, M., Negrin, R., Blume, K. & Chao, N. (1992). In vitro and in vivo activity of murine lymphokine-activated killer cells after cryopreservation. *Transfusion* 32, 42-45.
202. Wells, M., Ennis, F. & Albrecht, P. (1981). Recovery from a viral respiratory infection. II. Passive transfer of immune spleen cells to mice with influenza pneumonia. *J Immunol* 126, 1042-1046.
203. Many, M., Drexhage, H. & Denef, J. (1993). High frequency of thymic ectopy in thyroids from autoimmune prone nonobese diabetic female mice. *Lab Invest* 69, 364-367.
204. Vladutiu, A. & Rose, N. (1972). Aberrant thymus tissue in rat and mouse thyroid. *Experientia* 28, 79-81.
205. Wu, S., Gupta, D. & Connelly, J. (2001). Adult ectopic thymus adjacent to thyroid and parathyroid. *Arch Pathol Lab Med* 125, 842-3.
206. Skelton-Stroud, P. & Ishmael, J. (1986). Naturally occurring lesions in some endocrine glands of laboratory maintained baboons. *Vet Pathol* 23, 380-5.
207. Smith, C. & Clifford, C. (1962). Histochemical study of aberrant parathyroid glands associated with the thymus of the mouse. *Anat Rec* 143, 220-38.
208. Stewart, F. (1918). On the (so-called) thymus IV and the ultimobranchial body of the cat (felis domestica). *Am J Anat.* 24, 191-223.
209. Hilfer, S. & Brown, J. (1984). The development of pharygeal endocrine organs in mouse and chick embryos. *Scan Electron Microsc* 4, 2009-22.
210. Cordier, A. & Haumont, S. (1980). Development of thymus, parathyroids, and ultimo-branchial bodies in NMRI and nude mice. *Am J Anat.* 157, 227-63.
211. Bleul, C. & Boehm, T. (2000). Chemokines define distinct microenvironments in the developing thymus. *European Journal of Immunology* 30, 3371-3379.
212. Vermot, J., Niederreither, K., Garnier, J.-M., Chambon, P. & Dolle, P. (2003). Decreased embryonic retinoic acid synthesis results in a DiGeorge syndrome phenotype in newborn mice. *PNAS* 100, 1763-1768.

213. Xu, P.-X., Zheng, W., Laclef, C., Maire, P., Maas, R. L., Peters, H. & Xu, X. (2002). Eya1 is required for the morphogenesis of mammalian thymus, parathyroid and thyroid. *Development* 129, 3033-3044.
214. Gordona, J., Bennetta, A., Blackburn, C. & Manley, N. (2001). Gcm2 and Foxn1 mark early parathyroid- and thymus-specific domains in the developing third pharyngeal pouch. *Mechanisms of Development* 103, 141-143.
215. Su, D.-m. & Manley, N. R. (2000). Hoxa3 and Pax1 Transcription Factors Regulate the Ability of Fetal Thymic Epithelial Cells to Promote Thymocyte Development. *J Immunol* 164, 5753-5760.
216. Hetzer-Egger, C., Schorpp, M., Haas-Assenbaum, A., Balling, R., Peters, H. & Boehm, T. (2002). Thymopoiesis requires Pax9 function in thymic epithelial cells. *Eur J Immunol* 32, 1175-1181.
217. Gregoire, C. (1942). Recherches sur les facteurs de l'hyperplasie du thymus et du tissu lymphoide dans la maladie de Basedow. *Arch Internat Pharmacodynam Therapie* 68, 263.
218. Scheiff, J., Cordier, A. & Haumont, S. (1977). Epithelial cell proliferation in thymic hyperplasia induced by triiodothyronine. *Clin Exp Immunol* 27, 516-521.
219. Panda, D. K., Miao, D., Tremblay, M. L., Sirois, J., Farookhi, R., Hendy, G. N. & Goltzman, D. (2001). Targeted ablation of the 25-hydroxyvitamin D 1alpha -hydroxylase enzyme: Evidence for skeletal, reproductive, and immune dysfunction. *PNAS* 98, 7498-7503.
220. Matti, H. (1912). Uber die kombination von morbus Basedowii mit thymushyperplasie. *Cor Bl Schweiz Aerzte* 42, 1345-47.
221. Halsted, W. (1915). Significance of the thymus gland in Graves' disease. *Bull Johns Hopkins Hosp* 25, 223-234.
222. Van Herle, A. & Chopra, I. (1971). Thymic hyperplasia in Graves' disease. *J Clin Endocrinol Metab.* 32, 140-146.
223. Gunn, A., Michie, W. & Irvine, W. (1964). The thymus in thyroid disease. *Lancet* ii, 776-777.
224. Michie, W., Swanson Beck, J., Mahaffy, R., Honein, E. & Fowler, G. (1967). Quantitative radiological and histological studies of the thymus in thyroid disease. *Lancet* i, 691-695.
225. Vincent, A. (2002). Unravelling the pathogenesis of myasthenia gravis. *Nat Rev Immunol* 2, 797-804.
226. Gronseth, G. S. & Barohn, R. J. (2000). Practice parameter: Thymectomy for autoimmune myasthenia gravis (an evidence-based review): Report of the Quality Standards Subcommittee of the American Academy of Neurology. *Neurology* 55, 7-15.
227. Chu, W. & Metreweli, C. (2002). Ectopic thymic tissue in the paediatric age group. *Acta Radiologica* 43, 144-146.
228. Murakami, M., Hosoi, Y., Negishi, T., Kamiya, Y., Miyashita, K., Yamada, M., Iriuchijima, T., Yokoo, H., Yoshida, I., Tsushima, Y. & Mori, M. (1996). Thymic Hyperplasia in Patients with Graves' Disease . Identification of Thyrotropin Receptors in Human Thymus. *J. Clin. Invest.* 98, 2228-2234.
229. Wortsman, J., McConnachie, P., Baker, J. & Burman, K. (1988). Immunoglobulins that cause a thymocyte proliferation from a patient with Graves' disease and an enlarged thymus. *Am J Med* 85, 117-121.
230. Farr, A. G., Dooley, J. L. & Erickson, M. (2002). Organization of thymic medullary epithelial heterogeneity: implications for mechanisms of epithelial differentiation. *Immunological Reviews* 189, 20-27.
231. Volpe, R. (2001). The immunomodulatory effects of anti-thyroid drugs are mediated via actions on thyroid cells, affecting thyrocyte-immunocyte signalling: a review. *Curr Pharm Des* 7, 451-460.
232. Caturegli, P., Rose, N., Kimura, M., Kimura, H. & Tzou, S. (2003). Studies on murine thyroiditis: new insights from organ flow cytometry. *Thyroid* 13, 419-26.
233. Farr, A. G. & Rudensky, A. (1998). Medullary Thymic Epithelium: A Mosaic of Epithelial "Self"? *J. Exp. Med.* 188, 1-4.
234. Wild, P. & Setoguti, T. (1995). Mammalian parathyroids: morphological and functional implications. *Microsc Res Tech* 32, 120-8.
235. Porter, J., Baker, R., Ragusa, R. & Brueckner, J. (1995). Extraocular muscles: basic and clinical aspects of structure and function. *Surv Ophthalmol* 39, 451-484.
236. Briggs, M. M. & Schachat, F. (2002). The superfast extraocular myosin (MYH13) is localized to the innervation zone in both the global and orbital layers of rabbit extraocular muscle. *J Exp Biol* 205, 3133-3142.
237. Muhlendyck, H. & Syed, A. (1978). Fixation artifacts in the external eye muscles in biopsy examinations. (A light microscopy and electron microscopy study). *Buch Augenarzt.* 73, 181-191.
238. Simons, P. J., Delemarre, F. G. A. & Drexhage, H. A. (1998). Antigen-Presenting Dendritic Cells as Regulators of the Growth of Thyrocytes: A Role of Interleukin-1{beta} and Interleukin-6. *Endocrinology* 139, 3148-3156.

239. Bagriacik, E. U. & Klein, J. R. (2000). The Thyrotropin (Thyroid-Stimulating Hormone) Receptor Is Expressed on Murine Dendritic Cells and on a Subset of CD45RBhigh Lymph Node T Cells: Functional Role for Thyroid-Stimulating Hormone During Immune Activation. *J Immunol* 164, 6158-6165.
240. Hou, W., Wu, Y., Sun, S., Shi, M., Sun, Y., Yang, C., Pei, G., Gu, Y., Zhong, C. & Sun, B. (2003). Pertussis Toxin Enhances Th1 Responses by Stimulation of Dendritic Cells *J Immunol* 170, 1728-1736.
241. Ulmer, J., Donnelly, J., Parker, S., Rhodes, G., Felgner, P., Dwarki, V., Gromkowski, S., Deck, R., DeWitt, C. & Friedman, A. (1993). Heterologous protection against influenza by injection of DNA encoding a viral protein. *Science* 259, 1745-1749.
242. Ulmer, J., DeWitt, C., Chastain, M., Friedman, A., Donnelly, J., McClements, W., Caulfield, M., Bohannon, K., Volkin, D. & Evans, R. (1999). Enhancement of DNA vaccine potency using conventional aluminum adjuvants. *Vaccine* 18, 18-28.
243. Chattergoon, M. A., Kim, J. J., Yang, J.-S., Robinson, T. M., Lee, D. J., Dentchev, T., Wilson, D. M., Ayyavoo, V. & Weiner, D. (2000). Targeted antigen delivery to antigen–presenting cells including dendritic cells by engineered Fas-mediated apoptosis. *Nat Biotechnol* 18, 974-979.
244. Sasaki, S., Amara, R., Oran, A., Smith, J. & Robinson, H. (2001). Apoptosis-mediated enhancement of DNA-raised immune responses by mutant caspases. *Nat Biotechnol* 19, 543-7.
245. Sasaki, S., Xin, K., Okudela, K., Okuda, K. & Ishii, N. (2002). Immunomodulation by apoptosis-inducing caspases for an influenza DNA vaccine delivered by gene gun. *Gene Ther* 9, 828-31.
246. White, J. & Engel, F. (1958). Lipolytic action of corticotropin on rat adipose tissue in vitro. *J Clin Invest* 37, 1556-63.
247. Freinkel, N. (1961). Extrathyroidal actions of pituitary thyrotropin: effects on the carbohydrate lipid and respiratory metabolism of rat adipose tissue. *J. Clin. Invest.* 40, 476-89.
248. Rodbell, M. (1964). Metabolism of isolated fat cells. I. Effects of hormones on glucose metabolism and lipolysis. *J Biol Chem* 239, 375-80.
249. Kendall-Taylor, P. & Munro, D. (1971). The lipolytic activity of long-acting thyroid stimulator. *Biochim Biophys Acta* 231, 314-9.
250. Hart, I. & McKenzie, J. (1971). Comparison of the effects of thyrotropin and the long-acting thyroid stimulator on guinea pig adipose tissue. *Endocrinology* 88, 26-30.
251. Winand, R. J. & Kohn, L. D. (1975). Stimulation of adenylate cyclase activity in retro-orbital tissue membranes by thyrotropin and an exophthalmogenic factor derived from thyrotropin. *J. Biol. Chem.* 250, 6522-6526.
252. Mullin BR, L. G., Ledley FD, Winand RJ, Kohn LD. (1976). Thyrotropin interactions with human fat cell membrane preparations and the finding of soluble thyrotropin binding component. *Biochem Biophys Res Commun* 69, 55-62.
253. Davies, T., Teng, C., McLachlan, S., Smith, B. & Hall, R. (1978). Thyrotropin receptors in adipose tissue, retro-orbital tissue and lymphocytes. *Mol Cell Endocrinol* 9, 303-10.
254. Marcus, C., Ehren, H., Bolme, P. & Arner, P. (1988). Regulation of lipolysis during the neonatal period. Importance of thyrotropin. *J Clin Invest* 82, 1793-7.
255. Janson, A., Karlsson, F., Micha-Johansson, G., Bolme, P., Bronnegard, M. & Marcus, C. (1995). Effects of stimulatory and inhibitory thyrotropin receptor antibodies on lipolysis in infant adipocytes. *J Clin Endocrinol Metab* 80, 1712-1716.
256. Hellstrom, L., Wahrenberg, H., Reynisdottir, S. & Arner, P. (1997). Catecholamine-Induced Adipocyte Lipolysis in Human Hyperthyroidism. *J Clin Endocrinol Metab* 82, 159-166.
257. Nagayama Y, K. K., Seto P, Rapoport B. (1989). Molecular cloning, sequence and functional expression of the cDNA for the human thyrotropin receptor. *Biochem Biophys Res Commun.* 165, 1184-90.
258. Feliciello, A., Porcellini, A., Ciullo, I., Bonavolonta, G., Avvedimento, E. & Fenzi, G. (1993). Expression of thyrotropin-receptor mRNA in healthy and Graves' disease retro-orbital tissue. *Lancet* 342, 337-8.
259. Paschke, R., Metcalfe, A., Alcalde, L., Vassart, G., Weetman, A. & Ludgate, M. (1994). Presence of nonfunctional thyrotropin receptor variant transcripts in retroocular and other tissues. *J Clin Endocrinol Metab* 79, 1234-1238.
260. Mengistu, M., Lukes, Y., Nagy, E., Burch, H., Carr, F., Lahiri, S. & Burman, K. (1994). TSH receptor gene expression in retroocular fibroblasts. *J Endocrinol Invest.* 17, 437-41.
261. Heufelder, A., Dutton, C., Sarkar, G., Donovan, K. & Bahn, R. (1993). Detection of TSH receptor RNA in cultured fibroblasts from patients with Graves' ophthalmopathy and pretibial dermopathy. *Thyroid.* 3, 297-300.
262. Chelly, J., Concordet, J., Kaplan, J. & Kahn, A. (1989). Illegitimate transcription: transcription of any gene in any cell type. *Proc Natl Acad Sci U S A.* 86, 2617-21.

263. Wu, S., Yang, C., Wang, H., Liao, C., Chang, T. & Chang, T. (1999). Demonstration of thyrotropin receptor mRNA in orbital fat and eye muscle tissues from patients with Graves' ophthalmopathy by in situ hybridization. *J Endocrinol Invest.* 22, 289-95.
264. Haraguchi, K., Shimura, H., Lin, L., Saito, T., Endo, T. & Onaya, T. (1996). Functional Expression of Thyrotropin Receptor in Differentiated 3T3-L1 Cells: A Possible Model Cell Line of Extrathyroidal Expression of Thyrotropin Receptor. *Biochemical and Biophysical Research Communications* 223, 193-198.
265. Haraguchi, K., Shimura, H., Lin, L., Endo, T. & Onaya, T. (1996). Differentiation of rat preadipocytes is accompanied by expression of thyrotropin receptors. *Endocrinology* 137, 3200-3205.
266. Valyasevi, R. W., Erickson, D. Z., Harteneck, D. A., Dutton, C. M., Heufelder, A. E., Jyonouchi, S. C. & Bahn, R. S. (1999). Differentiation of Human Orbital Preadipocyte Fibroblasts Induces Expression of Functional Thyrotropin Receptor. *J Clin Endocrinol Metab* 84, 2557-2562.
267. Endo, T., Ohta, K., Haraguchi, K. & Onaya, T. (1995). Cloning and Functional Expression of a Thyrotropin Receptor cDNA from Rat Fat Cells. *J. Biol. Chem.* 270, 10833-10837.
268. Shimura, H., Haraguchi, K., Endo, T. & Onaya, T. (1997). Regulation of Thyrotropin Receptor Gene Expression in 3T3-L1 Adipose Cells is Distinct from Its Regulation in FRTL-5 Thyroid Cells. *Endocrinology* 138, 1483-1490.
269. Shimura, H., Miyazaki, A., Haraguchi, K., Endo, T. & Onaya, T. (1998). Analysis of Differentiation-Induced Expression Mechanisms of Thyrotropin Receptor Gene in Adipocytes. *Mol Endocrinol* 12, 1473-1486.
270. Haraguchi, K., Shimura, H., Ikeda, M., Endo, T. & Onaya, T. (1998). Effects of cytokines on expression of thyrotropin receptor mRNA in rat preadipocytes. *Thyroid* 8, 687-692.
271. Haraguchi, K., Shimura, H., Kawaguchi, A., Ikeda, M., Endo, T. & Onaya, T. (1999). Effects of thyrotropin on the proliferation and differentiation of cultured rat preadipocytes. *Thyroid.* 9, 613-9.
272. Bell, A., Gagnon, A., Dods, P., Papineau, D., Tiberi, M. & Sorisky, A. (2002). TSH signaling and cell survival in 3T3-L1 preadipocytes. *Am J Physiol Cell Physiol* 283, C1056-1064.
273. Bell, A., Gagnon, A., Grunder, L., Parikh, S. J., Smith, T. J. & Sorisky, A. (2000). Functional TSH receptor in human abdominal preadipocytes and orbital fibroblasts. *Am J Physiol Cell Physiol* 279, C335-340.
274. Yang, V. W., Christy, R. J., Cook, J. S., Kelly, T. J. & Lane, M. D. (1989). Mechanism of Regulation of the 422(aP2) Gene by cAMP during Preadipocyte Differentiation. *PNAS* 86, 3629-3633.
275. Antras, J., Lasnier, F. & Pairault, J. (1991). Beta-adrenergic-cyclic AMP signalling pathway modulates cell function at the transcriptional level in 3T3-F442A adipocytes. *Mol Cell Endocrinol* 82, 183-90.
276. Bahn, R., Gorman, C., Woloschak, G., David, C., Johnson, P. & Johnson, C. (1987). Human retroocular fibroblasts in vitro: a model for the study of Graves' ophthalmopathy. *J Clin Endocrinol Metab* 65, 665-670.
277. Diascro, D., Vogel, R., Johnson, T., Witherup, K., Pitzenberger, S., Rutledge, S., Prescott, D., Rodan, G. & Schmidt, A. (1998). High fatty acid content in rabbit serum is responsible for the differentiation of osteoblasts into adipocyte-like cells. *J Bone Miner Res* 13, 96-106.
278. Ogston, N., Harrison, A., Cheung, H., Ashton, B. & Hampson, G. (2002). Dexamethasone and retinoic acid differentially regulate growth and differentiation in an immortalised human clonal bone marrow stromal cell line with osteoblastic characteristics. *Steroids* 67, 895-906.
279. De Roux, N., Polak, M., Couet, J., Leger, J., Czernichow, P., Milgrom, E. & Misrahi, M. (1996). A neomutation of the thyroid-stimulating hormone receptor in a severe neonatal hyperthyroidism. *J Clin Endocrinol Metab* 81, 2023-2026.
280. Fuhrer, D., Wonerow, P., Willgerodt, H. & Paschke, R. (1997). Identification of a New Thyrotropin Receptor Germline Mutation (Leu629Phe) in a Family with Neonatal Onset of Autosomal Dominant Nonautoimmune Hyperthyroidism. *J Clin Endocrinol Metab* 82, 4234-4238.
281. Fuhrer, D., Holzapfel, H.-P., Wonerow, P., Scherbaum, W. A. & Paschke, R. (1997). Somatic Mutations in the Thyrotropin Receptor Gene and Not in the Gs{alpha} Protein Gene in 31 Toxic Thyroid Nodules. *J Clin Endocrinol Metab* 82, 3885-3891.
282. Duprez, L., Parma, J., Van Sande, J., Allgeier, A., Leclere, J., Schvartz, C., Delisle, M., Decoulx, M., Orgiazzi, J. & Dumont, J. (1994). Germline mutations in the thyrotropin receptor gene cause non-autoimmune autosomal dominant hyperthyroidism. *Nat Genet.* 7, 396-401.
283. Pear, W., Nolan, G., Scott, M. & Baltimore, D. (1993). Production of High-Titer Helper-Free Retroviruses by Transient Transfection. *PNAS* 90, 8392-8396.
284. Green, H. & Kehinde, O. (1975). An established preadipose cell line and its differentiation in culture. II. Factors affecting the adipose conversion. *Cell.* 5, 19-27.

285. Ashworth, R., Ham, J. & Cockle, S. (1994). The effects of pyroglutamylglutamylprolineamide, a peptide related to thyrotrophin-releasing hormone, on rat anterior pituitary cells in culture. *J Endocrinol.* 142, 111-8.
286. Smith, T. J., Koumas, L., Gagnon, A., Bell, A., Sempowski, G. D., Phipps, R. P. & Sorisky, A. (2002). Orbital Fibroblast Heterogeneity May Determine the Clinical Presentation of Thyroid-Associated Ophthalmopathy. *J Clin Endocrinol Metab* 87, 385-392.
287. Gesta, S., Lolmede, K., Daviaud, D., Berlan, M., Bouloumie, A., Lafontan, M., Valet, P. & Saulnier-Blache, J. (2003). Culture of human adipose tissue explants leads to profound alteration of adipocyte gene expression. *Horm Metab Res.* 35, 158-63.
288. Aubert, J., Saint-Marc, P., Belmonte, N., Dani, C., Negrel, R. & Ailhaud, G. (2000). Prostacyclin IP receptor up-regulates the early expression of C/EBPbeta and C/EBPdelta in preadipose cells. *Mol Cell Endocrinol* 160, 149-56.
289. Aubert, J., Dessolin, S., Belmonte, N., Li, M., McKenzie, F. R., Staccini, L., Villageois, P., Barhanin, B., Vernallis, A., Smith, A. G., Ailhaud, G. & Dani, C. (1999). Leukemia Inhibitory Factor and Its Receptor Promote Adipocyte Differentiation via the Mitogen-activated Protein Kinase Cascade. *J. Biol. Chem.* 274, 24965-24972.
290. Belmonte, N., Phillips, B. W., Massiera, F., Villageois, P., Wdziekonski, B., Saint-Marc, P., Nichols, J., Aubert, J., Saeki, K., Yuo, A., Narumiya, S., Ailhaud, G. & Dani, C. (2001). Activation of Extracellular Signal-Regulated Kinases and CREB/ATF-1 Mediate the Expression of CCAAT/Enhancer Binding Proteins β and δ in Preadipocytes. *Mol Endocrinol* 15, 2037-2049.
291. Chen, J. & Iyengar, R. (1994). Suppression of Ras-induced transformation of NIH 3T3 cells by activated G alpha s. *Science* 263, 1278-81.
292. Houslay, M. D. & Kolch, W. (2000). Cell-Type Specific Integration of Cross-Talk between Extracellular Signal-Regulated Kinase and cAMP Signaling. *Mol Pharmacol* 58, 659-668.
293. Dhillon, A. S., Pollock, C., Steen, H., Shaw, P. E., Mischak, H. & Kolch, W. (2002). Cyclic AMP-Dependent Kinase Regulates Raf-1 Kinase Mainly by Phosphorylation of Serine 259. *Mol. Cell. Biol.* 22, 3237-3246.
294. Inoue, M., Tawata, M., Yokomori, N., Endo, T. & Onaya, T. (1998). Expression of thyrotropin receptor on clonal osteoblast-like rat osteosarcoma cells. *Thyroid* 8, 1059-64.
295. Parma, J., Van Sande, J., Swillens, S., Tonacchera, M., Dumont, J. & Vassart, G. (1995). Somatic mutations causing constitutive activity of the thyrotropin receptor are the major cause of hyperfunctioning thyroid adenomas: identification of additional mutations activating both the cyclic adenosine 3',5'-monophosphate and inositol phosphate-Ca2+ cascades. *Mol Endocrinol* 9, 725-733.
296. Jelsema, C. & Axelrod, J. (1987). Stimulation of phospholipase A2 activity in bovine rod outer segmentsby the βγ subunits of transducin and its inhibition by the α subunit. *PNAS* 84, 3623-3627.
297. Russell, T. & Ho, R. (1976). Conversion of 3T3 fibroblasts into adipose cells: triggering of differentiation by prostaglandin F2alpha and 1-methyl-3-isobutyl xanthine. *Proc Natl Acad Sci U S A.* 73, 4516-20.
298. Bennett, C. N., Ross, S. E., Longo, K. A., Bajnok, L., Hemati, N., Johnson, K. W., Harrison, S. D. & MacDougald, O. A. (2002). Regulation of Wnt Signaling during Adipogenesis. *J. Biol. Chem.* 277, 30998-31004.
299. Puigserver, P. & Spiegelman, B. M. (2003). Peroxisome Proliferator-Activated Receptor-γ Coactivator 1α (PGC-1α): Transcriptional Coactivator and Metabolic Regulator. *Endocr Rev* 24, 78-90.
300. Corbin, J. D., Reimann, E. M., Walsh, D. A. & Krebs, E. G. (1970). Activation of Adipose Tissue Lipase by Skeletal Muscle Cyclic Adenosine 3',5'-Monophosphate-stimulated Protein Kinase. *J. Biol. Chem.* 245, 4849-4850.
301. Brasaemle, D. L., Levin, D. M., Adler-Wailes, D. C. & Londos, C. (2000). The lipolytic stimulation of 3T3-L1 adipocytes promotes the translocation of hormone-sensitive lipase to the surfaces of lipid storage droplets. *Biochimica et Biophysica Acta (BBA) - Molecular and Cell Biology of Lipids* 1483, 251-262.
302. Spiegelman, B. & Green, H. (1981). Cyclic AMP-mediated control of lipogenic enzyme synthesis during adipose differentiation of 3T3 cells. *Cell* 24, 503-10.
303. Sequeira, M., Jasani, B., Fuhrer, D., Wheeler, M. & Ludgate, M. (2002). Demonstration of reduced in vivo surface expression of activating mutant thyrotrophin receptors in thyroid sections. *Eur J Endocrinol.* 146, 163-71.
304. Lalli, E. & Sassone-Corsi, P. (1995). Thyroid-Stimulating Hormone (TSH)-Directed Induction of the CREM Gene in the Thyroid Gland Participates in the Long-Term Desensitization of the TSH Receptor. *PNAS* 92, 9633-9637.
305. Prummel, M. & Wiersinga, W. (1993). Smoking and risk of Graves' disease. *JAMA.* 269, 479-82.
306. Hagg, E. & Asplund, K. (1987). Is endocrine ophthalmopathy related to smoking? *Br Med J* 295, 634-5.

307. Pfeilschifter, J. & Ziegler, R. (1996). Smoking and endocrine ophthalmopathy: impact of smoking severity and current vs lifetime cigarette consumption. *Clin Endocrinol* 45, 477-81.
308. Metcalfe, R. & Weetman, A. (1994). Stimulation of extraocular muscle fibroblasts by cytokines and hypoxia: possible role in thyroid-associated ophthalmopathy. *Clin Endocrinol (Oxf).* 40, 67-72.
309. Prummel, M., Van Pareren, Y., Bakker, O. & Wiersinga, W. (1997). Anti-heat shock protein (hsp)72 antibodies are present in patients with Graves' disease (GD) and in smoking control subjects. *Clin Exp Immunol.* 110, 292-5.
310. Mack, W., Stasior, G., Cao, H., Stasior, O. & Smith, T. (1999). The effect of cigarette smoke constituents on the expression of HLA-DR in orbital fibroblasts derived from patients with Graves ophthalmopathy. *Ophthal Plast Reconstr Surg.* 15, 260-71.
311. Smyth, L., Machado, D., Upton, A., Good, S., Aufderheide, M. & Helm, B. (2000). Assessment of the Molecular Basis of the Proallergenic Effects of Cigarette Smoke. *Environ Sci Technol.* 34, 1370-74.
312. Hufnagel, T., Hickey, W., Cobbs, W., Jakobiec, F., Iwamoto, T. & Eagle, R. (1984). Immunohistochemical and ultrastructural studies on the exenterated orbital tissues of a patient with Graves' disease. *Ophthalmology.* 91, 1411-9.
313. Eckstein, A., Quadbeck, B., Mueller, G., Rettenmeier, A. W., Hoermann, R., Mann, K., Steuhl, P. & Esser, J. (2003). Impact of smoking on the response to treatment of thyroid associated ophthalmopathy. *Br J Ophthalmol* 87, 773-776.
314. Khurana, A., Sunder, S., Ahluwalia, B. & Malhotra, K. (1992). Tear film profile in Graves' ophthalmopathy. *Acta Ophthalmol (Copenh).* 70, 346-9.
315. Gilbard, J & Farris, R. (1983). Ocular surface drying and tear film osmolarity in thyroid eye disease. *Acta Ophthalmol (Copenh).* 61, 108-16.
316. Cher, I. (2003). Blink-related microtrauma: when the ocular surface harms itself. *Clin Exp Ophthalmol* 31, 183-190.
317. Eckstein, A., Finkenrath, A., Heiligenhaus, A., Renzing-Kohler, K., Esser, J., Kruger, C., Quadbeck, B., Steuhl, K. & Gieseler, R. (2004). Dry eye syndrome in thyroid-associated ophthalmopathy: lacrimal expression of TSH receptor suggests involvement of TSHR-specific autoantibodies. *Acta Ophthalmol Scand* 82, 291-7.
318. Reese, A. (1935). Dacryadenitis in hyperthyroidism. *Arch Ophthalmol* 8, 855-7.
319. Trokel, S. & Jakobiec, F. (1981). Correlation of CT scanning and pathologic features of ophthalmic Graves' disease. *Ophthalmology.* 88, 553-64.
320. Allard, J., Lee, V. & Franklin, P. (1988). Thyroid uptake of gallium in Graves' disease. *Clin Nucl Med.* 13, 663-6.
321. Moncayo, R., Baldissera, I., Decristoforo, C., Kendler, D. & Donnemiller, E. (1997). Evaluation of immunological mechanisms mediating thyroid-associated ophthalmopathy by radionuclide imaging using the somatostatin analog 111In-octreotide. *Thyroid.* 7, 21-9.
322. Berta, A., Kalman, K., Patvaros, I. & Kelenhegy, C. (1986). Changes in tear protein composition in Graves' ophthalmopathy. *Orbit* 5, 97.
323. Khalil, H., De Keizer, R. & Kijlstra, A. (1988). Analysis of tear proteins in Graves' ophthalmopathy by high performance liquid chromatography. *Am J Ophthalmol.* 106, 186-90.
324. Weetman, A. (1987). IgA class and subclass thyroid auto-antibodies in Graves' disease and Hashimoto's thyroiditis. *Int Arch Allergy Appl Immunol.* 83, 432-5.
325. Rosen, C., Raikow, R., Burde, R., Kennerdell, J., Mosseri, M. & Scalise, D. (1992). Immunohistochemical evidence for IgA1 involvement in Graves ophthalmopathy. *Ophthalmology.* 99, 146-52.
326. Khalil, H., De Keizer, R., Bodelier, V. & Kijlstra, A. (1989). Secretory IgA and lysozyme in tears of patients with Graves' ophthalmopathy. *Doc Ophthalmol.* 72, 329-34.
327. Molloy, M., Bolis, S., Herbert, B., Ou, K., Tyler, M., van Dyk, D., Willcox, M., Gooley, A., Williams, K., Morris, C. & Walsh, B. (1997). Establishment of the human reflex tear two-dimensional polyacrylamide gel electrophoresis reference map: new proteins of potential diagnostic value. *Electrophoresis.* 18, 2811-5.
328. Bakheet, S., Hammami, M., Hemidan, A., Powe, J. & Bajaafar, F. (1998). Radioiodine secretion in tears. *J Nucl Med.* 39, 1452-4.
329. Solans, R., Bosch, J.-A., Galofre, P., Porta, F., Rosello, J., Selva-O'Callagan, A. & Vilardell, M. (2001). Salivary and Lacrimal Gland Dysfunction (Sicca Syndrome) After Radioiodine Therapy. *J Nucl Med* 42, 738-743.
330. Kloos, R. T., Duvuuri, V., Jhiang, S. M., Cahill, K. V., Foster, J. A. & Burns, J. A. (2002). Nasolacrimal Drainage System Obstruction from Radioactive Iodine Therapy for Thyroid Carcinoma. *J Clin Endocrinol Metab* 87, 5817-5820.
331. Tumilasci, O., Arqueros, M., Ostuni, M., El Tamer, E. & Houssay, A. (1996). Thyrotropin receptor antibodies in parotid saliva. *J Endocrinol Invest.* 19, 412-4.

332. Rapoport, B. (1976). Dog thyroid cells in monolayer tissue culture: adenosine 3',5'-cyclic monophosphate response to thyrotropic hormone. *Endocrinology* 98, 1189-97.
333. Kasagi, K., Konishi, J., Iida, Y., Ikekubo, K., Mori, T., Kuma, K. & Torizuka, K. (1982). A new in vitro assay for human thyroid stimulator using cultured thyroid cells: effect of sodium chloride on adenosine 3',5'-monophosphate release. *J Clin Endocrinol Metab* 54, 108-14.
334. Van Sande, J., Massart, C., Costagliola, S., Allgeier, A., Cetani, F., Vassart, G. & Dumont, J. (1996). Specific activation of the thyrotropin receptor by trypsin. *Mol Cell Endocrinol.* 119, 161-8.
335. Zhou, L., Beuerman, R., Barathi, A. & D., T. (2003). Analysis of rabbit tear proteins by high-pressure liquid chromatography/electrospray ionization mass spectrometry. *Rapid Commun Mass Spectrom* 17, 401-12.
336. Ng, V., Cho, P., Mak, S. & Lee, A. (2000). Variability of tear protein levels in normal young adults: between-day variation. *Graefes Arch Clin Exp Ophthalmol.* 238, 892-9.
337. Ohashi, Y., Ishida, R., Kojima, T., Goto, E., Matsumoto, Y., Watanabe, K., Ishida, N., Nakata, K., Takeuchi, T. & Tsubota, K. (2003). Abnormal protein profiles in tears with dry eye syndrome. *Am J Ophthalmol.* 136, 291-9.
338. Levay, P. & Viljoen, M. (1995). Lactoferrin: a general review. *Haematologica* 80, 252-67.
339. Mann, D., Romm, E. & Migliorini, M. (1994). Delineation of the glycosaminoglycan-binding site in the human inflammatory response protein lactoferrin. *J. Biol. Chem.* 269, 23661-23667.
340. Massucci, M., Giansanti, F., Di Nino, G., Turacchio, M., Giardi, M., Botti, D., Ippoliti, R., De Giulio, B., Siciliano, R., Donnarumma, G., Valenti, P., Bocedi, A., Polticelli, F., Ascenzi, P. & Antonini, G. (2004). Proteolytic activity of bovine lactoferrin. *Biometals.* 17, 249-55.
341. Elrod, K., Moore, W., Abraham, W. & Tanaka, R. (1997). Lactoferrin, a Potent Tryptase Inhibitor, Abolishes Late-Phase Airway Responses in Allergic Sheep. *Am. J. Respir. Crit. Care Med.* 156, 375-381.
342. Kuizenga, A., van Haeringen, N. & Kijlstra, A. (1987). Inhibition of hydroxyl radical formation by human tears. *Invest Ophthalmol Vis Sci.* 28, 305-13.
343. Kijlstra, A., Kuizenga, A., van der Velde, M. & van Haeringen, N. (1989). Gel electrophoresis of human tears reveals various forms of tear lactoferrin. *Curr Eye Res.* 8, 581-8.
344. Ghafouri, B., Stahlbom, B., Tagesson, C. & Lindahl, M. (2002). Newly identified proteins in human nasal lavage fluid from non-smokers and smokers using two-dimensional gel electrophoresis and peptide mass fingerprinting. *Proteomics.* 2, 112-20.
345. Panda, K., Chattopadhyay, R., Chattopadhyay, D. & Chatterjee, I. (2001). Cigarette smoke-induced protein oxidation and proteolysis is exclusively caused by its tar phase: prevention by vitamin C. *Toxicol Lett.* 123, 21-32.
346. Rogan, M., Taggart, C., Greene, C., Murphy, P., O'Neill, S. & McElvaney, N. (2004). Loss of microbicidal activity and increased formation of biofilm due to decreased lactoferrin activity in patients with cystic fibrosis. *J Infect Dis* 190, 1245-53.
347. Britigan, B., Hayek, M., Doebbeling, B. & Fick, R. J. (1993). Transferrin and lactoferrin undergo proteolytic cleavage in the Pseudomonas aeruginosa-infected lungs of patients with cystic fibrosis. *Infect Immun.* 61, 5049-55.
348. Sakata, M., Sack, R., Sathe, S., Holden, B. & Beaton, A. (1997). Polymorphonuclear leukocyte cells and elastase in tears. *Curr Eye Res.* 16, 810-9.
349. Kamboh, M. & Ferrell, R. (1986). Genetic studies of low-abundance human plasma proteins. I. Microheterogeneity of zinc-alpha 2-glycoprotein in biological fluids. *Biochem Genet.* 24, 849-57.
350. Burgi, W. & Schmid, K. (1961). Preparation and Properties of Zn-agr2-glycoprotein of Normal Human Plasma. *J. Biol. Chem.* 236, 1066-1074.
351. Sanchez, L. M., Lopez-Otin, C. & Bjorkman, P. J. (1997). Biochemical characterization and crystalization of human Zn-alpha 2-glycoprotein, a soluble class I major histocompatibility complex homolog. *PNAS* 94, 4626-4630.
352. Kennedy, M. W., Heikema, A. P., Cooper, A., Bjorkman, P. J. & Sanchez, L. M. (2001). Hydrophobic Ligand Binding by Zn-alpha 2-glycoprotein, a Soluble Fat-depleting Factor Related to Major Histocompatibility Complex Proteins. *J. Biol. Chem.* 276, 35008-35013.
353. Russell, S., Hirai, K. & Tisdale, M. (2002). Role of beta3-adrenergic receptors in the action of a tumour lipid mobilizing factor. *Br J Cancer* 86, 424-8.
354. Russell, S., Zimmerman, T., Domin, B. & Tisdale, M. (2004). Induction of lipolysis in vitro and loss of body fat in vivo by zinc-alpha2-glycoprotein. *Biochim Biophys Acta.* 1636, 59-68.
355. Kuizenga, A., van Agtmaal, E., van Haeringen, N. & Kijlstra, A. (1990). Sialic acid in human tear fluid. *Exp Eye Res.* 50, 45-50.
356. Dickerson, T. J. & Janda, K. D. (2002). A previously undescribed chemical link between smoking and metabolic disease. *PNAS* 99, 15084-15088.

357. Mulvenna, I., Stapleton, F., Hains, P., Cengiz, A., Tan, M., Walsh, B. & Holden, B. (2000). Low molecular weight analysis of tears using matrix assisted laser desorption ionization-time of flight mass spectrometry. *Clin Experiment Ophthalmol* 28, 205-7.
358. Khoo, D., Ho, S., Seah, L., Fong, K., Tai, E., Chee, S., Eng, P., Aw, S. & Fok, A. (1999). The combination of absent thyroid peroxidase antibodies and high thyroid-stimulating immunoglobulin levels in Graves' disease identifies a group at markedly increased risk of ophthalmopathy. *Thyroid.* 9, 1175-80.
359. Rajala, M. W. & Scherer, P. E. (2003). Minireview: The Adipocyte--At the Crossroads of Energy Homeostasis, Inflammation, and Atherosclerosis. *Endocrinology* 144, 3765-3773.
360. Berg, A., Combs, T., Du, X., Brownlee, M. & Scherer, P. (2001). The adipocyte-secreted protein Acrp30 enhances hepatic insulin action. *Nat Med.* 7, 947-53.
361. Steppan, C. M., Bailey, S. T., Bhat, S., Brown, E. J., Banerjee, R. R., Wright, C. M., Patel, H. R., Ahima, R. S. & Lazar, M. A. (2001). The hormone resistin links obesity to diabetes. 409, 307-312.
362. Kadowaki, T. & Yamauchi, T. (2005). Adiponectin and Adiponectin Receptors. *Endocr Rev* 26, 439-451.
363. Kishore, U. & Reid, K. (1999). Modular organization of proteins containing C1q-like globular domain. *Immunopharmacology.* 42, 15-21.
364. Yamauchi, T., Kamon, J., Ito, Y., Tsuchida, A., Yokomizo, T., Kita, S., Sugiyama, T., Miyagishi, M., Hara, K., Tsunoda, M., Murakami, K., Ohteki, T., Uchida, S., Takekawa, S., Waki, H., Tsuno, N., Shibata, Y., Terauchi, Y., Froguel, P., Tobe, K., Koyasu, S., Taira, K., Kitamura, T., Shimizu, T., Nagai, R. & Kadowaki, T. (2003). Cloning of adiponectin receptors that mediate antidiabetic metabolic effects. *Nature* 423, 762-9.
365. Fruebis, J., Tsao, T.-S., Javorschi, S., Ebbets-Reed, D., Erickson, M. R. S., Yen, F. T., Bihain, B. E. & Lodish, H. F. (2001). Proteolytic cleavage product of 30-kDa adipocyte complement-related protein increases fatty acid oxidation in muscle and causes weight loss in mice. *PNAS* 98, 2005-2010.
366. Waki, H., Yamauchi, T., Kamon, J., Kita, S., Ito, Y., Hada, Y., Uchida, S., Tsuchida, A., Takekawa, S. & Kadowaki, T. (2005). Generation of Globular Fragment of Adiponectin by Leukocyte Elastase Secreted by Monocytic Cell Line THP-1. *Endocrinology* 146, 790-796.
367. Seo, J. B., Moon, H. M., Noh, M. J., Lee, Y. S., Jeong, H. W., Yoo, E. J., Kim, W. S., Park, J., Youn, B.-S., Kim, J. W., Park, S. D. & Kim, J. B. (2004). Adipocyte Determination- and Differentiation-dependent Factor 1/Sterol Regulatory Element-binding Protein 1c Regulates Mouse Adiponectin Expression. *J. Biol. Chem.* 279, 22108-22117.
368. Combs, T. P., Berg, A. H., Obici, S., Scherer, P. E. & Rossetti, L. (2001). Endogenous glucose production is inhibited by the adipose-derived protein Acrp30. *J. Clin. Invest.* 108, 1875-1881.
369. Hotta, K., Funahashi, T., Arita, Y., Takahashi, M., Matsuda, M., Okamoto, Y., Iwahashi, H., Kuriyama, H., Ouchi, N., Maeda, K., Nishida, M., Kihara, S., Sakai, N., Nakajima, T., Hasegawa, K., Muraguchi, M., Ohmoto, Y., Nakamura, T., Yamashita, S., Hanafusa, T. & Matsuzawa, Y. (2000). Plasma Concentrations of a Novel, Adipose-Specific Protein, Adiponectin, in Type 2 Diabetic Patients. *Arterioscler Thromb Vasc Biol* 20, 1595-1599.
370. Combs, T. P., Wagner, J. A., Berger, J., Doebber, T., Wang, W.-J., Zhang, B. B., Tanen, M., Berg, A. H., O'Rahilly, S., Savage, D. B., Chatterjee, K., Weiss, S., Larson, P. J., Gottesdiener, K. M., Gertz, B. J., Charron, M. J., Scherer, P. E. & Moller, D. E. (2002). Induction of Adipocyte Complement-Related Protein of 30 Kilodaltons by PPARγ Agonists: A Potential Mechanism of Insulin Sensitization. *Endocrinology* 143, 998-1007.
371. Kubota, N., Terauchi, Y., Yamauchi, T., Kubota, T., Moroi, M., Matsui, J., Eto, K., Yamashita, T., Kamon, J., Satoh, H., Yano, W., Froguel, P., Nagai, R., Kimura, S., Kadowaki, T. & Noda, T. (2002). Disruption of Adiponectin Causes Insulin Resistance and Neointimal Formation. *J. Biol. Chem.* 277, 25863-25866.
372. Yamauchi, T., Kamon, J., Waki, H., Terauchi, Y., Kubota, N., Hara, K., Mori, Y., Ide, T., Murakami, K., Tsuboyama-Kasaoka, N., Ezaki, O., Akanuma, Y., Gavrilova, O., Vinson, C., Reitman, M., Kagechika, H., Shudo, K., Yoda, M., Nakano, Y., Tobe, K., Nagai, R., Kimura, S., Tomita, M., Froguel, P. & Kadowaki, T. (2001). The fat-derived hormone adiponectin reverses insulin resistance associated with both lipoatrophy and obesity. *Nat Med.* 7, 941-6.
373. Yamauchi, T., Kamon, J., Waki, H., Imai, Y., Shimozawa, N., Hioki, K., Uchida, S., Ito, Y., Takakuwa, K., Matsui, J., Takata, M., Eto, K., Terauchi, Y., Komeda, K., Tsunoda, M., Murakami, K., Ohnishi, Y., Naitoh, T., Yamamura, K., Ueyama, Y., Froguel, P., Kimura, S., Nagai, R. & Kadowaki, T. (2003). Globular Adiponectin Protected ob/ob Mice from Diabetes and ApoE-deficient Mice from Atherosclerosis. *J. Biol. Chem.* 278, 2461-2468.
374. Ouchi, N., Kihara, S., Arita, Y., Okamoto, Y., Maeda, K., Kuriyama, H., Hotta, K., Nishida, M., Takahashi, M., Muraguchi, M., Ohmoto, Y., Nakamura, T., Yamashita, S., Funahashi, T. &

Matsuzawa, Y. (2000). Adiponectin, an Adipocyte-Derived Plasma Protein, Inhibits Endothelial NF-κB Signaling Through a cAMP-Dependent Pathway. *Circulation* 102, 1296-1301.

375. Combs, T. P., Pajvani, U. B., Berg, A. H., Lin, Y., Jelicks, L. A., Laplante, M., Nawrocki, A. R., Rajala, M. W., Parlow, A. F., Cheeseboro, L., Ding, Y.-Y., Russell, R. G., Lindemann, D., Hartley, A., Baker, G. R. C., Obici, S., Deshaies, Y., Ludgate, M., Rossetti, L. & Scherer, P. E. (2004). A Transgenic Mouse with a Deletion in the Collagenous Domain of Adiponectin Displays Elevated Circulating Adiponectin and Improved Insulin Sensitivity. *Endocrinology* 145, 367-383.
376. Viengchareun, S., Zennaro, M.-C., Pascual-Le Tallec, L. & Lombes, M. (2002). Brown adipocytes are novel sites of expression and regulation of adiponectin and resistin. *FEBS Letters* 532, 345-350.
377. Starkey, K., Heufelder, A., Baker, G., Joba, W., Evans, M., Davies, S. & Ludgate, M. (2003). Peroxisome Proliferator-Activated Receptor-γ in Thyroid Eye Disease: Contraindication for Thiazolidinedione Use? *J Clin Endocrinol Metab* 88, 55-59.
378. Levin, F., Kazim, M., Smith, T. J. & Marcovici, E. (2005). Rosiglitazone-Induced Proptosis. *Arch Ophthalmol* 123, 119-121.
379. Fu, Y., Luo, N., Klein, R. L. & Garvey, W. T. (2005). Adiponectin promotes adipocyte differentiation, insulin sensitivity, and lipid accumulation. *J. Lipid Res.* 46, 1369-1379.
380. Cinti, S., Cigolini, M., Sbarbati, A. & Zancanaro, C. (1986). Ultrastructure of brown adipocytes mitochondria in cell culture from explants. *J Submicrosc Cytol.* 18, 625-7.
381. Pischon, T., Hotamisligil, G. S. & Rimm, E. B. (2003). Adiponectin: Stability in Plasma over 36 Hours and Within-Person Variation over 1 Year. *Clin Chem* 49, 650-652.
382. Kishida, K., Nagaretani, H., Kondo, H., Kobayashi, H., Tanaka, S., Maeda, N., Nagasawa, A., Hibuse, T., Ohashi, K. & Kumada, M. (2003). Disturbed secretion of mutant adiponectin associated with the metabolic syndrome*1. *Biochemical and Biophysical Research Communications* 306, 286-292.
383. Saito, T., Kawano, T., Saito, T., Ikoma, A., Namai, K., Tamemoto, H., Kawakami, M. & Ishikawa, S. (2005). Elevation of serum adiponectin levels in Basedow disease. *Metabolism* 54, 1461-1466.
384. Nishida, Y., Tian, S., Isberg, B., Hayashi, O., Tallstedt, L. & Lennerstrand, G. (2002). Significance of orbital fatty tissue for exophthalmos in thyroid-associated ophthalmopathy. *Graefe's Archive for Clinical and Experimental Ophthalmology* 240, 515-520.
385. Iglesias, P., Alvarez Fidalgo, P., Codoceo, R. & Diez, J. J. (2003). Serum concentrations of adipocytokines in patients with hyperthyroidism and hypothyroidism before and after control of thyroid function. *Clin Endocrinol* 59, 621-629.
386. Freemark, M., Fleenor, D., Driscoll, P., Binart, N. & Kelly, P. A. (2001). Body Weight and Fat Deposition in Prolactin Receptor-Deficient Mice. *Endocrinology* 142, 532-537.
387. Zinger, M., McFarland, M. & Ben-Jonathan, N. (2003). Prolactin Expression and Secretion by Human Breast Glandular and Adipose Tissue Explants. *J Clin Endocrinol Metab* 88, 689-696.
388. Pohlenz, J., Maqueem, A., Cua, K., Weiss, R., Van Sande, J. & Refetoff, S. (1999). Improved radioimmunoassay for measurement of mouse thyrotropin in serum: strain differences in thyrotropin concentration and thyrotroph sensitivity to thyroid hormone. *Thyroid* 9, 1256-1271.
389. Shattock, S. (1909). The fat masses in the necks of cretins. *Proc R Soc Med* 2, 252-261.
390. Doniach, D. (1975). Possible stimulation of thermogenesis in brown adipose tissue by thyroid stimulating hormone. *Lancet* 2, 160-1.
391. Roselli-Rehfuss, L., Robbins, L. & Cone, R. (1992). Thyrotropin receptor messenger ribonucleic acid is expressed in most brown and white adipose tissues in the guinea pig. *Endocrinology* 130, 1857-1861.
392. Chaudhry, A. & Granneman, J. G. (1997). Effect of hypothyroidism on adenylyl cyclase activity and subtype gene expression in brown adipose tissue. *Am J Physiol Regul Integr Comp Physiol* 273, R762-767.
393. Murakami, M., Kamiya, Y., Morimura, T., Araki, O., Imamura, M., Ogiwara, T., Mizuma, H. & Mori, M. (2001). Thyrotropin Receptors in Brown Adipose Tissue: Thyrotropin Stimulates Type II Iodothyronine Deiodinase and Uncoupling Protein-1 in Brown Adipocytes. *Endocrinology* 142, 1195-1201.
394. Janus, D., Baker, G., Fuhrer, D. & Ludgate, M. (2005). Thyrotropin receptor (TSHR) activation in preadipocytes stimulates the early but inhibits the terminal stages of adipogenesis. *Endocrine Abstracts* 9, OC39.
395. Digby, J., Montague, C., Sewter, C., Sanders, L., Wilkison, W., O'Rahilly, S. & Prins, J. (1998). Thiazolidinedione exposure increases the expression of uncoupling protein 1 in cultured human preadipocytes. *Diabetes* 47, 138-141.
396. Klaus, S., Ely, M., Encke, D. & Heldmaier, G. (1995). Functional assessment of white and brown adipocyte development and energy metabolism in cell culture. Dissociation of terminal differentiation and thermogenesis in brown adipocytes. *J Cell Sci* 108, 3171-3180.

397. Gupta, O., Boynton, J., Sabini, P., Markowitch, W. J. & Quatela, V. (2003). Proptosis after retrobulbar corticosteroid injections. *Ophthalmology.* 110, 443-447.
398. Grus, F., Sabuncuo, P., Augustin, A. & Pfeiffer, N. (2002). Effect of smoking on tear proteins. *Graefes Arch Clin Exp Ophthalmol* 240, 889-92.
399. Kumar, S., Leontovich, A., Coenen, M. J. & Bahn, R. S. (2005). Gene expression profiling of orbital adipose tissue from patients with Graves' ophthalmopathy: a potential role for soluble frizzled related protein-1 in orbital adipogenesis. *J Clin Endocrinol Metab* 90, 4730-35.
400. Kumar, S. & Bahn, R. S. (2003). Relative Overexpression of Macrophage-Derived Cytokines in Orbital Adipose Tissue from Patients with Graves' Ophthalmopathy. *J Clin Endocrinol Metab* 88, 4246-4250.
401. Zipris, D., Lien, E., Xie, J. X., Greiner, D. L., Mordes, J. P. & Rossini, A. A. (2005). TLR Activation Synergizes with Kilham Rat Virus Infection to Induce Diabetes in BBDR Rats. *J Immunol* 174, 131-142.
402. Bhattacharyya, K., Kalyan, K., Coenen, M. & Bahn, R. (2005). *13th International Thyroid Congress, Buenos Aires, Argentina.*
403. Hu, H. & Kato, Y. (1995). Body composition assessed by bioelectrical impedance analysis (BIA) in patients with Graves' disease before and after treatment. *Endocr J.* 42, 545-50.
404. Miyakawa, M., Tsushima, T., Murakami, H., Isozaki, O. & Takano, K. (1999). Serum leptin levels and bioelectrical impedance assessment of body composition in patients with Graves' disease and hypothyroidism. *Endocr J.* 46, 665-73.
405. Wakasugi, M., Wakao, R., Tawata, M., Gan, N., Inoue, M., Koizumi, K. & Onaya, T. (1994). Change in bone mineral density in patients with hyperthyroidism after attainment of euthyroidism by dual energy X-ray absorptiometry. *Thyroid.* 4, 179-82.
406. Rosen, C. & Adler, R. (1992). Longitudinal changes in lumbar bone density among thyrotoxic patients after attainment of euthyroidism. *J Clin Endocrinol Metab* 75, 1531-1534.
407. Abe, E., Marians, R., Yu, W., Wu, X., Ando, T., Li, Y., Iqbal, J., Eldeiry, L., Rajendren, G., Blair, H., Davies, T. & Zaidi, M. (2003). TSH is a negative regulator of skeletal remodeling. *Cell.* 115, 151-62.

8 Appendicies

8.1 Appendix A

Agarose gel electrophoresis

TAE buffer x1	Tris base 40mM ph7.6	
	EDTA 1mM	
	Glacial acetic acid 20mM	

Culture Media

GPI	DMEM x1	177ml
DMEM/ 10%FCS	FCS	20ml
	PS x 100	2ml
	Fungizone x 100	1ml

LULU*	Hams F12	177ml
Hams F12 complete	FCS	20ml
	PS x 100	2ml
	Fungizone x 100	1ml

Hams F12 complete (charcoal stripped) as above but substitute FCS for charcoal stripped FCS.

Hams F12 (serum free) as above but omit FCS and use 197ml HamsF12.

Splenocytes	RPMIx10	10ml
RPMI 1640	Dist. water	85ml
	$NaHCO_3$ (7.5%)	2.7ml
	PSG x 100	2ml
	Fungizone x 100	1ml
	NaOH 10N	200µl
		100ml

RF10	RPMI 1640 (above)	89ml
	FCS	10ml
	β-mercaptoethanol (5mM)	1ml
		100ml

ECD/MBP protein production and purification

Column Buffer	Sodium Phosphate 0.5M	10ml
	Sodium chloride	14.6g
	Dist. water	490ml
		500ml

Luria Broth	LB medium	1.8g
	Dist. water	500ml
	Autoclaved, cooled and stored at 4 C.	

Luria rich broth	LB	1l
	Glucose (20mmol)	3.6g

Lysis buffer	Tris 20mM, pH 7.4	2mls	1M stock
	EDTA 1mM	200µl	0.5M stock
	Sodium chloride 200mM	20ml	1M stock
	β-mercaptoethanol	1ml	1M stock
	Lysozyme 1mg/ml	23mg	

Sodium Phosphate 0.5M

solution A	11.7ml
solution B	38.3ml
	50ml

where:	solution A	6.9g	NaH_2PO_4 in 100ml dH_20
	solution B	13.4g	Na_2HPO_4 in 100ml dH_20

ELISA reagents and buffers

1. ECD/MBP

Wash	NaCl		87.66g
	Tris base		24.23g
	Tween		5ml
	Dist. Water	6l	adjust to pH 7.4 and then make up to 10l.
Coating buffer	$NaHCO_3$		4.2g
	NaN_3		0.2g
	Dist. water		800ml
			pH to 9.3 and make up to 1l
Diluent	NaH_2PO_4		1.56g
	NaCl		9g
	NaN_3		0.2g
	Tween		0.5ml
	Dist. water		800ml
			pH to 7.4 and make up to 1l
Conjugate	NaCl 0.9%		3ml
	Anti mouse IgG HRP		1.5µl
	Sheep serum		60µl
Substrate	ABTS*	0.01g	
	Citrate phos buffer		25ml
	H_2O_2		10µl

(* 2-2azino-bis(3-ehtylbenzthiazolin 6-sulfonic acid))

Citrate phosphate Buffer	Citric acid		5.106g
	Na_2HPO_4		7.31g
	Dist. water		800ml pH to 5 and make up to 1l

2. IFN-γ and Il 4

Wash buffer	PBS
	Tween 20 0.05%

Blocking buffer	PBS Sucrose 5% NaN_3 0.5%		
Reagent diluent IFN-γ	PBS BSA 1%		
Reagent diluent Il 4	Tris buffered saline (Tris base 20mM and NaCl 150mM) PBS 0.1% Tween 20 0.05%		
Developing buffer	Citric acid Dist. Water	8.4g 160ml	 pH to 3.95 with 4M KOH and make up to 200ml
Tetramethylbenzidine (TMB) stock	TMB DMSO Ethanol	240mg 5ml 5ml	 store protected from light 4 C
Substrate soulution	Developing buffer TMB stock H_2O_2 (30%)	15ml 150µl 15 µl	
Stop solution	H_2SO_4 2N		

ELISA sample standard curve IL4 and IFN gamma

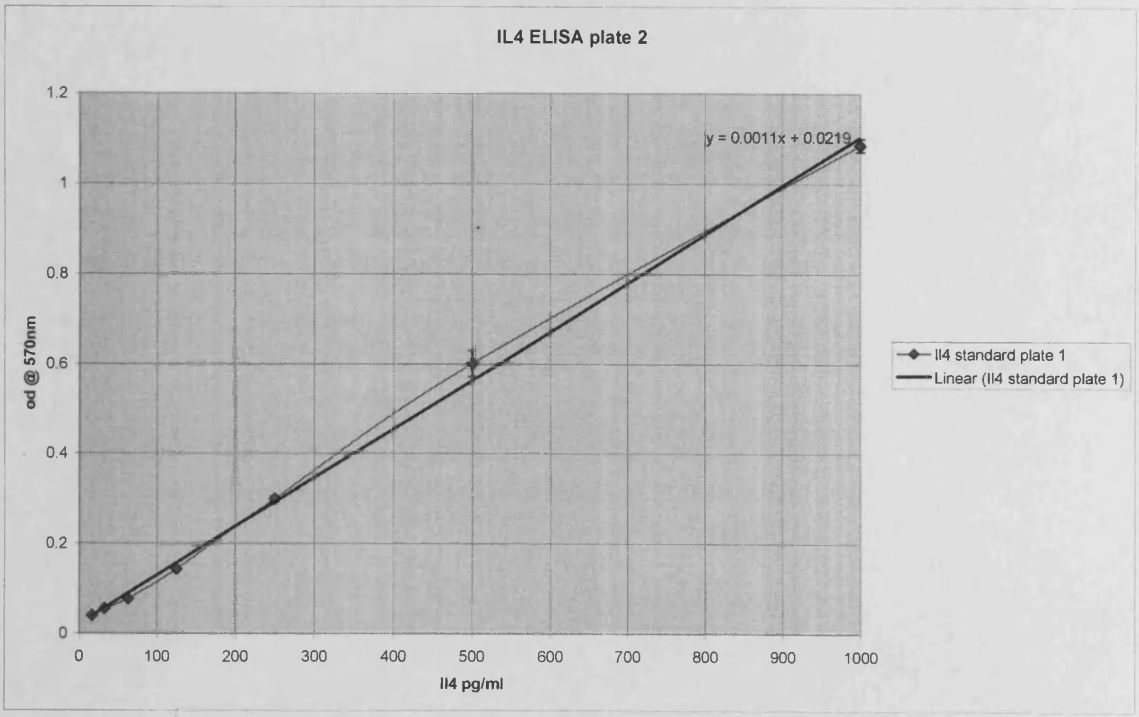

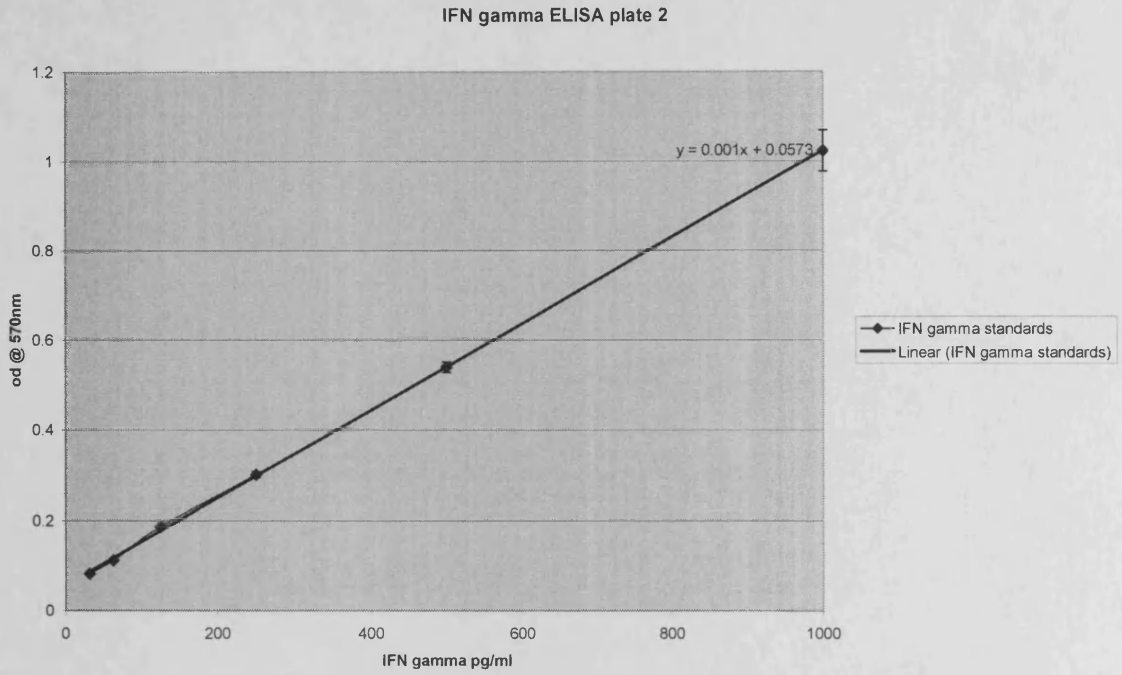

General Buffers

Phosphate buffered saline (PBS)	NaCl	20g	
	Na_2HPO_4	3.6g	
	NaH_2PO_4	0.6g	
	KCl	0.5g	
Dist. Water		2.5l	pH to 7.2 with NaOH 10N and autoclave.

Histology Processing

Paraffin processing schedule (26 hour)

Alcohol 50%		1 hr	
Alcohol 70%		2 hr	
Alcohol 80%		2 hr	
Alcohol 90%		2 hr	
Alcohol 100%		1 hr	
Alcohol 100%		2 hr	
Alcohol 100%		3 hr	
Cedar wood oil	2 hr		
Cedar wood oil	4 hr		
Wax		2 hr	All wax processing at 60C
Wax		3 hr	
Wax		2hr	

Partial dehydration in LR white for ultrastructure and immunoelectron microscopy

Dist. water x 3	10 min
Uranyl acetate 2%	2 hr
Dist. water x 3	10 min
Alcohol 50%	10 min
Alcohol 70% x 3	10 min
2:1 LR white monomer: Alcohol 70%	30 min
LR white monomer x 4	20 min

Embedding in LR white

LR white monomer (at 0 C)	10ml
LR white catalyst	15µl

Stir 30 seconds, place 0.65ml in gelatine capsules in an aluminum heat sink on ice, insert specimens, seal capsules, store overnight at 0 C and finally cure in an oven at 50 C for 1 hour.

Maxiprep buffers

Resuspension buffer	Tris-Cl 50mM ph8 EDTA 10mM RNase A 100µg/ml	store 2-8 C
Lysis buffer	NaOH 200mM SDS 1%	
Neutralisation buffer	Potassium acetate 3M pH5.5	store 2-8 C
QIAfilter wash	NaCl 750mM MOPS 50mM pH7 Isopropanol 15%	
Equilibration buffer	NaCl 750mM MOPS 50mM pH7 Isopropanol 15% Triton X-100 0.15%	
Wash buffer	NaCl 1M MOPS 50mM pH7 Isopropanol 15%	
Elution buffer	NaCl 1.25M MOPS 50mM pH8.5 Isopropanol 15%	
TE	Tris-Cl 10mM pH8 EDTA 1mM	

SDS PAGE

Resolving Gel (12%)	Acrylamide 30%	4ml	(1:29, bis:acrylamide)
	Dist. water	2.25ml	
	Tris-Cl 1M ph 8.8	3.75ml	
	SDS 10%	100µl	
	APS 10%	100µl	

Degas under vacuum then add:

	TEMED	3µl

Load between gel plates 3ml below level of stacking gel comb and seal with N-butanol. Set for 30-40mins.

Stacking Gel (4%)	Acrylamide 30%	1.3ml
	Dist. water	6.1ml
	Tris-HCl 0.5M ph 6.8	2.5ml
	SDS 10%	100µl
	APS 10%	100µl

Degas under vacuum then add:

	TEMED	10µl

Remove N-butanol from resolving gel, rinse, add stacking gel, insert comb and set for 20-30mins.

Loading buffer (Laemlli 1.8X)	SDS 20%	2ml	
	Glycerol	2ml	
	Tris-HCl 0.5M ph 6.8	2ml	
	β mercaptoethanol	200µl	
	Pyronin Y	200µl	
		6.4ml	
Running buffer 5X	Tris base	9g	
	Glycine	43.2g	
	SDS	3g	Make up to 600mls with Dist.water.
Coomassie Blue stain	Coomassie blue	250mg	
	Methanol	1ml	
	Glacial acetic acid	10ml	
	Propan-2-ol	25ml	
	Dist. water	64ml	
		100ml	
Coomassie wash	Methanol	20%	
	Acetic acid	10%	
	Dist. water	70%	
Coomassie drying	Methanol	50%	
	Glycerol	5%	
	Dist. water	45%	

TBII and TSAB buffers

HANKS balanced solution salt free buffer (SFB) 4X	KCl	0.4g	
	KH_2HPO_4	0.06g	
	$MgSO_4$	0.1g	
	$NaHCO_3$	0.35g	
	Na_2HPO_4	0.48g	Make up to 250mls with distilled water.
$CaCl_2$ stock	$CaCl_2$	1.85g	
	Dist. water	10ml	
Working buffer	SFB 4X	25mls	
	Glucose	0.1g	
	Sucrose	9.6g	
	BSA	1.5g	
	HEPES 1M	2ml	
	$CaCl_2$	100µl	Make up to 100mls with distilled water.

Thyrotropin Receptor Peptides

	TSHR residue	Amino Acid Sequence
Functional Receptor	34-53	EEDFRVTCKDIQRIPSLPPS
	48-67	PSLPPSTQTLKLIETHLRTI
	90-109	QQLESHSFYNLSKVTHIEIR
	104-123	THIEIRNTRNLTYIDPDALK
	118-137	DPDALKELPLLKFLGIFNTG
	132-151	GIFNTGLKMFPDLTKVYSTD
	146-165	KVYSTDIFFILEITDNPYMT
	188-207	GFTSVQGYAFNGTKLDAVYL
	216-235	IDKDAFGGVYSGPSLLDVSQ
	230-249	LLDVSQTSVTALPSKGLEHL
	286-305	FKNQKKIRGILESLMCNESS
	300-319	MCNESSMQSLRQRKSVNALN
	306-325	MQSLRQRKSVNALNSPLHQE
	356-375	FEEQEDEIIGFGQELKNPQE

Restriction endonuclease buffer

Buffer K	Tris-Cl 200mM pH8.5	
	$MgCl_2$ 100mM	
	Dithiothreitol 10mM	
	KCl 1M	

Western blotting

Blotting buffer	Glycine	13.7gm
	Tris base	3.02gm
	Dist. water	800ml

Dissolve fully before adding methanol.

	Methanol	200ml

TBS-T 10X	Tris base	24.2g
	Sodium chloride	80g
	Dist. water	1000ml Adjust to pH 7.6, store at 4 C.

For 1X solution dilute 1:10, then to 999ml add 1ml of Tween to give 0.1%.

Blocking buffer	TBS-T	100ml
	Marvel	5g

Blotting cassette Open cassette black side down in blotting buffer, then lay on in turn: fibre pad, filter paper x3, gel, membrane, filter paper x3 and fibre pad. (Ensuring all bubbles removed between gel and membrane). Close cassette and load into blotting tank "black to black".

8.2 Appendix B

Culture Media

3T3-L1	DMEM x1	177ml
DMEM/10% CS	Calf serum	20ml
	Pen/strep x100	2ml
	Fungizone x100	1ml
		200ml
Human Preadipocytes	DMEM x1	88.5ml
DMEM/HAMS/	HamsF12 x1	88.5ml
10% FCS	FCS	20ml
	Pen/strep x100	2ml
	Fungizone x100	1ml
		200ml
HC C1	MEM x1	177ml
MEM/10% FCSFCS		20ml
	Pen/strep x100	2ml
	Fungizone x100	1ml
		200ml
MG 63	see app.A	
DMEM/10%FCS		
HBSS	HBSS x10	10ml
	$NaHCO_3$ (7.5%)	470µl
	Dist. water	89.5ml

FCS Heat inactivated30 minutes at 56 C

HEPES x 2	NaCl	1.64g
	Na2HPO4	0.054g
	HEPES	4.99ml (1M stock)
		100mls made up with dist. water
		pH to 7.1 and filter through 0.2µm

Red blood cell	Ammonium chloride (0.154M)	0.822g
lysis solution	Potassium hydrocarbonate (10mM)	0.1g
	EDTA (0.1mM)	20µl (0.5M stock)
	Dist. water	100ml

Mix then autoclave.

Immunocytochemistry

PGT

	PBS	500ml
	Gelatine (dissolved @ 50C)	100mg
	Tween 20	250µl
Periodic acid 0.025%	PGT	10ml
	Periodic acid 50%	50µl

Ligation reaction

BstEII (New England Biolabs) has endonuclease activity in the following region:

5′ ... G^G T N A C C ... 3′
3′ ... C C A N T G^G ... 5′

BstEII	0.5µl	
Buffer NE3	2µl	
Plasmid DNA (2-3µg)	5µl	
Dist. water	12.5µl	
	20µl	2 hours at 60C.

PCR reaction

cDNA (from RT step)	2.5µl
Taq polymerase	0.5µl
Mg x10 buffer	5µl
dNTP 10mM	2µl
forward primer	1µl
reverse primer	1µl
Dist.water	39.5µl

PCR program (Thermal cycler Genius Techne)

Initially denature	1 minute @95 C
followed by 35 cycles of :	1 minute @95 C
	1 minute @55 C
	2 minutes @72 C
final elongation	10 minutes @72 C (then hold at 4C)

Retroviral handling considerations

If possible learn safe handling techniques from someone experienced in Level 2 conditions. In brief the guidelines are as follows.

1. Work in a biosafety level 2 tissue culture facility, clearly labeled with biohazard warning signs and use a system of un-recirculated exhaust air.
2. Use a regularly serviced and maintained biological safety cabinet (Class II laminar flow hood with HEPA filter).
3. Perform work behind closed doors and restrict access when working with virus particles.
4. Use gloves, a lab coat and do not use sharps. Use quills and syringes and avoid forming aerosols, if unavoidable use eye and face protection.

5. All virus contaminated waste, medium/plasticware should be soaked in concentrated bleach overnight before autoclaving and disposal.
6. All spills to be washed exhaustively with bleach.

Further information can be found at: http://bmbl.od.nih.gov

RNA reverse transcription

RT master mix	RT buffer x5	4µl
	DEPC water	0.5µl
	RNAse inhibitor (25u)	0.5µl
	Oligo(dt)	2µl
	dNTPs	2µl
	MMLV RT (200u)	1µl
		10µl

All reagents from Promega.

Sequencing reaction

Big dye	2µl
Primer (10pM/µl)	1µl
PCR product	3µl
Dist. water	4µl
	10µl

Vortex then pulse centrifuge.

Sequencing program (Thermal cycler Genius Techne)

Initially denature	3 minute @96 C
followed by 30 cycles of :	0.5 minute @96 C
	4 minutes @60 C
	0 minutes @70 C (then hold at 4C)

Transformation of competent cells and small scale plasmid preparation

SOC	Luria broth (appA)	96ml
	$MgCl_2$ (10mM)	1ml (1M stock)
	$MgSO_4$ (10mM)	1ml (1M stock)
	Glucose (20mM)	2ml (1M stock)

LB agar	LB agar	7.4g
	Dist. water	200ml
	Autoclave, allow to cool, melt gently in a microwave, add ampicillin 100µg/ml, plate and store at 4C until use.	

SET	Sucrose 20%	5g
	Tris HCl 50mM	1.25ml (1M stock pH 7.5)
	EDTA 50mM	5ml (250mM stock)
		25ml made up with sterile dist. water.

DNAse free RNAse A	RNAse A 10mg/ml in 10mM Tris HCl (pH7.5) and 15mM NaCl. Dissolved at 100 C for 15 mins, cooled to RT, aliquoted and stored at -20 C.	
Sodium acetate 3M pH4.8	CH_3COONa	24.61g
	H_20	45ml
Lysis solution	NaOH 0.2N	1ml (2N stock)
	SDS 1%	1ml (10% stock)
	Dist. water	8ml

Sample information sheet

Adipogenesis in Thyroid Eye Disease

Thyroid eye disease (TED) develops in some patients with an overactive thyroid gland, some with an under-active thyroid gland and a few with a normally functioning gland. It is important that the disease is recognised and treated early in order to reduce the risk of double vision or visual loss. Even more vital is the search for effective treatment. We currently believe that this may be due to an abnormality in the fat tissue of the eye sockets in these patients. To investigate this we would like to test fat samples from patients with and without TED.

You are currently about to undergo surgery and tissue that is normally discarded can be useful in furthering research. We would like to ask for your consent to retain a small piece of fat tissue so that we can use it in our studies to help investigate TED and its potential cause. There will be no other incision made, only the one your surgeon has to make for your particular operation and there will be no other scarring or post-operative effects from removing this tissue.

You are not obliged to take part in this study. Participating or declining to participate will have no effect on the treatment you receive.

Thank you for taking time to read this and please ask your surgeon if you have any further questions about participating in this study.

Sample consent

Adipogenesis in Thyroid Eye Disease

I consent to the removal of a small piece of fat tissue whilst undergoing my prearranged operation, to be sent to the laboratory for testing and storage in relation to thyroid eye disease. I have read and understood the attached information sheet.
Signed _____

Date_____

Preadipocyte cultures

Sample	M/F	Age	Diagnosis	History Summary
1. GH lid bx	F	49	TED	Euthyroid initially then thyrotoxic, smoker, on prednisolone
2. CH decomp	M	49	TED	Thyrotoxic now euthyroid, radio-iodine 1988, ex smoker
3. DJ decomp	F	38	TED	Thyrotoxic now hypothyroid, radio-iodine 1994, smoker, previous immunosuppression therapy
4. PSN lid bx	M	64	TED	Euthyroid, non smoker, high TSAB.
5. HM decomp	M	69	TED	Thyrotoxic relapse, smoker, on carbimazole, previous radio-iodine and orbital radiotherapy.
6. PSM decomp	F	59	TED	Thyrotoxic now euthyroid, non smoker, previous orbital radiotherapy, on immunosuppression.
7. NF decomp	F	44	TED	Thyrotoxic now euthyroid, smoker, previous thyroidectomy, on immunosuppression.
8. ED decomp right	F	22	TED	Prolonged thyrotoxicosis, smoker.
9. DR decomp	M	50	TED	Thyrotoxic now euthyroid, smoker, previous radio-iodine.
10. ED decomp left	F	22	TED	Prolonged thyrotoxicosis, smoker.
11. GC decomp	F	73	TED	Thyrotoxic now hypothyroid, previous orbital radiotherapy, on immunosuppression.
12. AJ bleph bx	F	62	Dermatochalasis	No thyroid history and euthyroid.
13. X bleph bx	F	70	Dermatochalasis	No thyroid history and euthyroid.
14. JU bleph bx	F	78	Ptosis Right	No thyroid history and euthyroid.
15. RT bleph bx	M	43	Dermatochalasis	No thyroid history and euthyroid.
16. JU bleph bx	F	78	Ptosis Left	No thyroid history and euthyroid.
17. WH bleph bx	F	38	Ptosis	No thyroid history and euthyroid.
18. IL bleph bx	F	65	Dermatochalasis	No thyroid history and euthyroid.
19. PSB bleph bx	M	58	Dermatochalasis	No thyroid history and euthyroid.
20. MS LCS bx	F	73	Ectropion	No thyroid history and euthyroid.
21. TT bleph bx	F	44	Dermatochalasis	No thyroid history and euthyroid.

patient	Age	sex	CAS	propt sum	cigs	cbz	I131	dxt	thy	Steroid	TSH	T4	T3	spegTSAB	sfmTSAB	tsfmTSAB	tpegtsab
1	39	0	0	38	0	0	0	0	1	0	6.31	15	4.9	7.7	1.02	1.74	0.96
2	62	1	3	43	1	0	0	0	0	0	0.02	22.1	8.3	2.6	1.17	1.74	1.03
3	63	0	3	31	0	0	0	1	0	0	0.02	31.4	13.8	6.2		1.61	1.2
4	62	0	1	49	1	0	1	0	0	0	2.28	17.4		5.2	1.03	1.36	1.1
5	59	0	1	46	1	0	0	0	1	1	1.27	16.5		1.1	0.72	1.81	1.11
6	32	0	0	39	0	0	0	0	0	0	1.6	13.6		1	0.86	1.38	0.8
7	66	0	1	38	1	1	0	0	0	0	0.02	12.3	4.5	7.7	0.93	1.33	1.37
8	49	0	3	44	0	0	0	0	1	0	0.02	24.6	4.4	6.7	1.02	1.76	1.21
9	18	0	2	50	1	0	0	0	1	0	0.39	29.7	4.6	2.7	0.64	1.5	0.74
10	57	0	3	43	1	0	1	0	1	0	0.02	27.5	5.1	13.9	11.4	1.69	2.61
11	73	0	5	42	0	0	0	1	0	1	0.02	30.8		9.9	5.07	1.8	1.42
12a	41	1	4	50	0	0	1	0	0	0	0.14	21.1	5.2	6.1	0.94	1.39	1.09
12b	41	1	2	53	0	0	1	0	0	0	0.06	24.2	5.6	1	0.97	1.26	
13	22	0	3	56	1	1	0	0	0	0	0.02	46.9	16	7.2	1.97	1.66	0.83
14	56	0	3	50	0	1	0	0	0	0	0.02	23.9	6.9	9.7	5.39	1.91	0.89
15	51	0	0	46	0	0	0	0	1	0	0.02	21	7.6	2.7	0.66	1.02	
16	66	0	2	44	0	0	0	.1	0	0	0.02	19.4	4.4	15.5	2.8	1.79	
17	53	0	3	42	1	0	0	0	1	0	1.54	18.5		3.5	0.86	1.84	
18	49	0	4	34	1	0	0	0	0	1	0.08	20.1		6.6	0.88	1.77	1.04
19	19	0	1	36	1	0	1	0	0	0	3.17	19		6.6	0.86	1.61	0.92
20	48	1	2	55	1	0	0	0	1	0	9.8	11.5		0.8		1.71	1.13
21	38	0	3	42	1	0	1	0	0	0	3.54	17		5.1	1.09	1.67	0.68
22	32	0	0	43	0	0	0	0	0	0	0.62	15.3		1.2	0.82	1.36	0.85
23a	69	1	9	48	1	1	1	1	0	1	0.61	9.5		13.6	1.43	1.61	0.93
23b	69	1	7	49	1	0	1	1	0	1	0.69	11.9		5.8	1.19	1.46	
24	39	0	2	51	0	0	1	0	0	0	0.04	23.9		4.4	1.06	1.46	0.99
25	49	0	2	37	1	0	0	0	0	0	1.4	19.8		1.7	1.12	1.49	1.06
26	48	0	3	43	0	0	0	0	0	1	1.34	14.6		2.7	0.92	1.96	1.07

Clinical data Graves' ophthalmopathy patients chapter 4 (0=yes, 1=no)

patient	Age	sex	CAS	propt sum	cigs	cbz	I131	dxt	thy	Steroid	TSH	T4	T3	spegTSAB	sfmTSAB	tsfmTSAB	tpegtsab
27	43	0	3	34	0	0	1	0	0	0	0.26	20.7	4.2	1.9	0.72	1.26	0.72
28	54	0	3	47	1	0	0	0	1	0	6.76	17.4		13	16.5	1.48	1
29	57	0	7	49	0	0	1	0	0	1	0.91	16.8		7.8	3.93	2.23	1.35
30	63	0	2	41	0	0	0	0	0	1	1.13	15		1.2	0.62	1.22	
31	59	0	1	46	0	0	1	0	0	0	1.44	20.2	3.7	0.7	0.84	1.74	
32	45	0	9	44	0	0	0	0	0	0	0.02	42.7		5.9	1.08	1.69	
33	45	0	1	38	0	0	0	0	0	0	0.81	12.1		9.1	0.99	1.4	1.17
34	59	0	6	59	0	0	0	1	0	1	0.26	28.3		7.5	0.88	1.59	
35	60	0	3	49	1	0	0	0	0	0	0.02	28.1	8.8	3.7	0.97	1.35	1.46
36	48	1	0	45	0	1	0	1	0	0	1.02	15.6		2.4	0.93	1.73	
37	64	0	0	37	0	0	1	0	0	0	0.02	22.2	5.2	0.9	1.1	2.26	1.62
38	27	1	4	37	1	0	0	0	0	0	0.67	13.6		2.5	1.65	0.83	0.78

Clinical data Graves' ophthalmopathy patients chapter 4